Novel Regulatory Mechanisms of Autophagy in Human Disease: Implications for the Development of Therapeutic Strategies

Maneka Chitiprolu

A thesis submitted to the

Faculty of Graduate and Postdoctoral Studies

in partial fulfillment of the requirements for the

Doctorate in Philosophy degree in Cellular and Molecular Medicine

Department of Cellular and Molecular Medicine

Faculty of Medicine

University of Ottawa

Authorizations

Manuscript #1:

Maneka Chitiprolu, Chantal Jagow, Veronique Tremblay, Emma Bondy-Chorney, Geneviève Paris, Alexandre Savard, Gareth Palidwor, Francesca A. Barry, Lorne Zinman, Julia Keith, Ekaterina Rogaeva, Janice Robertson, Mathieu Lavallée-Adam, John Woulfe, Jean-François Couture, Jocelyn Côté, Derrick Gibbings. “A complex of C9ORF72 and p62 uses arginine methylation to eliminate stress granules by autophagy”. Nature Communications 2018 Jul 18;9:2794.

Manuscript #2:

Huishan Guo, Maneka Chitiprolu, David Gagnon, Lingrui Meng, Carol Perez-Iratxeta, Diane Lagace and Derrick Gibbings. “Autophagy supports genomic stability by degrading retrotransposon RNA”. Nature Communications 2014 Nov 4;5:5276.

Manuscript #3:

Huishan Guo, Maneka Chitiprolu, Luc Roncevic, Charlotte Javalet, Fiona J. Hemming, My Tran Trung, Lingrui Meng, Elyse Latreille, Christiano Tanese de Souza, Danielle McCulloch, R. Mitchell Baldwin, Rebecca Auer, Jocelyn Côté, Ryan Charles Russell, Rémy Sadoul, Derrick Gibbings. “Atg5 Disassociates the V1V0-ATPase to Promote Exosome Production and Tumor Metastasis Independent of Canonical Macroautophagy”. Developmental Cell 2017 Dec 18;43(6):716-730.

Abstract

The dysfunction of autophagy pathways has been linked to the development and progression of numerous human diseases, in particular neurological disorders and cancer. Investigating these pathological autophagy mechanisms is essential to gain insights into the underlying disease mechanisms, identify novel biomarkers, and develop targeted therapies. In this thesis, I present three manuscripts that investigate the regulatory mechanisms of autophagy machinery in human diseases.

In the first manuscript (Chitiprolu et al., 2018), we investigated the mechanism of p62-mediated selective autophagic clearance of RNA stress granules implicated in Amyotrophic Lateral Sclerosis (ALS). Repeat expansions in C9ORF72, the major cause of ALS, reduce C9ORF72 levels but how this impacts stress granules is uncertain. By employing mass spectrometry, high resolution imaging and biochemical assays, we demonstrated that the autophagy receptor p62 associates with C9ORF72 to eliminate stress granules by autophagy. This requires p62 to associate with proteins that are symmetrically methylated on arginines. Patients with C9ORF72 repeat expansions accumulate symmetric arginine dimethylated proteins which co-localize with p62. This suggests that C9ORF72 initiates a cascade of ALS-linked proteins (C9ORF72, p62, SMN, FUS) to recognize stress granules for degradation by autophagy and hallmarks of a defect in this process are observable in ALS patients.

The second manuscript (Guo, Chitiprolu et al., 2014) describes the mechanism by which autophagy degrades retrotransposon RNA from both long and short interspersed elements, thereby preventing new retrotransposon insertions into the genome. By employing quantitative imaging tools, we demonstrated that retrotransposon RNA localizes to RNA granules that are selectively degraded by the autophagy receptors NDP52 and p62. Mice lacking a copy of Atg6/Beclin1, a gene critical for autophagy, also

accumulate both retrotransposon RNA and genomic insertions. This suggests a mechanism for the increased tumorigenesis upon autophagy inhibition and therefore a role for autophagy in tempering evolutionary change.

Finally, the third manuscript (Guo, Chitiprolu et al., 2017) examines the intersection of autophagy machinery with exosome release and function in cancer metastasis. By employing dynamic light scattering, Nanosight particle tracking, electron microscopy, super-resolution imaging and Western blotting, we robustly quantified exosome identity and purity in multiple cell lines. We demonstrated that exosome production is strongly reduced in cells lacking Atg5 and Atg16L1, but this is independent of Atg7 and canonical autophagy. The effect of Atg5 on exosome production promotes the migration and in vivo metastasis of orthotopic breast cancer cells. These findings delineate autophagy-independent pathways by which autophagy-related genes can contribute to metastasis.

Taken together, data presented in the three manuscripts highlight the molecular mechanisms of autophagy core machinery proteins and selective receptors such as Atg5, p62 and NDP52, in the pathogenesis of cancer and neurodegeneration. In these diseases characterized by mutations in autophagy pathways, the mechanisms we uncover provide insights into their causes and serve as potential therapeutic targets.

Contents

List of Tables

List of Figures

List of Abbreviations

3-MA: 3-Methyladenine

AAV9: Adeno-Associated Virus

ACB1: Acyl-CoA-Binding Protein

ALIX: ALG-2-Interacting Protein X

ALS: Amyotrophic Lateral Sclerosis

Alu: Arthrobacter Luteus

ANOVA: Analysis of Variance

APP: Amyloid Precursor Protein

As: Sodium Arsenite

ASO: Anti-Sense Oligonucleotide

ASYM: Asymmetrically Dimethylated Proteins

ATG: Autophagy-Related Gene

ATP6V1E1: ATPase H+ Transporting V1 Subunit E1

ATPase: Adenylpyrophosphatase

ATXN2: Ataxin-2

BAC: Bacterial Artificial Chromosome

BAF, Baf A1: Bafilomycin A1

BECN1: Beclin1

BFDR: Bayesian False Discovery Rate

BFP: Blue Fluorescent Protein

Bif-1: Bax-Interacting Factor 1

BNIP3: BCL2/Adenovirus E1B 19 kDa Protein-Interacting Protein 3

BRCA1: Breast Cancer type 1 Susceptibility Protein

BSA: Bovine Serum Albumin

C9, C9ORF72: Chromosome 9 Open Reading Frame 72

CALCOCO2: Calcium Binding and Coiled-Coil Domain 2

CARM1: Coactivator-Associated Methyltransferase-1

cDNA: Complementary DNA

CIRP: Cold-Inducible RNA-Binding Protein

CMA: Chaperone-Mediated Autophagy

Co-IP: Co-Immunoprecipitation

CQ: Chloroquine

CRISPR: Clustered Regularly Interspaced Short Palindromic Repeats

Ctl: Control

DCP: Decapping Protein

DDX3: Dead-Box Protein

DMEM: Dulbecco's Modified Eagle Medium

DNA: Deoxyribonucleic Acid

EDC: Enhancer of Decapping Protein

EGF: Epidermal Growth Factor

eIF4E: Eukaryotic Translation Initiation Factor 4E

EM: Electron Microscopy

ER: Endoplasmic Reticulum

ESCRT: Endosomal Sorting Complexes Required for Transport

EWSR1: Ewing Sarcoma Breakpoint Region 1

fALS: Familial ALS

FBS: Fetal Bovine Serum

FDA: Food and Drug Administration

FDR: False Discovery Rate

FIP2000: Family Integrating Protein

FISH: Fluorescence In Situ Hybridization

FMRP: Fragile X Mental Retardation Protein

FUNDC1: FUN14 Domain Containing 1

FUS, TLS: Fused in Sarcoma, Translocated in Sarcoma

FYCO1: FYVE and Coiled-coil Protein 1

G3BP1: Ras GTPase-Activating Protein-Binding Protein 1

GAPDH: Glyceraldehyde 3-Phosphate Dehydrogenase

GFP: Green Fluorescent Protein

GIPC: GAIP Interacting Protein C-terminus

GLUT4: Glucose Transporter Type 4

GO: Gene Ontology

G-Q structure: G-Quadruplex

gRNA: Guide Ribonucleic Acid

GST: Glutathione S-Transferase

HA: Human influenza Hemagglutinin

HBSS: Hank's Balanced Salt Solution

HCQ: Hydroxychloroquine

HCT-116: Human Colorectal Carcinoma Cells

HDAC6: Histone Deacetylase 6

HEK293: Human Embryonic Kidney Cells T Antigen of SV40

HeLa: Henrietta Lacks

HER2: Human Epidermal Growth Factor Receptor 2

HIV: Human Immunodeficiency Virus

hnRNP: Heterogeneous Nuclear Ribonucleoprotein

HRP: Horseradish Peroxidase

HuR: Hu Antigen R

IF: Immunofluorescence

IgG: Immunoglobulin G

IL: Interleukin

IP: Immunoprecipitate

IP/MS: Immunoprecipitation followed by Mass Spectrometry

iPSCs: Induced Pluripotent Stem Cells

JACoP: Just Another Co-localization Plugin

JmjC: Jumonji C

KEAP1: Kelch-like ECH-Associated Protein 1

LAMP: Lysosomal-Associated Membrane Protein

LC3: Light Chain 3

LC-MS: Liquid Chromatography–Mass Spectrometry

LINE-1: Long Interspersed Nucleotide Elements

LIR: LC3 Interacting Region

MATR3: Matrin 3

MCF7: Michigan Cancer Foundation-7

MEF: Mouse Embryonic Fibroblasts

MEP50: Methylosome Protein 50

miRNAs: microRNAs

MN1: Murine Motor Neuron Line

mRNA: Messenger Ribonucleic Acid

mRNPs: Messenger Ribonucleoprotein Complexes

MSC: Mesenchymal Stromal Cells

MTA: Methylthioadenosine

mTOR: Mammalian Target of Rapamycin

MVB: Multivesicular Body

NBR1: Neighbor of BRCA1 Gene 1

NDP52: Nuclear Dot Protein 52

NRF2: Nuclear Factor Erythroid 2–Related Factor 2

NRhPE: N-lissamine Rhodamine Phosphatidylethanolamine

nt: Nucleotide

OPTN: Optineurin

OVCA: Human Ovarian Carcinoma Cells

PABP1: Poly-A Binding Protein 1

P-bodies, PBs: Processing Bodies

PBS: Phosphate-Buffered Saline

PE: Phosphatidylethanolamine

PHB2: Prohibitin-2

PI3K: Phosphatidylinositol 3-Kinase

PLA: Proximity Ligation Assay

PRMT: Protein Arginine Methyltransferase

PrP: Prion Protein

PSF: Point Spread Function

PTEN: Phosphatase and Tensin Homolog

PVDF: Polyvinylidene Fluoride

RBPs: RNA-Binding Proteins

rDNA: Ribosomal DNA

RIPA: Radioimmunoprecipitation

RNA: Ribonucleic Acid

RNAi: RNA Interference

rRNA: Ribosomal Ribonucleic Acid

RT-PCR: Reverse Transcriptase Polymerase Chain Reaction

RT-qPCR: Reverse Transcriptase Quantitative Polymerase Chain Reaction

SAINT: Significance Analysis of INTeractome

sALS: Sporadic ALS

SAM: S-Adenosylmethionine

SD: Standard Deviation

SEM: Standard Error of the Mean

SERBP1: SERPINE1 mRNA Binding Protein 1

SGs: Stress Granules

shRNA: Short Hairpin RNA

SILAC: Stable Isotope Labeling by Amino Acids in Cell Culture

SINE: Short Interspersed Nucleotide Elements

siRNA: Small Interfering RNA

SMN: Survival Motor Neuron

SMURF1: SMAD Specific E3 Ubiquitin Protein Ligase 1

Sm[Y12]: Smith Antigen Y12

snRNP: Small Nuclear Ribonucleoproteins

SNX18: Sorting Nexin 18

SOD1: Superoxide Dismutase 1

SQSTM1, p62: Sequestosome-1

SQUASSH: Segmentation and Quantification of Subcellular Shapes

STBD1: Starch-Binding Domain-Containing Protein 1

STED: Stimulated Emission Depletion microscopy

SYM: Symmetrically Dimethylated Proteins

TAF15: TATA-Box Binding Protein Associated Factor 15

TAX1BP1: Tax1-Binding Protein 1

TBK1: TANK-Binding Kinase 1

TDP-43: TAR DNA-Pinding Protein 43

TDRD3: Tudor Domain Containing 3

TECPR1: Tectonin Beta-Propeller Repeat Containing 1

TIA1: T-Cell Intracellular Antigen 1

TIAR: TIA-1-Related Protein

TOLLIP: Toll Interacting Protein

TRIM5: Tripartite Motif-Containing Protein 5

tRNA: Transfer Ribonucleic Acid

Tsc: Tuberous Sclerosis

TSG101: Tumor Susceptibility Gene 101

TUBA: Tubulin Alpha Chain

Ub: Ubiquitin

UBA: Ubiquitin-Associated Domain

UBQLN2: Ubiquilin-2

ULK1: Unc-51 Like Autophagy Activating Kinase 1

UTR: Untranslated Region

UVRAG: UV Radiation Resistance-Associated Gene Protein

VCP: Valosin-Containing Protein

WB: Western Blotting

WT: Wild-type

XRN1: 5'-3' Exoribonuclease 1

ZCCHC6: Zinc Finger, CCHC Domain Containing 6

Acknowledgements

I would like to express my heartfelt gratitude towards my supervisor Dr. Derrick Gibbings for his unwavering faith in my capabilities, throughout the journey of my MSc/PhD. His involvement in shaping my outlook not only strengthened my spirit to seek light at the end of the tunnel, but also to emerge out of it as a *Philosopher* with love for wisdom. I cannot think of another supervisor who would risk recruiting and funding an international student with a bachelor's degree from an overseas engineering institute. His training provided me a firm grounding in the rigors of proper scientific research and inspired me to adopt his logical, structured writing and critical reasoning skills. Going forward, I hope to lead by example like him.

My TAC members - Dr. Jocelyn Côté, Dr. Ruth Slack, Dr. Johnny Ngsee and Dr. William Stanford have been instrumental to my scientific progress over the past 5 years. If not for their honest commendations and criticisms, I would not have grown to be a well-rounded scientist. In particular, I will always be grateful to Dr. Côté's approachability that not only impacted my overall technical competence but also facilitated my understanding of administrative responsibilities.

I've always found my lab environment congenial, interactive and fun. Alyssa's positivity, Olanta's ambition and Danielle's determination taught me attitude is everything that brings us closer to our dreams. These three friends personify the fun component of my graduate studies. I've been fortunate to share my lab experiences with accomplished and humble teammates - Annie, Maisa, Matteo, Ryan and James. I will always cherish the memories with Nasim, Andréanne, Emma and Tara who made me feel welcome in Canada since day 1. I feel blessed to have found a true friend in Tanya Foley whose articulacy and passion for science never ceases to amaze me.

To the three pillars of my life, my parents and brother - Anitha Chiluveru, Nagender Chitiprolu and Nikhilesh Chitiprolu, you are the reason why I dream big and why I fight back with twice the effort to make those dreams come alive. Every phase of my Ottawa chapter is filled with one person, my dance partner - Farhan Khan, who introduced me to work-life balance. Lastly Sri Teja - my partner for life, you continue to inspire me to explore my untapped potential, turn challenges into opportunities and become multifaceted.

Chapter 1 - Introduction

"Survival of the fittest" is a concept that originated from Darwinian evolutionary theory to describe the mechanism of natural selection. Multicellular organisms have evolved to resolve internal cellular conflicts. This is illustrated by two predominant cellular quality control pathways - (i) autophagy and (ii) proteasomal degradation (Varshavsky, 2017). These sophisticated machineries eliminate suboptimal proteins from functioning aberrantly, thereby protecting the internal organization of an individual cell. In other words, autophagy and proteasomal degradation ensure survival of the fittest proteins or organelles in living cells.

Proteins are continuously turned over within a cell. The turnover rate varies significantly across proteins and is impacted by the balance between synthesis and degradation. With the half-life of individual proteins ranging from a few minutes to months (~100,000-fold variability), protein surveillance pathways play a central role in maintaining steady-state levels of healthy proteins (proteostasis) by clearing aggregated or dysfunctional counterparts. These processes are particularly critical to normal cell growth and development, and in response to environmental stress conditions. Although both the catabolic systems serve a similar purpose of degrading and recycling proteins, the proteins targeted and their final products released by autophagy and proteasome are radically different. While the proteasome degrades short-lived regulatory proteins individually (Hershko & Ciechanover, 1998), autophagy targets long-lived proteins, sugars, lipids, nucleic acids and other large cytosolic structures for bulk degradation (Levine & Klionsky, 2004). Further, proteasomal degradation results in short peptide products whereas autophagic degradation yields constituting amino acids. Here, we focus on deconvoluting the growing complexity within the autophagy pathway.

1.1 Autophagy - a master recycler

In 1963, a Belgian cytologist and biochemist Christian De Duve coined the term *autophagy* from the Ancient Greek αὐτόφαγος, meaning “self-eating” (Deter & De Duve, 1967). Autophagy is a conserved ubiquitous process that helps eukaryotic cells function as recyclers for efficient nutrient reuse as well as disposal of proteins and large obsolete organelles. When organelles such as mitochondria, the power house of the cell, become damaged or dysfunctional, cells don’t leave this debris lying around. Instead, the autophagy pathway is activated to collect it all within a double membrane structure called autophagosome and bring it to the lysosome (in higher eukaryotes) or to the vacuole (in lower eukaryotes/plants), where the substrates are broken down into constituent parts that can be reused elsewhere in the cell. Such cellular recycling is critical to organismal survival.

While initially thought to lead exclusively to cell death, it is now well understood that induction of autophagy can lead to a variety of outcomes, including cell survival under adverse conditions of nutrient deprivation, pathogen attack, or organelle dysfunction (Kundu & Thompson, 2008). For instance, neonates use autophagy to eliminate parts of themselves to survive in the first few hours after birth (Kuma et al., 2004). This ensures quick access to energy and nutrients. It is important to note that autophagy is basally active in all cells and is upregulated in response to environmental stresses and developmental changes (C. He & Klionsky, 2009).

1.2 Forms of autophagy

Three types of autophagy have been described – macroautophagy, microautophagy and chaperone-mediated autophagy. All 3 forms are capable of routing cytosolic components to the lysosome for degradation.

1.2.1 Microautophagy and endosomal microautophagy

In microautophagy, cytoplasmic entities destined for degradation are directly internalized by invagination of the lysosomal membrane to form small vesicles containing cytoplasmic contents inside lysosomes/vacuoles (Uttenweiler & Mayer, 2008). A similar mechanism involving protein internalization by late endosomes (multivesicular bodies) via direct membrane invagination is commonly known as endosomal microautophagy (Sahu et al., 2011). Interestingly, some proteins spared from degradation are released into the extracellular space, when multivesicular bodies fuse with the plasma membrane releasing their intraluminal vesicles called exosomes (Record, Carayon, Poirot, & Silvente-Poirot, 2014). While microautophagy uses some components of the macroautophagy pathway (Krick et al., 2008), endosomal microautophagy requires multiple endosomal sorting complexes required for transport (ESCRT) systems (X. M. Liu et al., 2015). Overall, microautophagy degrades large substrates in bulk as well as selectively (Farre & Subramani, 2004; Mukherjee, Patel, Koga, Cuervo, & Jenny, 2016).

1.2.2 Chaperone-mediated autophagy

In chaperone-mediated autophagy (CMA), soluble cytosolic proteins destined for degradation are directly delivered to the lysosome via translocation across the lysosomal membrane (Kaushik & Cuervo, 2012). CMA substrates in the cytosol form a complex with chaperone proteins that bind the lysosomal membrane receptor LAMP-2A for translocation (Bandyopadhyay, Kaushik, Varticovski, & Cuervo, 2008). Unlike micro- and macro-autophagy, CMA cannot degrade large substrates such as organelles or macromolecules.

1.2.3 Macroautophagy

Macroautophagy is a homeostatic process conserved in all eukaryotes. It is the best characterized process of autophagy thus far and stronger connections to cellular metabolism and diseases have been established for it. Here, we focus on macroautophagy (hereafter referred to as autophagy). Unlike microautophagy and CMA, autophagy is associated with morphological changes involving 0.5–1.5 μm double-membraned vesicles called autophagosomes (Z. Yang & Klionsky, 2010). These vesicles occupying a significant volume of the cytoplasm can engulf large parts of the cytosol consisting of macromolecules and damaged organelles.

1.3 Molecular machinery of autophagy

The molecular machinery that is required for autophagy has been extensively studied in yeast, nematodes, flies, and mammals (Noda & Inagaki, 2015). Efficient autophagic responses are mechanistically divided into distinct steps. The first step involves selection of cargo, followed by nucleation of a limiting membrane called a phagophore. Under the governance of autophagy (ATG) genes and two ubiquitin-like conjugation systems, microtubule-associated protein 1 light chain 3 beta (LC3-I) is covalently modified with the lipid phosphatidylethanolamine (PE) to form LC3-II that is then integrated into the growing phagophore for substrate uptake. Eventually, the phagophore seals encapsulating cytoplasmic contents inside the double-membraned autophagosome. Subsequent fusion of autophagosomes with lysosomes delivers hydrolases and other catabolic enzymes for complete degradation of autophagosome contents.

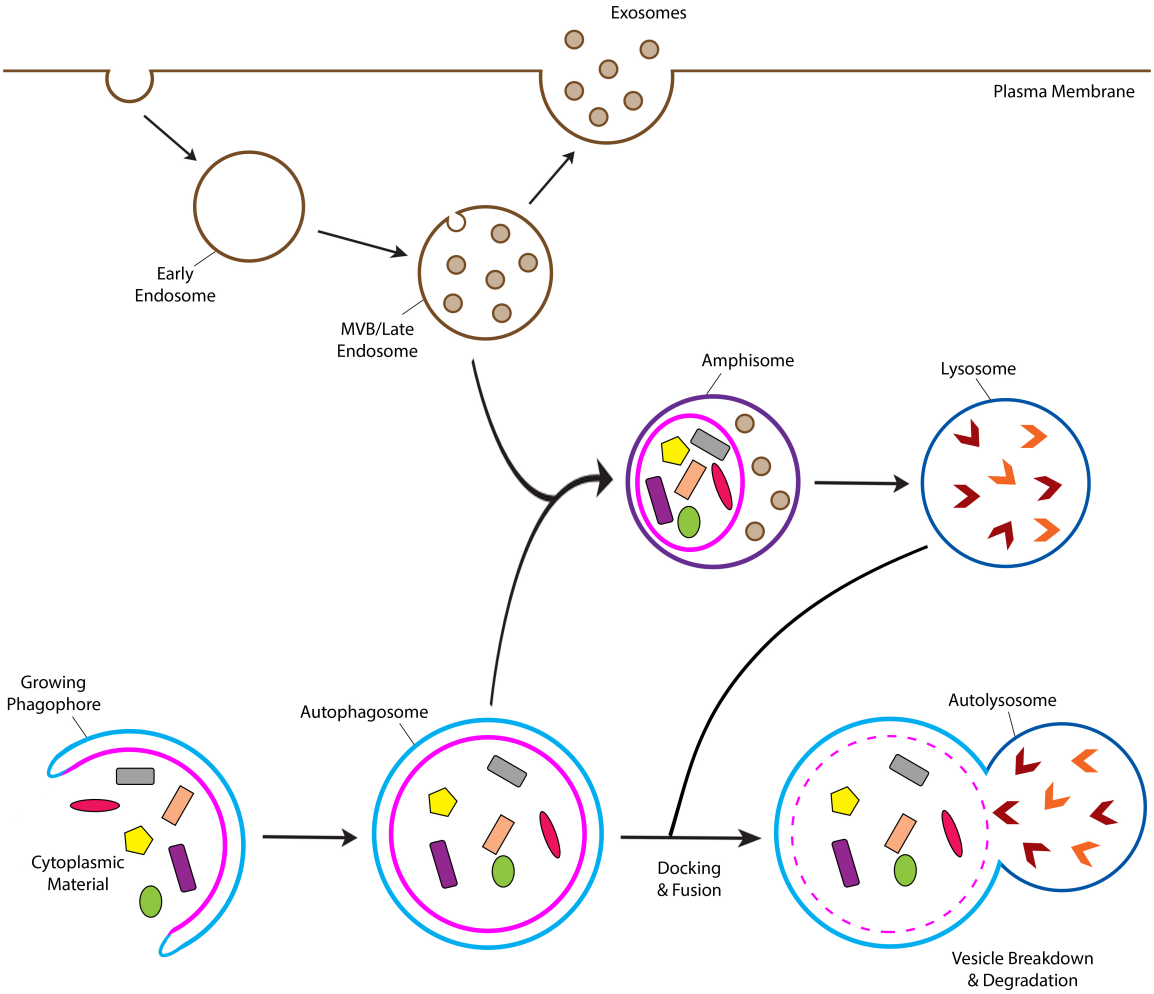

Schematic view of the autophagy and endocytic pathways

In response to inducing stimuli, autophagosome formation is initiated by the assembly of a multimeric complex containing ATG13, ATG101, FIP2000 and ULK1 at ATG9-positive membranes (Karanasios et al., 2016). Activated ULK1 then mediates phosphorylation of ATG9 to trigger the elongation of phagophore, utilizing membranes from various sources such as the endoplasmic reticulum, mitochondria and recycling late endosomes (Lamb, Yoshimori, & Tooze, 2013; Papinski et al., 2014). To further aid the process, another multimeric complex called the class III phosphatidylinositol 3-kinase (PI3K) complex is recruited to the site of initial phagophore membrane (Kihara, Noda, Ishihara, & Ohsumi,

2001). PI3K complex containing BECN1 and VPS34 produces PI3P, which recruits ubiquitin-like conjugation systems for the expansion and closure of the membranes.

One of the two ubiquitin-like systems functioning in autophagy relies on ATG7 and ATG10, which promote ATG5 and ATG12 conjugation. Conjugated ATG5-ATG12 then forms a multiprotein complex with ATG16L1 to subsequently associate with the extending phagophore (Mizushima et al., 1998). The second ubiquitin-like system comprising of ATG3 and ATG7, promote conjugation of phosphatidylethanolamine to LC3B following its proteolytic maturation (cleavage) by ATG4 (Ichimura et al., 2000). Lipidated LC3 (LC3-II), generated onto the inner and outer surfaces of autophagosomes, promotes hemifusion of the membranes (Kabeya et al., 2000).

The next step following encapsulation of the autophagy substrates within autophagosomes is the fusion of autophagosomes with late endosomes or lysosomes forming amphisomes or autolysosomes. The molecular machinery required for this fusion event comprises various proteins, also operating in the endocytic pathway, such as the activated small GTPase RAB7A (GTP-bound state) and the lysosomal membrane protein LAMP2 (Amaya, Fader, & Colombo, 2015; Antonioli, Di Rienzo, Piacentini, & Fimia, 2017). Evidence suggests that fusion of autophagosomes with endosomes lowers the pH within organelles prior to lysosomal fusion and subsequent delivery of acid preoteases (Mindell, 2012). Acidification of the lysosomal lumen, mediated by V-type ATPase, degrades the vesicle contents/substrates including the inner autophagosomal membrane.

1.4 Non-canonical autophagy

Multiple core autophagy proteins including ATG5 and ATG7 have been considered critical to elicit autophagic responses (Codogno, Mehrpour, & Proikas-Cezanne, 2011).

Specifically, genetic ablations of *ATG5* and *ATG7* in mice cause embryonic or post-natal lethality (Komatsu et al., 2005; Kuma et al., 2004). However, recent evidence of autophagic responses independent of ATG5/ATG7 suggests that non-canonical forms of autophagy also exist. One such autophagy pathway forms autophagosomes from late endosomes and trans-Golgi, independent of LC3 processing (Nishida et al., 2016). The existence of these pathways is indicative (i) that multiple independent pathways may be able to form autophagosomes and maybe (ii) of a high degree of redundancy among the molecular mechanisms of autophagy. However, these pathways may also be rare or unable to turnover large amounts of substrate as canonical autophagy. Owing to this redundancy and/or complexity, precise molecular signatures for autophagy may be difficult to understand.

1.5 Non-selective and selective types of autophagy

Autophagic responses constitute both (i) non-selective bulk disposal of cytoplasmic material, and (ii) selective clearance of distinct types of substrates by dedicated molecular factors called receptors (Zaffagnini & Martens, 2016).

1.5.1 Autophagy substrates

Selective autophagic responses can preferentially engulf and degrade a large and heterogeneous combination of cytoplasmic entities ranging from mitochondria (mitophagy), peroxisomes (pexophagy), nucleus (nucleophagy), endoplasmic reticulum (reticulophagy), ribosomes (ribophagy), protein aggregates (aggrephagy), lipid droplets (lipophagy), bacteria or virions (xenophagy), proteasomes (proteaphagy), lysosomes (lysophagy) to RNA stress granules (granulophagy) (Galluzzi, Baehrecke, et al., 2017).

1.5.2 Autophagy receptors and adaptors

Autophagy receptors are proteins that physically link specifc cargos to LC3 in the nascent autophagosome membrane for degradation within the lysosome. To this end, most receptors contain unique cargo recognition motifs and evolutionarily conserved domains for binding LC3 (LIR). This is applicable to autophagy receptors including p62, NDP52, NBR1, OPTN, BNIP3, BNIP3L, ATG34, FUNDC1, PHB2, TRIM5, TAX1BP1, Atg19, and Atg32 (Birgisdottir, Lamark, & Johansen, 2013). Besides cargo recognition, some autophagy receptors including p62 serve other regulatory functions to further aid the catabolic process by binding upstream machinery such as the ATG12-ATG5:ATG16L1, ULK1 or VPS34 complexes (Fracchiolla et al., 2016).

Autophagy adaptors on the other hand, are proteins that bind LC3 but with no role in cargo recognition. As a result, the adaptors remain resistant to autophagic degradation unlike the receptors. Several ATG proteins are regarded as adaptors. A few other adaptors include FYCO1, which links autophagosomes to the cytoskeleton, and SNX18, which promotes autophagosome biogenesis (Stolz, Ernst, & Dikic, 2014).

1.6 Autophagy in cell survival and cell death

In the recent past, self-digestion by autophagy has been recognized as a critical biological phenomenon promoting organismal health. An outstanding question in the field revolves around autophagy acting as a double-edged sword i.e., whether activating or inactivating autophagy would prevent disease progression (Mizushima, Levine, Cuervo, & Klionsky, 2008). The pro-survival function of autophagy has been studied in response to various cellular contexts such as nutrient deprivation, pathogen attack and organelle dysfunction. However, uncontrolled activation of autophagy can yield cell death as a result of non-specific degradation of vast amounts of cytoplasmic material that the cell cannot sustain. Additionally, the pro-survival function of autophagy can be

maladaptive and facilitate tumour cell growth under unfavourable cellular contexts such as the tumour microenvironment. Analysis of mice lacking core autophagy machinery genes has revealed the link between dysfunctional autophagy and human diseases, in particular neurodegeneration and cancer (Nixon, 2013; White, 2012). Here, we focused on investigating autophagy-dependent disease mechanisms.

1.7 Neurodegeneration and ALS

Autophagy is essential for basal neuronal homeostasis, especially in post-mitotic neurons where toxic components are not diluted by cell division. Predominant evidence comes from studies where mice lacking *Atg5* or *Atg7* in neurons suffered from neurodegeneration and progressive motor deficits due to their inability to clear abnormal protein accumulations (Hara et al., 2006; Komatsu et al., 2006). The dependence on autophagic degradation is further increased under stressed disease conditions. Toxic protein aggregates are observed as autophagy substrates in various neurodegenerative diseases including Parkinson's, Huntington's, Alzheimer's, amyotrophic lateral sclerosis, and prion diseases (Menzies et al., 2017). Therefore, activating autophagy may be beneficial in these disease contexts (Barmada et al., 2014).

1.7.1 Molecular mechanisms of ALS

Amyotrophic lateral sclerosis (ALS) is a degenerative disease killing upper and lower motor neurons. Consequent deficiency of motor neurons, which are required for transmitting messages from brain to the muscle, causes muscle weakness, paralysis and ultimately death. An estimated 3000 Canadians are living with ALS, with no access to viable treatment options that cure the disease. The disease strikes usually between the ages of 40 and 60, causing loss of motor function and death within 2–5 years in 80% of the diagnosed cases (Cleveland & Rothstein, 2001).

ALS-linked mutations can be broadly classified as those that impair cellular degradative systems such as autophagy or those that affect RNA splicing, metabolism or RNA granule dynamics (S. C. Ling, Polymenidou, & Cleveland, 2013). Both kinds of mutations result in the accumulation of cytoplasmic aggregates, the most common pathogenic theme in ALS. Hexanucleotide (G4C2) repeat expansion in the first intron of C9ORF72 gene is the most common genetic cause of ALS (DeJesus-Hernandez et al., 2011; Renton et al., 2011). Mutations in this locus are linked to 25% of familial ALS cases and 10% of sporadic ALS cases highlighting the importance to understand their role in C9ORF72-mediated neurodegeneration (Majounie et al., 2012; Taylor, Brown, & Cleveland, 2016). Repeat expansions are transcribed into RNA and translated into dipeptide proteins via a non-canonical repeat-associated non-ATG-dependent translation (Zu et al., 2011). Atleast 3 pathogenic mechanisms may result from the mutation. First, loss of function of C9OFR72 is mediated by decreased levels of C9ORF72 mRNA and protein (Almeida et al., 2013; DeJesus-Hernandez et al., 2011; Donnelly et al., 2013; Gijselinck et al., 2012; Waite et al., 2014). Drivers of this haploinsufficiency in patients include hypermethylation of CpG islands upstream of the predominant transcript variant (Xi et al., 2013), trimethylation of histones (Belzil et al., 2013), formation of G-quadruplex and R-loop structures by repeats (Kumar, Kashav, Islam, Ahmad, & Hassan, 2016). Although no deleterious mutations have been found in the coding region of *C9ORF72* (Harms et al., 2013), lack of C9ORF72 sensitizes human induced motor neurons to degenderation (Shi et al., 2018). Second, gain of function of C9ORF72 via RNA repeat toxicity is mediated by sequesteration of RNA binding proteins and splicing factors such as SRSF2, ALYREF and hnRNPA1 away from their normal function (Y. B. Lee et al., 2013). However, expression of stop codon interrupted untranslated repeats causes no toxicity or lethality in *Drosophila* (Mizielinska et al., 2014). Third, gain of function of C9ORF72 via dipeptide repeat toxicity is mediated by

impaired nucleocytoplasmic transport (Jovicic et al., 2015) and stress granule dynamics (K. H. Lee et al., 2016). Over-expression of dipeptide repeats induces ALS-like pathology (Chew et al., 2015; Haeusler, Donnelly, & Rothstein, 2016). Evidence from *Drosophila* suggests dipeptide repeats as primary drivers of eye degeneration and lethality (Mizielinska et al., 2014). However, clinicopathological analysis of human post-mortem samples reveals no correlation between dipeptide repeat pathology and neurodegeneration (Davidson et al., 2014; Mackenzie et al., 2015; Mackenzie, Frick, & Neumann, 2014). Taken together, a combination of all three pathomechanisms may be driving the disease. For example, loss of C9ORF72 function could make neurons vulnerable to other pathologies mediated by RNA foci or dipeptide repeats.

1.7.2 Autophagy genes and mechanisms implicated in ALS

A key hallmark of ALS pathology is the accumulation of cytoplasmic aggregates containing proteins whose corresponding genes are mutated in ALS patients. These include SOD1, TDP-43, FUS and C9ORF72 among others (Blokhuis, Groen, Koppers, van den Berg, & Pasterkamp, 2013). ALS cases are categorized as sporadic (90 - 95%) or familial (5-10%). Mutations in more than a hundred genes have been linked to ALS (Wroe, Wai-Ling Butler, Andersen, Powell, & Al-Chalabi, 2008). Fascinatingly, a number of these genes encode proteins that function in the autophagy pathway suggesting a defect in autophagy-mediated protein degradation in ALS patients. Indeed, impaired autophagy has been observed in the post-mortem tissue sections of sporadic ALS patients (Morimoto et al., 2007; Soo et al., 2015). Autophagy dysregulation in ALS may be caused by mutations in autophagy receptors such as p62/SQSTM1 (Fecto et al., 2011), OPTN (Maruyama et al., 2010), UBQLN2 (Williams et al., 2012) and autophagy regulators involved in the formation or maturation of autophagosome such as VCP (Ju et al., 2009; Tiloca et al., 2012) and C9ORF72 (Sullivan et al., 2016; Webster et al., 2016).

Evidence demonstrates that p62 deficiency in mice leads to neurodegeneration via aberrant hyperaccumulation of insoluble aggregates of K63-polyubiquitin chains (Ramesh Babu et al., 2008; Wooten et al., 2008). Further, depletion of p62 in zebrafish causes axonal anomalies in motor neurons and locomotor deficits that are rescued upon rapamycin treatment (Lattante et al., 2015). In addition to being mutated in some forms of ALS, p62 is commonly found in cytoplasmic aggregates associated with almost all forms of ALS including patients with C9ORF72 repeat expansions (Majcher, Goode, James, & Layfield, 2015; Schludi et al., 2015). Another ALS-linked gene - TBK1 has also been reported to function in autophagy as an enzyme phosphorylating p62 and OPTN to increase the efficiency of degradation (Freischmidt et al., 2015; Pilli et al., 2012; Richter et al., 2016). Overall, mutations in the autophagy pathway likely cause ALS because their ability to degrade cytoplasmic aggregates is impaired.

1.7.3 RNA metabolism and stress granule dynamics linked to ALS

Several mutations genetically-linked to ALS impair nuclear localization of RNA-binding proteins such as FUS, TDP-43, TIA1, hnRNPA1, hnRNPA2B1 and MATR3, causing them to accumulate in cytoplasmic foci and insoluble aggregates in patient neurons (Arai et al., 2006; Belzil et al., 2009; Bentmann et al., 2012; Bosco et al., 2010; Bruijn et al., 1998; Corrado et al., 2010; Daigle et al., 2013; Deng et al., 2010; Dormann et al., 2010; Fernandes, Eshleman, & Buchan, 2018; Forman, Trojanowski, & Lee, 2004; Gal et al., 2011; Hart, 2006; Ito, Seki, Tsunoda, Uchiyama, & Suzuki, 2011; Kabashi et al., 2008; H. J. Kim et al., 2013; Kino et al., 2011; Kwiatkowski et al., 2009; Lagier-Tourenne & Cleveland, 2009; Lemmens, Moore, Al-Chalabi, Brown, & Robberecht, 2010; Matsumoto, Stojanovic, Holmberg, Kim, & Morimoto, 2005; Neumann et al., 2006; Piao et al., 2003; Sreedharan et al., 2008; Stieber, Gonatas, & Gonatas, 2000a, 2000b; Tu et al., 1996; Ugras & Shorter, 2012; van Blitterswijk & Landers, 2010; Van Deerlin et al.,

2008; Vance et al., 2009; Watanabe et al., 2001; Wolozin, 2012). These proteins function in RNA metabolism activities such as splicing and mRNA export to the cytoplasm. Although the critical events leading to ALS remain elusive, it is well known that pathology is often associated with the accumulation of intracellular mutant proteins within foci or aggregates in degenerating neurons of brain and spinal cord (Forman et al., 2004; Piao et al., 2003). Strikingly, aggregates of ALS-linked mutant proteins such as TDP-43 and FUS are identified as derivatives of RNA-rich stress granules (Acosta et al., 2014; Baron et al., 2013; Bentmann et al., 2012; Bosco et al., 2010; Colombrita et al., 2009; Daigle et al., 2013; Dewey et al., 2011; Dewey et al., 2012; Dormann et al., 2010; Gal et al., 2011; D. Ito et al., 2011; Kino et al., 2011; Lenzi et al., 2015; Liu-Yesucevitz et al., 2010; McDonald et al., 2011; Parker et al., 2012; Sama et al., 2013; Wolozin, 2012).

Stress granules (SGs) are dynamic membrane-less organelles, composed largely of stalled pre-initiation complexes (nontranslating messenger ribonucleoprotein complexes (mRNPs)) that contain polyadenylated mRNAs, RNA-binding proteins, translation initiation factors and small ribosomal subunits (Fan & Leung, 2016). It is believed that stress granules help cells conserve energy and adapt to stress by sequestering select groups of RNA-binding proteins, mRNA and signaling proteins while promoting the translation of proteins involved in the stress response program. This correlates with a rapid global reduction in translation initiation that otherwise consumes significant amounts of cellular resources (Anderson & Kedersha, 2008; Buchan & Parker, 2009). Stress granules form minutes after cells encounter stress of many types (oxidative, heat, viral) and largely disappear within an hour after removal of stress. While many stress granules disassemble, a significant proportion relies on autophagy for their elimination (Buchan, Kolaitis, Taylor, & Parker, 2013). The physiological relevance of stress granules remains unclear but their sequestration of select RNA-binding proteins

controlling splicing and translation is postulated to re-shape the post-transcriptional landscape to rapidly tailor cellular responses to stress (Panas, Ivanov, & Anderson, 2016; Protter & Parker, 2016).

Stress granules are formed upon liquid-liquid phase separation of RNA-binding proteins driven by homo and heterotypic protein-protein interactions once a critical local concentration of proteins is achieved (Han et al., 2012; Y. Lin, Protter, Rosen, & Parker, 2015; Molliex et al., 2015). Often the phase separation is facilitated by the presence of low complexity aggregation-prone domains in RNA-binding proteins. It should be noted that proteins interacting at slow off rates will result in solid phases whereas fast off rates will yield liquid assemblies. Stress granules containing core structures surrounded by dilute shells represent a mix of both solid and liquid phases (Protter & Parker, 2016). Consistent with stress granules being critical for neurological pathogenesis in ALS, multiple ALS-linked mutations occur in stress granule proteins or proteins that alter stress granule dynamics such as C9ORF72, FUS, SMN, VCP, TIA1, ATXN2, TDP-43, hnRNPA2B1/hnRNPA1, MATR3, TAF15 and EWSR1 among others (Fernandes et al., 2018). Several of these proteins including FUS, TDP-43, hnRNPA1 and TIA1 can phase separate to form liquid droplets in vitro (Y. Lin et al., 2015; Molliex et al., 2015). Over time, these droplets mature and form less dynamic foci called fibrillar aggregates; this process of phase separation is further accelerated by ALS-causing mutations in FUS, C9ORF72, TDP-43 and hnRNPA1 (Boeynaems et al., 2017; Conicella, Zerze, Mittal, & Fawzi, 2016; Kato et al., 2012; Murakami et al., 2015; A. Patel et al., 2015). This suggests that ALS-linked mutations perturb stress granule dynamics that lengthen the persistence of granules in diseased cells, thus seeding the formation of intractable aggregates. The continued presence of pathological stress granules in neurons of patients (Forman et al., 2004; Piao et al., 2003) is indicative of impaired physiological

functions of sequestered RNA binding and signaling proteins and thus, disrupted neuronal hoemostasis in ALS.

Evidence suggests that pathology in ALS is caused not only by the toxic gain of function in the cytoplasm mediated by protein aggregates, but also the loss of splicing capacity in the nucleus of proteins like TDP-43 and FUS (J. P. Ling, Pletnikova, Troncoso, & Wong, 2015; Scekic-Zahirovic et al., 2016). Indeed, alteration in FUS-dependent splicing events is central to the pathogenesis of ALS (Anthony & Gallo, 2010; Da Cruz & Cleveland, 2011; Lagier-Tourenne & Cleveland, 2009; Lagier-Tourenne et al., 2012; Qiu et al., 2014; Rabin et al., 2010; Zhou, Liu, Liu, Ozturk, & Hicks, 2013). In ALS patients with FUS mutations, the normal nuclear localization of FUS is disrupted resulting in accumulation of FUS-positive aggregates in neuronal cytoplasm and dendrites of spinal motor neurons and cerebral cortex neurons as well as nuclei of brainstem (Huang et al., 2010; Kwiatkowski et al., 2009; Mackenzie et al., 2011; Vance et al., 2009). FUS physiologically binds both DNA and RNA (Baechtold et al., 1999; Zinszner, Sok, Immanuel, Yin, & Ron, 1997). It is involved in multiple stages of RNA metabolism including pre-mRNA splicing (Cleaver, Lam, & Revet, 2009; Kornblihtt, de la Mata, Fededa, Munoz, & Nogues, 2004; Lagier-Tourenne, Polymenidou, & Cleveland, 2010; Munoz et al., 2009). Importantly, FUS is one of the ~50 non-snRNP proteins in the pre-spliceosome (Wahl, Will, & Luhrmann, 2009), further establishing the implications of FUS in splicing regulation. Especially in the nervous system, tight regulation of splicing is necessary to generate a vast majority of transcripts that control cell fate determination, axon guidance, dendritic growth, and synaptic functions (Q. Li, Lee, & Black, 2007; Martin & Ephrussi, 2009). Evidence demonstrates that a fALS-linked mutation in FUS – R521G changes its binding preference on target RNAs from the intronic sequences to sequences in the 3′ UTR (Hoell et al., 2011). Furthermore in several sALS patients, FUS

RNA targets are found to be substantially downregulated (Lagier-Tourenne et al., 2012) suggesting that widespread mRNA splicing defects mediated by aggregation-prone mutant of FUS in ALS may add to the loss of neuronal integrity and neurodegeneration.

1.7.4 Stress granules at the intersection of autophagy and ALS

Stress granules may serve critical cellular survival functions, consistent with their evolutionary conservation in all eukaryotic cells. Their dynamics are regulated by balancing mechanisms that assemble and disassemble them. Pathways turning over intracellular components such as autophagy are required to maintain this balance in healthy and especially disease states where persistent stress granules may seed the formation of pathological aggregates (Acosta et al., 2014). Owing to the large size (>1.5 μm) of mature stress granules and protein aggregates, autophagy is better suited to eliminate them than the ubiquitin-proteasome degradation (Venkatraman, Wetzel, Tanaka, Nukina, & Goldberg, 2004).

Emerging genetic and therapeutic evidence suggests that autophagy is required to eliminate stress granules linked to ALS. Activating autophagy with rapamycin promotes stress granule clearance, while selective autophagy inhibitors demonstrate the converse effect (Buchan et al., 2013). Autophagy is involved in the elimination of cytoplasmic aggregates of FUS and TDP-43 (Barmada et al., 2014; Caccamo et al., 2009; Matus, Bosco, & Hetz, 2014; Ryu et al., 2014; Soo et al., 2015; X. Wang et al., 2010). Recent reports link mutations in the autophagy receptors - p62, OPTN, UBQLN2 and autophagy effectors - C9ORF72, VCP, TBK1 to the pathogenesis of ALS (Belzil et al., 2011; Deng et al., 2011; Freischmidt et al., 2015; Gal et al., 2009; Hirano et al., 2013; Kwon et al., 2012; Le Ber et al., 2013; Maruyama et al., 2010; Millecamps et al., 2011; Rubino et al., 2012; Sugihara, Maruyama, Kamada, Morino, & Kawakami, 2011; Teyssou et al., 2013).

All of these autophagy proteins co-localize with pathological cytoplasmic aggregates, often containing TDP-43 and FUS (Brady, Meng, Zheng, Mao, & Hu, 2011; H. Ito et al., 2011; Korac et al., 2013). ALS-linked TDP-43 aggregates also co-localize with the autophagosome marker LC3 (Brady et al., 2011; X. Wang et al., 2010). Many types of aggregates in ALS patients are labeled with the autophagy receptor p62. Indeed, there is evidence that autophagy regulates stress granules by targeting them for degradation (Buchan et al., 2013). ALS-associated protein - VCP, which is essential for autophagy (Ju et al., 2009), is required for degradation of stress granules by autophagy (Buchan et al., 2013). Furthermore, in the absence of other mechanisms to degrade mRNAs such as decapping or direct 5′ to 3′ digestion, autophagic flux to clear stress granules is enhanced. Therefore, disease-linked mutations in autophagy machinery likely cause ALS because their ability to degrade a specific substrate - stress granules is disrupted. The coalescence of so many proteins genetically implicated in ALS with autophagy (p62, C9ORF72, OPTN, VCP, TBK1, UBQLN2) and stress granules (FUS, SMN, C9ORF72, VCP, hnRNPA2B1/hnRNPA1, TDP-43, TIA1, ATXN2, etc.) suggests that failure to clear stress granules by autophagy may promote ALS pathogenesis (Belzil et al., 2011; Fimia, Kroemer, & Piacentini, 2013; Gal et al., 2009; Hirano et al., 2013; Kwon et al., 2012; Maruyama et al., 2010; Millecamps et al., 2011; Renton et al., 2011; Sugihara et al., 2011; Teyssou et al., 2013; Tiloca et al., 2012).

1.7.5 Targeting post-translational modifications

The specificity and efficiency of selective autophagy is often regulated by post-translational modifications that allow interaction of the cargo with autophagy receptors. Most selective autophagy receptors such as p62, NDP52, OPTN and NBR1 are equipped with ubiquitin binding domains to recognize ubiquitinated substrates (Rogov, Dotsch, Johansen, & Kirkin, 2014; Shaid, Brandts, Serve, & Dikic, 2013). Autophagy

allocates its receptors to target intracellular ubiquitinated aggregates (p62, NBR1, OPTN, TOLLIP) (Kirkin et al., 2009; Pankiv et al., 2007; J. Zhou, J. Wang, et al., 2013), bacteria (p62, NDP52, OPTN) (Thurston, Ryzhakov, Bloor, von Muhlinen, & Randow, 2009; Wild et al., 2011; Y. T. Zheng et al., 2009), peroxisomes (NRB1) (Deosaran et al., 2013), or mitochondria (OPTN, NDP52, Tax1BP1) (Lazarou et al., 2015; Sarraf et al., 2013; Wong & Holzbaur, 2014). The affinity to polyubiquitinated protein aggregates for subsequent autophagic degradation is further enhanced by phosphorylation of the polyubiquitin-binding protein p62 in its ubiquitin-associated domain (Matsumoto, Wada, Okuno, Kurosawa, & Nukina, 2011). Similarly, TBK1-mediated phosphorylation of OPTN results in its stronger binding to LC3 for xenophagy (Wild et al., 2011). In most published cases, ubiquitination of substrates is required for their recognition by selective autophagy receptors. Nonetheless, in some cases degradation of substrates such as proteins, lipids and sugars by autophagy appears to be independent of ubiquitination (Gal et al., 2009; Khaminets, Behl, & Dikic, 2016; Korac et al., 2013; Matsumoto et al., 2011; Shaid et al., 2013). For instance, p62 can recognize SOD1 mutants in ALS in an ubiquitin-independent fashion for degradation by autophagy–lysosome pathway. Selective autophagy of bacterial pathogens by Tecpr1 is also ubiquitin independent as Shigella avoid polyubiquitin tagging (Ogawa et al., 2011). Autophagic clearance of damaged mitochondria by Nix does not require ubiquitination (Novak et al., 2010). Other identified receptors include BNIP3, FUNDC1, Atg32 (mitophagy) (Hanna et al., 2012; Kanki, Wang, Cao, Baba, & Klionsky, 2009; L. Liu et al., 2012; Okamoto, Kondo-Okamoto, & Ohsumi, 2009; Quinsay, Thomas, Lee, & Gustafsson, 2010), Atg30, Atg36, NBR1 (pexophagy) (Farre, Manjithaya, Mathewson, & Subramani, 2008; Motley, Nuttall, & Hettema, 2012), SMURF1, TRIM5α (virophagy) (Mandell et al., 2014; Orvedahl et al., 2011), and Stbd1 (glycophagy) (S. Jiang, Wells, & Roach, 2011). Growing evidence also points to deacetylation by HDAC6, as essential for autophagosome maturation,

autophagosome and lysosome fusion, and subsequent degradation of protein aggregates (Iwata, Riley, Johnston, & Kopito, 2005; J. Y. Lee et al., 2010).

Recently, arginine methylation of proteins has been demonstrated to recruit proteins for degradation by autophagy (S. Li, Yang, Tian, & Zhang, 2013). This frequently occurring modification involves addition of one or two methyl groups to the guanidino nitrogen atoms of arginine by protein arginine methyltransferase enzymes (PRMTs) (Larsen et al., 2016). PRMTs transfer methyl groups from S-adenosylmethionine (SAM) to the nitrogen atoms of arginine, resulting in the formation of methylarginine and S-adenosylhomocysteine. Type I PRMTs including – PRMT1, PRMT2, PRMT3, PRMT4/CARM1, PRMT6 and PRMT8 generate asymmetric dimethylarginine residues by adding two methyl groups on one of the terminal guanidino nitrogen atoms. Type II PRMTs including – PRMT5 (predominant) and PRMT9 generate symmetric dimethylarginine residues by adding one methyl group on each of the terminal guanidino nitrogen atoms (Bedford & Clarke, 2009; Y. Yang et al., 2015). Type III PRMTs including - PRMT7 generate monomethylarginine residues by adding one methyl group on one of the two terminal gaunidino nitrogen atoms.

PRMTs are known to functionally affect protein-protein interactions between methylarginine sites and methylarginine-binding proteins. Most PRMTs favour the arginine- and glycine-rich amino acid motif GAR, while PRMT4 and PRMT7 display unique specificity to PGM and RXR motifs. Recent evidence suggests that certain JmjC histone lysine demethylases also demethylate methylarginine indicating that the modification is dynamic (Walport et al., 2016). One family of proteins that contain a conserved 60-amino acid motif to bind methylarginine-containing proteins is the Tudor domain-containing proteins including TDRD3 and SMN (C. Chen, Nott, Jin, & Pawson, 2011). While arginine methylated FUS interacts with SMN-Tudor, interactions with

arginine methylated DDX3 are specific to TDRD3-Tudor (Goulet, Boisvenue, Mokas, Mazroui, & Cote, 2008). The RNA-binding capacity of several Tudor domain-containing proteins suggests the role of arginine methylation in RNA metabolism. For instance, symmetric arginine methylation of Sm proteins by PRMT5 is required for their binding to the Tudor domain of SMN for cytoplasmic core-UsnRNP assembly and subsequent pre-mRNA splicing (Meister et al., 2001). Interestingly, a large proportion of arginine-methylated proteins or arginine-methylation binding proteins localize to stress granules including TDRD3, SMN, FUS and DDX3 (Baron et al., 2013; Cote & Richard, 2005; Goulet et al., 2008). Both TDRD3 and SMN do not localize to stress granules upon deletion of their Tudor domains and/or inhibition of methylation (Goulet et al., 2008; Hua & Zhou, 2004). Indeed, arginine methylation recruits several proteins into stress granules. Hypomethylation of FMRP, a potential PRMT substrate and a component of stress granules, affects its recruitment into stress granules (Dolzhanskaya, Merz, Aletta, & Denman, 2006; Mazroui et al., 2002). Similarly hypomethylation of another protein recognized by both SMN and TDRD3 – SERBP1, delays its recruitment to stress granules (Goulet et al., 2008; Y. J. Lee, Wei, Chen, & Li, 2014). Fascinatingly, localization of ALS-linked pathological FUS to the cytoplasm and stress granules is dependent on its arginine methylation (Dormann et al., 2012; Scaramuzzino et al., 2013; Tradewell et al., 2012). Methylated mutant FUS is detected in stress granules as well as diseased tissues. Other arginine methylated RNA-binding proteins recruited to stress granules include hnRNPA2B1/hnRNPA1, TAF15, DDX3, G3BP1, EWS, PABP1 (PRMT4 substrate) and CIRP (De Leeuw et al., 2007; J. Lee & Bedford, 2002). Therefore we hypothesize that this post-translational modification found on many stress granule proteins allows recruitment of autophagy receptors for subsequent degradation. This idea is also supported by a recent study performed in *C. elegans* wherein posttranslational arginine methylation of P (germ) granule components by a PRMT1

homolog enhanced their association with a scaffold protein which itself is selectively targeted for degradation by autophagy (S. Li et al., 2013). Taken together, we propose that arginine methylation of proteins in stress granules allows them to be recognized for degradation by autophagy. This mechanism may play a role in eliminating some types of cytoplasmic aggregates closely associated with ALS pathology.

1.7.6 Current ALS therapeutic approaches

There is currently no cure for ALS. Only one drug, Riluzole, is approved for the treatment of ALS, but it improves survival by only 2 - 3 months in a subset of patients (Traynor, Alexander, Corr, Frost, & Hardiman, 2003). Another FDA-approved drug, Radicava, scavenges free radicals and slows down the impairment in physical function (Abe et al., 2014; Ittner et al., 2015; Yoshino & Kimura, 2006). Therefore, there is a pressing need for therapeutic strategies to treat ALS.

Autophagy upregulation presents an area of therapeutic potential. Autophagy impacting drugs have been tested in various neurodegenerative diseases including ALS (Ballou & Lin, 2008). Activating autophagy with trehalose (AMPK activator) or the FDA-approved drug rapamycin (mTOR inhibitor), clears pathological cytoplasmic aggregates and confers neuroprotection against cytotoxicity in animal models of ALS (Caccamo et al., 2009; Castillo et al., 2013; Y. Li et al., 2015; I. F. Wang et al., 2012; I. F. Wang, Tsai, & Shen, 2013; K. Zhang et al., 2013; X. Zhang et al., 2014). Furthermore, rapamycin also reduces FUS-positive stress granules, neurite fragmentation and cell death in cell-based FUS ALS models (Ryu et al., 2014). However, trehalose has been effective only in the early stages of ALS and rapamycin has demonstrated contradictory evidence of worsening motor neuron death and lifespan in SOD1 ALS mice (X. Zhang et al., 2011). Another inducer of autophagy – lithium carbonate reduces motor neuron loss and

promotes survival of ALS mice and patients (Fornai et al., 2008). However, other studies with similar experimental conditions have presented conflicting results with earlier onset of disease and reduced lifespans (Gill, Kidd, Vieira, Thompson, & Perrin, 2009; Pizzasegola et al., 2009). Although autophagy promises a druggable therapeutic strategy for ALS, current studies highlight the need to develop more specific and targeted therapeutics

Several novel small molecule regulators of autophagy have been identified with no cytotoxic effects, by employing high-throughput library screens (Kuo et al., 2015; L. Zhang et al., 2007). Some of these have also been explored in the neurodegeneration context (Sarkar & Rubinsztein, 2008). Two compounds in particular - fluphenazine and methotrimeprazine, have rescued the mislocalized TDP-43 and improved cell survival in TDP-43 ALS mice (Barmada et al., 2014). A natural herb - berberine (AMPK activator), has also reduced TDP-43 aggregates by activating autophagy (C. F. Chang et al., 2016).

Strategies involving antisense oligonucleotides (ASOs) are nearing clinical trials for ALS. This strategy, targeting mRNA of interest, decreases the target protein levels. Thus, ASOs can be advantageous in gain-of-toxicity mediated pathogenesis. Phase I clinical testing of ASOs targeting SOD1 mRNA have shown no toxicities (Miller et al., 2013). However, the inability to reduce mutant SOD1 protein paved the way for a reformulated ASO, which is currently undergoing phase I trials. Additional ASO strategies targeting expanded repeats in C9ORF72 in neurons differentiated from patient iPSCs have reduced toxic RNA aggregates without impacting the C9ORF72 mRNA levels (Donnelly et al., 2013). In a BAC mouse model expressing 450 human C9ORF72 repeats, ASOs have improved ALS phenotypes (J. Jiang et al., 2016; Lagier-Tourenne et al., 2013). Finally, targeting Atxn2 in TDP-43 ALS mice has reduced inclusions and improved survival (Becker et al., 2017). In C9ORF72-mediated pathogenesis, a small molecule

targeting of the G-quadruplex (G-Q) structure of the repeat RNA alleviates the hallmark of dipeptide repeat toxicity with a moderate survival benefit and thereby presents a promising therapy (Schludi & Edbauer, 2018). In parallel, RNA interference based approaches employing viral vectors such as AAV9 in combination with shRNA against SOD1 have delayed disease onset and improved survival (van Zundert & Brown, 2017). Certain stem-cell based therapies employing adult mesenchymal stromal cells (MSC) show promise for neuroprotection in ALS patients (Forostyak & Sykova, 2017).

Taken together, the evidence from pharmacological studies suggests that autophagy induction holds promise as a therapeutic strategy. However, the point of intervention in the autophagy pathway is critical to tailoring the therapeutic approach for ALS. Unlike upstream mTOR inhibitors or autophagy activators that cannot overcome downstream dysfunctions in eliminating specific substrates, drugs activating degradation of disease-specific substrates such as stress granules offer a viable strategy to treat this debilitating disease.

1.8 Hallmarks of Cancer

Paradoxical roles of autophagy have been implicated in tumour suppression and tumour progression. Therefore to understand how autophagy functions at various stages of tumorigenesis, it is critical to establish links between autophagy and hallmarks of cancer. Cancer initiation and progression is linked to cellular traits that impact underlying molecular and biochemical processes to convert a normal cell into a malignant cell. These traits represent the hallmarks of cancer: (1) selective growth and proliferative advantage, (2) altered stress response favouring overall survival, (3) induced vascularization, (4) activated invasion and metastasis, (5) metabolic rewiring, (6) an abetting microenvironment, and (7) immune modulation (Fouad & Aanei, 2017; Hanahan

& Weinberg, 2011). Moreover two enabling characteristics essential for the acquisition of these hallmarks have now been described as (i) genome instability and mutation, and (ii) tumour-promoting inflammation.

Genetic change is fundamental to each of the 200,000 cancers diagnosed each year in Canada. Individual cells in a tumour house a remarkable level of genetic heterogeneity (Almendro, Marusyk, & Polyak, 2013; Marusyk, Almendro, & Polyak, 2012). Tens to hundreds of mutations, deletions, amplifications and translocations differentiate normal tissue from tumours. Genetic differences are also common between metastases and the tumour of origin (Almendro et al., 2013; Marusyk et al., 2012), and among distinct regions of tumours in many cancers (Gerlinger et al., 2012) including ovarian cancer (Hoogstraat et al., 2014). Genetic change promotes the evolution of tumour aggression, metastasis (Almendro et al., 2013; Marusyk et al., 2012) and resistance to chemotherapeutics (Duesberg, Stindl, & Hehlmann, 2000; McClelland, Burrell, & Swanton, 2009; Swanton et al., 2009).

1.8.1 Retrotransposons in cancer

Human genomes harbour agents of genetic change, called retrotransposons or jumping genes, which replicate using an RNA intermediate that traffics through the cytoplasm before inserting into a new site in the genome (copy-and-paste mechanism). Two of the principal families of retrotransposons, Long Interspersed Nucleotide Elements (LINE-1) and Short Interspersed Nucleotide Elements (SINE), such as the dominant *Alu* family in primates, account for 20% and 13% of the human genome respectively (Batzer & Deininger, 2002; Beck, Garcia-Perez, Badge, & Moran, 2011; Kemp & Longworth, 2015). Retrotransposons are a major contributor to genetic variation between species, within species, and between cells in a single individual (Baillie et al., 2011; Beck et al.,

2010; Hormozdiari et al., 2011; E. Lee et al., 2012). They are highly active in somatic cells and particularly in cancers, generating an estimated 0.3-800 random insertions in the genome per cell (Baillie et al., 2011; Beck et al., 2011; E. Lee et al., 2012; Muotri et al., 2005; Muotri, Zhao, Marchetto, & Gage, 2009; Shukla et al., 2013; Solyom et al., 2012). Indeed, retrotransposons sporadically cause 65 diseases identified to date (Beck et al., 2011; Hancks & Kazazian, 2012), including many cancers (Hancks & Kazazian, 2012). Retrotransposon RNA accumulates in various types of cancer (L. Chen, Dahlstrom, Chandra, Board, & Rangasamy, 2012; Wang-Johanning et al., 2003; Wang-Johanning et al., 2008; J. Zhao et al., 2011) and recent articles demonstrate that up to 60 new retrotransposon insertions occur in the dominant tumour clone alone (E. Lee et al., 2012; Solyom et al., 2012). Moreover, LINE-1 and *Alu* retrotransposons instigate much more genetic instability than their insertions alone: LINE-1 generates double-stranded DNA breaks in the genome in great excess of those required for LINE-1 re-insertion (Pepin, Paradis, Perez-Iratxeta, Picketts, & Vanderhyden, 2013). LINE-1 and *Alu* are also a frequent cause of interchromosomal translocations, intrachromosomal deletions, inversions, and amplifications due to their numerous copies scattered throughout the genome (Fussner et al., 2011; Guevel et al., 2011; Perez-Iratxeta, Halloy, Moran, Martiel, & Goldbeter, 1998; Pratt et al., 2009; Sandie et al., 2009; Schrider et al., 2013). Taken together, retrotransposons are a highly active source of genetic change in tumorigenesis and tumour evolution.

Both *Alu* (SINE) and LINE-1 replicate using a copy-paste mechanism requiring two proteins encoded by LINE-1: ORF1p and ORF2p. RNA is transcribed from genome-integrated copies of retrotransposons to then transit through the cytoplasm (Goodier, Mandal, Zhang, & Kazazian, 2010). ORF1p is required for retrotransposition and binds LINE-1 and *Alu* RNA (Evans, Peddigari, Chaurasiya, Williams, & Martin, 2011) in the

cytoplasm (J. Lin et al., 2012). Retrotransposon RNA traffics back into the nucleus where the reverse-transcriptase and endonuclease functions of ORF2p copy retrotransposon RNA and generate double-stranded breaks to enable re-insertion in a new genomic location (Beck et al., 2011; Pepin et al., 2013). Nearly all LINE-1 and *Alu* elements are inactive due to excessive truncation or mutation, but approximately 80-100 LINE-1 elements remain active and account for >99% of new LINE-1 insertions in humans (Brouha et al., 2003; Myers et al., 2002). Similarly, *AluY* elements account for most *Alu* activity in the genome (Bennett et al., 2008). Mechanisms quelling retrotransposons have been the focus of recent studies (Goodier, Cheung, & Kazazian, 2013; Martin S. Taylor, 2013; K. Zhao et al., 2013).

1.8.2 Autophagy genes implicated in cancer

Molecular and clinical evidence linking autophagy activation and inhibition to cancer is striking. As a substrate-specific catabolic process, autophagy exerts a protective effect by minimizing genomic damage that results in instability, mutations and cancer. In contrast, as cancer progresses, tumour cells exploit autophagy for their own survival and growth under stressed conditions (White, 2012).

As a tumour-suppressive mechanism, impaired autophagy is linked to elevated intracellular levels of ROS, over-active growth factor signalling, tumorigenesis and malignant transformation (Grunt & Mariani, 2012; Kung, Budina, Balaburski, Bergenstock, & Murphy, 2011; Poillet-Perez, Despouy, Delage-Mourroux, & Boyer-Guittaut, 2015; Vaught et al., 2012; R. C. Wang et al., 2012). For instance, over 75% of breast cancers (Choi, Jung, & Koo, 2013; S. Kim, Kim do, Jung, & Koo, 2013) and 43% of ovarian cancers (Shen et al., 2008) have low or undetectable expression of proteins critical for autophagy (Choi et al., 2013; S. Kim et al., 2013); 40-70% of breast cancers

and 50% of ovarian cancers have reduced copy number of *BECN1* (Aita et al., 1999; Gao et al., 1995; Laddha, Ganesan, Chan, & White, 2014b; Liang et al., 1999; Saito et al., 1993; Thompson et al., 2011; X. Wang et al., 2014), and 35-50% of breast cancers lack a copy of *PTEN (Cancer Genome Atlas, 2012)*, a gene that (among other functions) activates autophagy (Errafiy et al., 2013). PTEN deletion is also one of the most common deletions in ovarian cancer (Cancer Genome Atlas Research, 2011). Overall, defects in several proteins that activate or are required for autophagy, such as *Becn1*, *Atg5*, *Atg7*, *Atg4,* UVRAG, Bif-1, *Tsc,* or *Pten* lead to the development of tumours in mice (Inami et al., 2011; Kimmelman, 2011; Liang et al., 1999; X. Qu et al., 2003; Takamura et al., 2011b; Yue, Jin, Yang, Levine, & Heintz, 2003). Moreover, mTOR inhibitors that activate autophagy are effective in many types of cancer, and FDA-approved in some (Baselga et al., 2012; Rubinsztein, Codogno, & Levine, 2012; Zagouri, Sergentanis, Chrysikos, Filipits, & Bartsch, 2012). Thus, autophagy has a critical role in tumour initiation and tumorigenesis.

As a tumour-promoting mechanism, autophagy enhances stress tolerance of cancer cells and powers their massive metabolic demand under prevalent conditions such as hypoxia and nutrient deprivation. Unsurprisingly, inhibiting autophagy pharmacologically or genetically (*FIP200* deletion) results in tumour regression (J. Y. Guo, Karsli-Uzunbas, et al., 2013; M. J. Kim et al., 2011; Wei et al., 2011; S. Yang et al., 2011).

Despite the clinical importance of autophagy, many of its consequences are not understood. For example, how inhibition of autophagy elicits genetic instability is unresolved (R. Mathew et al., 2009; R. Mathew et al., 2007). While the degradation of proteins and organelles by autophagy has been extensively studied, the ability of autophagy to degrade RNA has been relatively ignored. Here, we propose to return the focus to RNA.

1.8.3 RNA granule dynamics linked to cancer

Early metabolic studies have suggested that autophagy constitutively degrades RNA. Under stress, 65% of RNA degradation is performed by autophagy, which is blocked with inhibitors of lysosomal degradation (Balavoine, Feldmann, & Lardeux, 1990, 1993; Balavoine, Rogier, Feldmann, & Lardeux, 1992; Dirks et al., 1992; Heydrick, Lardeux, & Mortimore, 1991; Hillwig et al., 2011; Kraft, Deplazes, Sohrmann, & Peter, 2008; Lardeux, Heydrick, & Mortimore, 1987, 1988; Morales & Hecht, 1994; Shukla et al., 2013; P. Yu et al., 2012). Recent reports highlight that certain types of cytoplasmic RNA granules are also degraded by autophagy (Buchan et al., 2013; S. Li et al., 2013; Y. Zhang et al., 2009).

Of the several types of RNA granules, stress granules and processing bodies are the best researched. While stress granules constitute proteins involved in mRNA translation, processing bodies constitute proteins involved in translational repression, mRNA silencing (GW182, Argonautes) or mRNA decay (DCP1, DCP2, XRN1, EDC3, Hedls/EDC4, Pat1 LSm1-7, RCK/p54/DDX6) (Decker & Parker, 2012). Despite the difference in composition, processing bodies and stress granules do share some components (eIF4E, mRNA, and selected RBPs) and properties (liquid-liquid phase transition). Given that these RNA granules sequester diverse proteins functioning in stress response programs, metabolic machinery and cellular signalling pathways, it is not surprising that they are critical to the pathogenesis of cancer (Anderson, Kedersha, & Ivanov, 2015).

The hostile tumour microenvironment (hypoxia, starvation, reactive oxygen species, hyperosmolarity) and cancer therapeutics (mTOR inhibitors, inhibitors of growth factor receptor signalling) induce the formation of RNA granules (Anderson et al., 2015).

Indeed, stress granules are found in tumours of colorectal cancer, carcinomas, and glioblastomas (Adjibade et al., 2015; El-Naggar et al., 2015; Fournier, Gareau, & Mazroui, 2010; Gareau et al., 2011; Vilas-Boas Fde et al., 2016). Granules so formed promote cancer cell survival by responding and adapting to stress. Particularly in response to radio and chemotherapies, stress granules are induced in cancer cells to compromise cancer treatment (Moeller, Cao, Li, & Dewhirst, 2004; Szaflarski et al., 2016). Furthermore, stress granules enhance metastasis. In mouse sarcoma models, stress granule nucleating protein - G3BP1 drives the formation of stress granules, which then enhance resistance to chemotherapy and lung metastasis (Somasekharan et al., 2015). Similar induction of stress granules is mediated by anti-inflammatory lipid 15-deoxy-Δ-12,14-prostaglandin J2 that is secreted by cancer cells (Grabocka & Bar-Sagi, 2016). Therefore, preventing stress granule assembly or activating stress granule disassembly by autophagy may offer a valuable strategy to promote tumour death.

Taken together, we propose that activating autophagy to target RNA substrates causing genetic instability, drug resistance and tumour survival such as retrotransposon RNA or RNA granules, may allow us to treat a broad subset of cancers. Additionally, a combination therapy with autophagy upregulators may enhance cancer treatments.

1.8.4 Exosome-mediated cancer progression and metastasis

Increased exosome production is associated with many cancers (W. Guo et al., 2017; Peinado et al., 2012). Exosomes are extracellular vesicles of 40-120 nm facilitating intracellular communication; they are released by a variety of cell types (Raposo & Stoorvogel, 2013). They are formed by budding of endosomal membranes into the lumen of the endosome (Raposo & Stoorvogel, 2013) in a process involving ceramide (Trajkovic et al., 2008) and proteins associated with the Endosomal Sorting Complex

Required for Transport (ESCRT) (Baietti et al., 2012; Colombo et al., 2013; Stuffers, Sem Wegner, Stenmark, & Brech, 2009; Tamai et al., 2010). The resulting intraluminal vesicles, contained within an endosome, also known as a multivesicular body (MVB) have two potential fates. Fusion of MVB with the plasma membrane releases the intraluminal vesicles, exosomes, to the extracellular space (Ostrowski et al., 2010; Raposo & Stoorvogel, 2013). Alternatively, fusion of MVB with lysosomes results in degradation of MVB content (Buschow et al., 2009; Raposo & Stoorvogel, 2013).

Emerging evidence demonstrates roles for exosomes in cancer progression, metastasis and drug resistance (Azmi, Bao, & Sarkar, 2013). Exosomes may promote cancer progression by acting as vehicles of communication between cancer cells in the tumour microenvironment (Tian et al., 2013). Through horizontal transfer of oncogenic proteins, mRNA and miRNAs, exosomes can reprogram recipient cells into aggressive cancer cells (Al-Nedawi et al., 2008). Some tumour-promoting proteins transferred by exosomes include KRAS, EGFR, SRC family kinases, Amphiregulin and integrins. In doing so, exosomes promote growth and invasion of tumour cells (Higginbotham et al., 2011; D. Hoshino et al., 2013; Melo et al., 2014). Interestingly, melanoma-derived exosomes promote tumorigenesis and metastasis in mice (Melo et al., 2014; Peinado et al., 2012). Moreover, exosomes may confer drug resistance by expulsing chemotherapeutics from cells (Azmi et al., 2013; Safaei et al., 2005). For instance, transfer of a drug efflux pump - P-glycoprotein via exosomes, provides resistance against docexatel in sensitive cells (Lv et al., 2014). Therefore, targeting the exosome-mediated communication that tumours rely on to survive, may serve as an effective therapeutic strategy. To this end, understanding the mechanisms regulating exosome functions holds promise.

1.8.5 Intersection of the autophagy machinery with exosome function

Like exosomes, autophagy promotes tumour cell local invasion and distant metastasis, in part by controlling secretion (Kenific & Debnath, 2015; Lock, Kenific, Leidal, Salas, & Debnath, 2014; Vader, Breakefield, & Wood, 2014; White, 2012; H. G. Zhang & Grizzle, 2014). Most stressors in the tumour microenvironment increase autophagic flux as well as exosome release (W. S. He, Dai, Jin, Liu, & Rent, 2012; King, Michael, & Gleadle, 2012). Depletion of GIPC, a regulator of vesicular trafficking, enhances autophagic flux and exosome production in pancreatic cancer cells (Bhattacharya et al., 2014). Like exosomes, autophagy also helps tumour cells tolerate cancer therapeutics through multiple pathways (Sui et al., 2013). For instance, platinum-resistant ovarian cancer cells have reported increased autophagic flux and increased exosome release (Pasto et al., 2017; Yin et al., 2012). Together, this suggests that both autophagy and exosomes may function as stress response programs in cancer cells.

As described above, autophagosomes fuse with late endosomes including MVB before their content is degraded within lysosomes (Berg, Fengsrud, Stromhaug, Berg, & Seglen, 1998; Gordon & Seglen, 1988). Recent evidence suggests that Atg proteins affect trafficking in the endolysosomal system (McKnight et al., 2014; Peng et al., 2014). Atg proteins localize to several organelles including endoplasmic reticulum and endosomes and may use these organelles as sources of membrane to elongate the rapidly growing phagophore (Puri, Renna, Bento, Moreau, & Rubinsztein, 2013). However, Atg proteins may have alternative functions at these sites as well, sometimes engaging only subsets of Atg proteins (Bestebroer, V'Kovski, Mauthe, & Reggiori, 2013; Deretic, Jiang, & Dupont, 2012). Non-degradative roles for Atg proteins in release of proteins lacking conventional signal peptides and cytokines have been described (Bruns, McCaffery, Curwin, Duran, & Malhotra, 2011; Deretic et al., 2012; Hwang et al., 2012; Sorbara et al., 2013; Z. Zhao et al., 2008). Intriguingly, in at least one case in

Dictyostelium discoideum, release of Acb1, a protein lacking a signal peptide, requires Atg proteins and components of the ESCRT complex, and is hypothesized to involve exosomes (Bruns et al., 2011; Duran, Anjard, Stefan, Loomis, & Malhotra, 2010). In mammals, autophagy is required for release of HIV-1 from macrophages (Kyei et al., 2009), a process that closely parallels the endogenous pathway for exosome biogenesis and release (Izquierdo-Useros, Puertas, Borras, Blanco, & Martinez-Picado, 2011). Similarly, knockdown of autophagy genes - BECN1 or ATG7 impairs the release of exosome-associated hepatitis C virus (Shrivastava et al., 2016). Together, this evokes the possibility that autophagy proteins may impact production of exosomes.

Indeed, autophagy machinery proteins have been found to contribute to exosome biogenesis. ATG9 depletion in *Drosophila* decreases the number of intraluminal vesicles of MVB within amphisomes and autolysosomes (Bader, Shandala, Ng, Johnson, & Brooks, 2015). Further, ATG12-ATG3 complex interacts with ALIX, an ESCRT-associated protein critical for exosome composition and/or formation (Baietti et al., 2012; Colombo et al., 2013; Murrow, Malhotra, & Debnath, 2015). Various components of the PI3K complex are shared between and required for both autophagy and endocytosis. Indeed, Beclin1 suppression impairs both autophagic flux and exosomes release in chronic myeloid leukemia cells likely by affecting Vps34 activity (J. Liu et al., 2016). Strikingly, autophagy-dependent exosome secretion through amphisomes has been recently reported (Y. D. Chen et al., 2017). ATG5 along with RAB11 and 27A facilitate the colocalization of LC3 on amphisomes and exosome release. Therefore, targeting autophagy to prevent exosomal transfer of tumour-promoting information between cells warrants further investigation.

Taken together, we propose that targeting stress response programs such as autophagy and exosome-mediated communication in cancer cells would prevent these cells from adapting to and surviving the tumour microenvironment.

1.8.6 Current therapies for cancer treatment

Existing treatment options for cancer include: surgery, immunotherapy, chemotherapy, radiation therapy, hormonal therapy, stem cell transplantation, and precision medicine wherein patient's unique cancer-driving genetic abnormalities are identified and targeted drugs or immunotherapies are employed to kill the cancer cells alone. Several drugs undergoing clinical trials act as autophagy inducers or autophagy inhibitors due to the context-dependent role of autophagy in cancer (Singh et al., 2018). While it suppresses tumour initiation at the early stages, autophagy leads to tumour survival under metabolic and therapeutic stress in the later stages of cancer.

mTOR inhibitors such as temsirolimus and everolimus have been shown to induce autophagy and prevent tumour growth in lymphoma and leukemia (Crazzolara et al., 2009; Yazbeck et al., 2008). Combination chemotherapy with temozolomide and dasatinib induces autophagy and kills glioblastoma (Milano, Piao, LaFortune, & de Groot, 2009). Similar anti-cancer effects have resulted from autophagy activation of HDAC inhibitors (Y. L. Liu et al., 2010). Everolimus (rapamycin analog) has been FDA-approved for its anti-angiogenesis effects in advanced breast cancer, renal carcinoma and pancreatic neuroendocrine tumours (Motzer et al., 2008). Together, this indicates that excessive induction of autophagy could lead to autophagic cell death.

Genetic or pharmacological inhibition of autophagy sensitizes cancer cells to therapy. Genetic deletion of *Atg5*, *Atg7* or *beclin1* has been shown to sensitize ER-positive breast cancer cells to tamoxifen (Cook, Shajahan, & Clarke, 2011). Atg5 depletion in cisplatin-

resistant ovarian cancer cells induces cell death (J. Wang & Wu, 2014). Combination of autophagy inhibitor 3-MA and trastuzumab increases the response to chemotherapy in HER2-positive breast cancer cells (K. Jain, Paranandi, Sridharan, & Basu, 2013). Currently, CQ/HCQ is the only autophagy inhibitor to be FDA-approved for clinical trials. CQ blocks lysosomal acidification thereby preventing the digestion of engulfed cargo. It has been shown to sensitize glioblastoma and colorectal cancer cells to anti-angiogenesis and chemotherapy drugs (Hu et al., 2012; Selvakumaran, Amaravadi, Vasilevskaya, & O'Dwyer, 2013). These findings are clinically the most relevant as tumours acquiring resistance is the toughest obstacle in chemotherapy.

Taken together, both autophagy inducers as well as inhibitors hold promise as cancer therapeutics depending on the stage, type and genetic context of cancer. Several off-target effects of CQ demand the development of more potent and specific autophagy modulators to treat cancer. Therefore, dissecting the cellular and functional mechanisms of autophagy in the context of tumours would facilitate identification of viable targets and biomarkers specific to each stage of cancer progression and thereby aid better translation of research from the bench-to-bedside.

1.9 Description of rationales and hypotheses

The complex cellular and molecular aspects of autophagy need to be better understood prior to developing autophagy modulators as interventions to treat multiple human diseases. To this end, **my overarching hypothesis is that defects in autophagy pathways contribute to human disease**. Therefore, the thesis presents both critical and novel mechanisms implicating specialized autophagy pathways in diseases such as ALS and cancer.

1.9.1 Selective autophagy clears RNA/protein granules linked to ALS

1.9.1.1 Rationale

ALS is pathologically associated with the accumulation of cytoplasmic aggregates that are positive for various stress granule proteins. A striking majority of ALS-linked mutations either occur in cytoplasmic stress granule proteins (FUS, SMN) or cell degradative systems such as autophagy (p62, C9ORF72), suggesting that defects in the clearance of cytoplasmic substrates by autophagy can cause ALS.

1.9.1.2 Hypothesis

We hypothesized that *C9ORF72*, *p62*, *FUS* and *SMN*, all genes linked to ALS, operate in a pathway critical for autophagic degradation of stress granules.

1.9.2 Selective autophagy quells genomic instability

1.9.2.1 Rationale

Tumour suppressive roles have been attributed to autophagy. While inhibition of autophagy results in genetic instability, the mechanism whereby autophagy elicits genetic instability is unresolved. Interestingly, random genomic insertions leading to

genetic instability can be driven by retrotransposons or jumping genes. They are a highly active source of genetic change in tumorigenesis and tumour evolution. Together with the ability of autophagy to degrade RNA constitutively and under stress, this suggests that autophagy may buffer evolutionary change by targeting retrotransposons.

1.9.2.2 Hypothesis

We hypothesized that autophagy degrades retrotransposon RNA to restrict their genomic insertion and thereby quell genomic instability.

1.9.3 Autophagy machinery promotes exosome release and tumour metastasis

1.9.3.1 Rationale

In cancer, autophagy has been attributed roles in tumour growth and metastasis. While autophagy activators (mTOR inhibitors) are approved to treat cancer, the mechanism whereby autophagy genes or these drugs affect tumour growth and metastasis is unclear. Interestingly, exosomes released by tumour cells establish niches in distant sites for metastasis. Cross-talk between the pathways of autophagy and exosome biogenesis is prevalent at the amphisome, suggesting that the tumour-promoting role of autophagy may be mediated by exosomes.

1.9.3.2 Hypothesis

We hypothesized that the core autophagy machinery proteins impact exosome production and thereby promote metastasis.

Chapter 2 - Manuscript #1

A complex of C9ORF72 and p62 uses arginine methylation to eliminate stress granules by autophagy

Publication information:

Maneka Chitiprolu, Chantal Jagow, Veronique Tremblay, Emma Bondy-Chorney, Geneviève Paris, Alexandre Savard, Gareth Palidwor, Francesca A. Barry, Lorne Zinman, Julia Keith, Ekaterina Rogaeva, Janice Robertson, Mathieu Lavallée-Adam, John Woulfe, Jean-François Couture, Jocelyn Côté & Derrick Gibbings. “A complex of C9ORF72 and p62 uses arginine methylation to eliminate stress granules by autophagy”. Nature Communications 2018 Jul 18;9:2794.

Author’s contribution:

Designed the experiments: MC, CJ, VT, GPalidwor, JFC, JC, DG. Performed the experiments: MC, CJ, VT, EBC, GP, AS. Analyzed the data: MC, EBC, GPalidwor, FAB, MLA, JW, JFC, JC, DG. Contributed ALS tissues: LZ, JK, ER, JR. Conceived the study and wrote the paper: MC, DG.

MC contributions by figure: Figure 1, Figure 2, Figure 3a-g,l-o, Figure 4a-d,f-i, Figure 5, Figure 6a-f,h-n, Figure 7a-i,m, Figure 8, Figure 9a-i, Western blots: j-n, Figure 10a-g, Figure 11, Figure 12, Figure 13, Figure 14

A complex of C9ORF72 and p62 uses arginine methylation to eliminate stress granules by autophagy

Maneka Chitiprolu[1,2], Chantal Jagow[1,2], Veronique Tremblay[2,3], Emma Bondy-Chorney[1], Geneviève Paris[1], Alexandre Savard[1,2], Gareth Palidwor[4], Francesca A. Barry[2,3], Lorne Zinman[5], Julia Keith[5], Ekaterina Rogaeva[6], Janice Robertson[6], Mathieu Lavallée-Adam[2,3], John Woulfe[7], Jean-François Couture[2,3], Jocelyn Côté[1], Derrick Gibbings[1,2]

1. Department of Cellular and Molecular Medicine, University of Ottawa, 451 Smyth Road, Ottawa, Ontario, Canada K1H 8M5

2. Ottawa Institute of Systems Biology, Department of Biochemistry, Microbiology and Immunology, University of Ottawa, 451 Smyth Road, Ottawa, Ontario, Canada K1H 8M5

3. Department of Biochemistry, Microbiology and Immunology, University of Ottawa, 451 Smyth Road, Ottawa, Ontario, Canada K1H 8M5

4. Ottawa Bioinformatics Core Facility, Ottawa Hospital Research Institute, 501 Smyth Road, Ottawa, Ontario, Canada K1H 8L6

5. Sunnybrook Health Sciences Centre, 2075 Bayview Avenue, Toronto, Ontario, Canada M4N 3M5

6. Tanz Centre for Research in Neurodegenerative Disease, University of Toronto, Krembil Discovery Tower, 60 Leonard Avenue, Toronto, Ontario, Canada M5T 2S8

7. Department of Pathology and Laboratory Medicine, University of Ottawa, 501 Smyth Road, Ottawa, Ontario, Canada K1H 8L6

2.1 Abstract

Mutations in proteins like FUS which cause Amyotrophic Lateral Sclerosis (ALS) result in the aberrant formation of stress granules while ALS-linked mutations in other proteins impede elimination of stress granules. Repeat expansions in *C9ORF72*, the major cause of ALS, reduce C9ORF72 levels but how this impacts stress granules is uncertain. Here, we demonstrate that C9ORF72 associates with the autophagy receptor p62 and controls elimination of stress granules by autophagy. This requires p62 to associate via the Tudor protein SMN with proteins, including FUS, that are symmetrically methylated on arginines. Mice lacking p62 accumulate arginine-methylated proteins and alterations in FUS-dependent splicing. Patients with C9ORF72 repeat expansions accumulate symmetric arginine dimethylated proteins which co-localize with p62. This suggests that C9ORF72 initiates a cascade of ALS-linked proteins (C9ORF72, p62, SMN, FUS) to recognize stress granules for degradation by autophagy and hallmarks of a defect in this process are observable in ALS patients.

2.2 Introduction

In autophagy, a phagophore elongates to engulf and then enclose cytoplasmic contents in an autophagosome. Fusion of the autophagosome with lysosomes generates an autophagolysosome and results in cargo degradation (Mizushima & Komatsu, 2011). Cargoes are frequently recruited for degradation by autophagy in a selective manner. Autophagy receptors such as p62 (Sequestosome-1 [SQSTM1]) bind both specific cargoes and LC3, an integral part of the elongating phagophore, thereby directing the selective recruitment of cytoplasmic cargoes into autophagosomes (Johansen & Lamark, 2011; Pankiv et al., 2007). In most published cases ubiquitination of substrates is required for their recognition by selective autophagy receptors, but in some cases degradation appears to be independent of ubiquitination (Khaminets et al., 2016).

Early studies demonstrated that a large proportion of RNA degradation in stress is performed by autophagy (Heydrick et al., 1991). It is now increasingly clear that cytoplasmic RNA granules, including stress granules, are degraded by autophagy (Buchan et al., 2013; H. Guo et al., 2014; S. Li et al., 2013). Stress granules coalesce RNA and RNA-binding proteins in large cytoplasmic clusters within minutes of stresses such as oxidative stress (Panas et al., 2016; Protter & Parker, 2016). When stressors are removed, many stress granules disassemble, but a significant proportion relies on autophagy for their elimination (Buchan et al., 2013).

The rapid concentration of select RNA-binding proteins controlling splicing and translation in stress granules is postulated to re-shape the post-transcriptional landscape to rapidly tailor cellular responses to stress (Panas et al., 2016; Protter & Parker, 2016). Interestingly, several mutations genetically-linked to ALS impair nuclear localization of RNA-binding proteins like FUS and TDP-43 causing them to accumulate in cytoplasmic

stress granules and insoluble inclusions in patient neurons (Lagier-Tourenne & Cleveland, 2009). Importantly, evidence suggests that pathology in ALS is caused not only by loss of the splicing capacity in the nucleus of proteins like FUS, but also by a toxic gain of function in the cytoplasm (Scekic-Zahirovic et al., 2016). This has led to a model in which inappropriate induction of stress granules or their derivatives may play a role in ALS pathology (Y. R. Li, King, Shorter, & Gitler, 2013).

Intriguingly, mutations in Valosin-Containing Protein (VCP), which are an inherited cause of ALS, control elimination of stress granules by autophagy (Buchan et al., 2013). P62 localizes to many types of inclusions in ALS patients. We previously demonstrated that p62, which is genetically linked to ALS (Teyssou et al., 2013), degrades stress granule-like cytoplasmic aggregates by selective autophagy (H. Guo et al., 2014). This suggests that either instigating formation of inclusions related to stress granules or impeding their clearance by selective autophagy may have a role in ALS.

Repeat expansions in an intron of C9ORF72 are the most common genetic cause of ALS (DeJesus-Hernandez et al., 2011; Renton et al., 2011). Repetitive RNAs and dipeptide repeat proteins are produced by transcription and translation of these repeat expansions and over-expression of these can induce ALS-like pathology (Haeusler et al., 2016). C9ORF72 repeat expansions also cause decreased levels of C9ORF72 mRNA and protein, suggesting that alongside repeat-induced pathology certain aspects of ALS pathology could be caused by loss of C9ORF72 function (Waite et al., 2014; Xiao et al., 2015).

Here, we show that symmetric arginine-methylation of stress granules by Protein Arginine Methyltransferase 5 (PRMT5) is required for a complex of C9ORF72 and p62 to

associate with stress granules and eliminate them by autophagy. Additionally, *p62*$^{-/-}$ mice and patients with C9ORF72 repeat expansions show signs of defects in this process.

2.3 Results

C9ORF72 associates with stress granule proteins and p62

To identify new functions of C9ORF72 during oxidative stress we immunoprecipitated endogenous C9ORF72 from cells exposed to arsenite-induced oxidative stress (+As) and untreated counterparts (-As, Figure 1a). C9ORF72 was detected as expected at 50 kDa with a secondary antibody specific for IgG light chain (Figure 1a). This band was diminished in cells treated with a C9ORF72 siRNA (Figure 1a, Figure 2a-b) confirming the specificity of the immuno-enrichment. C9ORF72 immunoprecipitated a known C9ORF72 interactor (hnRNPA2B1) (Figure 1b). Mass spectrometry of three biological replicates of C9ORF72 immunoprecipitates compared to IgG controls identified 309 proteins putatively interacting with C9ORF72 (Bayesian False Discovery Rate < 0.05) as assessed by the Significance Analysis of INTeractome (SAINT) algorithm (Figure 2c, Table 1). Stringently limiting candidates to those enriched in C9ORF72 immunoprecipitation vs. IgG control in each of the three biological replicates yielded 36 high-confidence interactors including multiple previously identified C9ORF72 interactors (Figure 1c, Table 1). Strikingly, 8 (22%) of the C9ORF72 interactors during oxidative stress were known stress granule components (Cooper-Knock et al., 2014; Farg et al., 2014; S. Jain et al., 2016) including two ALS-linked proteins (hnRNPA2B1 and hnRNPA1, Figure 1c, Table 1). FUS and SMN, two other ALS-linked proteins that localize to stress granules, also immunoprecipitated with C9ORF72-myc (Figure 1c, Figure 2d-e). Putative C9ORF72 interactors were enriched in RNA binding and RNA splicing GO terms (Table 2). Upon exposure to oxidative stress induced by arsenite multiple RNA binding proteins including PABP, TIAR, FMRP, FUS, SMN and DDX3 were

recruited into stress granules (Figure 2d-e). Consistent with putative interactions of C9ORF72 with stress granules, C9ORF72 was recruited into 93% of FMRP+ stress granules (Figure 1d, Figure 2f-g). This suggests that C9ORF72 has a role in stress granule biology.

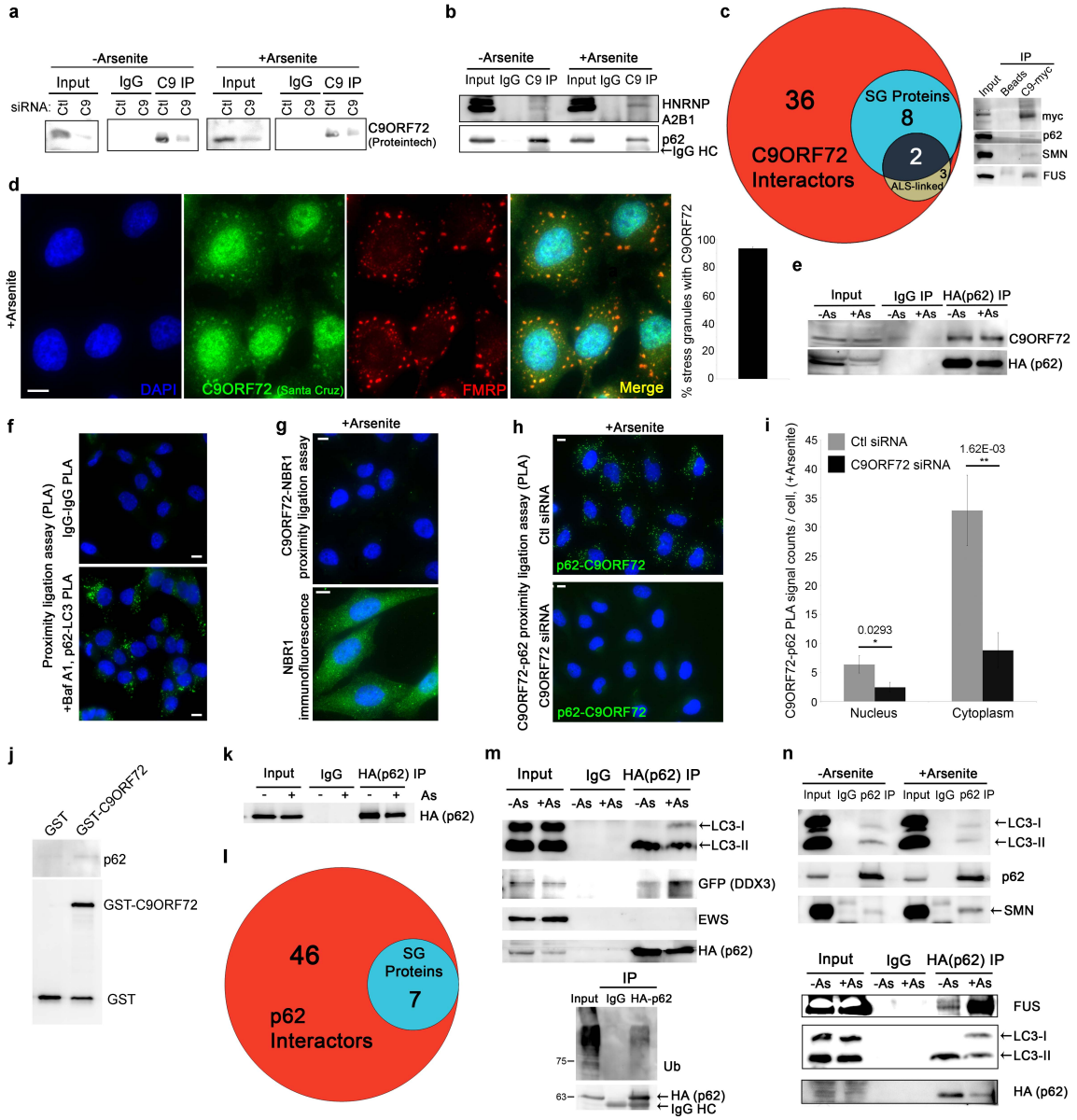

Figure 1: C9ORF72 associates with ALS-linked stress granule proteins including p62

(**a**) Western blot of endogenous C9ORF72 immunoprecipitates compared to immunoprecipitation with non-specific IgG from cell lysates (input) transfected with control or C9ORF72 siRNA. Secondary antibody specific for IgG light chain was used. (**b**) Western blot of endogenous C9ORF72 immunoprecipitates with and without arsenite treatment. (**c**) Left, venn-diagram depicting the number of proteins in the putative C9ORF72 interactome that localize to stress granules (SGs, blue) or contain mutations linked to ALS (olive); Right, Western blot of immunoprecipitation of C9ORF72-myc for p62 and SG proteins (FUS, SMN). (**d**) Immunofluorescence of endogenous C9ORF72 and SGs (FMRP) after 30 min incubation with Sodium Arsenite, (0.5 mM); Right, quantification of the percentage of SGs (FMRP+) co-localizing with foci of C9ORF72 (quantified 3916 C9ORF72 punctae and 3331 SGs). (**e**) Western blot of HA-p62 immunoprecipitates with and without arsenite treatment. (**f**) PLA co-labeling with species controlled IgG (top, negative control) and known interactors p62 and LC3 (bottom, positive control); p62-LC3 association was tested in cells treated with Bafilomycin A1 (Baf A1). (**g**) Top, proximity ligation assay (PLA) for C9ORF72 and NBR1 in arsenite treated cells; Bottom, immunofluorescence for NBR1 showing antibody does label cells. (**h**) PLA for endogenous p62 and C9ORF72 in cells treated with arsenite and transfected with control (Ctl) or C9ORF72 (C9) siRNA. (**i**) Quantification of PLA signals for C9ORF72 and p62 in the cytoplasm and nucleus in identical conditions to (h) (n=3, mean ± SD, Student's *t*-test). (**j**) Western blot of recombinant p62 and GST-C9ORF72 from *in vitro* pulldown assay. (**k**) Representative immunoprecipitation of HA-p62 used for identification of putative p62 interacting proteins using LC-MS/MS. (**l**) Venn-diagram depicting number of proteins in predicted p62 interactome that localize to SGs (blue). (**m**) Western blot of immunoprecipitates of HA-p62 detecting known interactors (LC3, ubiquitinated proteins), candidate interactors identified by LC-MS/MS (GFP-DDX3) and control RNA binding proteins that don't associate with p62 (EWS) in cells treated or not

with arsenite. (**n**) Western blot of immunoprecipitations of endogenous p62 (top) and HA-p62 (bottom) for other SG proteins (FUS, SMN). HeLa cells were used in all experiments. Scale bar = 10 µm. Molecular weight markers for blots, where not shown, are included in the uncropped versions.

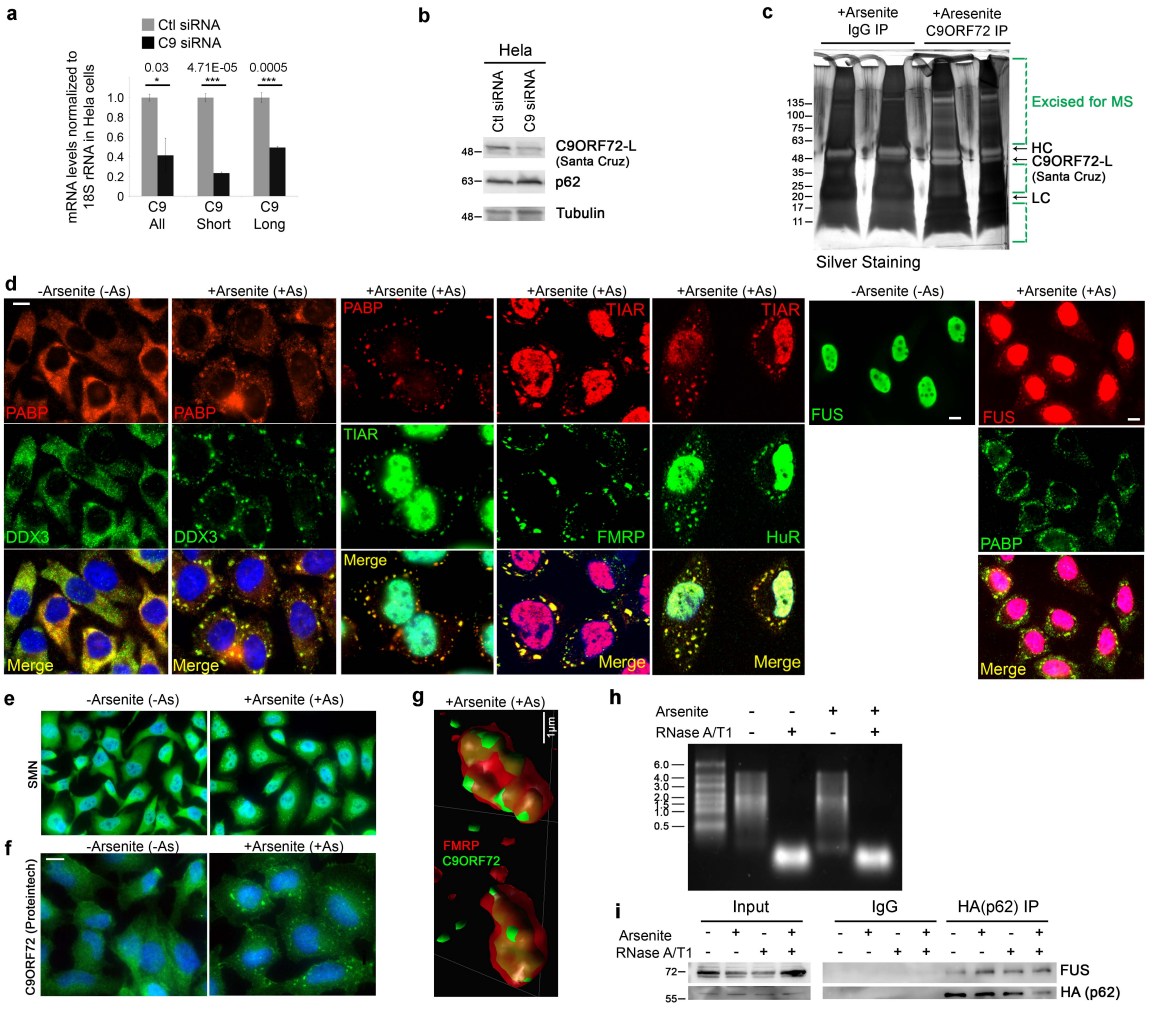

Figure 2: C9ORF72 localizes to stress granules

(**a**) RT-qPCR of C9ORF72 in cells treated with siRNA targeting control (Ctl) or *C9ORF72* (C9); RT-qPCR primers were designed to detect all *C9ORF72* mRNA, or only the long (C9 long) or short isoforms (C9 short) of *C9ORF72* mRNA. (**b**) Western blot of C9ORF72 in cells treated with control or C9ORF72 targeting siRNA; C9ORF72-L indicates C9ORF72 long isoform. (**c**) Silver stained gel of C9ORF72 immunoprecipitates

from lysates treated with arsenite (As) prior to mass spectrometry; two samples of IgG control immunoprecipitations and C9ORF72 immunoprecipitations are included on the representative gel; regions of gel excised for mass spectrometric analyses are highlighted with green dashed lines. (**d**) Immunofluorescence of stress granules upon oxidative stress using various markers (PABP, TIAR, FMRP, DDX3, HuR, FUS) to demonstrate the specificity of labeling with the antibodies and the ability to use alternate stress granule markers. (**e**) Immunofluorescence of SMN in cells untreated or treated with arsenite. (**f**) Immunofluorescence of C9ORF72 in cells untreated or treated with arsenite. (**g**) 3-D reconstruction of Z-stacks acquired by confocal microscopy of cells treated with arsenite and labeled with C9ORF72 and FMRP. (**h**) Ethidium bromide stained agarose gel showing total cellular RNA subjected to identical RNAse treatment as used to treat immunoprecipitates in (i). (**i**) Western blot of HA-p62 immunoprecipitates from lysates with and without arsenite treatment as indicated (+, -); immunoprecipitates were treated with a combination of RNAse A and T1 or treated with vehicle control as indicated. HeLa cells were used in all experiments. Scale bar = 10 μm.

Table 1: C9ORF72 mass spectrometric analyses in arsenite-treated HeLa cells

Putative C9ORF72-associated proteins identified by LC-MS/MS in arsenite-treated HeLa cells. See also Supplementary Data 1.

Throughout Tables 1 to 6, putative C9ORF72 and p62 interacting proteins were intersected with known stress granule proteins (S. Jain et al., 2016) and ALS-linked genes (Abel, Powell, Andersen, & Al-Chalabi, 2012). Interactomes were also overlapped with consolidated published datasets of arginine dimethylated proteins or potential PRMT5 substrates (Bremang et al., 2013; A. Guo et al., 2014; Larsen et al., 2016; Sylvestersen, Horn, Jungmichel, Jensen, & Nielsen, 2014; Uhlmann et al., 2012). Potential PRMT5 substrates were derived from Supplementary Table 1 of (Larsen et al.,

2016) with SILAC H/L ratio > 1.02 for at least two out of the 3 following treatment conditions: (i) EPZ015666 – selective PRMT5 inhibitor, (ii) siPRMT5_Exp1 and (iii) siPRMT5_Exp2.

*Due to the size of this table please refer to Appendix A

Supplementary Data 1: Unprocessed output files generated by MaxQuant and SAINT analysis of LCMS/MS results, related to Table 1-2. C9ORF72 LC-MS/MS. File contains 3 Excel sheets: (i) protein groups interacting with C9ORF72 after arsenite treatment, (ii) dimethyl (KR) sites interacting with C9ORF72 after arsenite treatment and (iii) SAINT analysis of C9ORF72 interactors after arsenite treatment. Project accession: PXD009759

*Due to the size of this table please refer to Appendix B

Table 2: Gene ontology terms based on analysis of C9ORF72 proteome upon oxidative stress

Gene ontology terms based on analysis of C9ORF72 interactome upon oxidative stress.

GO Category	GO Term	Corrected *p*-Value	Cluster Frequency
Molecular function	RNA binding	4.7131E-9	36.3%
	Nucleic acid binding	8.0499E-6	56.8%
	Nucleotide binding	2.5634E-5	45.4%
	rRNA binding	6.5744E-4	6.8%
	Single-stranded RNA binding	1.7181E-2	4.5%
	Ribonucleotide binding	2.4969E-2	27.2%
Cellular Component	Cytosolic ribosome	4.2193E-11	20.9%
	Non-membrane bound organelle	4.3547E-11	62.7%
	Ribonucleoprotein complex	4.3547E-11	34.8%
	Macromolecular complex	2.3891E-10	67.4%
	Cytosolic small ribosomal subunit	4.9731E-7	11.6%
	Spliceosomal complex	1.8059E-4	11.6%

Biological process	Translation elongation	6.8141E-11	23.8%
	Cellular macromolecular complex assembly	2.7869E-7	26.1%
	Protein polymerization	4.6117E-7	14.2%
	Cellular macromolecular complex organization	4.8840E-7	26.1%
	Translation	8.0371E-7	23.8%
	Cellular protein complex assembly	2.1154E-4	14.2%
	RNA splicing	3.3182E-3	14.2%
	mRNA processing	4.5402E-3	14.2%
	Protein complex assembly	9.5164E-3	16.6%
	Nuclear mRNA splicing via spliceosome	3.1006E-2	7.1%

Intriguingly, a third ALS-linked protein that is a high-confidence candidate interactor with C9ORF72 is p62 (Table 1). C9ORF72 immunoprecipitated p62, and HA-p62 reciprocally immunoprecipitated C9ORF72 both in the absence and presence of oxidative stress (Figure 1a-b,e). Proximity ligation assays (PLA) confirmed that in intact cells p62 and C9ORF72 closely associate. While no PLA signal was detected with control non-specific antibodies (Figure 1f), or between C9ORF72 and another autophagy receptor NBR1 (Figure 1g), prominent PLA signals were obtained between p62 and a known interactor (LC3) as well as between C9ORF72 and p62 (Figure 1f,h). PLA signal between C9ORF72 and p62 was lost upon knockdown of C9ORF72 (Figure 1h-i). Finally, more recombinant p62 was pulled down with recombinant purified GST-C9ORF72 than with beads containing GST alone (Figure1j). Together, this suggests that C9ORF72 and p62 are part of a physically-associated complex.

We investigated whether C9ORF72 and p62 have a shared role in stress granule biology. We immunoprecipitated HA-p62 (Figure 1k). p62 interactors (vs. IgG control immunoprecipitates) with and without oxidative stress were identified by mass spectrometry analysis using SAINT (Table 3, Figure 1l). In addition to immunoprecipitating LC3 and ubiquitinated proteins as anticipated, p62 immunoprecipitated candidate interactor DDX3, but not EWS another RNA-binding protein (Figure 1m). Candidate p62 interactors overlapped with putative p62 interactors

from other studies curated in iRefWeb (Turinsky, Razick, Turner, Donaldson, & Wodak, 2014) by 26.3% (20/76 proteins) in untreated cells and 26.1% (12/46 proteins) in arsenite-treated cells compared to random overlap of 2.9% (431 putative interactors/15,000 proteins in the proteome). Like C9ORF72, candidate p62 interactors were strongly enriched in RNA splicing functions and 29% of p62 interacting proteins were RNA-binding proteins (Table 4). Seven (15%) of the candidate p62 interactors were known stress granule components (Figure 1l, Table 5). p62 also interacted with SMN and other RNA binding proteins including FUS (Figure 1n), which localize to stress granules (Figure 2d-e). p62 interaction with FUS was independent of RNA (Figure 2h-i). Strikingly, p62 and C9ORF72 interactomes upon oxidative stress significantly overlapped ($p < 0.0001$, Chi-test) including RNA binding proteins known to localize to stress granules (Table 6). This strongly suggests that a complex of C9ORF72 and the autophagy receptor p62 (Figure 1b,e-j, Table 1) associates with stress granule proteins in cells exposed to oxidative stress (Figure 1b-d,k-n).

Table 3: Comparison of p62/SQSTM1 interactome with and without arsenite treatment

Comparison of p62/SQSTM1 interactome with and without arsenite treatment. See also Supplementary Data 2.

*Due to the size of this table please refer to Appendix C

Supplementary Data 2: Unprocessed output files generated by MaxQuant and SAINT analysis of LCMS/MS results, related to Table 3-5. p62 LC-MS/MS. File contains 4 Excel sheets: (i) protein groups interacting with HA-p62/SQSTM1 from cells with and without arsenite treatment, (ii) dimethyl (KR) sites interacting HA-p62/SQSTM1 from cells with

and without arsenite treatment, (iii-iv) SAINT analysis of HA-p62/SQSTM1 interactors (iii) without and (iv) with arsenite treatment. Project accession: PXD009741

*Due to the size of this table please refer to Appendix D

Table 4: Gene ontology terms based on analysis of putative p62/SQSTM1 interactors in arsenite-treated HeLa cells

Gene ontology terms significantly enriched in the putative p62/SQSTM1 interactome in cells treated with arsenite. Putative p62 interactors with SAINT FDR < 0.01 and enriched in all three immunoprecipitations were used.

GO Category	GO Term	Corrected *p*-Value	Cluster Frequency
Molecular function	RNA binding	1.5706E-6	29.4%
	Nucleic acid binding	5.2963E-5	52.9%
	Nucleotide binding	7.3112E-4	39.2%
	Unfolded protein binding	1.1727E-3	9.8%
	rRNA binding	2.7362E-3	5.8%
	Protein binding	3.0936E-3	78.4%
Cellular Component	Macromolecular complex	1.6345E-11	68.0%
	Ribonucleoprotein complex	4.5913E-11	32.0%
	Non-membrane bound organelle	5.8026E-7	48.0%
	Cytosolic ribosome	3.5825E-5	10.0%
	Spliceosomal complex	4.0265E-2	6.0%
Biological process	Cellular macromolecular complex assembly	5.6645E-9	26.0%
	Cellular macromolecular complex subunit organization	2.0836E-8	26.0%
	mRNA metabolic process	2.3421E-6	22.0%
	RNA splicing	2.3421E-6	20.0%
	mRNA processing	4.3838E-6	20.0%
	Translation elongation	4.0521E-5	12.0%
	Nuclear mRNA splicing via spliceosome	4.3680E-4	10.0%
	Macromolecule metabolic process	2.4346E-3	54.0%
	Spliceosome assembly	4.7159E-3	6.0%
	Translation	1.0676E-2	12.0%
	Response to unfolded protein	2.9928E-2	6.0%
	Ribonucleoprotein complex assembly	4.4298E-2	6.0%

Table 5: Putative p62/SQSTM1 interactors in arsenite-treated HeLa cells

p62/SQSTM1-associated proteins identified by LC-MS/MS in arsenite-treated HeLa cells. Putative p62 interactors with SAINT FDR < 0.01 and enriched in all three immunoprecipitations were used.

P62/SQSTM1 Putative Interactors upon Oxidative Stress			
Stress Granule Components (S. Jain et al., 2016)	Di-methylated Arginine Proteins	Potential PRMT5 Substrates (Larsen et al., 2016)	Di-methylated R sites interacting with p62
CASC3 DDX1 HSPA9 LMNA NUFIP2 PABPC1 PRDX1	BCLAF1 HIST3H3 HSPA1A HSPA8 ILF2 PABPC1;PABPC3 RBMX;RBMXL1 THRAP3 TRA2B	ALYREF_R45 FUS_R218, R259, R394 HNRNPA0_R139, R291 HNRNPA1_R206, R218, R232, R225, R194, R213, R196, R215, R265 HNRNPA1L2_R194, R196 HNRNPU_R715, R720, R709, R755, R572 HNRNPUL1_R181, R620 KHDRBS1_R304, R320 NDUFV1_R88 RBMX;RBMXL1_R144 SFPQ_R25 TAF15_R373, R293, R206, R286, R185, R338, R308, R315, R331, R195, R301, R124, R348, R137, R234 THRAP3_R101, R825 TRA2B_R224, R238, R251	ALYREF_R45, R70, R204 FUS_R216, R218 HIST2H3A;HIST3H3;H3F3B;H3F3A;HIST2H3PS2;H3F3C_R37 HNRNPA0_R291 HNRNPA1;HNRNPA1L2_R206; R194, R196 HNRNPU_R733, R739 HNRNPUL1_R529, R531 KHDRBS1_R325 MYH9_R1145 NDUFV1_R28, R36 PABPC1;PABPC3_R493 PABPC4_R489 SFPQ_R19, R25 TAF15_R525, R532 TRA2B_R241

Table 6: Common components of the putative C9ORF72 and p62/SQSTM1 interactomes in arsenite-treated HeLa cells and gene ontology analyses of these common components

Gene ontology analyses of shared components of the putative C9ORF72 and p62/SQSTM1 interactomes in arsenite-treated HeLa cells. Putative interactors with SAINT FDR < 0.01 and enriched in all three immunoprecipitations were used.

Putative interactors of both C9ORF72 and p62/SQSTM1 in arsenite-treated HeLa cells					
Putative Interactors of Both C9ORF72 and p62	Stress Granule Components (S. Jain et al., 2016)	Di-methylated Arginine Proteins	Potential PRMT5 Substrates (Larsen et al., 2016)	Di-methylated R sites	ALS-linked Proteins (Abel et al., 2012)
HIST1H2AC;HIST3H2A;HIST1H2AB HIST1H2BN;HIST1H2BL;HIST1H2BM;HIST1H2BH;HIST2H2BF;HIST1H2BC;HIST1H2BD;H2BFS;HIST1H2BK HIST1H4A HSPA8 MYH9 PABPC1 RBMX;RBMXL1 RPS11 RPS18 RPS27A;UBB;UBC;UBA52;UBBP4 SQSTM1 SRSF7	PABPC1	HSPA8 PABPC1 RBMX;RBMXL1	FUS_R218, R259, R394 HNRNPA1_R206, R218, R232, R225, R194, R213, R196, R215, R265 HNRNPU_R715, R720, R709, R755, R572 HNRNPUL1_R181, R620 RBMX;RBMXL1_R144 TAF15_R373, R293, R206, R286, R185, R338, R308, R315, R331, R195, R301, R124, R348, R137, R234 TRA2B_R224, R238, R251	FUS_R216, R218 HNRNPA1_R206 HNRNPU_R733, R739 HNRNPUL1_R529, R531 TAF15_R525, R532	SQSTM1

Gene ontology analyses of Putative interactors of both C9ORF72 and p62/SQSTM1 in arsenite-treated HeLa cells			
GO Catergory	GO Term	Corrected *p*-Value	Cluster Frequency
Molecular function	Structural constituent of ribosome Nucleic acid binding rRNA binding RNA binding	1.0638E-3 1.6349E-3 7.0741E-3 1.0151E-2	25.0% 68.7% 12.5% 31.2%

Cellular Component	Macromolecular complex Cytosolic small ribosomal subunit Ribonucleoprotein complex Cytosolic ribosome Non-membrane bound organelle Spliceosomal complex	2.1212E-7 5.6874E-7 3.0019E-6 7.1685E-6 1.1804E-5 2.0259E-2	87.5% 25.0% 43.7% 25.0% 68.7% 12.5%
Biological process	Cellular macromolecular complex subunit organization Translation elongation Translation RNA splicing mRNA processing	4.5774E-5 8.8696E-5 4.3873E-3 3.3178E-2 3.7218E-2	37.5% 25.0% 25.0% 18.7% 18.7%

C9ORF72 and p62 help eliminate stress granules by autophagy

To test if C9ORF72 and p62 control elimination of stress granules, p62 or C9ORF72 were depleted with siRNA. Depletion of C9ORF72 had minimal effect on p62 levels (Figure 2b). Cells depleted of p62 or C9ORF72 formed similar numbers of stress granules (30 min arsenite) as control cells (Figure 3a-d). In contrast, during recovery from stress (1 hour recovery after 30 min arsenite), 88% or 84% of cells respectively treated with siRNA targeting *p62* (Figure 3a-b) or *C9ORF72* (Figure 3c-d) failed to eliminate stress granules, closely mimicking the effect of inhibiting autophagy with ATG5 siRNA (Figure 4a-b). p62 knockdown had no effect on stress granule numbers in *ATG5*$^{-/-}$ cells suggesting that p62 operates in a ATG5-dependent autophagy pathway to clear stress granules (Figure 4c). In contrast, depletion of other autophagy receptors including NBR1 and OPTN did not affect clearance of stress granules (Figure 4d). Consistent with degradation of cytoplasmic stress granules by p62-dependent autophagy, cytoplasmic fractions, but not nuclear fractions, accumulated the stress granule protein FUS in cells treated with siRNA targeting p62, or genes required for autophagy (ATG5 and ATG7, Figure 3e-f, Figure 4b).

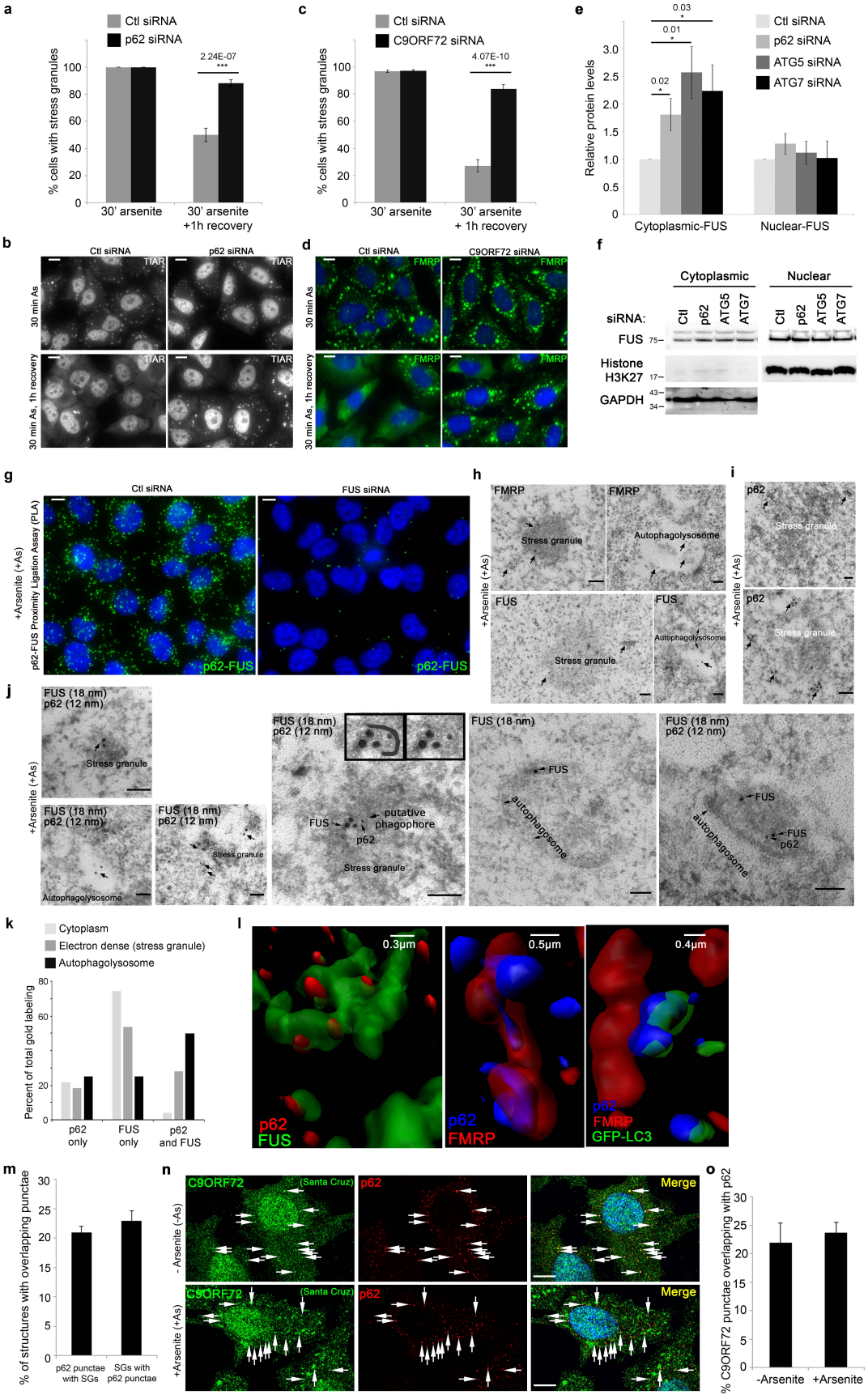
a
Ctl siRNA
p62 siRNA
% cells with stress granules
2.24E-07
***
30' arsenite
30' arsenite +1h recovery
c
Ctl siRNA
C9ORF72 siRNA
% cells with stress granules
4.07E-10
***
30' arsenite
30' arsenite + 1h recovery
e
Relative protein levels
0.03
0.01
0.02
Ctl siRNA
p62 siRNA
ATG5 siRNA
ATG7 siRNA
Cytoplasmic-FUS
Nuclear-FUS
b
Ctl siRNA
p62 siRNA
30 min As
30 min As, 1h recovery
TIAR
d
Ctl siRNA
C9ORF72 siRNA
FMRP
f
Cytoplasmic
Nuclear
siRNA:
Ctl
p62
ATG5
ATG7
FUS
Histone H3K27
GAPDH
g
Ctl siRNA
FUS siRNA
+Arsenite (+As)
p62-FUS Proximity Ligation Assay (PLA)
p62-FUS
h
FMRP
Stress granule
Autophagolysosome
FUS
i
p62
Stress granule
j
FUS (18 nm)
p62 (12 nm)
Stress granule
Autophagolysosome
putative phagophore
p62
autophagosome
k
Cytoplasm
Electron dense (stress granule)
Autophagolysosome
Percent of total gold labeling
p62 only
FUS only
p62 and FUS
l
0.3µm
0.5µm
0.4µm
p62
FUS
FMRP
GFP-LC3
m
% of structures with overlapping punctae
p62 punctae with SGs
SGs with p62 punctae
n
C9ORF72
(Santa Cruz)
p62
Merge
- Arsenite (-As)
+Arsenite (+As)
o
% C9ORF72 punctae overlapping with p62
-Arsenite
+Arsenite

Figure 3: C9ORF72 and p62 promote stress granule clearance by autophagy

(**a**) Percentage of cells containing stress granules in cells treated with control or p62 siRNA after 30 minutes arsenite, or one hour after removal of arsenite (n=3, mean ± SD, Student's *t*-test). (**b**) Representative images of stress granules used in (a). (**c**) Percentage of cells containing stress granules in cells treated with control or C9ORF72 siRNA after 30 minutes arsenite, or one hour after removal of arsenite (n=3, mean ± SD, Student's *t*-test). (**d**) Representative images of stress granules used in (c). (**e**) Quantification of FUS levels in cytoplasmic and nuclear extracts of cells treated with siRNA targeting p62, ATG5, ATG7 or control siRNA (n=5, mean ± SD, Student's *t*-test). (**f**) Representative Western blot of (e). (**g**) Proximity ligation assay for p62 and FUS in arsenite treated cells transfected with control siRNA or siRNA targeting FUS. Scale bar = 10 µm. (**h**) Immuno-electron micrographs of FUS and FMRP in cells treated with arsenite; arrows highlight antibody labeling within indicated stress-granule-like structures. (**i**) Immuno-electron micrographs of p62 in cells treated with arsenite. (**j**) Immuno-electron micrographs of p62 (12 nm gold) and FUS (18 nm gold) in cells treated with arsenite; arrows highlight co-labeled structures. Scale bar = 100 nm. (**k**) Quantification of 46 randomly selected immuno-electron micrographs co-labeled with p62 and FUS as in (j). Each electron-dense stress granule-like structure, autophagolysosome-like organelle or 50 nm radius area of cytoplasm with label was quantified as being labeled with p62 alone, FUS alone, or both p62 and FUS. (**l**) 3D reconstruction of Z-stack confocal images of cells. Images are zoomed-in on stress granules labeled with the indicated antibodies or fluorescent proteins (GFP-LC3). (**m**) Quantification of the percentage of p62 punctae co-labeled with stress granule markers and the percentage of stress granules with co-localized or docked p62 (quantified 12102 p62 punctae and 12627 stress granules, n=6, mean ± SD, Student's t-test). (**n**) Confocal image of endogenous C9ORF72 and p62 in cells treated with or without arsenite. Scale

bar = 10 µm. (**o**) Quantification of the percentage of C9ORF72 punctae overlapping with p62 in cells treated with or without arsenite (quantified C9ORF72 punctae without arsenite: 2688, with arsenite: 3778 punctae; p62 punctae without arsenite: 1805, with arsenite: 2942, n=2, mean ± SD, Student's t-test). HeLa cells were used in all experiments.

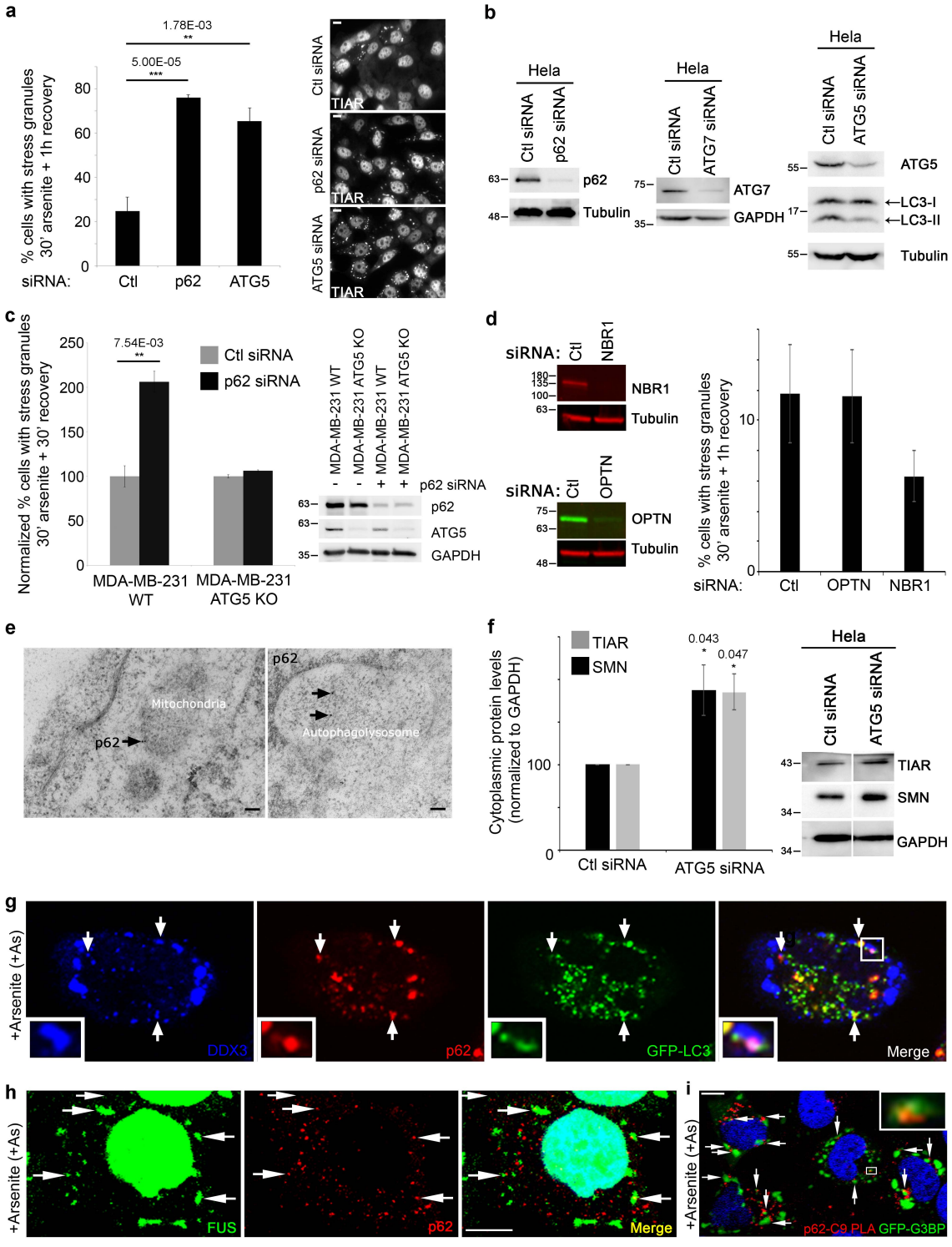

Figure 4: p62 docks on stress granules and is required for their elimination by autophagy

(**a**) Percentage of cells containing stress granules following 1 h of recovery from 30 minutes treatment with arsenite upon transfection with siRNA targeting p62, ATG5 or control siRNA (Ctl); Right, representative images. (**b**) Western blot of p62, ATG7 and ATG5 in cells treated with control siRNA (Ctl) or siRNA targeting p62, ATG7 or ATG5. (**c**) Percentage of wild-type or ATG5 knockout MDA-231 cells containing stress granules following 30 minutes of recovery from 30 minutes aresnite treatment upon transfection with siRNA targeting p62 or control siRNA (Ctl); Right, Western blot validating knockdown of p62 and knockout of ATG5 in MDA-231 cells. (**d**) Left, Western blot validating knockdown of NBR1 (top) and OPTN (bottom); Right, percentage of cells containing stress granules in cells treated with control (Ctl), OPTN or NBR1 siRNA after one hour recovery from 30 minutes arsenite (n=3, mean ± SD, Student's *t*-test). (**e**) Immuno-electron micrographs of p62; mitochondria (mito) and autophagolysosomes are indicated. Scale bar = 100 nm. (**f**) Left, quantification of TIAR and SMN cytoplasmic levels in cells treated with siRNA targeting ATG5 or control siRNA (n=5, mean ± SD, Student's *t*-test); Right, representative Western blot. (**g**) Immunofluorescent microscopy of arsenite treated cells labeled with antibodies recognizing DDX3, endogenous p62 and expressing GFP-LC3. (**h**) Immunofluorescent microscopy of arsenite treated cells labeled with antibodies recognizing endogenous FUS and p62. (**i**) Fluorescent microscopy image of proximity ligation assay for association of C9ORF72 and p62 in cells expressing the stress granule marker GFP-G3BP. HeLa cells were used in all experiments. Scale bar = 10 μm.

If p62 directly affects clearance of stress granules (Figure 3a-b, Figure 4a-c); it may localize to stress granules. P62 associated with the stress granule proteins FUS, SMN and DDX3 by immunoprecipitation (Figure 1m-n). PLA confirmed that p62 and FUS associate in intact cells (Figure 3g). To test whether p62 physically associates with

stress granules we used electron microscopy. As expected, p62 labeled mitochondria (Geisler et al., 2010; Wong & Holzbaur, 2014) as well as endolysosomal structures with heterogenous content resembling autophagolysosomes (Figure 4e). In arsenite-treated cells, stress granules were observed, as previously described (Souquere et al., 2009), as electron dense structures labeled with the stress granule markers FUS and FMRP (Figure 3h). p62 frequently clustered on the periphery of stress granules (Figure 3i). FUS and FMRP were also observed on similar electron-dense structures inside autophagolysosome-like structures (Figure 3h), suggesting their degradation by autophagy. In agreement, p62 and FUS were infrequently found in close proximity in the cytoplasm (Figure 3k) but 28% of structures co-labeled by p62 and FUS were stress granules and another 50% were inside autophagolysosomes (Figure 3j-k). In agreement with the role of autophagy in engulfment of stress granules, p62-labeled phagophore-like structures also associated with stress granules (Figure 3j), stress granules labeled with FUS and p62 were observed within double-membrane autophagosomes (Figure 3j) and stress granule proteins TIAR and SMN accumulated in cells depleted of ATG5 (Figure 4f). Together, this suggests that either entire stress granules or fragments of stress granules are degraded by p62-dependent autophagy and this is required for complete elimination of stress granules from cells (Figure 3a-f, Figure 4a-c).

Intriguingly, by electron microscopy p62 was frequently observed on the periphery of stress granules (Figure 3i-j), as required to remain accessible to LC3 and direct their degradation by autophagy. In agreement with this, 3-D reconstructions of confocal microscopy images demonstrated that p62 docked on stress granules and LC3 coated p62 on these stress granules (Figure 3l, Figure 4g-h). By immunofluorescence, p62 docked on 21% of stress granules (Figure 3m, Figure 4g-h), closely paralleling the percent of stress granules (28%) containing p62 by electron microscopy (Figure 3j-k).

Costes' test demonstrated that co-localization of p62 with TIAR in the cytoplasm is not random (in each of 88 cells, 100 iterations of randomized fluorescence found no images with greater co-localization than input images of p62 and TIAR). This closely resembles the type and amount of localization of autophagy receptors or LC3 to other autophagy substrates (Deosaran et al., 2013; Martinez-Vicente et al., 2010; Yamano, Fogel, Wang, van der Bliek, & Youle, 2014) including stress granules (Buchan et al., 2013). This amount of co-localization is also consistent with the fact that not all stress granules are degraded by autophagy (Buchan et al., 2013), p62 is involved in degradation of other substrates, and autophagic degradation is rapid (~10 min).

Since C9ORF72 and p62 form a complex (Figure 1b,e-j) and control elimination of stress granules (Figure 3a-d), they may dock on stress granules. Endogenous C9ORF72 and p62 co-localized both in untreated and arsenite treated cells (Figure 3n-o). PLA detected an association of C9ORF72 and p62 on the border of some stress granules (Figure 4i). Together, while C9ORF72 may also have effects on stress granules independent of p62, this suggests that C9ORF72 and p62 form a complex that docks on stress granules to control their elimination by autophagy either as large structures or portions of stress granules (Figure 1-4).

PRMT5 helps eliminate stress granules by autophagy

We inquired how a C9ORF72-p62 complex eliminates stress granules by autophagy. Canonically, p62 recruits ubiquitinated cargoes for degradation by autophagy (Pankiv et al., 2007). Ubiquitin was not enriched in stress granules despite forming punctae in cells treated with inhibitors of autophagic degradation and co-localizing with OPTN, a ubiquitin-binding autophagy receptor (Figure 5a, Figure 6a-b). This suggested that p62 may be recruited to stress granules by a non-canonical signal. Interestingly, arginine-

dimethylated proteins, particularly symmetrically dimethylated proteins (SYM), were strongly enriched in stress granules (Figure 5b-c). Asymmetrically dimethylated proteins (ASYM) were also found in stress granules (Figure 5b-c). Subcellular fractions were prepared according to established protocols (Sahu et al., 2011) to enrich autophagosomes and autophagolysosomes. Accordingly, these fractions were enriched in LC3-II (vs. LC3-I) compared to the LC3-II/LC3-I ratio in the corresponding total cell lysates (Figure 5d). Comparing the ratio of proteins in the autophagolysosome fractions to their level in the corresponding cell lysate indicates the propensity of proteins to be degraded by autophagy. Autophagolysosome fractions contained the canonical autophagy substrate p62, stress granule proteins degraded by autophagy such as FUS (Figure 3e-m), and symmetrically dimethylated proteins at similar autophagosome fraction/cell ratios (Figure 5d) suggesting that proteins with symmetrically dimethylated arginines are degraded at a rate comparable to p62 and stress granules. Additionally, symmetrically dimethylated proteins accumulated upon depletion of ATG7 and ATG12 (Figure 6c). p62 and LC3 also immunoprecipitated with proteins containing symmetrically dimethylated arginines (Figure 5e), alongside proteins known to contain (Sm) or bind to (SMN) this post-translational modification (Figure 5e). This suggests that proteins with symmetrically dimethylated arginines are enriched in stress granules, associate with p62 and are degraded by autophagy.

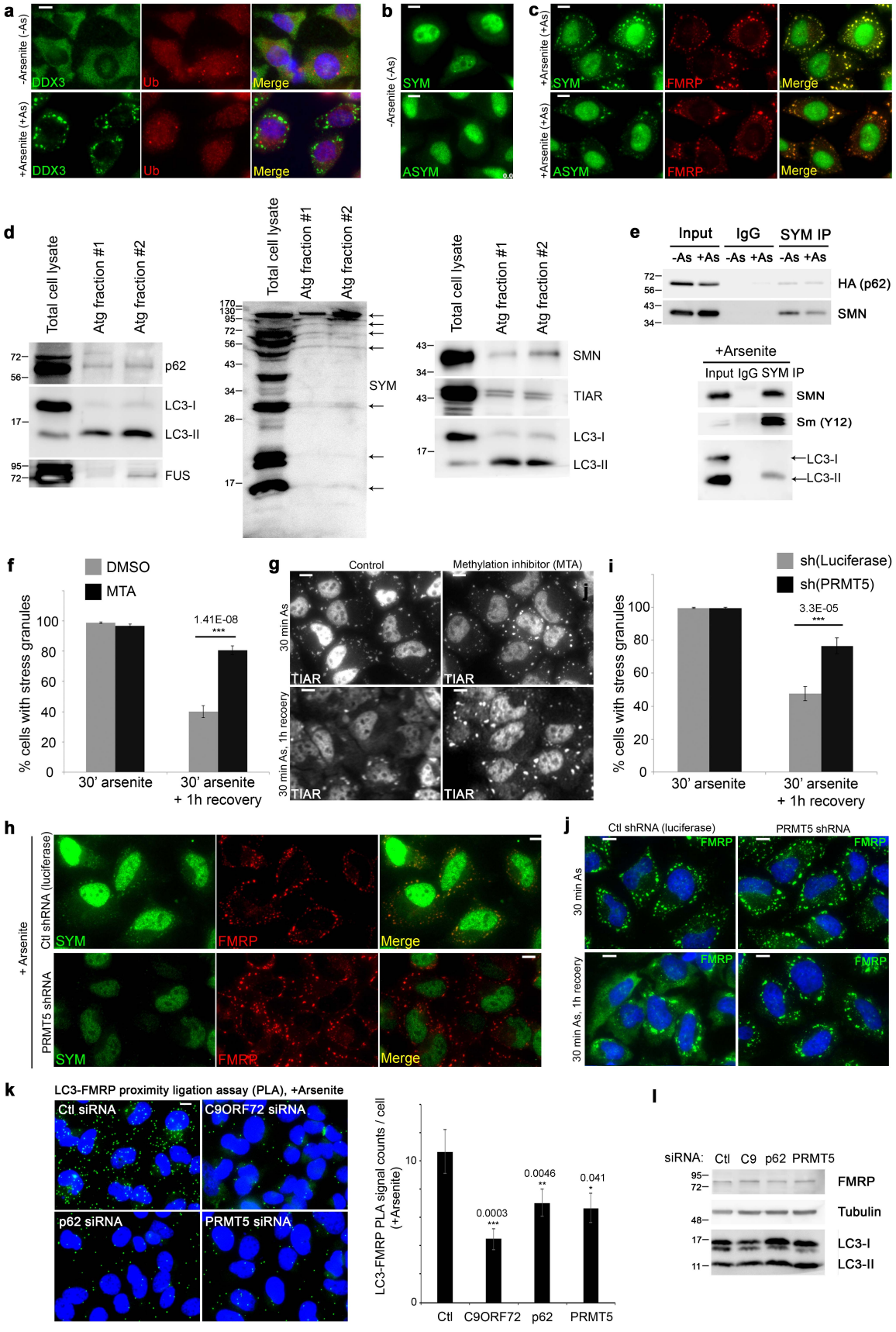
a
-Arsenite (-As)
+Arsenite (+As)
DDX3
Ub
Merge
b
SYM
ASYM
c
FMRP
d
Total cell lysate
Atg fraction #1
Atg fraction #2
p62
LC3-I
LC3-II
FUS
SYM
SMN
TIAR
e
Input
IgG
SYM IP
-As +As
HA (p62)
SMN
+Arsenite
Sm (Y12)
f
DMSO
MTA
% cells with stress granules
1.41E-08
***
30' arsenite
30' arsenite + 1h recovery
g
Control
Methylation inhibitor (MTA)
30 min As
30 min As, 1h recovery
TIAR
i
sh(Luciferase)
sh(PRMT5)
3.3E-05
h
+ Arsenite
Ctl shRNA (luciferase)
PRMT5 shRNA
j
k
LC3-FMRP proximity ligation assay (PLA), +Arsenite
Ctl siRNA
C9ORF72 siRNA
p62 siRNA
PRMT5 siRNA
LC3-FMRP PLA signal counts / cell (+Arsenite)
0.0003
0.0046
0.041
Ctl
C9ORF72
p62
PRMT5
l
siRNA: Ctl C9 p62 PRMT5
FMRP
Tubulin
LC3-I
LC3-II

Figure 5: Symmetric arginine methylation by PRMT5 is required for stress granule clearance by autophagy

(**a**) Immunofluorescent microscopy of DDX3 and ubiquitin (Ub) in cells treated with or without arsenite. (**b**) Immunofluorescent microscopy of cells labeled with antibodies for symmetric (SYM) or asymmetric (ASYM) dimethylated arginines. (**c**) Immunofluorescent microscopy of cells labeled with antibodies for FMRP and proteins containing symmetric (SYM) or asymmetric (ASYM) arginines after treatment with arsenite. (**d**) Western blot of total cell lysate and fractions enriched in autophagosomes (Atg fraction#1) and autophagolysosomes (Atg fraction#2) for known autophagy substrates (LC3-II, p62), stress granule proteins (FUS, SMN, TIAR) and symmetrically dimethylated proteins (SYM). (**e**) Western blot of immunoprecipitations of proteins containing symmetrically dimethylated arginines from cells expressing HA-p62 (top) or not (bottom); cells were treated with arsenite (+As) or not (-As). (**f**) Percentage of cells containing stress granules in cells treated with DMSO (control diluent) or MTA (methylthioadenosine 1 mM, 48 h) after 30 minutes arsenite treatment, or one hour after removal of arsenite (n=3, mean ± SD, Student's *t*-test). (**g**) Representative images of stress granules labeled with TIAR for (f). (**h**) Immunofluorescent images of cells labeled with antibodies specific for symmetrically dimethylated arginines (SYM) or FMRP (stress granule marker) in cells treated with arsenite and expressing either control shRNA or PRMT5 silencing shRNA. (**i**) Percentage of cells containing stress granules in cells treated with control shRNA or PRMT5 silencing shRNA after 30 minutes arsenite treatment, or one hour after removal of arsenite (n=5, mean ± SD, Student's *t*-test). (**j**) Representative images of stress granules labeled with FMRP for (i). (**k**) Left, PLA for endogenous LC3 and FMRP (in SGs) in cells treated with arsenite and transfected with control (Ctl), C9ORF72 (C9), p62 or PRMT5 siRNA; Right, quantification of proximity ligation assay signals (PLA) for LC3 and FMRP in cells under identical conditions to (k) (n=3, mean ± SD, Student's *t*-test).

(**l**) Western blot control for PLA in (k) in cells treated with control, C9ORF72, p62 or PRMT5 targeting siRNA. HeLa cells were used in all experiments. Scale bar = 10 μm.

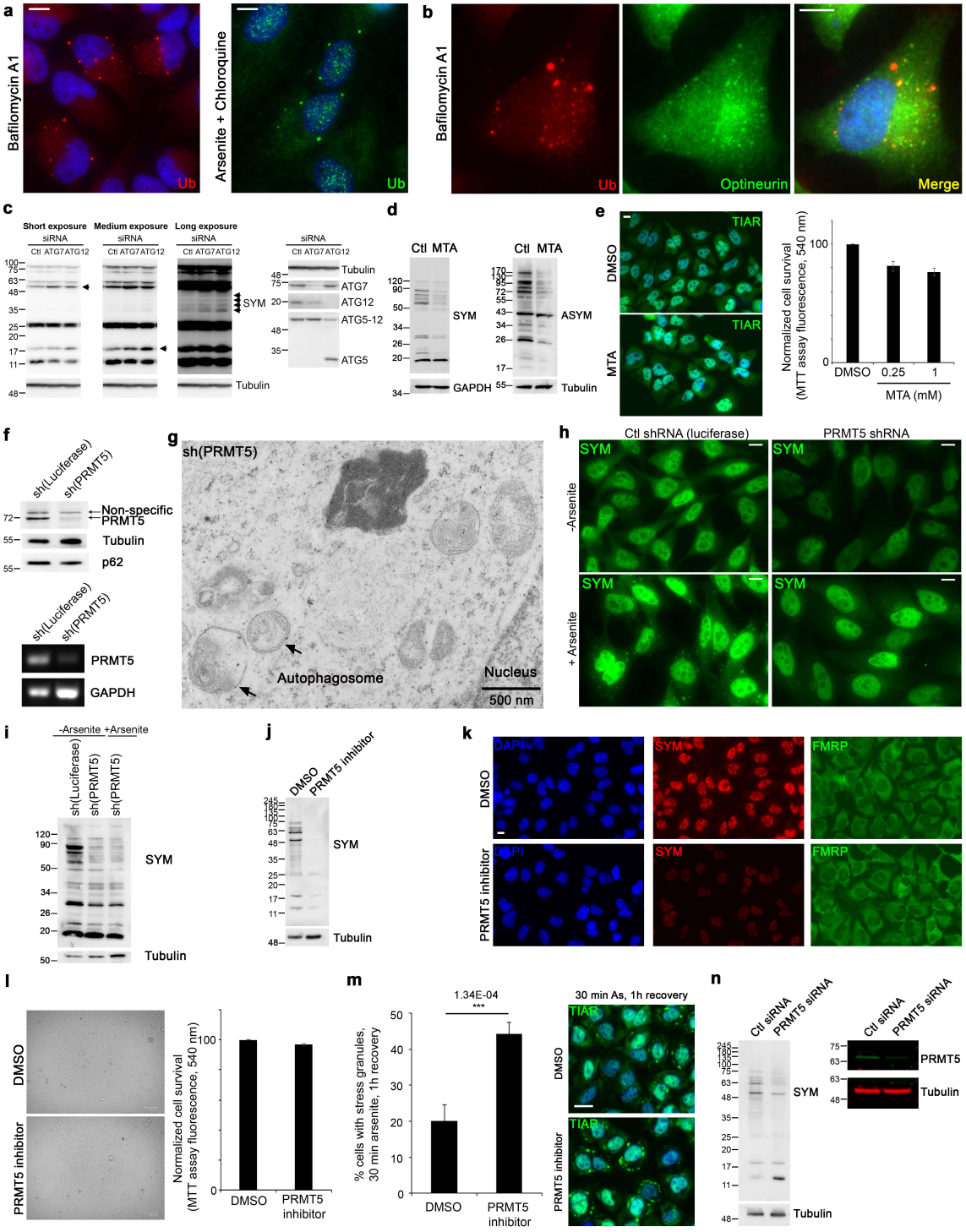

Figure 6: Stress granules are enriched in proteins modified with symmetrically dimethylated arginines

(**a, b**) Immunofluorescent microscopy of cells treated with (**a**) Bafilomycin A1 (left) or Arsenite and chloroquine (right) and labeled with Ubiquitin antibody and (**b**) Bafilomycin A1 and co-labeled with Ubiquitin and Optineurin. (**c**) Left, Western blot of proteins containing symmetrically (SYM) dimethylated arginines in total lysates of HEK293T cells treated with siRNA targeting *ATG7, ATG12*; Right, Western blot confirming ATG7, ATG12 knockdown. (**d**) Western blot of proteins containing symmetrically (SYM) and asymmetrically (ASYM) dimethylated arginines in total lysates of cells treated with vehicle or methylthioadenosine (MTA). (**e**) Left, immunofluorescent microscopy showing lack of stress granule induction in cells treated with vehicle or methylthioadenosine (MTA); Right, quantification of cell viability by MTT assay in cells treated with vehicle or methylthioadenosine. (**f**) Left, Western blot of PRMT5 and p62 in cells stably transduced with lentiviruses packaging shRNA targeting *PRMT5* (shPRMT5) or control shRNA targeting luciferase (shLuciferase); Right, RT-PCR of *PRMT5* mRNA in cells stably transduced as above. (**g**) Electron microscopy of autophagosomes (indicated by arrows) in shPRMT5 cells. (**h**) Immunofluorescent microscopy of proteins containing symmetrically dimethylated arginines (SYM) in shPRMT5 or shLuciferase cells treated or not with arsenite. (**i**) Western blot of total lysates from shPRMT5 or shLuciferase cells treated or not with arsenite and labelled with antibody specific for symmetrically dimethylated arginines. (**j**) Western blot of proteins containing symmetrically (SYM) dimethylated arginines in total lysates of cells treated with vehicle or PRMT5 inhibitor (EPZ015666). (**k**) Immunofluorescent microscopy showing lack of stress granule (FMRP) induction and diminished symmetric dimethylation signals in cells treated with vehicle or PRMT5 inhibitor. (**l**) Left, light microscopy of healthy cells upon treatment with PRMT5 inhibitor; Right, quantification of cell viability by MTT assay in cells treated with

PRMT5 inhibitor. (**m**) Left, percentage of cells containing stress granules following 1 hour recovery from 30 minutes arsenite treatment in the presence of PRMT5 inhibitor (n=4, mean ± SD, Student's *t*-test); Right, representative images. (**n**) Left, Western blot of proteins containing symmetrically (SYM) dimethylated arginines in total lysates of cells treated with siRNA targeting *PRMT5*; Right, Western blot confirming PRMT5 knockdown.

HeLa cells were used in all experiments. Scale bar = 10 µm.

We tested whether symmetric arginine dimethylation is required for elimination of stress granules. The methylation inhibitor, methylthioadenosine (MTA) (Figure 6d) alone did not induce stress granules and had minor effects on cell survival (Figure 6e). In cells treated with arsenite, MTA did not affect stress granule formation but prevented their elimination (Figure 5f-g). Depletion of the symmetric dimethylation enzyme PRMT5 (Figure 5h, Figure 6f,h-i) did not affect autophagosome formation or p62 levels (Figure 6f-g). PRMT5 depletion abrogated symmetric arginine dimethylation in stress granules (Figure 5h) and prevented their elimination during recovery from stress (Figure 5i-j). A PRMT5 inhibitor (EPZ015666) had similar effects (Figure 6j-m). Cumulatively, this suggests that like C9ORF72 and p62, symmetric arginine dimethylation of stress granule proteins by PRMT5 is required for their elimination. Knockdown of C9ORF72, p62, or PRMT5 decreased recruitment of LC3 to the stress granule marker FMRP as measured by PLA (Figure 5k, Figure 6n) independent of any change in LC3 or FMRP levels (Figure 5l). With evidence that p62 is epistatic to ATG5 in eliminating stress granules (Figure 4a-c), and the presence of stress granule markers with p62 in autophagosomes and autophagolysosomes by density gradient (Figure 5d), confocal microscopy (Figure 3l), and electron microscopy (Figure 3h-k), this strongly suggests that a complex of

C9ORF72 and p62 (Figure 1) requires PRMT5 to eliminate stress granules by autophagy.

Methylation of FUS by PRMT5 is required for binding to p62

Candidate interactors of C9ORF72 and p62 included several proteins containing dimethylated arginines by mass spectrometry, including FUS (Table 6). We asked whether FUS could be symmetrically dimethylated by PRMT5. PRMT1 is known to asymmetrically dimethylate arginines in FUS (Tradewell et al., 2012), however FUS is not known to be symmetrically dimethylated, or dimethylated by PRMT5. FUS was detected in immunoprecipitates of proteins with symmetrically dimethylated arginines (Figure 7a), and a protein at the mass of FUS was detected with antibodies specific for symmetrically dimethylated arginines in FUS immunoprecipitates (Figure 7b). PRMT5 was detected in FUS immunoprecipitates along with SMN which binds symmetrically dimethylated proteins (Figure 7c), suggesting PRMT5 may symmetrically dimethylate FUS. In agreement, symmetric dimethylation of arginine residues on FUS was reduced upon PRMT5 depletion (Figure 7b) and PRMT5 methylated GST-FUS, but not GST in an *in vitro* radiolabeling assay (Figure 7d). This suggests that PRMT5 symmetrically dimethylates FUS *in vitro* and *in vivo*.

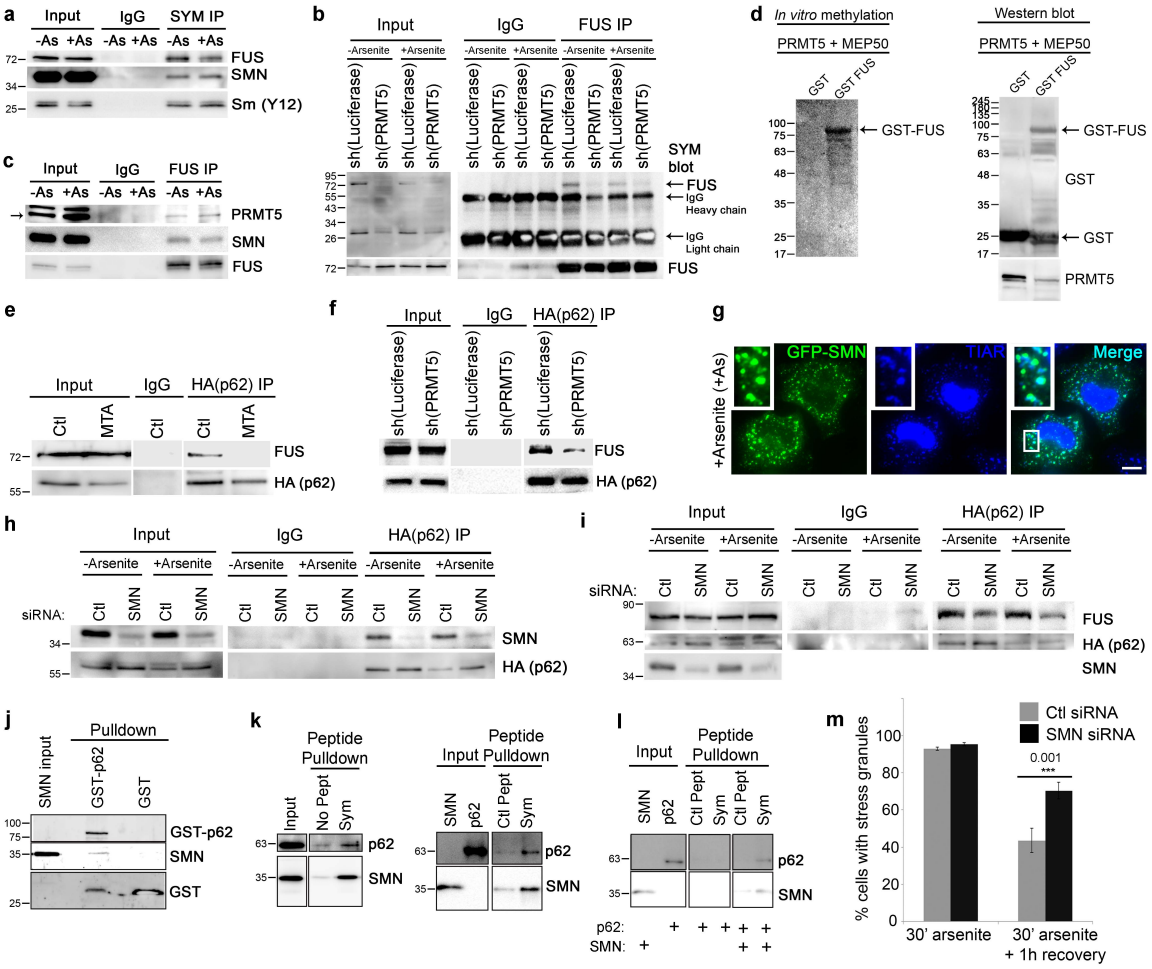

Figure 7: SMN mediates the interaction of p62 with FUS methylated by PRMT5 for degradation by autophagy

(**a**) Western blot of immunoprecipitates of endogenous proteins containing symmetrically dimethylated arginines from cells treated with arsenite (+As) or not (-As). (**b**) Western blot for proteins containing symmetrically dimethylated arginines in immunoprecipitates of FUS from cells stably expressing PRMT5 shRNA or control shRNA; top arrow indicates mass of FUS on Western blots and bottom arrows indicate bands due to detection of immunoprecipitating IgG heavy and light chain. (**c**) Western blot of immunoprecipitates of FUS from cells with and without arsenite treatment (+As, -As); A non-specific band appears above PRMT5 in PRMT5 input Western blots that is not depleted by shRNA targeting PRMT5 (see Figure 6e). (**d**) Left, autoradiograph of (3)H

after *in vitro* methylation assay of GST or GST-FUS incubated with PRMT5-MEP50; Right, Western blot of PRMT5 and GST in samples used for *in vitro* methylation assays (Right). (**e**) Western blot of HA-p62 immunoprecipitates in cells treated with DMSO (Ctl) or MTA (methylthioadenosine 1 mM, 48 h). (**f**) Western blot of FUS in HA-p62 immunoprecipitates from cells stably expressing PRMT5 or control shRNA. (**g**) Immunofluorescent microscopy of GFP-SMN and TIAR (stress granule marker) in cells treated with arsenite. (**h**) Western blot of SMN in immunoprecipitates of HA-p62 from cells treated with SMN or control siRNA and either treated or not with arsenite. (**i**) Western blot of FUS in immunoprecipitates of HA-p62 from cells treated with siRNA targeting SMN or control (Ctl) and either treated or not with arsenite. (**j**) Western blot of recombinant SMN and GST-p62 from *in vitro* GST-pulldown assay. (**k**) Western blot of recombinant p62 and SMN from *in vitro* pulldown of control (Ctl) or symmetrically dimethylated peptides (Sym) incubated with recombinant p62 and SMN. (**l**) Western blot of recombinant p62 and SMN from *in vitro* pulldown of peptides incubated with recombinant p62 alone or p62 and SMN. (**m**) Percentage of cells transfected with control (Ctl) or SMN siRNA containing stress granules following 30 min arsenite treatment or following 1 hour recovery from arsenite (n=6, mean ± SD, Student's *t*-test). HeLa cells were used in all experiments. Scale bar = 10 µm.

Intriguingly, FUS was only detected in p62 immunoprecipitates by mass spectrometry in its arginine dimethylated form (Table 5-6). This suggests that dimethylation of FUS may be required for its binding to p62. In agreement, FUS immunoprecipitated with p62 and this association was strongly reduced in cells treated with the methylation inhibitor MTA or depleted of PRMT5 (Figure 7e-f).

The Tudor protein SMN mediates association of FUS and p62

We investigated how p62 associates with arginine-methylated FUS. Tudor domains bind dimethylated arginines (Bedford & Clarke, 2009). Survival Motor Neuron protein (SMN) is a Tudor protein that preferentially binds symmetrically-methylated arginines (Cote & Richard, 2005), frequently co-localizes with or docks on stress granules like p62 (Figure 7g) (Hua & Zhou, 2004), and associates with FUS (Sun et al., 2015) (Figure 7c, Figure 8a). Like FUS, SMN immunoprecipitated with p62 in the absence or presence of oxidative stress (Figure 1n, 7h). This suggests that SMN may link FUS to p62. Supporting this mechanism, association of FUS with p62 was reduced when SMN was depleted with siRNA (Figure 7i, Figure 8b).

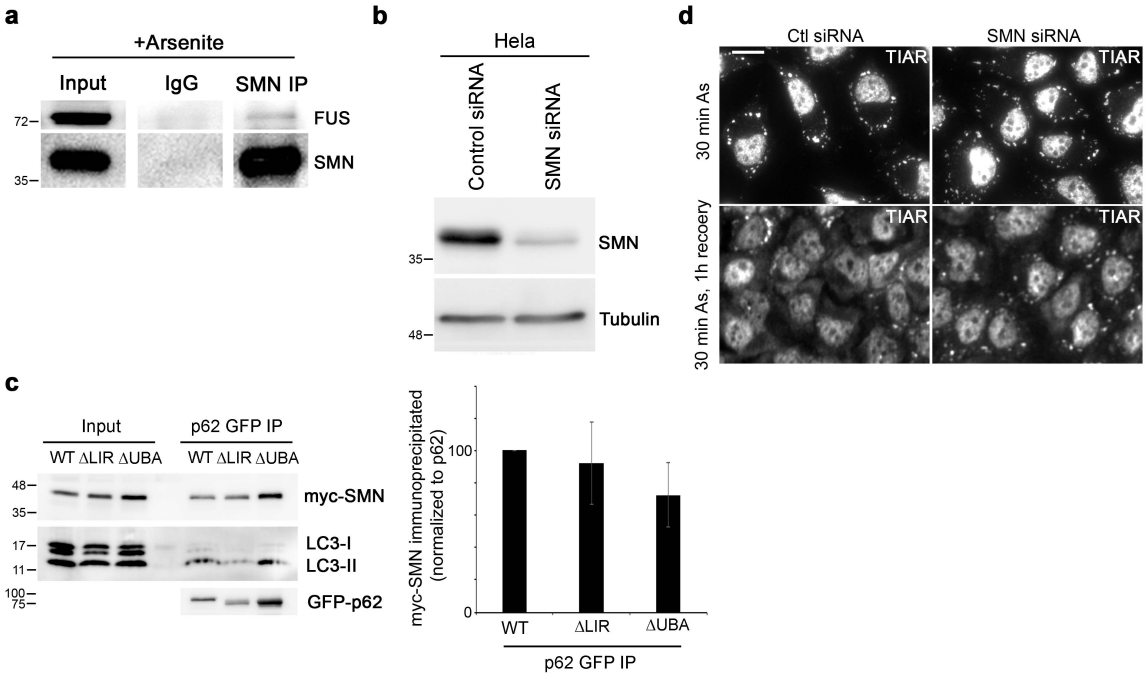

Figure 8: FUS associates with SMN

(**a**) Western blot of FUS in immunoprecipitates of SMN from cells treated with arsenite. (**b**) Western blot of SMN in cells treated with control siRNA or siRNA targeting *SMN*. (**c**) Left, Western blot of immunoprecipitates of wild-type (WT) and p62 mutants; Right, quantification of myc-SMN pulled down with indicated p62 expression constructs (n=2). (**d**) Representative images of cells transfected with control (Ctl) or SMN siRNA

containing stress granules (TIAR) following 30 min arsenite treatment or following 1 hour recovery from arsenite. HeLa cells were used in all experiments. Scale bar = 10 μm.

We sought to investigate binding of p62 to symmetrically-methylated arginines and SMN in more detail using recombinant proteins. Recombinant SMN was pulled down with recombinant GST-p62, but not GST alone (Figure 7j). In agreement with direct binding of recombinant p62 and SMN, p62 binding to SMN in cells did not require the p62 ubiquitin-binding domain (UBA) or its LC3 interacting region (LIR) (Figure 8c). In subsequent assays, peptides containing symmetrically dimethylated peptides were biotin-labelled and used for pulldowns compared to no peptide or identical peptides lacking symmetric dimethylation. As expected (Cote & Richard, 2005), SMN exhibited more binding to peptides containing symmetric arginine dimethylation (Figure 7k). p62 exhibited some background binding to beads likely due to its tendency to oligomerize and aggregate, but in the presence of SMN, p62 bound more to beads containing symmetrically-dimethylated peptides (Figure 7k). This demonstrates that p62 can bind the Tudor protein SMN (Figure 7j) and requires SMN to bind to peptides containing symmetric dimethylation (Figure 7k-l). Replicating the phenotype of p62 and PRMT5 knockdown (Figure 3a-b, Figure 5i-j), depletion of SMN did not impede formation of stress granules but blocked their elimination during recovery from stress (Figure 7m, Figure 8d). This suggests that p62 uses SMN to recognize arginine dimethylated proteins including FUS in stress granules for clearance by autophagy.

PRMT5 methylates FUS on R218 for autophagic degradation

PRMT5-mediated symmetric dimethylation promotes FUS association with p62 (Figure 7a-f). FUS was previously observed to associate with symmetrically arginine-dimethylated proteins (Boisvert, Cote, Boulanger, & Richard, 2003), but whether and

where it was directly symmetrically methylated remained unclear. FUS detected by mass spectrometry in both p62 and C9ORF72 immunoprecipitates was dimethylated exclusively on a peptide encompassing two arginines (R216, R218, Table 6). Other dimethylation sites were identified; however methylation at R218 was the only site consistently identified in assays including p62 and C9ORF72 interactomes, increasing in methylation assays with PRMT5 (Figure 7d, Table 7), and decreasing in cells expressing PRMT5 shRNA (Figure 9a). In some cases, FUS peptides were fragmented between R216 and R218, and this confirmed FUS is dimethylated on R218 (Figure 9b). To confirm this, R218K mutation of FUS strongly decreased its symmetric arginine dimethylation detected by Western blot (Figure 10a, Figure 9c). This suggests that R218 is a principal site of PRMT5-dependent symmetric dimethylation on FUS.

Table 7: Symmetric arginine dimethylation sites detected on FUS

Symmetric arginine dimethylation sites on FUS identified by MaxQuant analysis of LC-MS/MS. See also Supplementary Data 3.

Amino acid position	Method of detection (MaxQuant, FDR < 0.01)
R216, R218 and R503	Mass spectrometric analysis of immuno-precipitated FUS with and without PRMT5 depletion; summarized dimethyl (R) sites were enriched more in FUS immuno-precipitates in the presence of PRMT5
R218, R371, R394 and R407	Mass spectrometric analysis of FUS following its *In vitro* methylation assay with and without purified PRMT5/MEP50; summarized dimethyl (R) sites were enriched in the presence of PRMT5/MEP50
R218	Western blotting immuno-enriched R218K point mutant form of FUS with an antibody that recognizes symmetrically dimethylated proteins

Supplementary Data 3: Unprocessed output files generated by MaxQuant and SAINT analysis of LCMS/MS results, related to Table 7 - FUS Dimethyl(KR)Sites LC-MS/MS.

File contains 3 Excel sheets: (i) dimethyl (KR) sites detected on FUS with and without PRMT5, with and without arsenite treatment of cells, (ii) dimethyl (KR) sites detected on FUS following its in vitro methylation by purified PRMT5/MEP50 complex and (iii) dimethyl (KR) sites detected on FUS following its in vitro methylation in the presence or absence of purified PRMT5/MEP50 complex. Project accession: PXD009760

*Due to the size of this table please refer to Appendix E

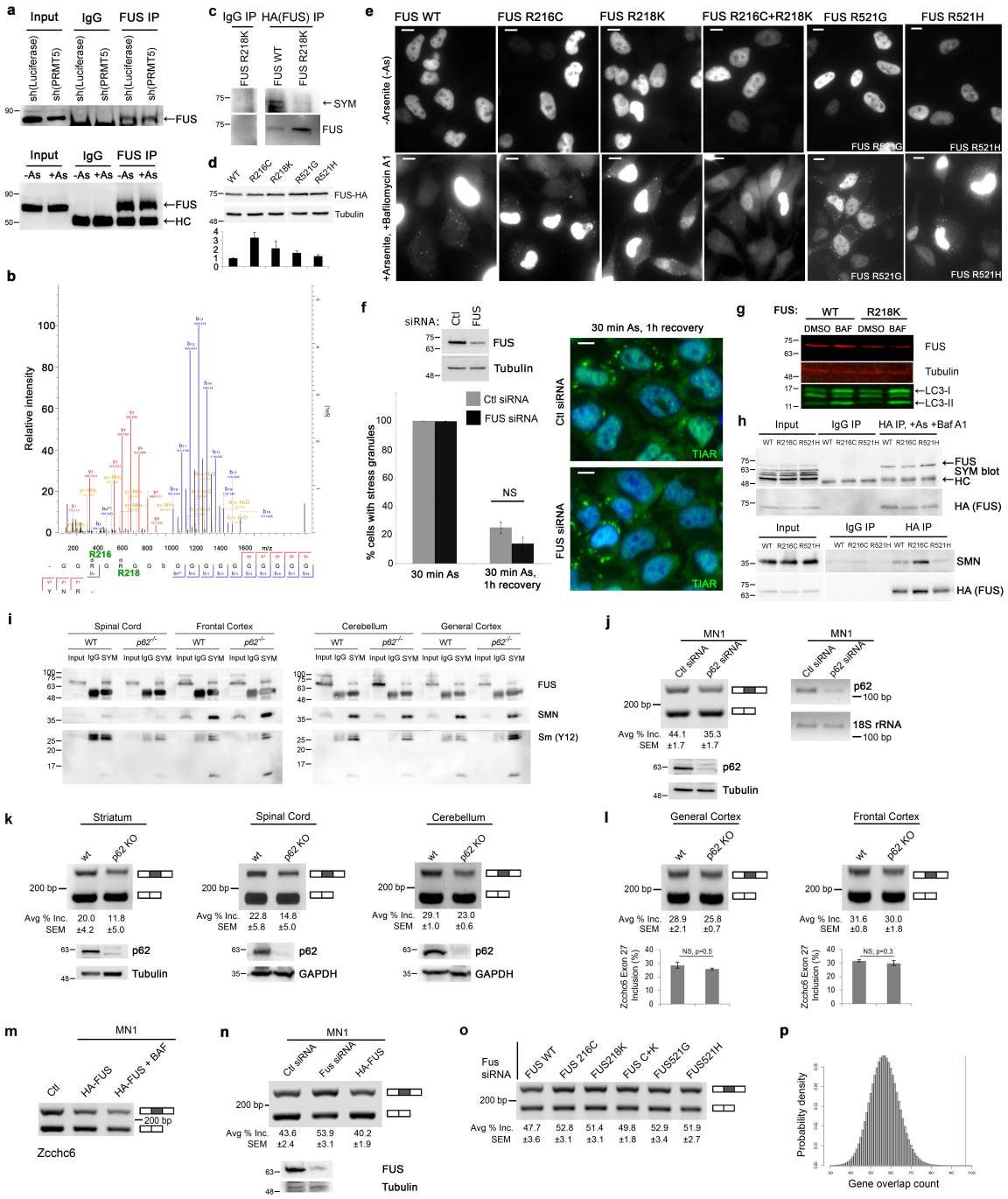

Figure 9: FUS mutants distribute in the cytoplasm of cells and exert splicing defects shared with p62 depleted cells and mice

(**a**) Western blot of FUS immunoprecipitates from HeLa cells used for MS/MS; Top, cells expressing shRNA targeting PRMT5 (shPRMT5) or luciferase control (shLuciferase); Bottom, cells treated with arsenite (+As) or vehicle (-As). (**b**) Annotated spectrum from

LC-MS/MS of dimethylated FUS peptide 214-GGRGRGGSGGGGGGGGGGYNR-234. (**c**) Western blot for symmetrically dimethylated arginines (SYM) in immunoprecipitates of wild-type or R218K HA-FUS HeLa cells (n=3-6, mean ± SD). (**d**) Western blot of wild-type and mutant FUS in HeLa cells. (**e**) Immunofluorescent microsocopy of wild type or FUS mutants in HeLa cells. (**f**) Top, Western blot of FUS in HeLa cells treated with FUS targeting siRNA; Left, percentage of transfected cells containing SGs following 30 min arsenite or 1 hour recovery from arsenite (n=2, mean ± SD, Student's *t*-test); Right, representative images. (**g**) Western blot of FUS wild-type and R218K mutant upon Bafilomycin A1 treatment of HeLa cells. (**h**) Western blot of immunoprecipitates of wild-type and FUS mutants from HeLa cells treated with arsenite and Bafilomycin A1. (**i**) Western blot of immunoprecipitates of symmetrically dimethylated proteins from wild-type and *p62*$^{-/-}$ mice; Sm (Y12) serves as a positive control. (**j**) Left, RT-PCR of splice variants of Zcchc6 mRNA in MN1 cells treated with siRNA; Right, RT-PCR and Bottom, Western blot of p62 in the corresponding cells. (**k**) Top, RT-PCR of splice variants of Zcchc6 mRNA from wild-type or *p62*$^{-/-}$ mice; Bottom, Western blot of p62. (**l**) Top, RT-PCR of splice variants of Zcchc6 mRNA from wild-type or *p62*$^{-/-}$ mice; Bottom, quantification from 3 mice. (**m**) RT-PCR of splice variants of Zcchc6 mRNA in MN1 cells mock transfected, transfected with HA-FUS and/or treated with Bafilomycin A1. (**n**) Top, RT-PCR of splice variants of Zcchc6 mRNA in MN1 cells treated with control siRNA or siRNA targeting FUS or transfected with HA-FUS; Bottom, Western blot of FUS. (**o**) RT-PCR of splice variants of Zcchc6 mRNA in MN1 cells treated with siRNA targeting FUS 3'UTR and co-transfected with wild-type or FUS mutants. (**p**) Normal probability distribution of number of mRNAs bound to FUS and alternatively spliced in *FUS*$^{-/-}$ brain; red line indicates probability of observed overlap with mRNAs with putative alternative splicing in *p62*$^{-/-}$ brain. Scale bar = 10 μm.

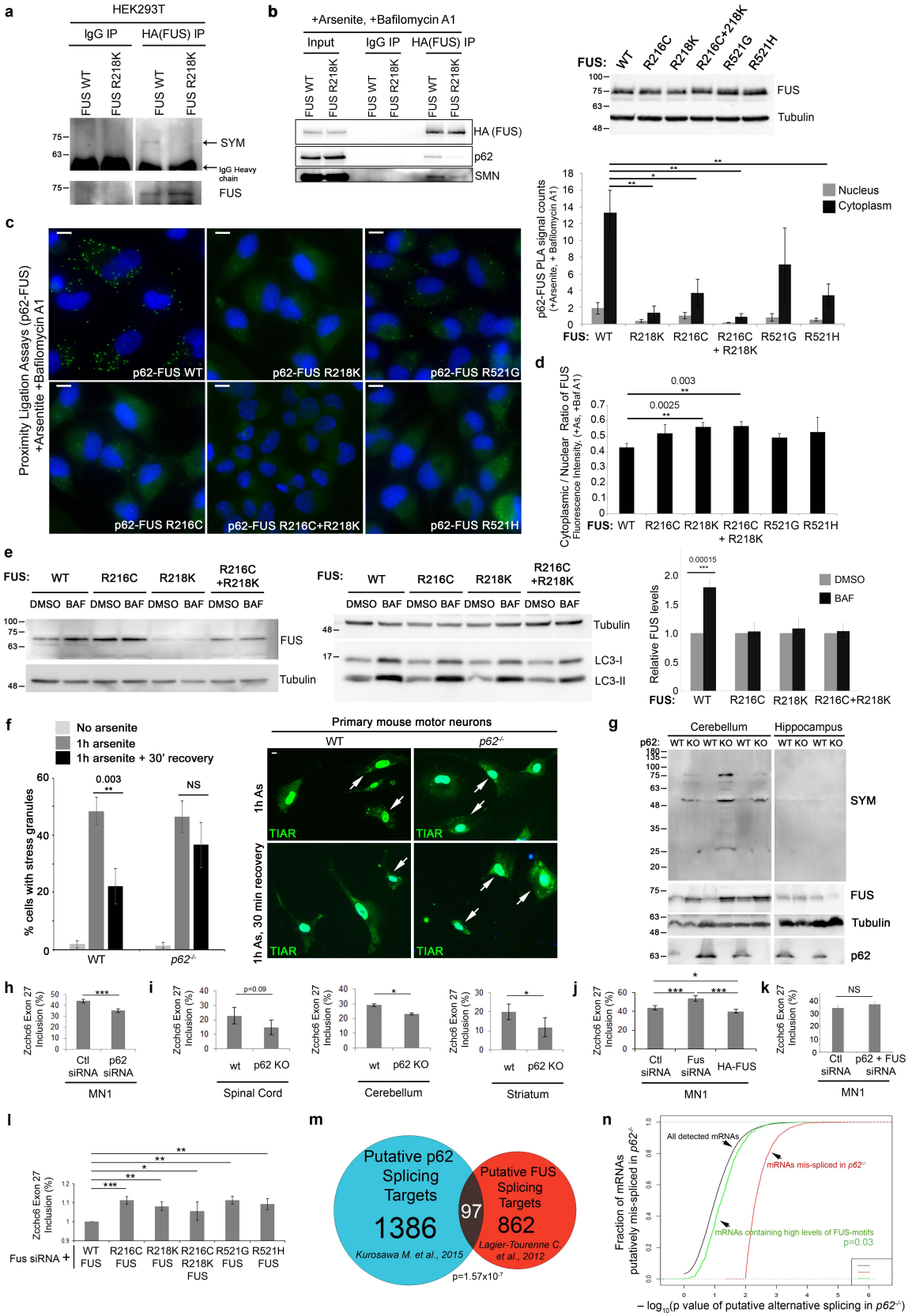
a
HEK293T
IgG IP
HA(FUS) IP
FUS WT
FUS R218K
SYM
IgG Heavy chain
FUS
b
+Arsenite, +Bafilomycin A1
Input
IgG IP
HA(FUS) IP
HA (FUS)
p62
SMN
FUS: WT R216C R218K R216C+218K R521G R521H
FUS
Tubulin
c
Proximity Ligation Assays (p62-FUS) +Arsenite +Bafilomycin A1
p62-FUS WT
p62-FUS R218K
p62-FUS R521G
p62-FUS R216C
p62-FUS R216C+R218K
p62-FUS R521H
p62-FUS PLA signal counts (+Arsenite, + Bafilomycin A1)
Nucleus
Cytoplasm
FUS: WT R218K R216C R216C + R218K R521G R521H
d
Cytoplasmic / Nuclear Ratio of FUS Fluorescence Intensity, (+As, +Baf A1)
0.003
0.0025
FUS: WT R216C R218K R216C + R218K R521G R521H
e
FUS: WT R216C R218K R216C +R218K
DMSO BAF DMSO BAF DMSO BAF DMSO BAF
FUS
Tubulin
LC3-I
LC3-II
Relative FUS levels
0.00015
DMSO
BAF
f
No arsenite
1h arsenite
1h arsenite + 30' recovery
% cells with stress granules
0.003
NS
WT
p62-/-
Primary mouse motor neurons
1h As
1h As, 30 min recovery
TIAR
g
Cerebellum
Hippocampus
p62: WT KO WT KO WT KO WT KO WT KO
SYM
FUS
Tubulin
p62
h
Zcchc6 Exon 27 Inclusion (%)
Ctl siRNA
p62 siRNA
MN1
i
p=0.09
wt
p62 KO
Spinal Cord
Cerebellum
Striatum
j
Ctl siRNA
Fus siRNA
HA-FUS
MN1
k
NS
Ctl siRNA
p62 + FUS siRNA
MN1
l
Fus siRNA +
WT FUS
R216C FUS
R218K FUS
R216C R218K FUS
R521G FUS
R521H FUS
m
Putative p62 Splicing Targets
1386
Kurosawa M. et al., 2015
97
Putative FUS Splicing Targets
862
Lagier-Tourenne C. et al., 2012
p=1.57x10-7
n
Fraction of mRNAs putatively mis-spliced in p62-/-
All detected mRNAs
mRNAs mis-spliced in p62-/-
mRNAs containing high levels of FUS-motifs
p=0.03
– log10(p value of putative alternative splicing in p62-/-)

Figure 10: p62 regulates turnover of FUS and splicing of its targets

(**a**) Western blot of symmetrically dimethylated arginines in FUS immunoprecipitates from HEK293T cells. (**b**) Left, Western blot of FUS immunoprecipitates from HeLa cells treated with arsenite and Bafilomycin A1; Right, Western blot of FUS in HeLa cells in conditions used for PLA in (c). (**c**) Left, PLA of p62 and wild-type or indicated FUS mutants in HeLa cells treated with arsenite and Bafilomycin A1; Right, quantification of PLA; images counted (>10 cells/image): wild-type (11), R218K (9), R216C (8), R216C+R217K (8), R521G (9), R521H (9) (n=3, mean ± SD, Student's *t*-test). (**d**) Quantification of nuclear/cytoplasmic distribution of wild-type and mutant FUS by fluorescence intensity in HeLa cells treated with arsenite and Bafilomycin A1; cells counted: wild-type (32), R218K (19), R216C (8), R216C+R218K (16), R521G (31), R521H (21) (mean ± SD, Student's *t*-test). (**e**) Left, Western blot of FUS wild-type, indicated mutants and LC3 upon Bafilomycin A1 treatment of HeLa cells; Right, quantification of Western blots normalized to Tubulin (n=6, mean ± SD, Student's *t*-test). (**f**) Left, percentage of cells containing SGs in primary motor neuron cultures of wild-type and *p62*$^{-/-}$ mice (n=2-4); 35-150 cells were counted per condition (mean ± SD, Student's *t*-test); Right, representative images. (**g**) Western blot of lysates from wild-type (WT) and *p62*$^{-/-}$ (KO) mice. (**h-l**) RT-PCR analysis of Zcchc6 splice variants in (**h**) p62 depleted MN1 cells (n=4), (**i**) indicated tissues of WT and *p62*$^{-/-}$ mice (n=3), (**j**) FUS depleted and overexpressing MN1 cells (n=4), (**k**) FUS and p62 depleted MN1 cells (n=3) and (**l**) MN1 cells depleted of endogenous FUS with siRNA targeting FUS 3'UTR and expressing FUS wild-type or indicated mutants (n=4, mean ± SEM, Student's *t*-test). (**m**) Venn-diagram depicting overlap between mRNAs putatively alternatively spliced in *p62*$^{-/-}$ brains and those bound to FUS and mis-spliced in *FUS*$^{-/-}$ brains. (**n**) A plot of the fraction of mRNAs putatively mis-spliced in *p62*$^{-/-}$ brain (y-axis) vs. the increasing significance of this ($-\log_{10}$ p-value, x-axis); black line – all detected mRNAs, green line – mRNAs

enriched in FUS binding motifs, red line – only mRNAs putatively mis-spliced in *p62*$^{-/-}$ brain. p =0.0357 that putative mRNAs mis-spliced in *p62*$^{-/-}$ brains are enriched in FUS binding motifs. Scale bar = 10 μm.

PRMT5-dependent methylation of FUS promotes its binding to SMN and p62 (Figure 7f-l). FUS R218K mutants and others were expressed at similar or slightly higher levels in cells (Figure 10b, Figure 9d). In agreement with R218 of FUS being the principal site of symmetric dimethylation by PRMT5, the immunoprecipitation of p62 and SMN with FUS was reduced by mutation of R218 (Figure 10b). In agreement, similar amounts of FUS R218K and other FUS mutants localized to the cytoplasm as wild-type FUS during oxidative stress (Figure 10d, Figure 9e), but in PLA p62 association with FUS was ablated by the R218K mutation (Figure 10c). Nonetheless, depletion of FUS with siRNA did not alter formation or elimination of stress granules (Figure 9f), suggesting that p62 recognizes multiple proteins methylated by PRMT5 to promote elimination of stress granules. If p62 can also eliminate symmetrically methylated proteins individually or in small clusters then mutating methylation sites should block their turnover by autophagy. Wild-type FUS significantly accumulated when autophagic degradation was blocked with Bafilomycin A1 whereas R218K mutant was unperturbed demonstrating that it is no longer targeted for degradation by autophagy (Figure 10e, Figure 9g). This strongly suggests that symmetric arginine dimethylation of FUS at R218 by PRMT5 is required for its association with p62 and clearance by autophagy (Figure 5i-k, Figure 7, Figure 10a-e), while methylation of multiple proteins in stress granules is likely required for their elimination by autophagy.

Like FUS R218K, the association of FUS R216C and R521H but not R521G with p62 was strongly decreased, despite accumulating similarly in the cytoplasm and being

expressed at similar levels (Figure 10b-d, Figure 9e). The association of FUS with p62 could be impaired at multiple levels. For example, PRMT5 or SMN may no longer be able to access R218, or the FUS-SMN complex could be otherwise altered to impair p62 binding. Symmetric dimethylation of FUS was not decreased in R216C or R521H mutants (Figure 9h). While FUS R216C association with SMN was not impaired, FUS R521H mutant associated poorly with SMN (Figure 9h), suggesting that the C-terminus of FUS may be required with R218 for optimal interaction with SMN. FUS R216C was also unperturbed upon inhibiting autophagic degradation (Figure 10e). Together, this suggests that multiple mutations in FUS have an impaired association with p62 caused by defects at multiple levels in the pathway elucidated here and this can prevent p62-dependent autophagy.

p62$^{-/-}$ mice accumulate symmetrically methylated proteins

We assessed whether p62 may affect elimination of stress granules in cell types relevant to ALS. Elimination of arsenite-induced stress granules in motor neurons derived from *p62*$^{-/-}$ mice was impaired compared to their wild-type counterparts (Figure 10f). Both FUS and SMN immunoprecipitated with symmetrically dimethylated proteins in mouse cortex, cerebellum and spinal cord (Figure 9i), suggesting that FUS is methylated by PRMT5 in relevant mouse tissues. Symmetrically dimethylated proteins and FUS accumulated in cerebellum, but not the hippocampus of *p62*$^{-/-}$ mice (Figure 10g). While we cannot exclude that p62 promotes symmetric arginine dimethylation, this data suggests that p62 controls turnover of stress granules in neurons and proteins containing symmetrically dimethylated arginines in some regions of the mouse brain.

p62$^{-/-}$ mice exhibit FUS-dependent mRNA splicing defects

P62 may impact the amount and nuclear-cytoplasmic distribution of FUS and other splicing regulators that are symmetrically dimethylated resulting in alternative splicing. In brain of *p62*$^{-/-}$ mice (Kurosawa et al., 2015), while no mRNAs besides p62 exhibited changes in expression, 1386 mRNAs exhibited signatures of alternative splicing. A predicted p62-dependent splicing event in *Zcchc6* (exon 27 inclusion) was impaired in p62 knockdown MN-1 cells and in several brain regions of *p62*$^{-/-}$ mice (Figure 10h-i, Figure 9j-l). Zcchc6 uridylates the 3' end of select miRNA and mRNAs including *let-7* (B. Kim et al., 2015) whereby it may impact formation of neuromuscular junctions (Bussing, Slack, & Grosshans, 2008) and ALS-associated phenotypes (Emde et al., 2015). Exon 27 inclusion of *Zcchc6* mRNA was increased when FUS was depleted with siRNA, reversed when wild-type FUS, but not FUS mutants (R218K, R216C, R521G, R521H) were expressed and further enhanced by blocking autophagic degradation of FUS with Bafilomycin (Figure 10j,l, Figure 9m-o). The decreased inclusion of Zcchc6 exon 27 induced by loss of p62 (Figure 10h-i) was prevented by depletion of FUS (Figure 10k), demonstrating that p62 effects on splicing of *Zcchc6* require FUS. Overall, this strongly suggests that p62 and FUS regulate shared alternative splicing events that depend in part on methylation of R218 on FUS and its ability to associate with p62 and be degraded by autophagy (Figure 10a-l, Figure 9a-o).

More broadly, mRNAs putatively mis-spliced in *p62*$^{-/-}$ brains included a highly significant proportion of mRNAs (97 of 862, $p=1.57x10^{-7}$) that bound to FUS and were mis-spliced in FUS-deficient brains (Lagier-Tourenne et al., 2012) (Figure 10m, Figure 9p). Furthermore, mRNAs mis-spliced in *p62*$^{-/-}$ brain were significantly enriched in a FUS-binding motif (Lagier-Tourenne et al., 2012) (Figure 10n). This suggests that p62 and FUS regulate alternative splicing of a large shared pool of transcripts.

Patient inclusions contain arginine-methylated proteins

C9ORF72 associates with p62 and moderately lowering the levels of C9ORF72 prevents clearance of stress granules (Figure 1b,e-j, Figure 3a-d). ALS patients with C9ORF72 repeat expansions have reduced levels of C9ORF72 (Haeusler et al., 2016) and may therefore exhibit signatures of impaired p62-dependent clearance of proteins with symmetrically methylated arginines.

In patients with C9ORF72 expansions, inclusions were observed in the lumbar spinal cord containing TDP-43 and p62 as expected (Figure 11a,b). Validating the specificity of antibodies recognizing symmetrically dimethylated arginines, staining was reduced in PRMT5-depleted cells (Figure 6h), and exhibited prominent staining of the nucleus, without evident cytoplasmic foci in non-ALS patients as expected (Figure 12a-b). In both cerebellum and hippocampus, but not spinal cord of patients with *C9ORF72* repeat expansions inclusions containing p62 frequently also contained proteins with symmetrically dimethylated arginines (Figure 12c-f, Figure 11b). While we cannot exclude that p62 promotes symmetric dimethylation of arginines of inclusions, with evidence above, this suggests that p62 is recruited to inclusions containing symmetrically dimethylated arginines in patients with *C9ORF72* repeat expansions, but is unable to efficiently eliminate them, potentially due of the loss of C9ORF72 (Figure 3c-d).

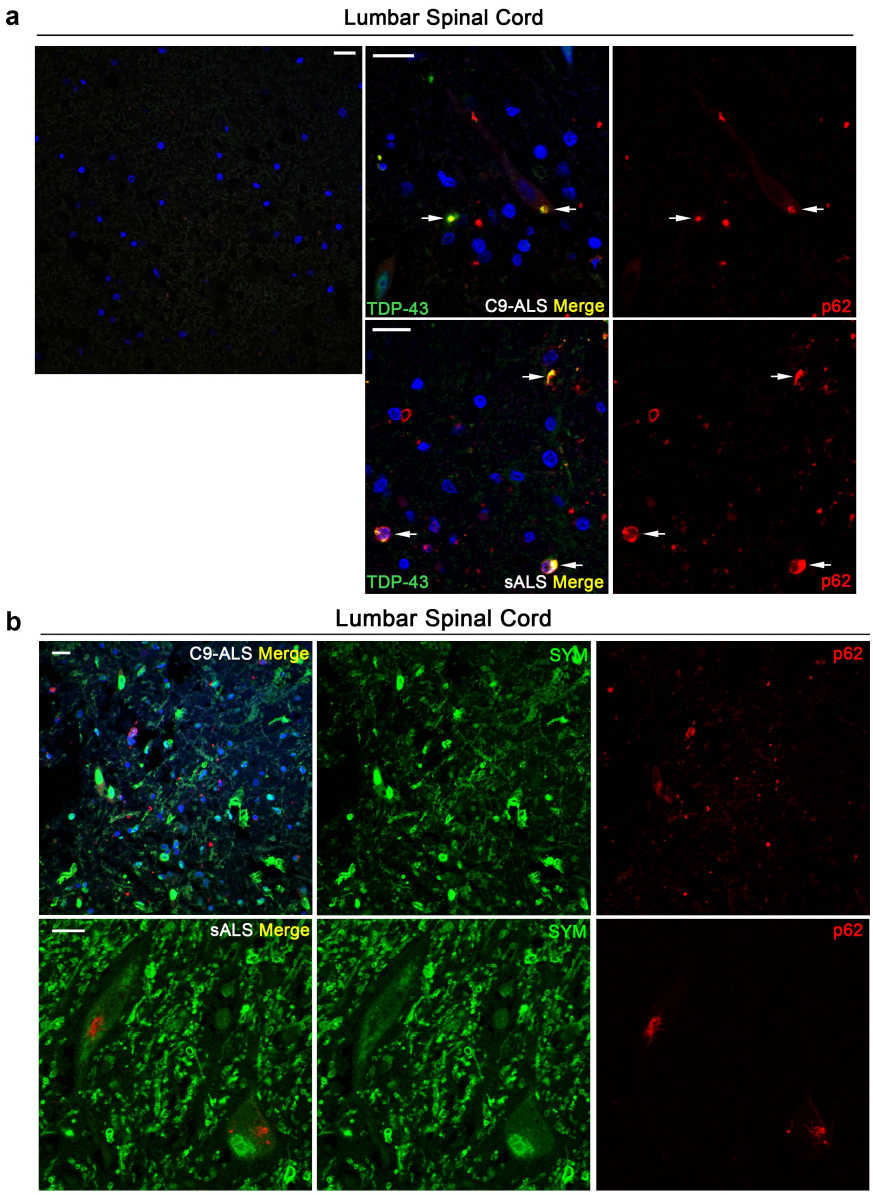

Figure 11: Lumbar spinal cord of ALS patients with sporadic disease or C9ORF72 repeat expansions exhibit p62+ inclusions that are not enriched in symmetrically dimethylated arginines

(**a**) Two-color immunofluorescence staining of lumbar spinal cord sections from patients with C9ORF72 repeat expansions (C9-ALS) or sporadic ALS (sALS) with isotype control non-specific antibody or antibodies to p62 and TDP-43 (Left, merged image); arrows represent inclusions and co-localization. (**b**) Two-color immunofluorescence staining of

lumbar spinal cord sections of patients with C9ORF72 repeat expansions (C9ORF72) and sporadic ALS (sALS) with antibodies to p62 and proteins with symmetrically dimethylated arginines (SYM). Scale bar = 20 µm.

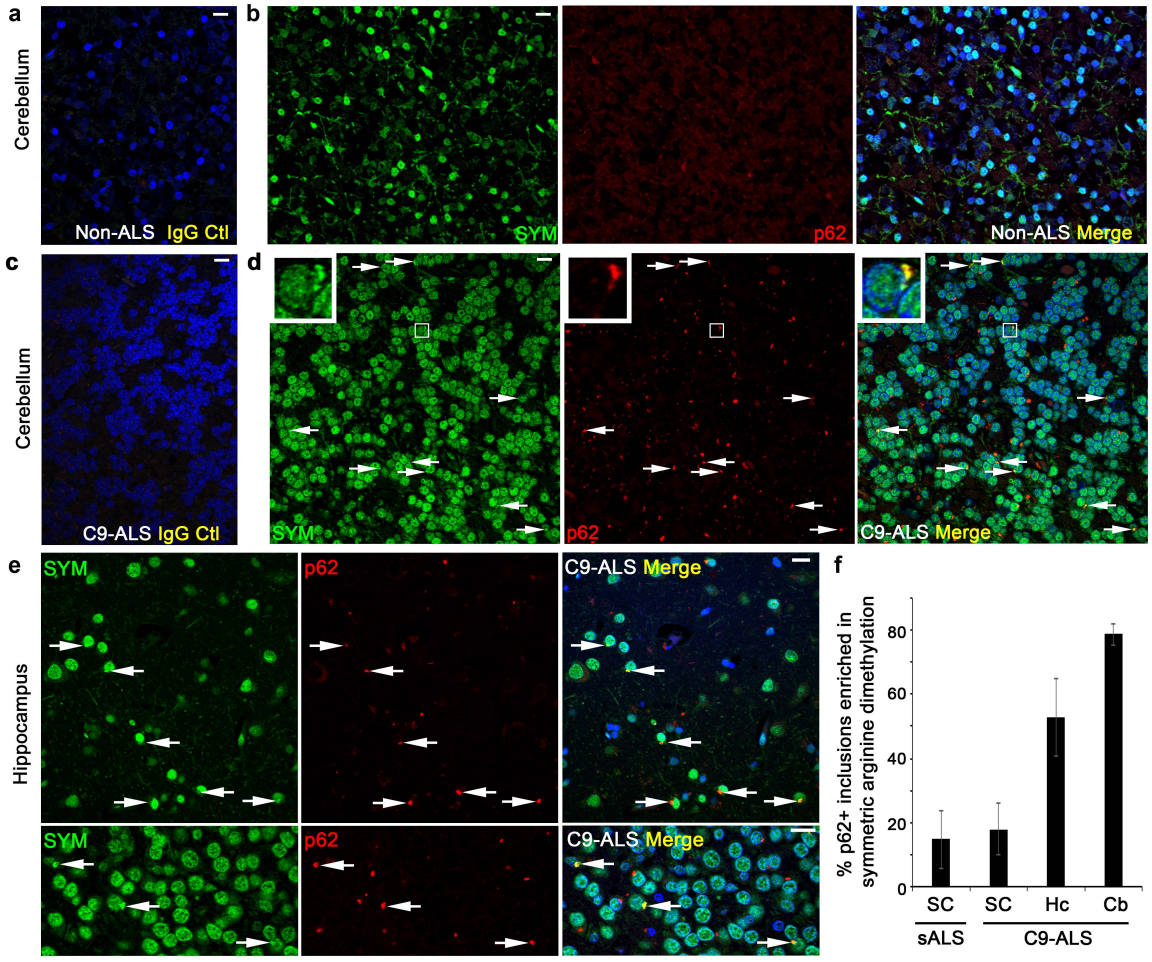

Figure 12: Patients with C9ROF72 repeat expansions exhibit inclusions rich in symmetrically arginine-dimethylated proteins

(**a,b**) Immunofluorescent microscopy of non-ALS human cerebellum labeled with (**a**) control non-specific antibodies or (**b**) antibodies specific for p62 and symmetrically dimethylated arginines. (**c,d**) Immunofluorescent microscopy of cerebellum of patient with C9ORF72 repeat expansions labeled with (**c**) control non-specific antibodies or (**d**) antibodies specific for p62 and symmetrically dimethylated arginines; arrows highlight

inclusions containing p62 and symmetrically dimethylated arginines. (**e**) Immunofluorescent microscopy of hippocampus of patient with C9ORF72 repeat expansions labeled with antibodies specific for p62 and symmetrically dimethylated arginines; arrows highlight inclusions containing p62 and symmetrically dimethylated arginines. (**f**) Quantification of fraction of p62 inclusions positive for symmetrically dimethylated arginine proteins as observed in spinal cords (SC), hippocampi (Hc) and cerebellums (Cb) of patients with C9ORF72 repeat expansions (C9-ALS) and sporadic ALS (sALS). Scale bar = 10 µm. sALS Spinal Cord (n=2); C9 ALS Spinal Cord (n=2); C9 Hippocampus (n=1); C9 Cerebellum (n=3), mean ± SD, Student's t-test. Cytoplasmic p62 inclusions were counted across 3-10 frames (10-80 p62 inclusions) in each sample.

Together, this suggests that C9ORF72 and p62 form a complex that recognizes proteins like FUS containing symmetrically dimethylated arginines to eliminate them individually or as clusters in stress granules by autophagy (Figure 13). Interruption of this process can cause accumulation of symmetrically methylated proteins as demonstrated in the mouse brain and in the cytoplasm of patients with C9ORF72 repeat expansions.

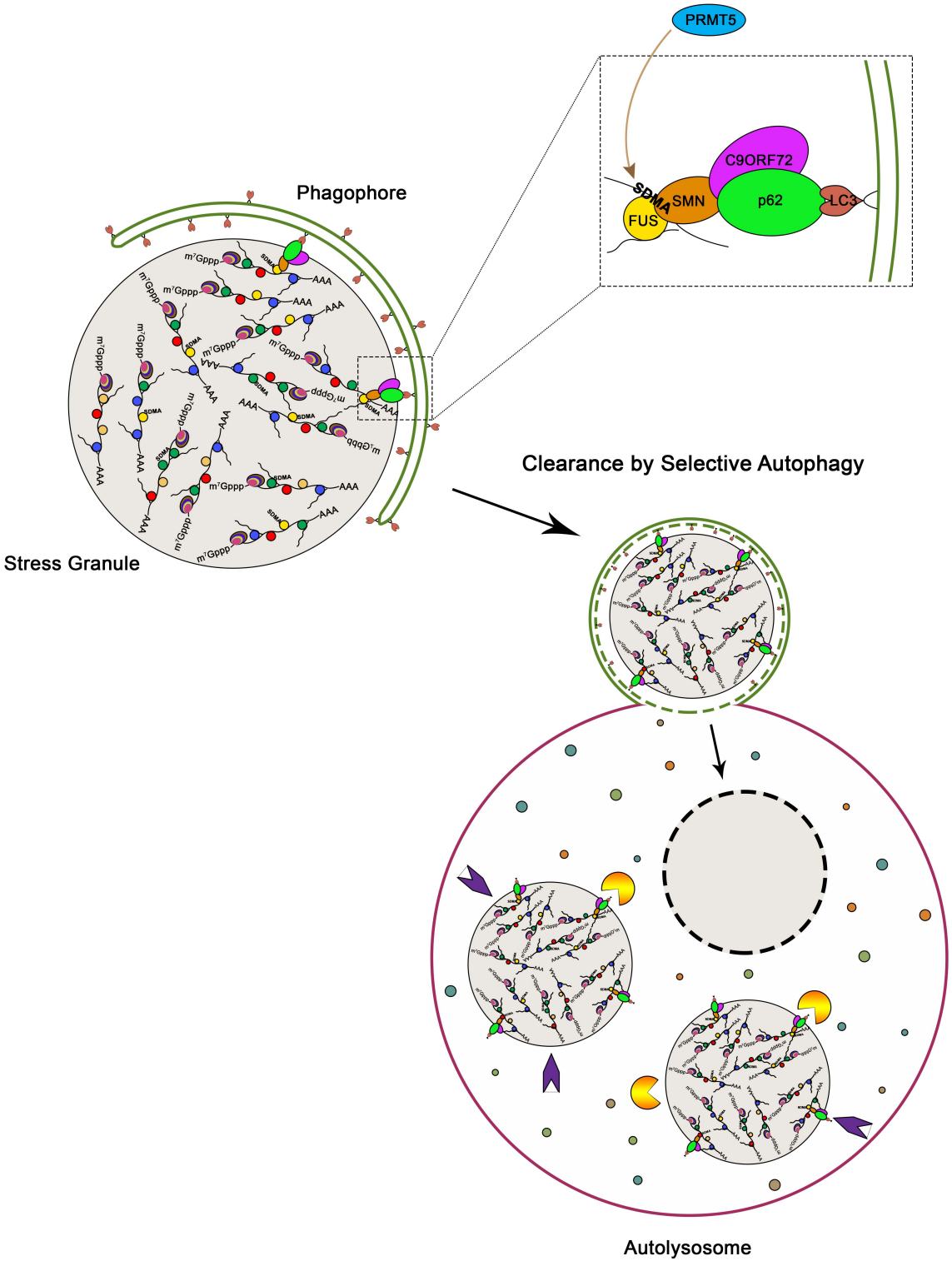

Figure 13: Schematic model of p62-C9ORF72 mediated autophagy

Stress granule proteins such as FUS are symmetrically dimethylated on arginines by PRMT5 to bind tudor-domain containing protein SMN for subsequent recruitment and degradation by p62-C9ORF72 mediated selective autophagy.

2.4 Discussion

Canonically, autophagy receptors bind ubiquitin on cargoes to direct their degradation by selective autophagy (Matsumoto et al., 2011), but this is not always the case (Khaminets et al., 2016). While ubiquitin was not enriched in stress granules in our analyses, we cannot exclude that elimination of stress granules requires ubiquitination in addition to symmetric arginine methylation. Recent reports highlight the ability of alternative post-translational modifications to target cargoes for autophagic degradation. For example, P granules, an RNA-containing structure unique to *C.elegans* germline cells, are eliminated by autophagy (Y. Zhang et al., 2009). Notably, this process is distinct from that described here in that it requires asymmetric, not symmetric arginine methylation of P granule proteins, and is independent of the *C. elegans* p62 homologue (S. Li et al., 2013). Arginine-methylated proteins are enriched in RNA binding domains (Boisvert et al., 2003; A. Guo et al., 2014). In the absence of an enzyme known to remove arginine methylation from proteins in cells, autophagy is one mechanism which enables turnover of arginine methylated proteins regrouped in diverse RNA granules.

PRMT1 asymmetrically methylates arginines on FUS (Tradewell et al., 2012) causing FUS mutants associated with ALS to accumulate in the cytoplasm in stress granules (Dormann et al., 2012). Similarly, PRMT1-mediated methylation of FMRP and other proteins drives their recruitment to stress granules (Dolzhanskaya et al., 2006). The current data suggests that an independent type of arginine methylation by PRMT5 at

FUS R218 controls a subsequent step, the targeting of cytoplasmic FUS for degradation by autophagy.

ALS-linked C9ORF72 with repeat expansions that decrease levels of endogenous C9ORF72 were previously shown to increase stress granule number, but the mechanism remained unknown (Maharjan, Kunzli, Buthey, & Saxena, 2016). Mimicking these conditions with a partial knockdown of C9ORF72, we observed a defect in elimination of stress granules (Figure 3c-d). C9ORF72 also has a role in controlling the initiation of phagophore formation by interacting with Rab1a (Webster et al., 2016). Intriguingly, Rab1a was identified in stress granules (S. Jain et al., 2016). We found that C9ORF72 and p62 decorated stress granules to initiate their elimination by autophagy. This suggests C9ORF72 and p62 are part of a broader complex, potentially including Rab1a at stress granules to promote engulfment of stress granules or fragments thereof within autophagosomes. At the same time, we cannot exclude that C9ORF72 effects independent of p62, or p62 functions independent of autophagy also promote elimination of stress granules.

Electron microscopy exhibited p62 and FUS co-localized on small electron dense clusters (~20-80 nm) on the periphery of stress granules (Figure 3h-k) and p62 is required to eliminate stress granules (Figure 3a-b, h-m). It is possible that p62 and autophagy achieve these effects by repeatedly eliminating parts of stress granules, rather than engulfing and degrading entire stress granules in a single autophagosome. Indeed, p62 bound to SMN and FUS both in the presence and absence of oxidative stress when stress granules are rare (Figure 1n, Figure 7h-i). Additionally, while methylation of FUS alone is insufficient to direct degradation of stress granules (Figure 9f), it is sufficient to cause degradation of FUS by autophagy (Figure 10e). Together, this suggests that turnover of submicroscopic complexes of FUS and possibly individual

FUS proteins may constitutively occur by p62-dependent autophagy and the clustering of multiple symmetrically dimethylated proteins into large granules during stress renders this process more readily observable with a microscope.

Multiple RNA surveillance mechanisms patrol the cytoplasm to prevent translation of mRNAs that contain errors or are unspliced (Brandman & Hegde, 2016; Lykke-Andersen & Jensen, 2015). Symmetrically-methylated proteins are highly enriched in the nucleus and many are involved in RNA processing. Our data suggests that symmetrically methylated proteins that escape into the cytoplasm are targeted for degradation by p62-dependent autophagy. The mechanism we describe may be a constitutive RNA surveillance and quality control mechanism that detects escape of nuclear RNA processing complexes into the cytoplasm and restricts production of toxic proteins from immature mRNA or mRNA with errors.

One model suggests that stress granules or a related derivative underlie the pathology of at least some forms of ALS (Y. R. Li et al., 2013). Mutations in another protein genetically-linked to ALS, VCP, inhibit its normal function in promoting elimination of stress granules by autophagy (Buchan et al., 2013). Our data demonstrates a cascade of events governing the recognition and degradation of stress granules that requires a protein genetically linked to ALS at each step (FUS, SMN, p62, C9ORF72) (Figure 13). This reinforces a unifying model in which mutations that instigate cytoplasmic accumulation of RNA splicing proteins or impinge on their elimination by autophagy can culminate in ALS.

Interestingly, multiple proteins modified with dimethyl-arginines associated with both C9ORF72 and p62. Proteins bearing these dimethyl sites included several proteins genetically-linked to ALS such as FUS, HNRNPA1 and TAF15 (Table 6). This suggests

that arginine dimethylation of these multiple ALS-linked substrates may drive association with p62 and elimination of stress granules. As we describe for ALS-linked FUS mutants (Figure 10a-c,e), it is possible that some ALS-linked mutations in these other proteins disrupt the ability of p62 to recognize and eliminate stress granule-linked substrates by autophagy.

Repeat expansions in *C9ORF72* are the most common genetic cause of ALS (DeJesus-Hernandez et al., 2011; Renton et al., 2011). Over-expression of dipeptide repeats translated from these repeat expansions causes cytoplasmic accumulation of RNA binding proteins usually concentrated in the nucleus and can initiate the formation of inclusions (Chew et al., 2015; Mizielinska et al., 2014). However, repeat over-expression does not replicate all facets of the spinal cord motor neuron pathology and other symptoms observed in ALS patients (Peters et al., 2015). Cells depleted of C9ORF72 to mimic reduced C9ORF72 expression in patients (Haeusler et al., 2016) were incapable of targeting stress granules for p62-dependent autophagy (Figure 1,3). In ALS patients with C9ORF72 repeat expansions symmetrically arginine-methylated proteins accumulate in cytoplasmic foci often co-labeled with p62 (Figure 12d-f).

Our evidence, thus suggests that loss of C9ORF72 may be required to generate the complete spectrum of ALS pathology, by preventing stress granule components from being eliminated and thereby contributing to inclusion formation, misregulation of splicing and attendant pathology in these ALS patients.

2.5 Methods

Animal studies

p62 WT and p62$^{-/-}$ mice were a gift from Dr. Herbert W. Virgin (Washington University - School of Medicine) (Komatsu et al., 2007). Animal husbandry was performed in

accordance with federal guidelines and the University of Ottawa Animal Care Committee. Information of *p62 WT* and *p62*$^{-/-}$ mice used in the study is included in Table 8.

Table 8: Information of *p62 WT* and *p62*$^{-/-}$ mice used in the study

Genotype	Case Number	Sex	Age	Application
p62 WT	1	M	35-36w	Splicing (Figure 10i)
	2	F	24w +0d	Splicing (Figure 10i)
	3	F	33w +0d	Splicing (Figure 10i); Co-IPs (Figure 9i)
	4	F	7w +0d	Cerebellum - WB (Figure 10g)
	5	F	3w +0d	Cerebellum - WB (Figure 10g)
	6	F	9w +0d	Cerebellum - WB (Figure 10g)
	7	F	31w +0d	Hippocampus - WB (Figure 10g)
	8	F	31w +0d	Hippocampus - WB (Figure 10g)
p62 KO	1	M	37w +5d	Splicing (Figure 10i)
	2	F	37w +5d	Splicing (Figure 10i)
	3	M	42w +3d	Splicing (Figure 10i); Co-IPs (Figure 9i)
	4	F	7w +0d	Cerebellum - WB (Figure 10g)
	5	F	3w +0d	Cerebellum - WB (Figure 10g)
	6	F	9w +0d	Cerebellum - WB (Figure 10g)
	7	M	26w +3d	Hippocampus - WB (Figure 10g)
	8	F	6w +6d	Hippocampus - WB (Figure 10g)

Isolation of mixed motor neurons

Mice embryos were collected from pregnant mice between day E13.5 and E14.5. Spinal cords and cortices were dissected using Zeiss Stereo Discovery V20 microscope (Carl Zeiss, Oberkochen, Germany). Clean spinal cords were then placed in dissection buffer

(sucrose 40 g/L, dextrose 1 g/L and HEPES 2.4 g/L in PBS), minced with scissors and incubated with trypsin (Sigma-Aldrich) for 30 min at 37 ºC. Cells were separated using a 1 mL pipette and placed in S.C. NFeed (MEM/HBSS, Hyclone, hormones (insulin 10 ug/mL, transferrin 200 ug/mL, BSA 10 ug/mL, putrescine 32 ug/mL, selenium 26 ng/mL, T3 20 ng/mL, hydrocortisone 9.1 ng/mL, progesterone 13 ng/mL and NGF 5 ng/mL) Sigma-Aldrich, Horse serum 1.4%, Multicell and ABAM 1%, Multicell) neuronal culture media. Cells were then counted and seeded at 300000 cells/well in 12 well plates pre-treated with poly-D-Lysine 1 mg/mL (Sigma-Aldrich) and Matrigel 0.5% (S.C., Corning, VWR). After 4-7 days, mitotic cells were killed using Arabinofuranosylcytosine 1.4 ug/mL (S.C., Calbiochem).

Cell culture, transfections and treatments

HeLa (CCL2, ATCC) and MDA-MB-231 (HTB-26, ATCC) were cultured in Dulbecco's Modified Eagle's Medium containing 10% fetal bovine serum, 2 mM L-glutamine and penicillin-streptomycin. MDA-MB-231 (HTB-26, ATCC) cells were genetically deleted of ATG5 using CompoZr Zinc Fingers technology (Sigma-Aldrich). Motor neuron-derived MN-1 cells were cultured in DMEM (GIBCO) supplemented with 10% fetal bovine serum. All stable lines were maintained in 2 µg/ml of puromycin.

For transient transfection with DNA, Lipofectamine2000 (11668-019, Invitrogen) was used. Silencer Select siRNAs (Life Technologies) were transfected at 10 nM concentration with RNAiMax (13778150, Invitrogen). Cells were harvested for analyses 48 h post transfection. siRNAs and plasmids used in the study are listed in Tables 9-10.

Table 9: Antisense sequences of siRNAs used in the study

Target	Thermo Fisher Scientific: Silencer® Select ID and Catalog #

Negative Control (Ctl)	4390847
ATG5 #1	s18160 - 4392420; 5’ – UAUCUCAUCCUGAUAUAGCgt – 3’
ATG5 #2	s18158 - 4392420; 5’ – UAGAGCUUCAAUUGCAUCCtt – 3’
ATG7 #1	s20650 - 4392420; 5’ – UGGUGUUAUACAGUGUUCCaa – 3’
ATG7 #2	s20651 - 4392420; 5’ – UGAACUCCAAUGUUAAGCGag – 3’
C9ORF72 #1	s47490 - 4392420; 5’ – UAUGCAUCCAUAUUCUUCCtt – 3’
C9ORF72 #2	s47491 - 4392420; 5’ – UUUCCAUCAAAGAUUAAUGaa – 3’
FUS	s5403 - 4392420; 5’ – AAUUGUAACAUUCUCACCCag – 3’
Fus	s107707 - 4390771; 5’ – UUUACCAUCAAACCAGUCGat – 3’
FUS-3’UTR	5’ – UUGGGUGAUCAGGAAUUGGaa – 3’
NBR1	s57876 - 4392420; 5’ – UAUGAUACUGCACCAGACCcg – 3’
OPTN	s19720 - 4392420; 5’ – UUGAGUGCAACUUCAAGUCtc – 3’
P62 #1	s16960 - 4392420; 5’ – UCUUUUCCCUCCGUGCUCCac – 3’
P62 #2	s16962 - 4392420; 5’ – UUUAAUGUAGAUUCGGAAGat – 3’
PRMT5	s20375 - 4390824; 5’ – AGAGUUCAUAGGCAUUAGGtg – 3’
SMN	s231507 - 4390827; 5’ – UCCAAUAUCAUUCAAAAUCta – 3’

Table 10: Plasmids used in the study

Name	**Manufacturer**
FLAG/HA-FUS	Addgene (26374)
FLAG/HA-FUS-R521G	Addgene (26380)
FLAG/HA-FUS-R521H	Addgene (26381)
FLAG/HA-FUS-R216C	Created by PCR from FLAG/HA-FUS
FLAG/HA-FUS-R218K	Created by PCR from FLAG/HA-FUS
FLAG/HA-FUS-R216C+R218K	Created by PCR from FLAG/HA-FUS
GFP-DDX3	Subcloned DDX3 into pcDNA 3.1 GFP plasmid
GFP-P62	(Pankiv et al., 2007)

GFP-P62ΔUBA	(Pankiv et al., 2007)
GFP-P62ΔLIR	(Pankiv et al., 2007)
GFP-SMN	Subcloned from pcDNA3.1-Myc-SMN (Bachand, Boisvert, Cote, Richard, & Autexier, 2002)
GFP-SMNΔTdr	Subcloned from GFP-SMN
pGST2	(Sheffield, Garrard, & Derewenda, 1999)
GST-FUS	Addgene (44978)
HA-P62	Addgene (28027)
Myc-DDK-C9ORF72	OriGene (RC209700)
Myc-SMN	(Bachand et al., 2002)
pLKO.1-sh(Luciferase)	TRC (The RNAi Consortium)
pLKO.1-sh(PRMT5)	TRC (The RNAi Consortium)

For all stress granule experiments, HeLa and MDA-MB-231 cells were induced with 0.5 mM sodium arsenite (71287, Sigma-Aldrich) for 30 min followed by a PBS wash and recovery in complete DMEM up to 1 h. Primary cultures of mixed motor neurons were induced with 0.5 mM sodium arsenite (71287, Sigma-Aldrich) for 1 h followed by a PBS wash and recovery up to 30 min. At least 100 cells were counted per experiment for quantification of cells containing stress granules. HeLa and MN-1 cells were treated with Bafilomycin A1 (196000, EMN Millipore) for 16 h at 400 nM. HeLa cells were treated with (i) Chloroquine (sc-205629A, Santa Cruz Biotechnology) for 16 h at 20 μM, (ii) MTA (Sigma-Aldrich) for 48h at 1 mM, (iii) PRMT5 inhibitor - EPZ015666 (SML1421, Sigma-Aldrich) for 48 h at 3 μM and (iv) Ubiquitin E1 inhibitor - PYR-41 (N2915, Sigma-Aldrich) for 3 h at 50 μM.

Lentiviral vector production and transduction

HeLa cells stably expressing shRNA targeting PRMT5 (sh(PRMT5)) or luciferase (sh(luciferase)) were generated via lentiviral transduction. Lentivirus was produced through transfection of 293T cells with the packaging plasmid pLKO.1-sh. The media was harvested 48h post transfection and filtered through a 0.45 uM PES membrane. HeLa cells were seeded in 10 cm plates (250 000 cells) 24 h before infection. The cells were infected with the lentivirus containing media along with 8 µg/mL of polybrene. After 48 h, media was changed and cells were selected with puromycin (2 µg/mL). Equivalent amounts of virions encoding shRNA targeting Luciferase as a control was used to transduce HeLa cells. Knockdown in stable lines was validated by RT-PCR and immunoblotting.

DNA constructions

The plasmid pDEST-FUS-WT was obtained from Addgene (#26374). Three different arginine (R) mutations were generated: (i) arginine to cysteine at position 216 (R216C), (ii) arginine to lysine at position 218 (R218K) and (iii) both mutations (R216C and R218K) by PCR using oligos indicated in the primers table. PCR reactions were digested with DPNI for 1 h and transformed in DH5α. DNA was purified from colonies and sent for sequencing. Constructs that were successfully mutated were then purified by MaxiPrep (Qiagen) as per manufacturer's guidelines.

Reverse Transcription (RT)- PCR and quantitative RT- PCR

After RNA extraction with Trizol, RT-qPCR was performed with Superscript II Reverse Transcriptase (Invitrogen) and GoTaq qPCR Master Mix (Promega, A6002). Fold change of transcripts was calculated using the ΔΔCt method, normalized to 18SrRNA. Sequences of primer pairs used in the study are listed in Table 11.

Table 11: Sequences of primer pairs used in the study

Target gene / locus		Sequence (5' – 3')	Application
18S rRNA	Fwd	GTAACCCGTTGAACCCCATT	
	Rev	CCATCCAATCGGTAGTAGCG	
C9ORF72 All	Fwd	CCCACTTCATAGAGTGTGTGTTG	
	Rev	TTCCATTCTCTCTGTGCCTTC	
C9ORF72 Short	Fwd	GAAATCACACAGTGTTCCTGAAGAA	
	Rev	ATCTGCTTCATCCAGCTTTTATGA	
C9ORF72 Long	Fwd	CATGGCTCAGGATACGATCA	Transcript-specific qRT-PCR primers
	Rev	GGAAGGCTTTCACTAGAGTGTCTC	
GAPDH	Fwd	ATCTTCTTGTGCAGTGCCAG	
	Rev	TTTGCCACTGCAAATGGCAG	
p62/ Sqstm1	Fwd	AGATGCCAGAATCGGAAGGG	
	Rev	GAGAGGGACTCAATCAGCCG	
PRMT5	Fwd	GGAACTCTGAAGCGGCTATG	
	Rev	TGATTAGACGGGAGGTCAGC	
Zcchc6/ Tut7	Fwd	GCCCACAGTTCAAAGGCTCT	Splice variant-specific RT-PCR primers
	Rev	GTGTCCTGTGCCATGAACCT	
FUS-R216C	Fwd	ACCGTGGAGGCTGCGGCAGGGGT	FUS mutant-specific PCR primers
	Rev	ACCCCTGCCGCAGCCTCCACGGT	
FUS-R218K	Fwd	GGAGGCCGCGGCAAGGGTGGCAGT	
	Rev	ACTGCCACCCTTGCCGCGGCCTCC	
FUS-216C+R218K	Fwd	CCGTGGAGGCTGCGGCAAGGGTGGCAGT	
	Rev	ACTGCCACCCTTGCCGCAGCCTCCACGG	

For RT-PCR, cDNA was synthesized with random hexamers and Promega AMV cDNA synthesis (Promega, M5101). PCRs were then set up using Promega GoTaq DNA

Polymerase (M5101) according to manufacturer's instructions. RT-PCR conditions were as follows for validation of splicing targets: 95 °C for 2 min, (95 °C for 30 sec, 55 °C for 30 sec, 72 °C for 45 sec) × 32 cycles, 72 °C for 10 min. Specific RT-PCR conditions used for particular primers are available upon request. Amplicons were run on a 2% agarose gel (containing 5 µL of EtBr 20 mg/mL) and visualized under UV light. For analysis of splice variants, densitometry was performed to measure percentage exon inclusion with or without normalization to wild-type condition.

Isolation of autophagosomal fractions

Autophagosomes were fractionated as described(Sahu et al., 2011). Briefly, twenty 160 cm^2 plates of HEK293 cells were harvested in 0.25 M sucrose 10 mM HEPES pH 7.2, washed several times in the same solution, transferred into 0.25 M sucrose containing protease inhibitor cocktail (Roche, EDTA-free) and disrupted by nitrogen cavitation (Parr Instruments, 100 p.s.i. 30 s, 50 p.s.i. 30 s, 25 p.s.i. 8 min). Lysate was centrifuged twice at 2,000 × g to eliminate intact cells and large debris. Supernatant was then centrifuged at 17,000 × g (12 min) to pellet organelles. The pellet was resuspended in 0.25 M sucrose 10 mM HEPES pH 7.2 and treated with a mixture of RNAse A/T1 (Fermentas) for 10 min, 37 °C. Organelles were then loaded at the bottom of a discontinuous Histodenz density gradient (26, 24, 20 and 15%) and centrifuged at 90,000 × g for 3 h in an SW41 rotor (Beckman). Fractions at the interface of 15–20% and 20–24% densities are enriched in autophagosomes and autophagolysosomes, respectively. Autophagosome-enriched fractions were used for all analyses.

Immunofluorescence and proximity ligation assay (PLA)

Five micron sections were cut from formalin-fixed, paraffin-embedded blocks of cerebellum and hippocampus and mounted onto coated glass slides. Paraffin embedded sections were deparaffinized in xylene (3 × 5 min) and rehydrated through graded EtOH to deionized water: 100% EtOH (2 x 5 min), 95% EtOH (2 x 5 min), 80%, 70% and 50% EtOH (1 x 5 min). Additionally, frozen tissues were sectioned and mounted onto coated glass slides prior to fixation in 4% PFA in PBS (10 min). Antigen retrieval was performed in 0.05% Tween 20, 10 mM sodium citrate buffer pH 6.0 (prepared with 0.1 M citric acid) using a decloaking chamber (Biocare Medical, Walnut Creek, CA,USA) at 125 ºC for 30 s and 90 ºC for 10 s. The sections were cooled to room temperature and rinsed with deionized water 5 times and PBS once. They were permeabilized in 0.2% Triton-X-100 in PBS for 45 min, washed three times in PBS, blocked in 10% normal goat serum (S-1000, Vector Laboratories) in PBS for 1 h and incubated with primary antibodies in blocking solution overnight at 4 ºC. The sections were then washed thrice in PBS, incubated in fluorescently labelled secondary antibodies (1/250 dilution in PBS for 1h), washed thrice in PBS, incubated in 0.5 µg/ml DAPI (D9542, Sigma-Aldrich) in PBS for 10 min, washed twice in PBS and mounted with ProLong Diamond Antifade (P36961, Invitrogen).

Cells were prepared for microscopy as previously described(D. Gibbings, Leblanc, et al., 2012; D. Gibbings, Mostowy, et al., 2012). Cells were grown on 0.17 mm glass coverslips prior to fixation in 4% PFA in PBS (10 min). Cells were rinsed in PBS and incubated 10 min in 0.2% Triton-X-100 in PBS containing 20 mM NH_4Cl. After washing with PBS, cells were blocked in 5% milk in PBS for 1 h, washed in PBS and incubated with 1/200 dilution of primary antibody or control non-specific antibody overnight at 4 °C. For PLA, cells were subsequently processed as per manufacturer's instructions (DUO82049, Sigma-Aldrich). For immunofluorescence, cells were subsequently washed

in PBS thrice and incubated with 1/300 dilution of secondary antibodies (goat anti-mouse Alexa Fluor 488 or 546, anti-rabbit Alexa Fluor 488 or 546 or donkey anti-goat Alexa Fluor 488 [Invitrogen]) for 1 h. After three PBS washes, cells were mounted with Vectashield media (H-1200, Vector Laboratories) and imaged on a Zeiss AxioObserver Z1 epifluorescent microscope, a Zeiss 510 confocal microscope or a Zeiss LSM880 AxioObserver Z1 confocal microscope. At least 3 images were taken for each experiment.

Quantification of cytoplasmic inclusions in ALS patients

P62 inclusions in the cytoplasm were manually counted across 3-10 frames of images per n. About 10-80 P62 inclusions were counted per n. The fraction of these P62 inclusions positive for symmetric-arginine dimethylation was then manually ascertained.

Quantification of microscopic data

Immunofluorescent images of punctae or stress granules containing P62, C9ORF72 and TIAR were first segmented using SQUASSH (Rizk et al., 2014). Segmented objects were then binarized prior to counting them using 'Analyze Particles' function of Fiji. Binarized images of objects from one channel were intersected with respective binarized objects from the other channel using 'AND' function of Fiji. The resulting number of overlapping punctae were then used to calculate % overlap. PLA dots were quantified using Duolink® ImageTool (DUO90806, Sigma-Aldrich).

3D reconstruction of Z-stacks

Z-stack images separated by 0.2 μm were acquired on a Zeiss LSM880 AxioObserver Z1 confocal microscope with Airyscan. 3D surfaces were rendered from Z-stack image files using Imaris.

Electron microscopy

For transmission electron microscopy, cells were fixed in 2.5% glutaraldehyde in a 0.1 M sodium cacodylate buffer and then incubated in OsO4 (2%) in a 0.1 M sodium cacodylate buffer. After washing in 0.1 M sodium cacodylate the cells were dehydrated in increasing concentrations of alcohol. The most concentrated alcohol was replaced with acetone. The material was permeabilized with increasing concentrations of Araldite diluted in acetone. Finally, the tissues were embedded in Araldite (Huntsman Advanced Materials LLC, United States). Ultra-thin sections (80 nm) were prepared using an Ultracut Leica UC6 ultramicrotome (Leica Microsystems, Germany) and placed onto copper grids coated with Formvar film. Sections were stained with uranyl acetate and lead citrate solutions and examined with a transmission electron microscope (JEOL JEM 1230, Japan).

For immungold labeling, cells were fixed in 4% paraformaldehyde and 0.5% glutaraldehyde in 0.1 M sodium cacodylate buffer (pH 7.4). After dehydrating the samples with increasing concentrations of ethanol, the pellets were embedded in LR White Resin. The blocks were sectioned with ultracut (Leica EM UC 6) using a diamond knife. The thin sections were mounted on Formvar-coated nickel grids. The grids were floated on drops of 1% BSA/0.01% Tween 20 for 1 h, then incubated for 1 h with primary antibody or a mixture of rabbit and mouse primary antibody diluted with PBS-0.05% Tween 20 (PBST) diluted 1/200. Next, the samples were washed in PBST and incubated for 2 h with a mixture of secondary antibody in PBST. The secondary antibodies were 12-nm colloidal gold-conjugated goat anti-rabbit IgG antibody (111-205-144, Jackson) and 18-nm colloidal gold-conjugated goat anti-mouse IgG antibody (115-215-068, Jackson) that were applied at a dilution of 1/50 for 2 h at room temperature. For control

staining the primary antibody was omitted and secondary only was used. After antibody labeling, the grids were washed three times in PBST, rinsed in distilled water, stained with uranyl acetate and lead citrate, and imaged with a transmission electron microscope (JEOL JEM 1230, Japan).

Quantification of electron microscopy

Forty-six electron microscopy images containing any signal for P62 or FUS were collected at random from the cytoplasm of cells and 193 electron-dense clusters, autophagolysosomes or cytoplasmic labels were counted. P62 and FUS staining was evaluated as being associated with electron dense stress granule-like structures whenever it or they were directly localized within a cluster of electron dense material of at least 100 nm resembling structures labeled in other cells with stress granule markers FUS and FMRP. P62 and FUS were considered as within autophagolysosomes if it was within a translucent membrane-bound structure of > 200 nm containing heterogenous contents. If more than one gold bead for P62 or FUS was associated with a single structure it was counted as a single co-localization event. P62 and FUS not localized to electron dense clusters or membrane bound organelles was labeled as cytoplasmic. If P62 and FUS were within 100 nm of each other in the cytoplasm they were considered co-localized.

Co-immunoprecipitation

Cells were washed in cold PBS and lysed in NP40 lysis buffer (50 mM Tris-HCl pH 7.5, 150 mM NaCl, 1% NP40, Roche Complete Protease Inhibitor Cocktail Tablet EDTA free) for 30 min at 4 °C and centrifuged at 1000 × g, 5 min prior to immunoprecipitation. Mouse brain and spinal cord tissues were homogenized in NP40 lysis buffer using Dounce homogenizer and centrifuged at 6000 × g, 10 min at 4 °C. For IP, 500 µg lysate

was pre-cleared with 5 µl (0.15 mg) protein G-Dynabeads (10004D, Life Technologies) for 20 min at 4°C and estimated for protein content (DC Protein Assay, Bio-Rad). Every 500 µg lysate was incubated with 1 µg antibody for 3 h at 4°C before incubation with 20 µl wet volume of protein G–Dynabeads (1.5 h, 4 °C). Alternatively, lysates with GFP or Myc-tagged proteins were directly incubated with 20 µl GFP-Trap®_A slurry (gta-20, ChromoTek) or 50 µl wet volume of anti-c-myc magnetic beads (PI88842, Thermo Fisher Scientific) for 2 h at 4 °C. Beads were collected by centrifugation or using a magnetic support (12321D, Thermo Fisher Scientific) and washed with 200 µl lysis buffer three times. SDS-sample buffer was added and the samples were boiled at 99 ºC for 5 min prior to Western blot analysis.

For RNAse treatments, equal amounts of lysate were untreated or treated with RNase A/T1 Mix (FEREN0551, Fermentas, 28 µg/ml RNase A and 70 U/ml RNase T1) for 15 min at 37 ºC prior to antibody incubation. RNA digestion was confirmed on a 1% agarose gel by electrophoresis.

Quantification of co-immunoprecipitation

Densitometry-based analyses were employed. For each protein in an experiment, an area encompassing the maximum band size was selected and mean intensity of this area was measured using the 'Histogram' function in Photoshop. Mean intensities of interacting proteins from control IgG immunoprecipitates were subtracted from those of respective test immunoprecipitates followed by normalization to the mean intensity of the target of the immunoprecipitating antibody.

Whole cell extracts and Western blotting

Cells were washed in cold PBS and lysed in 5 mM Tris pH 7.4, 75 mM NaCl, 0.5 mM EDTA, 0.5% Triton-X-100 with protease inhibitors. Lysate was then spun down at 1000 × g, 5 min at 4 ºC to estimate the protein content of supernatants. Where noted, cells were lysed in RIPA lysis buffer (10 mM Tris pH 7.4, 100 mM NaCl, 1 mM EDTA, 1% NP-40, 0.5% NaDOC, 0.1% SDS, 10 µg/ml PMSF with protease inhibitors) and spun down at 15000 × g, 10 min at 4 ºC. Mouse cerebellar and hippocampal tissues in NP40 lysis buffer were vortexed vigorously with 2 stainless steel beads per tissue (SSB32, Next Advance) every 10 min for 1 h, followed by end-to-end toppling at 4 ºC for 1 h. Homogenates in NP40 lysis buffer were then centrifuged at 6000 × g, 10 min at 4 ºC. For Western blotting, equal amounts of protein samples were resolved on 10% (w/v) acrylamide gels, transferred to PDVF membrane (IPVH00010, EMD Millipore), blocked with 5% milk in TBST (10 mM Tris-HCl pH 8, 150 mM NaCl, 0.05% Tween 20) for 1 h and probed with primary antibody in TBST overnight at 4 °C. All antibodies were used at 1/1000 dilution. Blots were then washed in TBST, probed with HRP labelled secondary antibodies (goat anti-mouse, goat anti-rabbit and donkey anti-goat), washed again in TBST and imaged with HRP substrate (WBLUR0100A, EMD Millipore) on an ImageQuant LAS 4000 system (GE Healthcare). Mean intensity levels were measured for densitometry-based normalization to tubulin levels. For each protein in an experiment, an area encompassing the maximum band size was selected and mean intensity of this area was measured using the Photshop ‘Histogram’ function. Full size uncropped blots are shown in Figure 14. Antibodies used in the study are listed in Table 12.

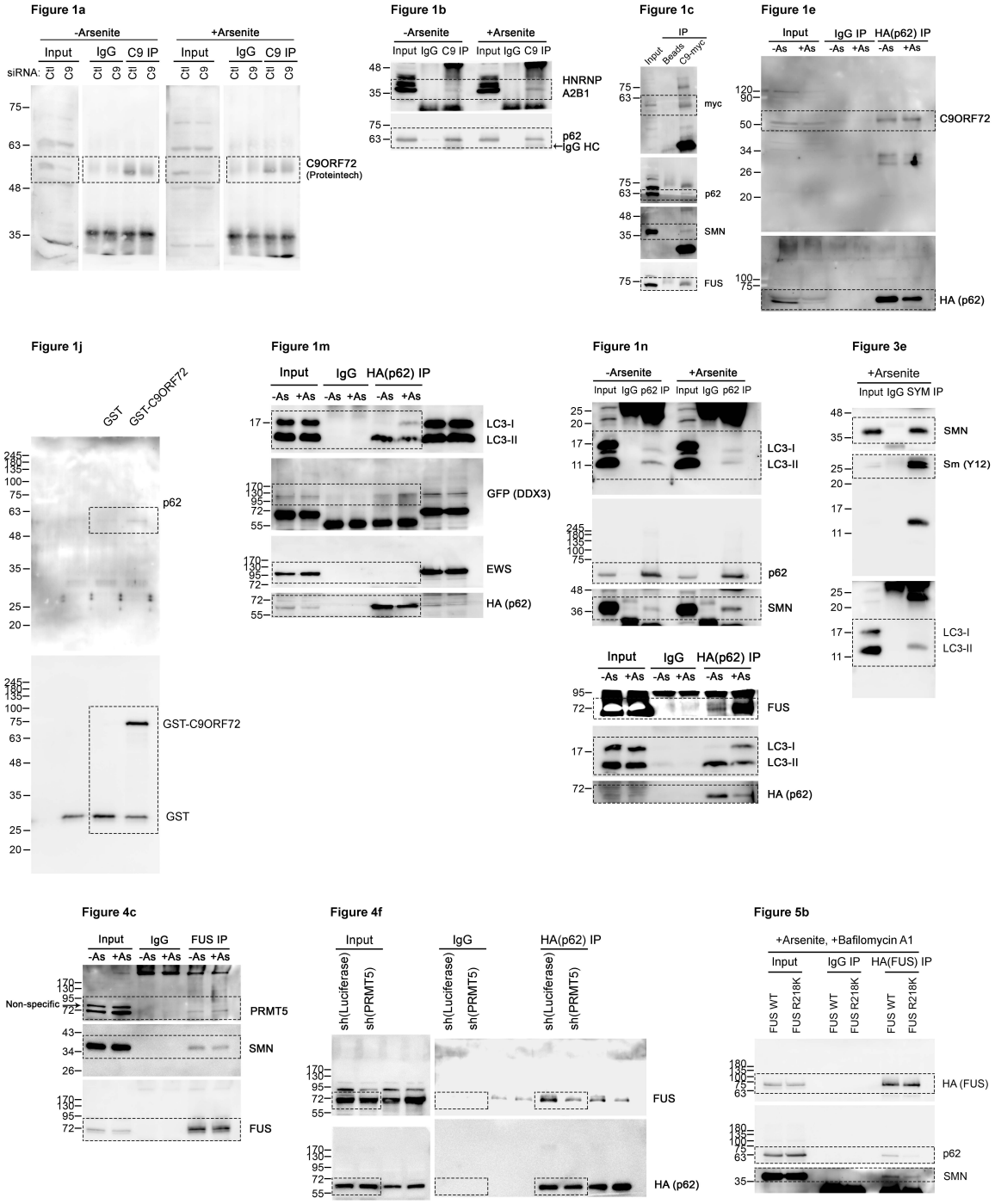

Figure 14: Uncropped Western blot images

Uncropped blots are shown for key experiments including co-immunoprecipitations and GST-pulldown assays. Molecular weight markers for these specific blots are shown only

in the uncropped versions (in this figure), unlike all the remaining blots where the size markers are included directly in the figure panels.

Table 12: Antibodies used in the study

Target	Manufacturer	Application
Dimethyl-Arginine, asymmetric – ASYM24/25	(Boisvert et al., 2003; Cote, Boisvert, Boulanger, Bedford, & Richard, 2003)	WB, IF
C9ORF72	Santa Cruz Biotechnology (sc-138763)	WB, IF, PLA, IP/MS
C9ORF72	Proteintech (22637-1-AP)	WB, IF, Co-IP
C9ORF72	Proteintech (66140-1-Ig)	IF
C9ORF72 Long	(Xiao et al., 2015)	WB
DDX3	Bethyl Laboratories (A300-474A)	WB, IF
EWS	Bethyl Laboratories (A300-417A)	WB
FMRP	EMD Millipore (MAB2160)	IF, EM
FUS	Bethyl Laboratories (A300-302A)	WB, Co-IP, IF, PLA, EM, IP/MS
GAPDH	BioLegend (919501)	WB
GST	(Cote & Richard, 2005)	WB
HA	EMD millipore (05-904)	WB, Co-IP, IF, PLA, IP/MS
HuR	Santa Cruz Biotechnology (sc-5261)	IF
LC3	Sigma-Aldrich (L7543)	WB, IF, PLA
LC3	Cell Signaling Technology (3868S)	WB, IF, PLA
Myc	ATCC Hybridoma (9E10)	WB
NBR1	Abnova (H00004077-M01)	IF, PLA, WB
Optineurin	Abcam (ab23666)	IF, WB
P62	BD Transduction Laboratories (610833)	WB, IF, PLA, IHC, EM

P62	Sigma-Aldrich (P0067)	WB, Co-IP, IF, PLA
PABP	Santa Cruz Biotechnology (sc-32318)	IF
PRMT5	(Boisvert et al., 2002)	WB
Smith Antigen [Y12]	Hybridoma from Robin Reed (Harvard University, Boston, MA)	WB
SMN	BD Biosciences (610647)	WB, Co-IP
SMN	Santa Cruz Biotechnology (sc-7804)	IF
Dimethyl-Arginine, symmetric – SYM10/11	(Boisvert et al., 2002; Boisvert et al., 2003)	WB, Co-IP, IF
Dimethyl-Arginine, symmetric	Cell Signaling Technology (13222S)	IF
TDP-43	Sigma-Aldrich (T1580)	IF
TIAR	Cell Signaling Technology (8509S)	IF
Tubulin	Thermo Fisher Scientific (PA5-22060)	WB
Ubiquitin	Cell Signaling Technology (3936S)	IF, WB
IgG mouse	eBioscience (14-4714-82)	Co-IP, IF, PLA, IP/MS
IgG rabbit	GeneTex (GTX35035)	Co-IP, IF, PLA, IP/MS
HRP secondary	Jackson ImmunoResearch (111-035-144, 115-035-174); GenScript (A00178)	WB
Fluorescent secondary	Invitrogen (Alexa Fluor® Dyes)	IF

p62 and SMN protein purification

P62 and SMN1 expressing plasmids were ordered from GenScript with the codon optimized for overexpression in E. coli. The DNA constructs contain a BamH1 and a Xho1 restriction site flanking each gene. After amplification of the vectors, the plasmids were digested with BamH1 and Xho1 and the DNA fragments were sub-cloned in a vector enabling the expression of P62 and SMN1 as TEV cleavable GST fusion proteins

(Sheffield et al., 1999). pGST2-p62 and pGST2-SMN1 were transformed in Rosetta cell and plated on amp-chloramphenicol. Pre-cultures were set up from colonies to grow overnight in 50 ml LB at 37 ºC. Culture volumes were increased to 500 ml and grown until OD 0.5. Temperature was then reduced to 18 ºC for induction with 0.1 mM IPTG (800-050-IG, Wisent) overnight. 1 L cultures were spun down; pellets were resuspended in binding buffer (50 mM NaPi pH 7, 500 mM NaCl, 10% Glycerol), sonicated thrice 1 min each at power 7 and centrifuged at 27216 × g for 30 min, 4 ºC. Soluble fractions were incubated with GST beads for 90 min at 4 ºC. For p62, beads were then washed and eluted in 10 mM glutathione, 50 mM Tris pH 8.6, 150 mM NaCl for 1 h at 4 ºC. The eluate was dialyzed overnight with and without TEV in 50 mM Tris pH 8, 150 mM NaCl, 0.5 mM EDTA and 5mM β-mercaptoethanol. Uncleaved GST-p62 (0.81 µg/ul) was frozen in 10% glycerol. Cleaved p62 was separated from GST by gel filtration and frozen in 10% glycerol (0.21 µg/ul). For SMN1, beads were washed and eluted overnight in 1M NaCl, 50 mM Tris pH 7 at 4 ºC to yield recombinant SMN1 (0.9 µg/ul). The protein was frozen in 10% glycerol.

GST-pulldown assay with recombinant proteins

Recombinant p62 was mixed in buffer A (20 mM HEPES pH 7.9, 150 mM NaCl, 0.5 mM EDTA, 1 mM DTT, 10% glycerol, 0.1% triton-X-100) and pre-cleared with 5 µl of a 50% slurry of glutathione-agarose beads(16100, Pierce) and 5 µg of GST for 2 h at 4 ºC with end-over-end mixing. Following centrifugation at 9000 × g, 10 min, 4 ºC, pre-cleared supernatants were collected and incubated with 5 µl of a 50% slurry of glutathione-agarose beads and either 0.25 µg of GST or GST-C9ORF72 (H00203228-P01, Abnova) for 1 h at 4 ºC. Upon precipitation, the mixtures were washed 5 times with buffer A, 2 min spins at 900 × g.

Recombinant GST or GST-p62 was bound to glutathione-agarose beads in buffer B (50 mM Tris pH 7.5, 200 mM NaCl, 0.1% triton-X-100) by end-to-end toppling at 4 ºC for 1 h 30 min. Beads were previously blocked with 3% BSA in PBS (overnight at 4 ºC). Following the incubation, bound beads were spun down at 9000 × g, 5 min, 4 ºC, and washed 3 times for 5 min each with buffer B, 1 min spins at 9000 × g. Recombinant SMN was pre-cleared with blocked glutathione-agarose beads bound to GST for 20 min at 4 ºC. Following centrifugation at 9000 × g, 5 min, 4 ºC, pre-cleared supernatant was collected and incubated with previously prepared glutathione-agarose beads bound to GST or GST-p62 for 1 h at 4 ºC. Upon precipitation, the mixtures were washed 5 times with buffer B, 1 min spins at 9000 × g.

The bound proteins were then analyzed by SDS-PAGE.

Peptide-pulldown assay

The peptide - KGRGRGRGRG was custom ordered from GenScript in two forms: all 4 arginines (i) symmetrically dimethylated, or (ii) asymmetrically dimethylated. 1mg of each of the peptides in 400 µl of PBS was incubated with 400µl of Affi-Gel 10 (1536099, Bio-Rad) media washed in cold deionized water to make 50% slurry. The uniform suspension was left to rotate on a wheel overnight at 4 ºC. 40 µl of 1M ethanolamine HCl in 0.5M Tris pH 8 was added to the slurry to block any active esters and left rotating for 2+ h at 4 ºC. Peptide bound media was then washed in 500 µl PBS thrice, resuspended in 1 ml of 0.1% sodium azide in PBS and stored at 4 ºC. For the pulldown assays, affi-gel 10 media – 10 µl per reaction was washed in PBS thrice and resuspended in 1 ml of binding buffer (20 mM HEPES pH 7.9, 200 mM NaCl, 10% Glycerol, 0.05% Tween 20) prior to pre-clearing 375 ng of recombinant p62 and/or SMN for 20 min at 4 ºC. Precleared proteins were separated from the beads upon centrifugation at 9000 × g, 5

min. As a positive control, 1% of the supernatant was frozen; remaining was incubated with 30 µl of affi-gel 10 media bound to (i) no peptide, (ii) symmetrically dimethylated or (iii) asymmetrically dimethylated RG(x4) peptide, on a rotating wheel for 1 h at 4 ºC. Mixture was then washed 6 times, each in 500 µl of binding buffer with 5 min rotations at 4 ºC and 9000 × g, 1 min spins at 4ºC. SDS-sample buffer was added and the reactions were boiled at 99 ºC for 5 min prior to Western blot analysis.

***In vitro* methylation assay**

a) **Substrate and enzyme preparation:** GST-FUS-WT (44978, Addgene) and pGST2 with no insert were transformed in BL21 strain. Colonies were picked to grow overnight cultures in 50 ml LB at 37 ºC. Culture volumes were increased to 1000 ml and grown at 37 ºC until OD 0.5. Protein expression was induced with 0.1 mM IPTG for 5 h at 37 ºC. Cultures were spun down at 1700 × g for 20 min, pellets lysed in PBS containing protease inhibitors, sonicated 5 times 15 s each with 10 s intervals at power 3 and centrifuged at 15309 × g for 20 min at 4 ºC. Supernatants were solubilized in 1% Triton-X-100 for 30 min, 4 ºC and incubated with 500 µl GST beads (16100, Pierce) overnight at 4 ºC. Washed beads were then stored in PBS at 4 ºC. Active human PRMT5 in complex with MEP50 was purchased (SRP0145, Sigma-Aldrich).
b) **Enzymatic reactions:** Equal amounts of protein on agarose beads were each incubated with 1 ug PRMT5-MEP50 and SAM in a 30 µl reaction buffer (50 mM Tris pH 8, 1 mM DTT, 10 mM NaCl) for 1 h at 30 ºC and 3 h at 37 ºC. For Western blot and mass spectrometry analyses, 80 uM cold SAM (A7007, Sigma-Aldrich) was used while 1 µCi SAM[3H] (NET155V250UC, PerkinElmer) was used per radioactive reaction. Reactions were stopped by adding SDS-sample buffer. To detect

radioactive signal, samples transferred to PVDF membrane were dried 1h, sprayed thrice with EN^{3}HANCE Spray (6NE970C, PerkinEmer) while allowing drying for 30 min and rotating 90º following each spray. Tritium signal was further enhanced with Transcreen LE (Z374253, Sigma-Aldrich) during the 2 week exposure at -80 ºC. Alternatively, radioactive polyacrylamide gels were soaked in EN^{3}HANCE liquid (6NE9701, PerkinElmer) for 30 min at room temperature, washed 6 times in water (5 min $\times$ 3 times and 15 min $\times$ 3 times), vacuum dried for 3 h at 60 ºC and exposed for 2 weeks at -80 ºC.

Nuclear/cytoplasmic subcellular fractionation

Cells washed with cold PBS were lysed in hypotonic lysis buffer (10 mM HEPES pH 7.9, 10 mM KCl, 1.5 mM $MgCl_2$, 0.5 mM DTT, protease inhibitors), incubated on ice for 10 min and homogenized with 15 strokes of a Dounce glass homogenizer. Supernatant was collected as the cytoplasmic extract after centrifuging the lysate at 2000 $\times$ g for 10 min. To collect the nuclear extract, pellet was washed in hypotonic lysis buffer, further centrifuged at 2000 $\times$ g for 10 min, resuspended in NP-40 buffer (50 mM Tris pH 8, 400 mM NaCl, 5 mM EDTA pH 8, 1% NP-40, 0.2% SDS) and sonicated for 15 s at power 3. For Western blotting, the fractions were run in equal volume proportions. For quantification, cytoplasmic fractions were normalized to GAPDH while nuclear fractions were normalized to methylated histone H3 on lysine 27 – H3K27.

Quantification of nuclear/cytoplasmic fluorescence

DAPI nuclear staining and brightfield images were used respectively to draw nuclear and cytoplasmic regions of interest on individual cells. Mean fluorescence intensity was

measured for each of the two regions per cell using Fiji and thereby represented as a ratio.

Mass spectrometry

Chemicals used include urea, dithiothreitol (DTT), ammonium bicarbonate (ABC), and iodoacetamide (IAA), all of which were purchased from Sigma-Aldrich (St. Louis, MO). HPLC grade water and acetonitrile (ACN) were from J.T Baker. Formic acid (FA) and citric acid were obtained from Merck (Darmstadt, Germany). Trypsin was purchased from Promega (Madison, WI). All the chemicals were of analytical purity grade except ACN and FA, which were of HPLC grade.

Sliced protein bands were digested as reported previously(Shevchenko, Tomas, Havlis, Olsen, & Mann, 2006). Briefly, gel slices were cut into smaller pieces, shrunk using 100% ACN, then reduced and alkylated sequentially. Trypsin solution of 10 ng/μL was used to cover the gel pieces for digestion overnight. Tryptic peptides were then extracted using 80% ACN. The solution was then dried down and reconstituted in 20 μL 0.5% formic acid, and 4 μL was loaded for MS analysis.

LCMS Analysis: Eksigent 2D+ nanoLC system (Dublin, CA) was connected to a Q-Exactive mass spectrometer (Thermo Electron, Waltham, MA), equipped with a nano-electrospray interface operated in positive ion mode. The solvent system consists of buffer A of 0.1% FA in water, and buffer B of 0.1%FA in 80% acetonitrile. Dried down protein digests were acidified with 0.5% (v/v) formic acid and loaded on a 75 μm I.D. × 150 mm fused silica analytical column packed in-house with 1.9 μm ReproSil-Pur C18 beads (100 Å; Dr. Maisch GmbH, Ammerbuch, Germany) at a flow rate of 500 nL/min for 15 min. Then the flow rate was changed to 200 nL/min to perform the peptide separation. Gradient elution was set as 5–35% buffer B per hour. The spray voltage was

set to 2.0 kV and the temperature of the heated capillary was set to 300 °C. The instrument method consisted of one full MS scan from 300 to 1800 m/z followed by data-dependent MS/MS scan of the 12 most intense ions, a dynamic exclusion repeat count of 1 in 30 s, and an exclusion duration of 30 s. The full mass was scanned in an Orbitrap analyzer with R = 70,000 (defined at m/z 400) for MS1 and 17,500 for MS2. To improve the mass accuracy, all the measurements in the orbitrap mass analyzer were performed with a real time internal calibration by the lock mass of background ion 445.120025. The charge state rejection function was enabled, and charge states with unknown and single charge state were excluded for subsequent MS/MS analysis. All data were recorded with Xcalibur software (Thermo Fisher Scientific, San Jose, CA).

Data Analysis: The peak lists of the raw files were processed and analyzed with MaxQuant (Version 1.5.2.8) (Cox & Mann, 2008) against UniProt human protein database, including commonly observed contaminants. Cysteine carbamidomethylation was selected as a fixed modification; methionine oxidation, protein N-terminal acetylation and arginine methylation were set as variable modifications. Enzyme specificity was set to trypsin, not allowing for cleavage N-terminal to proline. Up to two missing cleavages of trypsin were allowed. The precursor ion mass tolerances were 7 ppm, and fragment ion mass tolerance was 20 ppm. Razor and unique peptides were used for LFQ quantitation. FDR was set at 0.01 on protein, peptide and modification of specific sites; a minimum length of seven amino acids was used for peptide identification. For protein identification, if the identified peptide sequence of one protein was equal to or contained another protein's peptide set, these two proteins were grouped together by MaxQuant and reported as one protein group.

Bioinformatic analyses of splicing and FUS-motif enrichment

To analyze potential splicing events using published microarray data from p62 knockout mice the following MoGene-1_0-st-v1 chip files were used: (GSM1522557, GSM1522558 p62 knockout; GSM1522560, GSM1522562 wild type). The method outlined in (Lockstone, 2011) with Affymetrix Power Tools 1.17.0 and MoGene-1_0-st-v1.r4 annotation files was used to identify splicing candidate genes. Genomic locations for probesets were taken from Affymetrix annotations: MoGene-1_0-st-v1.na35.mm10.probeset.csv. Genomic locations for exons and genes, as well as gene to probeset associations were downloaded from ENSEMBL BioMart mmusculus_gene_ensembl, dec2015.archive.ensembl.org. Genomic introns sequences were determined by selecting the genomic interval of each ENSEMBL gene with status "known" and removing intervals for exons associated with that gene. Genes were considered putatively spliced if they had MIDAS p-values < 0.01. Instances of the motif GTGGT identified as the most frequent FUS-binding motif (Lagier-Tourenne et al., 2012) in intronic sequences were then counted and normalized to the total sequence length of mRNAs.

The list of 957 mRNAs whose splicing was putatively affected by FUS was taken from Table 6 in (Lagier-Tourenne et al., 2012) and 862 were found to be potentially mappable to the above derived genes based on MGI gene symbols in the ENSEMBL tcid annotations. 1481 putatively spliced MGI genes were identified in our analysis; there are 22509 unique MGI genes in the microarray gene expression set. Ninety-seven of the genes whose splicing was putatively affected by FUS (Lagier-Tourenne et al., 2012) were also found among the 1481 putatively spliced genes in p62 knockout mice. The predicted probability distribution was generated using the R dhyper function and the above parameters. The probability of seeing 97 or greater overlapping gene symbols by chance is 1.57e-07. The cumulative fraction of -log10 of the best probeset MIDAS p-

value per gene was plotted for all genes, as well as for the gene set matching FUS targets and those with MIDAS p-values 0.01. Additionally, the cumulative density of -log10 of the best probeset MIDAS p-value per gene was plotted for all genes, as well as the set with higher FUS motif (GTGGT (Lagier-Tourenne et al., 2012)) density than the mean (p-value 0.01) by a one-sided proportion test.

Analysis of putative interactomes of C9ORF72 and P62

Protein intensity values obtained from MaxQuant were used for the statistical confidence assessment of C9ORF72 and P62 interactions by SAINTq (Teo et al., 2016). For each protein, SAINTq compares its intensity values in the biological replicates of the immunoprecipitations (IPs) against those in the IgG control replicates under the same experimental conditions. SAINTq then assigns each protein a Bayesian False Discovery Rate (BFDR) that is based on the level of significance of the intensity difference between the IPs and the controls. Proteins with a BFDR < 0.05 were considered as high-confidence protein-protein interactions. C9ORF72 and P62 interacting proteins were intersected with known stress granule proteins (S. Jain et al., 2016) and ALS-linked genes (Abel et al., 2012). Interactomes were also overlapped with published datasets of arginine dimethylated proteins and potential PRMT5 substrates (Bremang et al., 2013; A. Guo et al., 2014; Larsen et al., 2016; Sylvestersen et al., 2014; Uhlmann et al., 2012). Potential PRMT5 substrates from Supplementary Table 1 of (Larsen et al., 2016) which had SILAC H/L ratio > 1.02 for at least two out of the 3 following treatment conditions: (i) EPZ015666 – selective PRMT5 inhibitor, (ii) siPRMT5_Exp1 and (iii) siPRMT5_Exp2 were included. Cytoscape 3.4.0 (Shannon et al., 2003) plugin BiNGO was used to perform GO term analyses. Overrepresented categories were chosen after Benjamini & Hochberg False Discovery Rate correction. Hypergeometric statistical test was used to ascertain the *p*-value of GO term enrichment.

Silver staining

Immunoprecipitations of P62, FUS and C9ORF72 were performed as described above except in a sterile environment to reduce keratin contamination. Following the final washes in NP-40 lysis buffer, magnetic beads were resuspended in 1% SDS (in lysis buffer), boiled at 99ºC for 5 min; then DTT was added to 10 mM and samples were boiled at 99 ºC for 5 min prior to silver staining. Samples were run on precast protein gels (4561094, Bio-Rad) and processed for silver staining as per manufacturer's instructions (17-1150-01, GE Healthcare). Protein lanes were then excised for trypsin digestion.

MTT Assay

Vybrant™ MTT Cell Proliferation Assay Kit (V13154, Thermo Fisher Scientific) was employed in accordance with manufacturer's guidelines.

Patient information, tissue collection, and consent

Patient tissues were collected with informed consent with approval from the Sunnybrook Health Sciences Centre Research Ethics Board and the Ottawa Hospital Research Ethics Board. Specimens were also provided by the Department of Veterans Affairs Biorepository. Overall, two non-ALS control cases, five ALS cases carrying C9ORF72 repeat expansions, and three ALS cases not carrying C9ORF72 repeat expansions were used in the study.

Statistical analysis

Statistical analyses were performed using two-tailed Student's *t*-tests in Microsoft Excel. A *p*-value of < 0.05 was considered statistically significant. Significance was denoted as follows: * *p*-value < 0.05, ** *p*-value < 0.01, *** *p*-value < 0.001.

Data Availability

The mass spectrometry proteomics data have been deposited to the ProteomeXchange Consortium via the PRIDE partner repository with the dataset identifiers PXD009759, PXD009741 and PXD009760. Dataset legends and reviewer account details are included in the Supplementary Information. The authors declare that all data supporting the findings of this study are available within the article and its Supplementary Information files, or from the corresponding author upon reasonable request.

2.6 Acknowledgements

We thank My Tran Trung and Charles Campbell for help with mouse work. We thank Herbert W. Virgin for *p62*$^{-/-}$ mice. Research in the D.G. group is supported by an open operating grant from Canadian Institutes of Health Research (#142174). E.R. was supported by the Canadian Consortium on Neurodegeneration in Aging. M.L.A. is supported by a Discovery Grant from the National Science and Research Council of Canada and startup funds from the University of Ottawa. J.C. was supported by grants from Canadian Institutes of Health Research (MOP86746) and CureSMA Canada. J.W. was supported by Partners Investing in Parkinson's Research group (Ottawa Hospital Foundation). J.R. was supported by the James Hunter and Family ALS Initiative and Brain Canada/ALS Canada. J.F.C. is supported by a grant from Canadian Institutes of Health Research (MOP136816). M.C. was supported alternately by a 2015 ALS Society Cycle of Hope Doctoral Research Award and a

Vanier Canada Graduate Scholarship from the Canadian Institutes of Health Research.

Chapter 3 - Manuscript #2

Autophagy supports genomic stability by degrading retrotransposon RNA

Publication information:

Huishan Guo, Maneka Chitiprolu, David Gagnon, Lingrui Meng, Carol Perez-Iratxeta, Diane Lagace and Derrick Gibbings. “Autophagy supports genomic stability by degrading retrotransposon RNA”. Nature Communications 2014 Nov 4;5:5276.

Author’s contribution:

Designed the experiments: MC, HG, DL, CP-I, DGibbings. Performed the experiments and analyzed the data: MC, HG, DG, LM, DGibbings. Helped write the paper: MC (Relevant Methods), HG, DGibbings. Conceived the study: DGibbings.

MC contributions by figure: Figure 21b-d, Figure 22i-j, Figure 23e-f, Figure 24a-e, Figure 25a-c

Autophagy supports genomic stability by degrading retrotransposon RNA

Huishan Guo[1], Maneka Chitiprolu[1], David Gagnon[1], Lingrui Meng[1], Carol Perez-Iratxeta[1,2], Diane Lagace[1] & Derrick Gibbings[1]

1. Department of Cellular and Molecular Medicine, University of Ottawa, Ottawa, Ontario, Canada K1H 8M5

2. Sprott Centre for Stem Cell Research, Ottawa Hospital Research Institute, Ottawa, Ontario, Canada K1H 8L6

3.1 Abstract

Many cytoplasmic substrates degraded by autophagy have been identified; however, the impact of RNA degradation by autophagy remains uncertain. Retrotransposons comprise 40% of the human genome and are a major source of genetic variation among species, individuals and cells. Retrotransposons replicate via a copy-paste mechanism involving a cytoplasmic RNA intermediate. Here we report that autophagy degrades retrotransposon RNA from both long and short interspersed elements, preventing new retrotransposon insertions into the genome. Retrotransposon RNA localizes to RNA granules, whose selective degradation is facilitated by the autophagy receptors NDP52 and p62. Accordingly, NDP52 and p62 control retrotransposon insertion in the genome. Mice lacking a copy of *Atg6/Beclin1*, a gene critical for autophagy, also accumulate both retrotransposon RNA and genomic insertions. Thus, autophagy physiologically buffers genetic variegation by degrading retrotransposon RNA. This may contribute to the increased tumorigenesis occuring when autophagy is inhibited and suggest a role for autophagy in tempering evolutionary change.

3.2 Introduction

Stress instigates cellular programs for adaptation. Critical among these is macroautophagy (hereafter autophagy), a mechanism of cytoplasmic degradation. In autophagy, a double membrane is formed *de novo* in the cytoplasm and expands to engulf cytoplasmic contents, eventually enclosing them within an autophagosome (Mizushima & Komatsu, 2011). Lysosomes subsequently fuse with autophagosomes delivering catabolic enzymes including RNAses (Mizushima & Komatsu, 2011). Autophagy can selectively degrade cytoplasmic content using autophagy receptors, such as NDP52 or p62 (official gene symbols CALCOCO2 and SQSTM1 respectively), which recruit selective cargo to the nascent autophagosome membrane (Shaid, Brandts, Serve, & Dikic, 2012). While the field of autophagy has focused on proteins and organelles degraded by autophagy, only recently has attention shifted to RNA degradation by autophagy (Buchan et al., 2013; D. Gibbings, Mostowy, S., Jay, F., Schwab, Y., Cossart, P., Voinnet, O., 2012).

Retrotransposons, ancient symbionts whose genetic material is sheltered and replicates within the human genome (Baillie et al., 2011; Beck et al., 2011; Evrony et al., 2012; Muotri et al., 2005), are a major contributor to genetic variation between species, within species, and between cells in a single individual. Two of the principal families of retrotransposons, Long Interspersed Nucleotide Elements (LINE-1) and Short Interspersed Nucleotide Elements (SINE), such as the dominant *Alu* family in primates, account for 17% and 10% of the human genome respectively (Hancks & Kazazian, 2012). By re-inserting themselves in the genome, retrotransposons drive genetic change but also cause over 65 diseases identified to date (Hancks & Kazazian, 2012). Increasing attention is therefore being devoted to mechanisms that control

retrotransposon insertions and balance the risks of unhindered retrotransposon replication with their potentially adaptive benefits (Cornelis et al., 2013).

Both *Alu* and LINE-1 replicate using a copy-paste mechanism requiring two proteins encoded by LINE-1: ORF1p and ORF2p (Beck et al., 2011). RNA is transcribed from genome-integrated copies of retrotransposons and transits through the cytoplasm (Goodier et al., 2010). ORF1p is required for retrotransposition and binds LINE-1 and *Alu* RNA in the cytoplasm (J. Lin et al., 2012). Retrotransposon RNA traffics back into the nucleus where ORF2p copies and re-inserts the retrotransposon in a new genomic location (Beck et al., 2011). Our understanding of the spectrum of mechanisms quelling retrotransposons is limited, but retrotransposon RNA is susceptible to repression during transit through the cytoplasm (Goodier et al., 2013).

Here we demonstrate that autophagy degrades LINE-1 RNA and tempers the rate of insertion of LINE-1 and *Alu* retrotransposons by using the autophagy receptors NDP52 and p62 to target P-bodies and stress granules for elimination. Our evidence suggests this mechanism causes genetic change in select tissues of mice lacking a copy of *Atg6/Becn1*, a gene critical for autophagy.

3.3 Results

Retrotransposon RNA co-localizes with autophagosomes

If LINE-1 and *Alu* RNA are degraded by autophagy, they should co-localize, in part, with autophagosomes. To visualize the subcellular localization of LINE-1 RNA, as previously (Goodier et al., 2010), we co-expressed LINE-1 RNA fused with six MS2 binding sites (LINE-1-MS2) and MS2-GFP. As described, LINE-1-MS2 accumulated in cytoplasmic foci (Goodier et al., 2010), 65% of which co-localized with a specific (Figure 16a-c) autophagosome marker LC3 (Figure 15a,b). Similarly, foci of *Alu*-MS2 RNA detected

with the MS2-GFP system co-localized with LC3 (Figure 15c). Consistent with autophagic elimination of LINE-1-MS2 RNA, the number of foci of LINE-1-MS2 increased when degradation of autophagosome content was blocked with Bafilomycin A1 (BAF) (Figure 15d). The number of foci of LINE-1-MS2 RNA that co-localized with the autophagosome marker, LC3, also increased when autophagic degradation was inhibited (Figure 15d). To exclude the possibility that co-localization of LINE-1 RNA with autophagosomes is an artifact of overexpression of LINE-1 fused with MS2 binding sites, we detected endogenous LINE-1 RNA using specific Fluorescence *In Situ* Hybridization (FISH) probes recognizing retrotransposition-active LINE-1 elements of the L1-HS family (Figure 16d,e). Cytoplasmic foci of endogenous LINE-1 RNA also co-localized with LC3 (Figure 15e,f). 3-D rendered Z-stacks of endogenous LINE-1 RNA and LC3 demonstrated that LINE-1 RNA is tightly associated with, or enclosed within autophagosomes (Figure 15g).

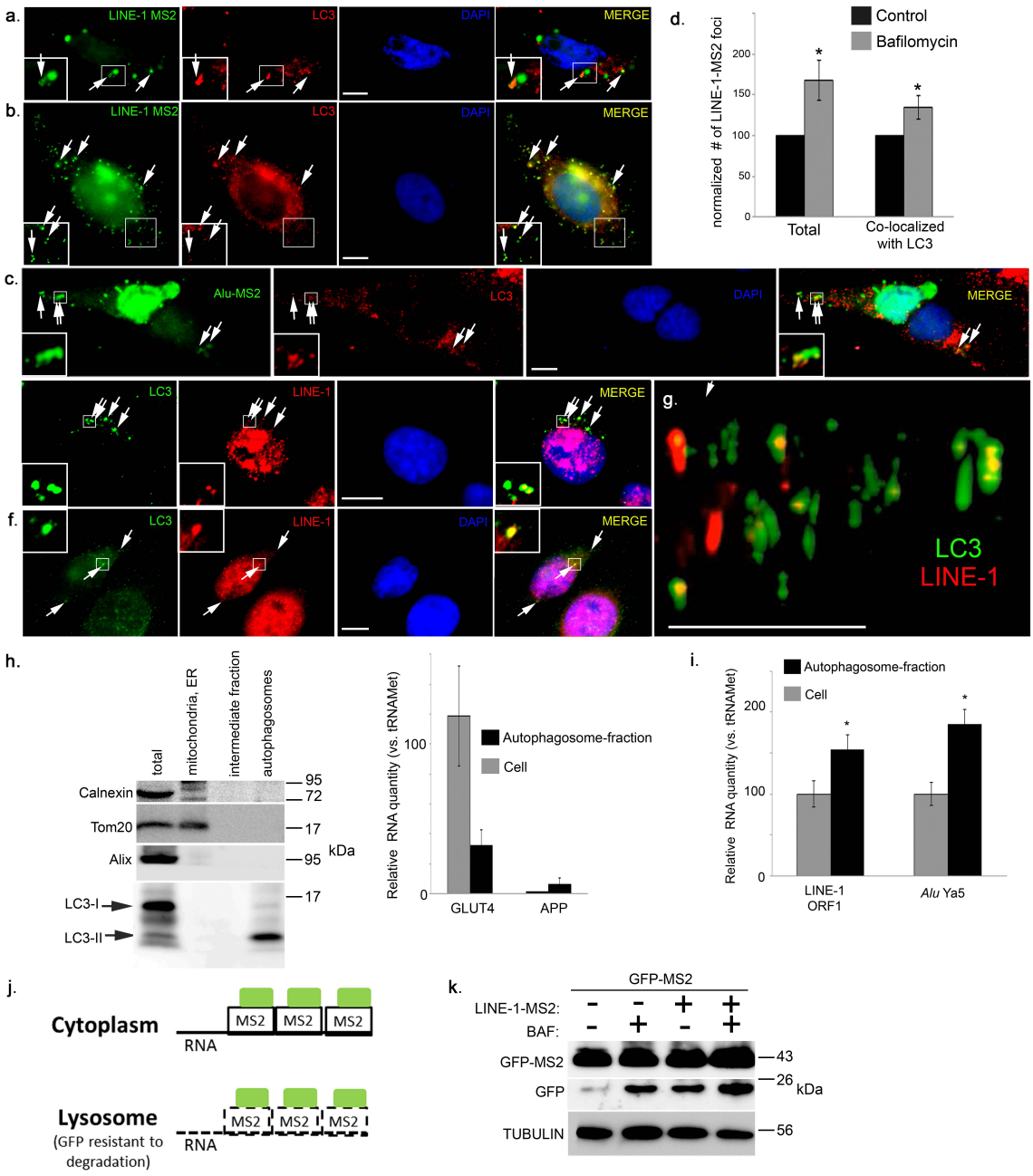

Figure 15: LINE-1 and *Alu* RNA are enclosed within autophagosomes

(**a**,**b**) Two representative images of fluorescent microscopy of LC3 and LINE-1 fused to six MS2-binding sites detected with MS2-GFP. (**c**) Fluorescent microscopy of LC3 and *Alu* fused to six MS2-binding sites detected with MS2-GFP. Li's correlation coefficient of co-localization (0.0232, s.e.m. 0.048). (**d**) Relative number of foci of LINE-1-MS2, or number of foci of LINE-1-MS2 co-localized with LC3 per cell in

randomly selected fields of cells treated with BAF1 (20 h, 400 nM). *n*=25 cells, total number of LINE-1-MS2 foci: control=104, BAF=175, total number of LINE-1-MS2 foci co-localized with LC3: control =68, BAF 167. *Total *P*=0.015, Co-localized with LC3 $P=5 \times 10^{-8}$, *t*-test). Li's correlation coefficient of co-localization (without BAF 0.19 s.e.m. 0.027; with BAF 0.213, s.e.m. 0.02). (**e**,**f**) Two representative images of fluorescent microscopy of FISH probes recognizing endogenous LINE-1 RNA and LC3. (**g**) Three-dimensional reconstruction of confocal microscopy z-stacks of endogenous LINE-1 RNA and LC3 prepared in Imaris. (**h**) Western blot of fractions enriched in autophagosomes compared with total cell extracts and ER/mitochondria-enriched fractions. RT-qPCR analysis of mRNA levels of two transmembrane proteins (GLUT4 and APP) in total cell RNA and autophagosome-enriched fractions. *n*=3, *P*>0.05. (**i**) RT-qPCR analysis of LINE-1 ORF1 and *AluYa5* in RNAse-treated autophagosome-enriched fractions or total cell RNA. *n*=3, **P*=0.043 LINE-1, *P*-0.01 *Alu*Ya5, *t*-test (**j**) Model of system to measure degradation of GFP-tagged substrates by autophagy. (**k**) Western blot analysis of GFP and alpha-tubulin (control) in cells transfected with MS2-GFP or LINE-1-MS2 and MS2-GFP and treated with control or Bafilomycin (2 h, 400 nM). All error bars represent s.e. of the mean. All experiments were replicated a minimum of three times.

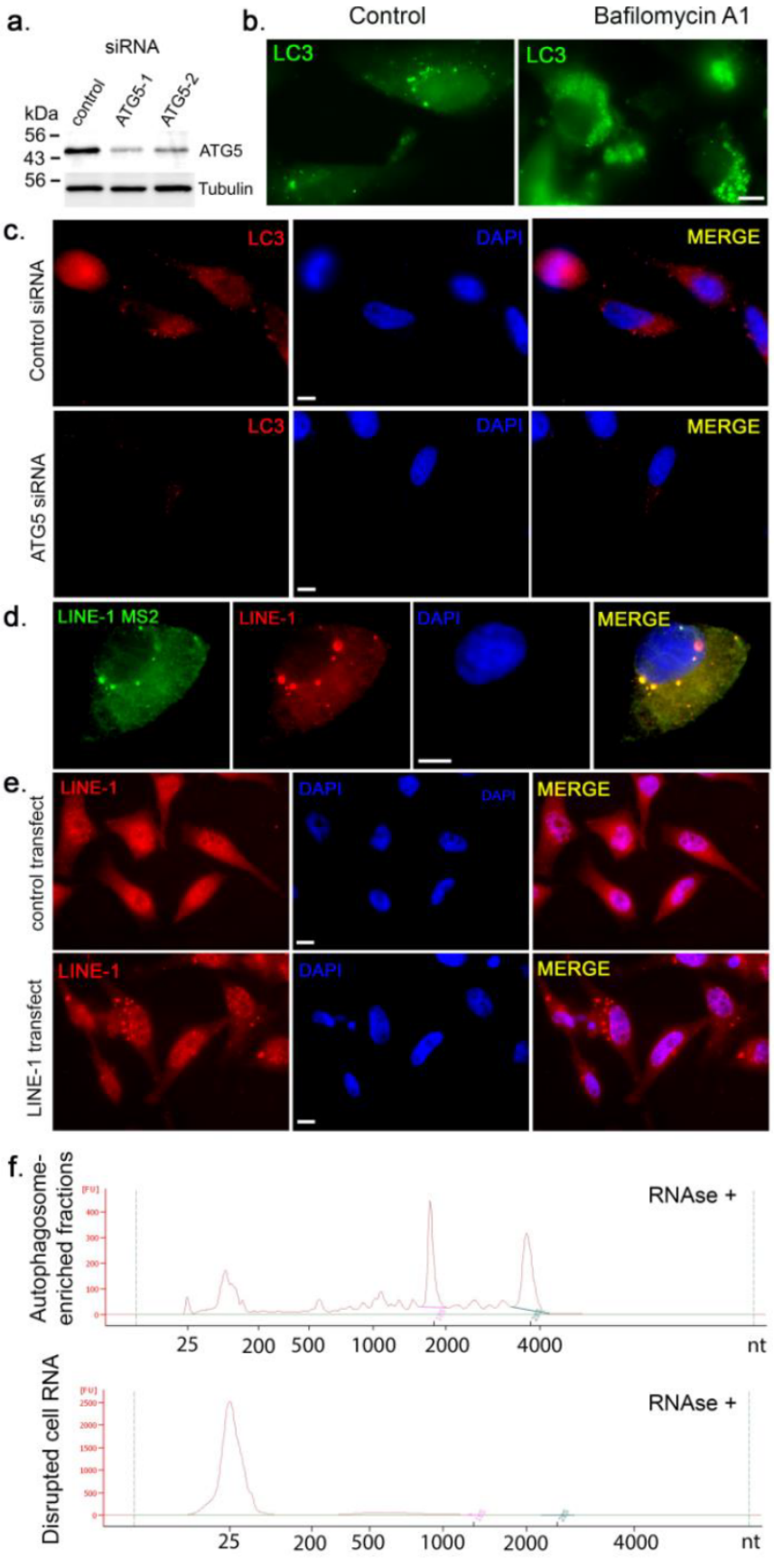
a.
siRNA
control
ATG5-1
ATG5-2
kDa
56
43
56
ATG5
Tubulin
b.
Control
Bafilomycin A1
LC3
LC3
c.
Control siRNA
ATG5 siRNA
LC3
DAPI
MERGE
LC3
DAPI
MERGE
d.
LINE-1 MS2
LINE-1
DAPI
MERGE
e.
control transfect
LINE-1 transfect
LINE-1
DAPI
MERGE
LINE-1
DAPI
MERGE
f.
Autophagosome-enriched fractions
RNAse +
25
200
500
1000
2000
4000
nt
Disrupted cell RNA
RNAse +
25
200
500
1000
2000
4000
nt

Figure 16: Reagents used to detect LC3 and LINE-1 are specific

(**a**) Western blot analysis of ATG5 and TUBA (loading control) cells treated with control siRNA or siRNA targeting ATG5. (**b**) Immunofluorescent detection of LC3 in cells treated with vehicle or Bafilomycin A1 (20 h, 400 nM). (**c**) Immunofluorescent detection of LC3 in cells treated with control siRNA or siRNA targeting ATG5. (**d**) Fluorescent microscopy of cells labeled with FISH probes recognizing LINE-1 (red) and transfected with LINE-1-MS2 and MS2-GFP. (**e**) Fluorescent microscopy of cells labeled with FISH probes recognizing LINE1 in cells transfected with control plasmid (pcDNA3.1) or plasmid expressing LINE-1 (99 RPS-GFP PUR). All scale bars are 10 μM. (**f**) Agilent Bioanalyzer analysis of RNA from disrupted total cells or from autophagosome-enriched fractions pre-treated with RNAse A and T1. Experiments were performed in triplicate.

Retrotransposon RNA co-purifies with autophagosomes

As a first step to test whether LINE-1 and *Alu* RNA are enclosed within autophagosomes, these were purified (Sahu et al., 2011). The lipid-modified form of LC3 (LC3-II) which is specifically incorporated in autophagosomes was selectively enriched in these fractions compared to unmodified LC3-I (Figure 15h). Autophagosome-enriched fractions were devoid of markers of other RNA-associated organelles such as mitochondria (TOM20), endoplasmic reticulum (Calnexin), endosomes and multivesicular bodies (Alix) (Figure 15h). Autophagosome-enriched fractions were also not consistently enriched in mRNA of transmembrane proteins (APP, GLUT4), further excluding contamination with significant amounts of endoplasmic reticulum (Figure 15h). Fractions enriched in intact autophagosomes were treated with RNAses to eliminate RNA attached to their external surface (Figure 16f). We measured abundance of retrotransposon RNA by RT-qPCR using primers specific for active LINE-1 and *Alu* family members (Figure 17). Autophagosome-enriched fractions contained abundant

RNAse-protected LINE-1 (L1-HS) and *Alu* (*AluYa5*) RNA compared to total cellular RNA by RT-qPCR (Figure 15i). Together, this suggests that a substantial quantity of LINE-1 and *Alu* RNA is enclosed within autophagosomes.

a.

Primers

```
Yb8 R:   CGGACTGCGGACTGCAGTG
Yb8 F:   ATCCTGGCTAACAAGGTGAAACCC
Ya5 R:   CTCCCAAGTAGCTGGGACTACAGG
Ya5 F:   TCCCGGCTAAAACGGTGAAA
```

b.

Sequence

```
Sx:       1 GGCCGGGCGCGGTGGCTCACGCCTGTAATCCCAGCACTTTGGGAGGCCGAGGCGGGCG 58
Yb8Ref:     ·····························································T·
Ya5Ref:     ·····························································

                                              87    AluYb8F Primer    110
                                              88  AluYa5F Primer 107
Sx:      59 GATCACCTGAGGTCAGGAGTTCGAGACCAGCCTGGCCAACATGGTGAAACCCCGTCTC 116
Yb8Ref:     ·····T--···········A·········T·····T····A·················
Yb8:                                87   ·T·····T····A·················
Ya5Ref:     ·····--···········A·········T··C···T··A·C·················
Ya5:                                87   TT··C···T··A·C··N·····N···N

                                                                158 AluYa5R Primer
Sx:     117 TACTAAAAATACAAAAA-TTAGCCGGGCGTGGTGGCGCGCGCCTGTAATCCCAGCTAC 173
Yb8Ref      ·················A···········C·······G·········G··········
Yb8:        ·················A···········C·······G·········G··········
Ya5Ref:     ·················A···········A·····G·········G··········
Ya5:        ·················A·····················G·····N··········

                  181
Sx:     174 TCGGGAGGCTGAGGCAGGAGAATCGCTTGAACCCGGGAGGCGGAGGTTGCAGTGAGCC 231
Yb8Ref      ·····················G··G··········A·····C·············
Yb8:        ·····················G··G··········A·····C·············
Ya5Ref:     ·T···················G··G···············C·············
Ya5:        ·T··N·· 181

                        243     AluYb8R Primer     261
Sx:     232 GAGATCGCGCCACTGCACTCC--A-----GCCTGGGCGACAGAGCGAGACTCCGTCTC 282
Yb8Ref      ·····T··········G···GC·GTCCG···························
Yb8:        ·····T·········· 247
Ya5Ref:     ·····C·····------·····------·····------·····------·····
```

Figure 17: Specificity of RT-qPCR analysis for *AluYb8* and *AluYa5* elements

(**a**) Primers used for RT-qPCR analysis of *AluYb8* and *AluYa5* elements. Nucleotides that differentiate *AluYb8* and *AluYa5* are highlighted in red. (**b**) Sequence alignment of reference sequences for *Alu* elements of the *Sx* (Sx Ref), *Ya5* (Ya5 Ref), and *Yb8* (Yb8 Ref) families. Products of RT-qPCR reactions with primers for *AluYa5* and *AluYb8* were sequenced to ensure the targeted RNAs were amplified (Yb8 Seq, Ya5 Seq). Conserved nucleotides are noted with a (-), while non-conserved nucleotides are highlighted in red, unidentified nucleotides from sequencing reactions are indicated by N. The position of the primers on reference sequences are indicated by bold lines. Sequenced *AluYb8* products match exactly the reference sequence for AluYb8. Sequenced *AluYa5* products match several diagnostic nucleotides that differentiate *AluYa5* from *AluYb8* and *AluSx*, but several nucleotides could not be confidently identified. These may be due to problems with SAP treatment of Sybrgreen qPCR products or polymorphisms among the 2640 copies of *AluYa5* in the genome.

Retrotransposon RNA is degraded by autophagy

Autophagosome content is degraded upon fusion with lysosomes containing catabolic enzymes. GFP has unusual resistance to proteolytic degradation in lysosomes; when GFP-tagged proteins are degraded by autophagy, a GFP fragment persists while the tagged protein is degraded (Figure 15j) (Klionsky et al., 2012). Background levels of free GFP were apparent in cells transfected with MS2-GFP alone (Figure 15k). Expression of LINE-1 with MS2 binding sites markedly increased the amount of free GFP and inhibiting lysosomal degradation with BAF caused GFP to accumulate further (Figure 15k). This suggests LINE-1 RNA with MS2-binding sites increases recruitment of MS2-GFP into autophagosomes. Cumulatively, this data strongly suggests that LINE-1 RNA is enclosed within, and degraded by autophagosomes.

If LINE-1 and *Alu* RNA are degraded by autophagy they should accumulate when autophagy is inhibited. Either of two independent siRNA targeting ATG5 (Figure 16a), which is critical for autophagosome biogenesis, caused levels of LINE-1 (measured either at 5'UTR or ORF1), *AluYa5* and *AluYb8* RNA to increase (Figure 18a,b). *Alu* inserts within longer RNAs are frequent (Faulkner et al., 2009). We performed two tests to determine whether independent *Alu* elements were affected by autophagy. First, RNA was separated on gels and 250-350 nt RNAs consistent with the size of *Alu* were extracted and RT-qPCR was performed. Levels of *AluYa5* and *AluYb8* increased among 250-350 nt RNA in cells treated with ATG5 siRNA compared to control siRNA (Figure 18c, Figure 19a). Second, RNA of ~300 nt detected by northern blot with probes for *AluYa5* and *AluYb8* also increased in cells treated with ATG5 siRNA compared to control siRNA (Figure 19b). This suggests that full-length *Alu* RNA accumulates when autophagy is inhibited, independent of longer RNAs containing *Alu* elements. LINE-1 and *Alu* RNA also accumulated when autophagic degradation was inhibited with BAF (Figure 19c). To ensure that increases in LINE-1 and *Alu* RNA levels when autophagy was inhibited were due to inhibited degradation and not activated transcription we measured RNA decay using two assays. Blocking transcription with actinomycin D caused decay of LINE-1 and *Alu*Yb8 RNA that was impeded when autophagic degradation was blocked with Bafilomycin (Figure 18d, Figure 19d). Decay of pulse-labeled LINE-1 and *Alu*Yb8 RNA was also inhibited in cells treated with ATG5 siRNA (Figure 18e, Figure 19e). The majority of LINE-1 elements in the genome are drastically truncated at the 5' end and inactive (Beck et al., 2011), but RNA from 5'UTR and ORF1 of LINE-1 both accumulate when autophagy is inhibited (Figure 18a). Cumulatively, this suggests that degradation of RNA from full-length, retrotransposition-competent LINE-1 and *Alu* is mediated by autophagy, in accord with its co-localization with and co-purification within autophagosomes (Figure 15).

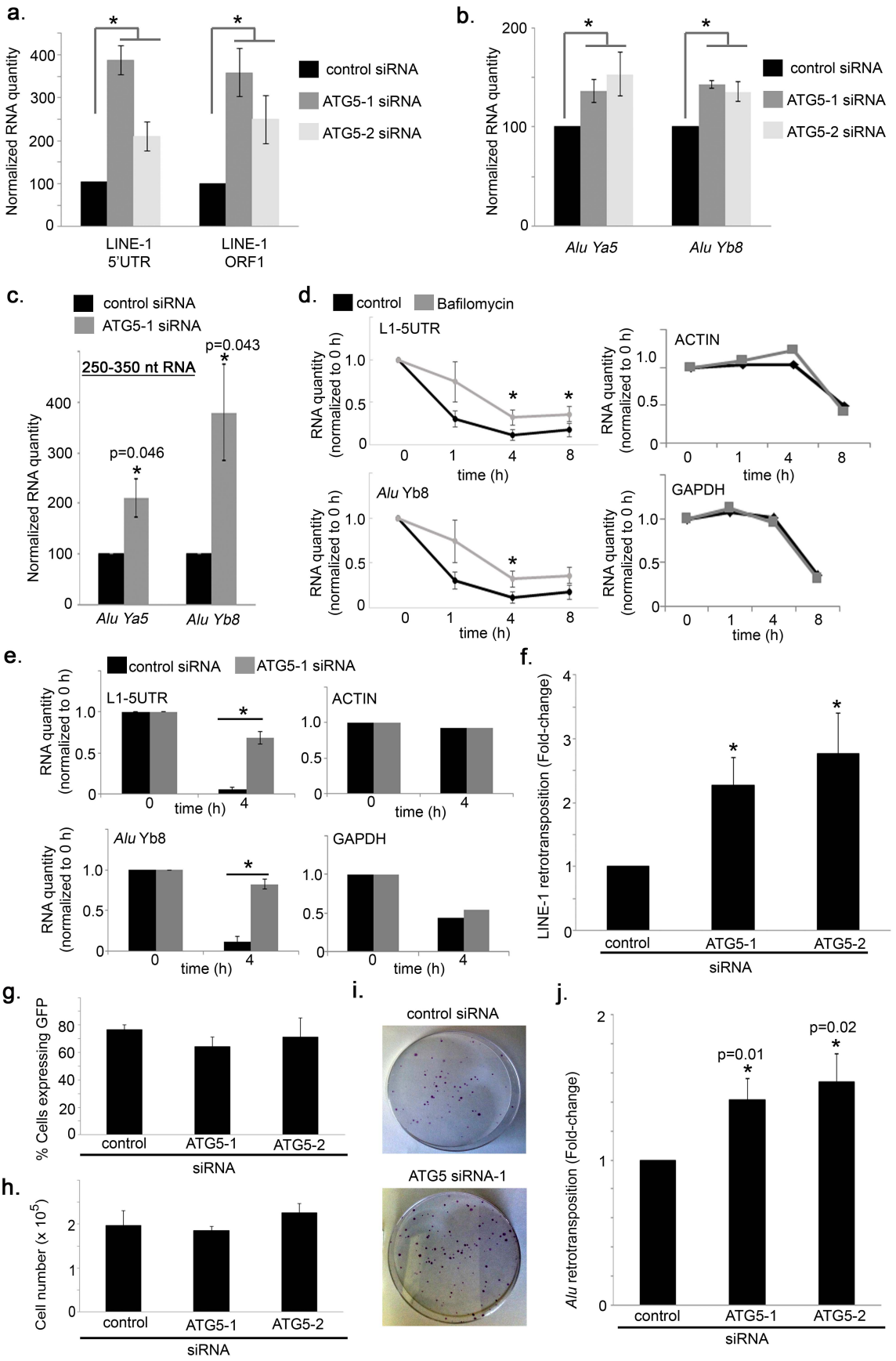
a.
Normalized RNA quantity
control siRNA
ATG5-1 siRNA
ATG5-2 siRNA
LINE-1 5'UTR
LINE-1 ORF1
b.
Alu Ya5
Alu Yb8
c.
250-350 nt RNA
p=0.046
p=0.043
d.
control
Bafilomycin
L1-5UTR
ACTIN
GAPDH
RNA quantity (normalized to 0 h)
time (h)
e.
f.
LINE-1 retrotransposition (Fold-change)
control
ATG5-1
ATG5-2
siRNA
g.
% Cells expressing GFP
h.
Cell number (x 10^5)
i.
ATG5 siRNA-1
j.
Alu retrotransposition (Fold-change)
p=0.01
p=0.02

Figure 18: Inhibiting autophagy increases levels of LINE-1 and *Alu* RNA and their corresponding genomic insertions

(**a**,**b**) RT-qPCR analysis of levels of (**a**) LINE-1 RNA (5′UTR, ORF1, n=3, *P=0.009 LINE-1 5′UTR, P=0.03 LINE-1 ORF1, t-test) and (**b**) *AluYa5* and *AluYb8* in cells (n=3, *P=0.0018 *Alu*Ya5, P=2 × 10^{-6} *Alu*Yb8, analysis of variance (ANOVA)) treated with siRNA-targeting ATG5 or control (10 nM, 48 h) (**c**) RT-qPCR analysis of *AluYa5* and *AluYb8* in 250–350 nt RNA isolated from cells treated with siRNA-targeting ATG5 or control (10 nM, 48 h, n=3, *P=0.046 AluYa5, P=0.043 *Alu*Yb8, ANOVA). (**d**) RT-qPCR analysis in cells treated with dimethylsulphoxide or Bafilomycin (400 nM) and actinomycin D. (5 nM, n=3, *P=0.01 LINE-1 both 4 and 8 h, P=0.04 *Alu*Yb8, ANOVA). (**e**) RT-qPCR analysis of pulse-labelled RNA recovered 0 and 4 h after pulse in cells transfected with siRNA-targeting ATG5 or control (10 nM, n=3, *P=0.01 both LINE-1 and *Alu*Yb8). (**f**) Percent of cells expressing GFP when co-transfected with LINE-1-RP GFP reporter of retrotransposition and siRNA-targeting ATG5 or control. Results are normalized to similar experiments with a retrotransposition-incompetent control (n=3, *P=0.045 ATG5-1, P=0.048 ATG5-2, ANOVA). (**g**) Relative number of cells at experiment's termination if cells were transfected with siRNA-targeting ATG5 or control. (**h**) Percent of cells expressing GFP when co-transfected with plasmid expressing GFP and siRNA-targeting ATG5 or control (n=3). (**i**) Representative plates from *Alu*-retrotransposition assay transfected with control siRNA or siRNA-targeting ATG5. (**j**) Relative number of G418-resistant colonies in cells transfected with siRNA-targeting ATG5 or control, *Alu*-retrotransposition reporter and retrotransposition-enhancer LINE-1 ORF2p (n=3, *P=0.01 ATG5-1, P=0.02 ATG5-2, ANOVA) All error bars represent s.e. of the mean. All experiments were performed with a minimum of three biological replicates.

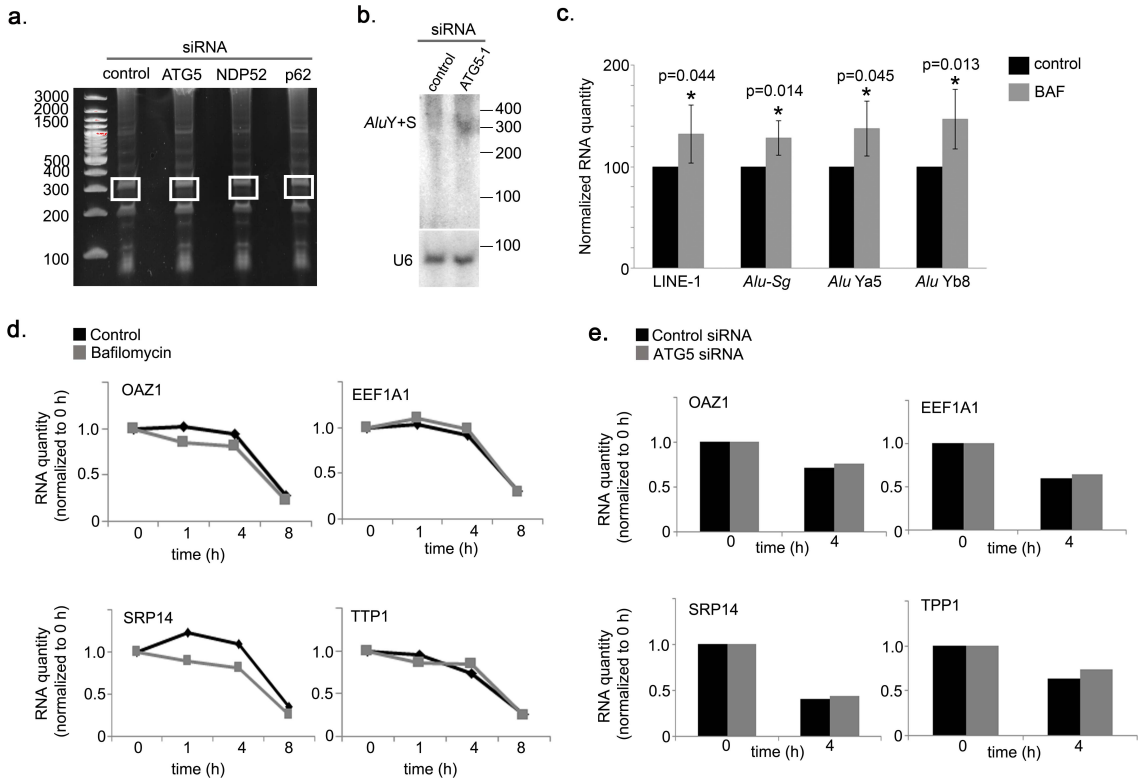

Figure 19: Inhibiting autophagy causes levels of retrotransposons to accumulate. Reagents used to detect ORF1p, NDP52 and p62 are specific

(**a**) Representative gel used to extract 250- 350 nucleotide RNA for RT-qPCR analysis of *Alu* RNA. Regions extracted are highlighted by white boxes. (**b**) Northern blot analysis of RNA from cells treated with siRNA targeting ATG5 or control, with probes recognizing *AluYa5* and *AluYb8*. U6 RNA serves as a loading control. (**c**) RT-qPCR analysis of the abundance of LINE-1 (5'UTR) and *AluYa5* and *AluYb8* in cells treated with vehicle or Bafilomycin A1 (20 h, 400 nM, n=3, p=0.044 LINE-1, p=0.014 *Alu*Sg, p=0.045 *Alu*Ya5, p=0.013 *Alu*Yb8, ANOVA). (**d**) RT-qPCR analysis of additional control RNAs in cells treated with DMSO or Bafilomycin (400 nM) and actinomycin D. (5nM). (**e**) RT-qPCR analysis of additional control RNAs in pulse-labeled RNA recovered 0 h and 4 h after pulse in cells transfected with siRNA targeting ATG5 or control (10 nM). All experiments were performed in three times.

Autophagy restricts retrotransposon insertion in the genome

To test directly whether autophagic degradation targets active LINE-1 RNA and prevents new insertions of LINE-1 in the genome we used an established LINE-1 retrotransposition reporter (Goodier et al., 2013). In this system, the LINE-1 that is expressed contains an intron with an inverted promoter and coding region for GFP (Ostertag, Prak, DeBerardinis, Moran, & Kazazian, 2000). When the LINE-1 is reverse-transcribed and inserted into the genome, GFP is correctly oriented and can be expressed. Percent GFP+ cells are enumerated by flow cytometry (Ostertag et al., 2000) comparing to cells transfected with GFP alone, or a GFP reporter with disabling mutations in LINE-1 (Goodier et al., 2013). In these systems, effects on retrotransposition are usually measured by over-expressing a protein of interest. To evaluate more accurately the endogenous effect of autophagy on retrotransposition we depleted cells of ATG5 using two independent siRNA (Figure 16a). In cells depleted of ATG5, ~2-fold more cells expressed GFP, when transfected with active LINE-1 GFP-reporter compared to a control with point mutations that abolish retrotransposition (Figure 18f) (J. Lin et al., 2012). ATG5 knockdown did not affect cell number or transfection efficiency (Figure 18g,h), suggesting that autophagic degradation of LINE-1 RNA quells retrotransposition of LINE-1 into the genome.

To test the effect of autophagy on *Alu* retrotransposition we utilized an established reporter designed similarly to the LINE-1 reporter, but substituting GFP expression for a geneticin resistance cassette (Dewannieux, Esnault, & Heidmann, 2003). In accord with abundant *Alu* RNA in autophagosome-enriched fractions (Figure 15i), co-localization of *Alu* RNA to autophagosomes (Figure 15c) and increased levels of *Alu* RNA upon inhibition of autophagy (Figure 18b-e, Figure 19c), depletion of ATG5 increased the

number of resistant colonies obtained when cells were transfected with the *Alu* retrotransposition reporter compared to vector alone (Figure 18i,j). Autophagy frequently enhances drug resistance (Gasior et al., 2007). Taken together these results strongly suggest that degradation of LINE-1 or *Alu* RNA by autophagy restricts their genomic insertion.

LINE-1 OR1p is also degraded by autophagy

LINE-1 encodes ORF1p, an RNA-binding protein, that binds LINE-1 RNA in the cytoplasm and is required for LINE-1 retrotransposition (J. Lin et al., 2012). GFP-ORF1p co-localized with the autophagosome marker LC3, and this co-localization increased when autophagy was inhibited (Figure 20a,b). Endogenous ORF1p detected with a specific antibody (Figure 21a) also co-localized with LC3 (Figure 20c) and was abundant in autophagosome-enriched fractions (Figure 20d). Consistent with autophagic degradation of ORF1p, free GFP accumulated in cells transfected with GFP-ORF1p when the cells were treated with BAF (Figure 20e) (Klionsky et al., 2012). This suggests that LINE-1 RNA is degraded by autophagy in complex with ORF1p.

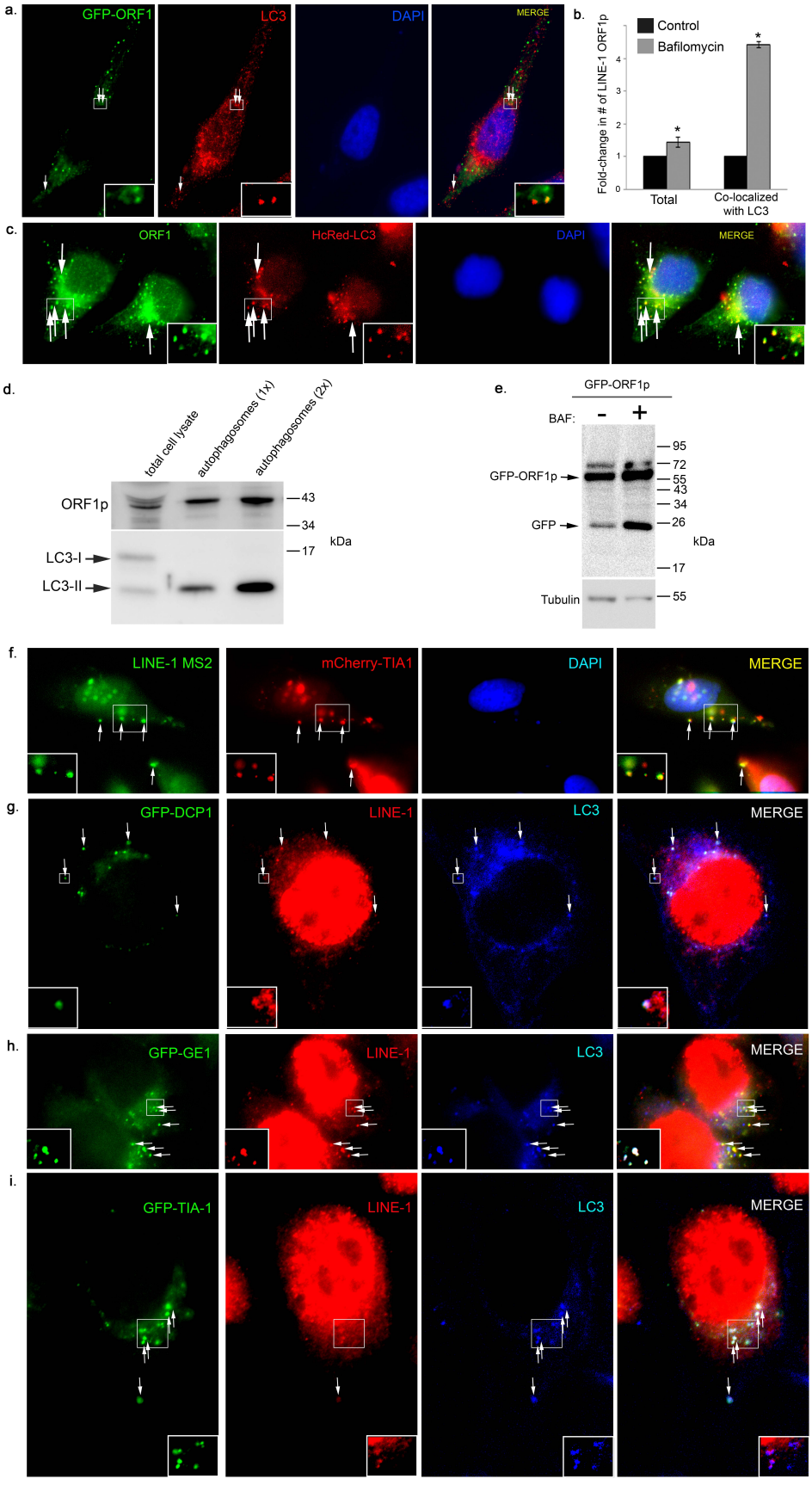
a.
GFP-ORF1
LC3
DAPI
MERGE
b.
Control
Bafilomycin
Fold-change in # of LINE-1 ORF1p
Total
Co-localized with LC3
c.
ORF1
HcRed-LC3
DAPI
MERGE
d.
total cell lysate
autophagosomes (1x)
autophagosomes (2x)
ORF1p
LC3-I
LC3-II
43
34
17
kDa
e.
GFP-ORF1p
BAF:
GFP-ORF1p
GFP
Tubulin
95
72
55
43
34
26
17
kDa
f.
LINE-1 MS2
mCherry-TIA1
DAPI
MERGE
g.
GFP-DCP1
LINE-1
LC3
MERGE
h.
GFP-GE1
LINE-1
LC3
MERGE
i.
GFP-TIA-1
LINE-1
LC3
MERGE

Figure 20: LINE-1 RNA in P-bodies and stress granules co-localizes with autophagosomes and is likely degraded by autophagy with ORF1p

(**a**) Fluorescent microscopy of GFP-ORF1p and LC3. (**b**) Relative number of foci of GFP-ORF1p, or number of foci of GFP-ORF1p co-localized with LC3 per cell in randomly selected fields of cells treated with Bafilomycin A1 (20 h, 400 nM, *n*=30 cells, total number of GFP-ORF1p foci: control=150, BAF=214, total number of GFP-ORF1p co-localized with LC3: control=32, BAF=199). **P*=0.007 Total, *P*=1 × 10^{-42} Co-localized with LC3, *t*-test. Li's correlation coefficient of co-localization (0.328, s.e.m. 0.019). Error bars represent s.e. of the mean. (**c**) Fluorescent microscopy of endogenous ORF1p and HcRed-LC3. (**d**) Western blot analysis of ORF1p in autophagosome-enriched fractions. LC3-II is a marker of autophagosomes. (**e**) Western blot analysis of GFP and alpha-tubulin (control) in cells transfected with GFP-ORF1p and treated with control or Bafilomycin (20 h, 400 nM). (**f**) Fluorescent microscopy of cells expressing LINE-1-MS2, MS2-GFP and mCherry-TIA-1. (**g**–**i**) Fluorescent microscopy of endogenous LINE-1 RNA in cells transfected with GFP-DCP1A (**g**), GFP-GE-1 (**h**) or GFP-TIA-1 (**i**). All experiments were performed with a minimum of three biological replicates.

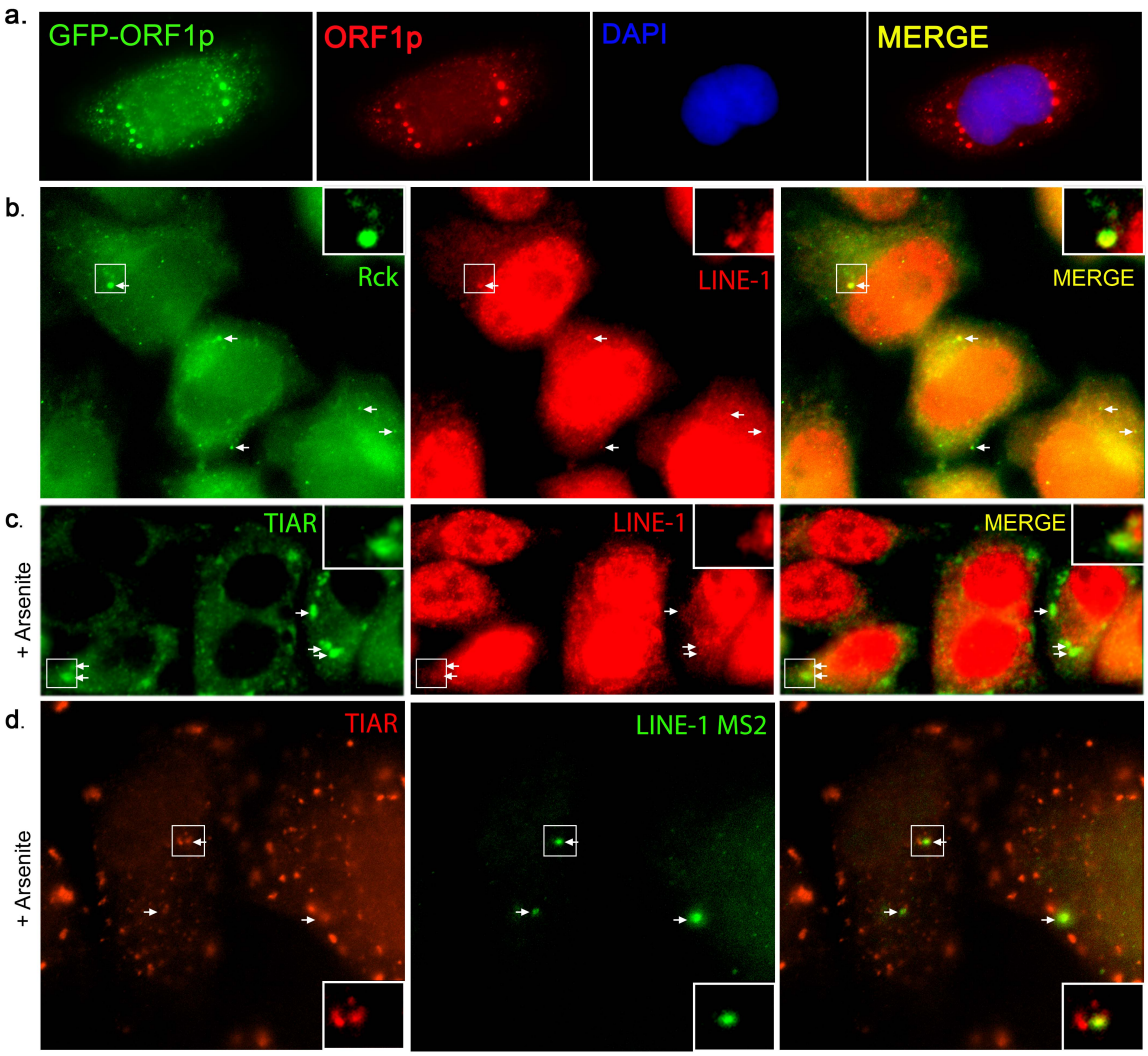

Figure 21: LINE-1 RNA localizes with P-bodies and stress granules

(**a**) Fluorescent microscopy of cells transfected with GFP-ORF1p and labeled with anti-ORF1p antibody. (**b**) Fluorescent microscopy of Rck and LINE-1 (FISH). (**c**) Fluorescent microscopy of TIAR (stress granules) and LINE-1 (FISH) in cells treated with arsenite (1 h, 0.5 mM). (**d**) Fluorescent microscopy of TIAR in cells transfected with LINE-1-MS2 and MS2-GFP and treated with arsenite (1 h, 0.5 mM). All scale bars are 10 μM. Experiments were performed a minimum of twice.

LINE-1 RNA co-localizes with P-bodies and stress granules

We next sought to determine how LINE-1 RNA is recruited to and degraded in autophagosomes. In accord with previous literature (Goodier et al., 2010), over-expressed LINE-1-MS2 RNA accumulated in stress granules (Figure 20f). In contrast, endogenous LINE-1 RNA co-localized strongly with markers of P-bodies that concentrate RNA decay enzymes (GFP-DCP1A, or GFP-Ge-1, Figure 20g,h), and to a lesser extent with stress granules (GFP-TIA-1, Figure 20i). Similar localization of endogenous LINE-1 RNA was observed when P-bodies and arsenite-induced stress granules were detected with antibodies to endogenous proteins (Rck, TIAR, Supplementary Figure 22b,c). LINE-1-MS2 also co-localized in part with arsenite-induced stress granules (Figure 21d). LINE-1 RNA that co-localized with GFP-DCP1A or GFP-TIA-1 also co-localized with LC3 (Figure 20g-i), suggesting that LINE-1 RNA in either stress granules or P-bodies can be targeted for autophagic degradation.

Autophagy receptors help selectively degrade RNA granules

Selective autophagy receptors, such as NDP52 and p62 recruit nascent autophagosome membranes to substrates of autophagy (Shaid et al., 2012). NDP52 or p62, labeled with specific antibodies (Figure 23a,b), co-localized with foci of endogenous LINE-1 RNA, LINE-1-MS2 (Figure 22a-d) and *Alu*-MS2 (Figure 23c,d). In four-color confocal microscopy exclusive markers of stress granules (mCherry-TIA-1) and P-bodies (GFP-DCP1A) were often adjacent, but not co-localized as expected (Kedersha et al., 2005) (Figure 22e). p62 preferentially co-localized with mCherry-TIA-1 compared to NDP52, while NDP52 preferentially co-localized with GFP-DCP1A (Figure 22e,f). NDP52 co-localized with a small proportion of stress granules (Figure 22f,g), but p62 was always also present in these stress granules (Figure 22h). Similarly, p62 co-localized with a small proportion of P-bodies, but NDP52 was virtually always co-present (Figure 22e-h). A third autophagy receptor, NBR1, also co-localized with a subset of P-bodies (Figure

23e,f). NDP52 and p62 also preferentially co-localized with markers of endogenous P-bodies (GW182) and arsenite-induced stress granules (DDX3) respectively (Figure 24a-e). This suggests that p62 and NDP52 are preferentially recruited to stress granules and P-bodies respectively, which frequently co-localize with autophagosomes (Figure 20g-i).

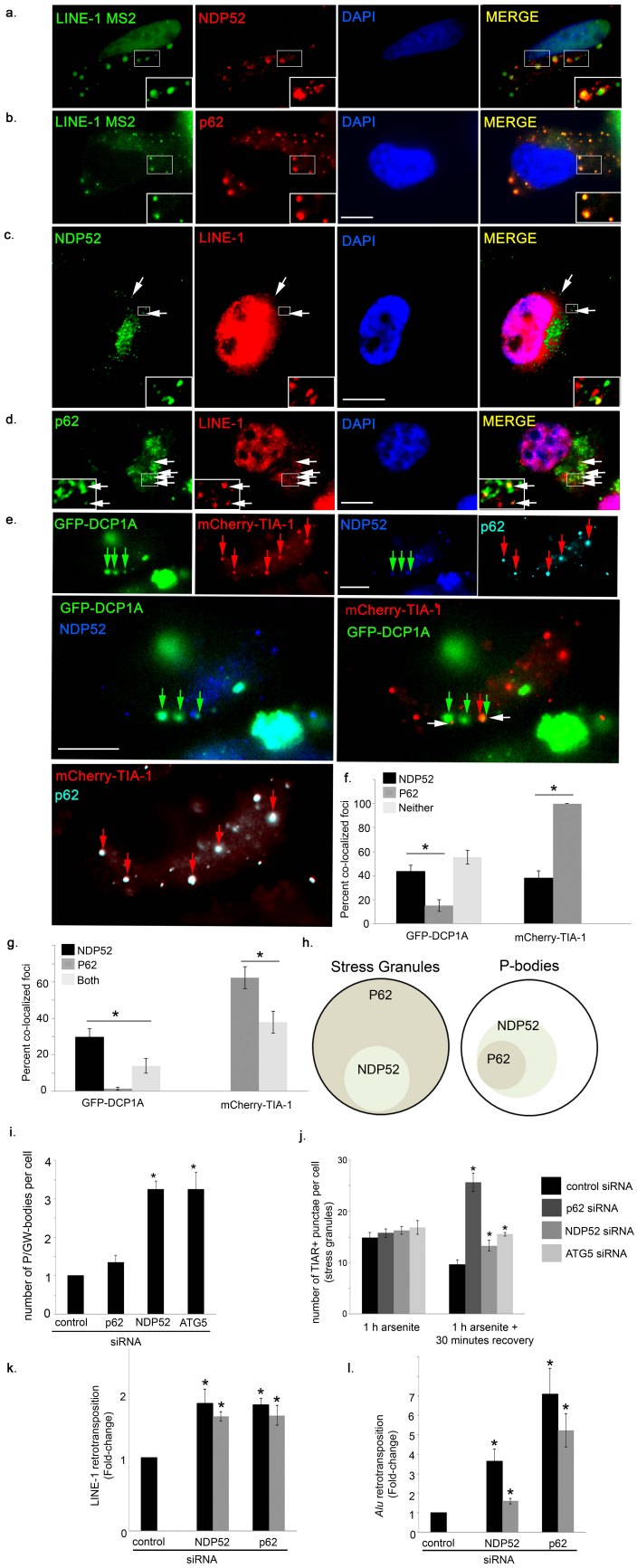
a.
LINE-1 MS2
NDP52
DAPI
MERGE
b.
LINE-1 MS2
p62
DAPI
MERGE
c.
NDP52
LINE-1
DAPI
MERGE
d.
p62
LINE-1
DAPI
MERGE
e.
GFP-DCP1A
mCherry-TIA-1
NDP52
p62
GFP-DCP1A
NDP52
mCherry-TIA-1
GFP-DCP1A
mCherry-TIA-1
p62
f.
NDP52
P62
Neither
Percent co-localized foci
GFP-DCP1A
mCherry-TIA-1
g.
NDP52
P62
Both
Percent co-localized foci
GFP-DCP1A
mCherry-TIA-1
h.
Stress Granules
P62
NDP52
P-bodies
NDP52
P62
i.
number of P/GW-bodies per cell
control
p62
NDP52
ATG5
siRNA
j.
number of TIAR+ punctae per cell (stress granules)
1 h arsenite
1 h arsenite + 30 minutes recovery
control siRNA
p62 siRNA
NDP52 siRNA
ATG5 siRNA
k.
LINE-1 retrotransposition (Fold-change)
control
NDP52
p62
siRNA
l.
Alu retrotransposition (Fold-change)
control
NDP52
p62
siRNA

Figure 22: LINE-1 RNA in P-bodies or stress granules is preferentially targeted for autophagic degradation by NDP52 and P62, respectively

(**a**,**b**) Fluorescent microscopy of (**a**) NDP52 or (**b**) P62 in cells expressing LINE-1-MS2 and MS2-GFP. (**c**,**d**) Fluorescent microscopy of endogenous LINE-1 RNA and (**c**) NDP52 or (**d**) P62. (**e**) Four-colour confocal microscopy of NDP52, P62, GFP-DCP1A and mCherry-TIA-1. (**f**) Percent of foci of NDP52, P62 or neither co-localizing with GFP-DCP1A or mCherry-TIA-1. **P*=0.007 GFP-DCP1A, *P*=0.00005 mCherry-TIA-1, analysis of variance (ANOVA). (**g**) Percent of foci of NDP52, P62 or both co-localizing with GFP-DCP1A or mCherry-TIA-1, *n*=674 stress granules, *n*=53 P-bodies. **P*=0.043 GFP-DCP1A, *P*=0.028 mCherry-TIA-1, ANOVA. (**h**) Venn diagram of the percent of P-bodies (GFP-DCP1A) or stress granules (mCherry-TIA-1) co-localizing with NDP52, P62, both or neither. (**i**) Relative number of P-bodies per cell (detected with 18033 serum-recognizing GW182) treated with indicated siRNAs. *n*=3, **P*=0.0002 NDP52, *P*=0.004 ATG5. (**j**) Relative number of stress granules (detected with antibody recognizing TIAR) 1 h after arsenite treatment and after 30 min recovery from 1 h treatment with arsenite. *n*=3, **P*=4x10^{-6} p62, *P*=0.019 NDP52, *P*=2 × 10^{-5} ATG5, ANOVA. (**k**) Percent of cells expressing GFP when co-transfected with LINE-1-RP retrotransposition GFP reporter and either of two independent siRNA (black and grey bars) targeting NDP52, P62 or control. Results are normalized to a retrotransposition-incompetent control (*n*=3, **P*=0.017, *P*=0.002 NDP52; *P*=0.001, *P*=0.013 p62, ANOVA). (**l**) Relative number of G418-resistant colonies in cells transfected with siRNA-targeting NDP52, P62 or control, *Alu*-retrotransposition reporter and retrotransposition-enhancer LINE-1 ORF2p (*n*=3, **P*=0.012, *P*=0.011 NDP52; *P*=0.008, *P*=0.011 p62, ANOVA). All error bars represent s.e. of the mean. All experiments were performed with a minimum of three biological replicates.

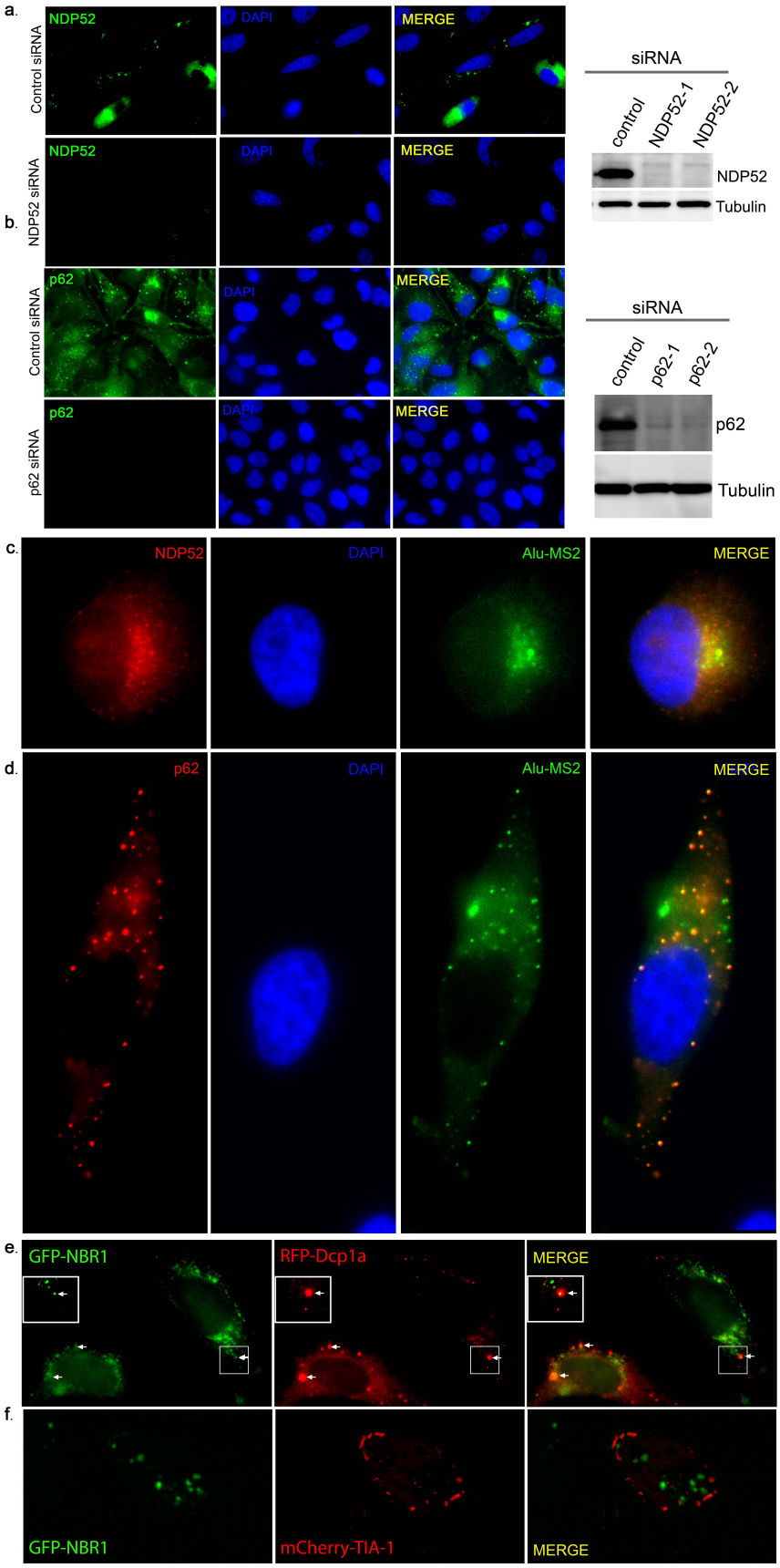
a.
Control siRNA
NDP52
DAPI
MERGE
b.
NDP52 siRNA
NDP52
DAPI
MERGE
siRNA
control
NDP52-1
NDP52-2
NDP52
Tubulin
Control siRNA
p62
DAPI
MERGE
p62 siRNA
p62
DAPI
MERGE
siRNA
control
p62-1
p62-2
p62
Tubulin
c.
NDP52
DAPI
Alu-MS2
MERGE
d.
p62
DAPI
Alu-MS2
MERGE
e.
GFP-NBR1
RFP-Dcp1a
MERGE
f.
GFP-NBR1
mCherry-TIA-1
MERGE

Figure 23: *Alu* RNA co-localizes with NDP52 and P62, NBR1 co-localizes with some P-bodies

(**a,b**) Western blot and immunofluorescent microscopy analysis of P62 and NDP52 in cells treated with control siRNA or siRNA targeting NDP52 (**a**) or P62 (**b**). (**c,d**) Fluorescent microscopy of NDP52 (**c**) or P62 (**d**) in cells transfected with *Alu*-MS2 and MS2-GFP. (**e,f**) Fluorescent microscopy of cells transfected with GFP-NBR1 and (**e**) RFP-DCP1A or (**f**) mCherry-TIA-1. GFP-NBR1 co-localizes with a subset of RFP-DCP1A foci (P-bodies), but no co-localization with foci of mCherry-TIA-1 (stress granules) was observed. All scale bars are 10 μM. Experiments were replicated at minimum two times.

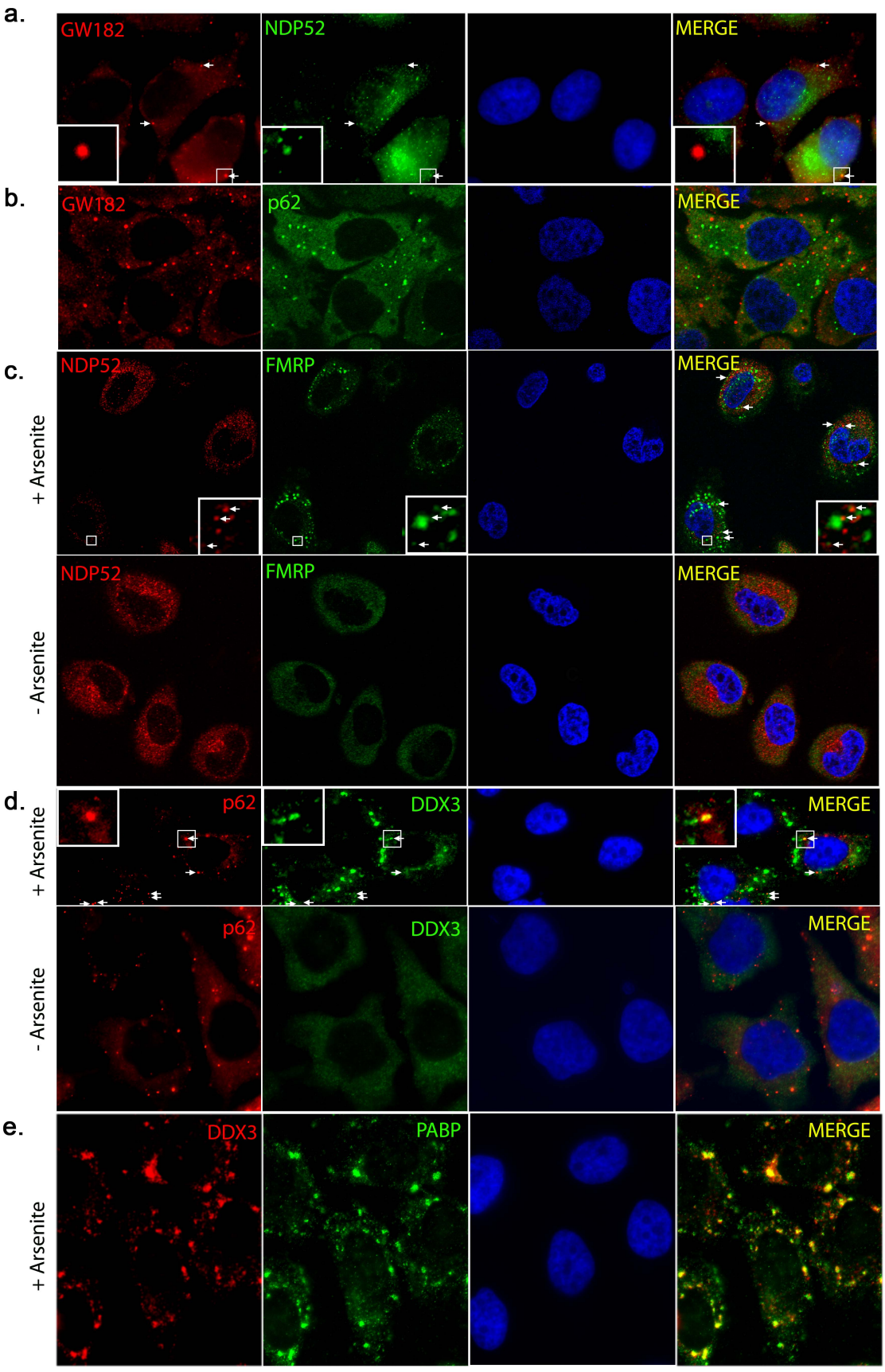
a.
GW182
NDP52
MERGE
b.
GW182
p62
MERGE
c.
+ Arsenite
NDP52
FMRP
MERGE
- Arsenite
NDP52
FMRP
MERGE
d.
+ Arsenite
p62
DDX3
MERGE
- Arsenite
p62
DDX3
MERGE
e.
+ Arsenite
DDX3
PABP
MERGE

Figure 24: NDP52 and P62 co-localize with endogenous markers of P-bodies and stress granules respectively

NDP52 (**a**) but not p62 (**b**) co-localizes with a subset of P-bodies labeled with serum recognizing GW182. (**c**) NDP52 does not co-localize with a marker of arsenite-induced stress granules (FMRP) (Mazroui et al., 2002) in the absence or presence of arsenite (1 h, 0.5 mM). (**d**) p62 co-localizes with a subset of arsenite-induced stress granules (1 h, 0.5 mM) labeled with DDX3 (Shih et al., 2012). (**e**) DDX3 co-localizes with a marker of stress granules (PABP) in cells treated with arsenite. All scale bars are 10 μM. Experiments were performed a minimum of two times each.

Previous work demonstrated that stress granules and P-bodies can be degraded by autophagy (Buchan et al., 2013). NDP52 selectively localized with P-bodies (Figure 22e-h, Figure 24a-d) and knockdown of NDP52, but not p62 caused a marked increase in the number of P-bodies per cell (Figure 22i, Figure 25a). Similarly, p62 selectively labeled stress granules (Figure 22e-h, Figure 24a-d) and knockdown of p62, and to a lesser extent NDP52, caused a marked increase in stress granules in cells during recovery from arsenite-induced stress (Figure 22j, Figure 25b,c). This suggests p62 and NDP52 selectively target stress granules and P-bodies respectively, for degradation by autophagy. NDP52 and p62 exhibited more co-operative effects on number of P-bodies labeled with GFP-Dcp1a and stress granules induced by over-expression of mCherry TIA-1 (Figure 25d,e). This closely resembles targeting of bacteria invading the cytoplasm in which p62 and NDP52 are also recruited independently, but collaboratively target bacteria for autophagic engulfment (Cemma, Kim, & Brumell, 2011).

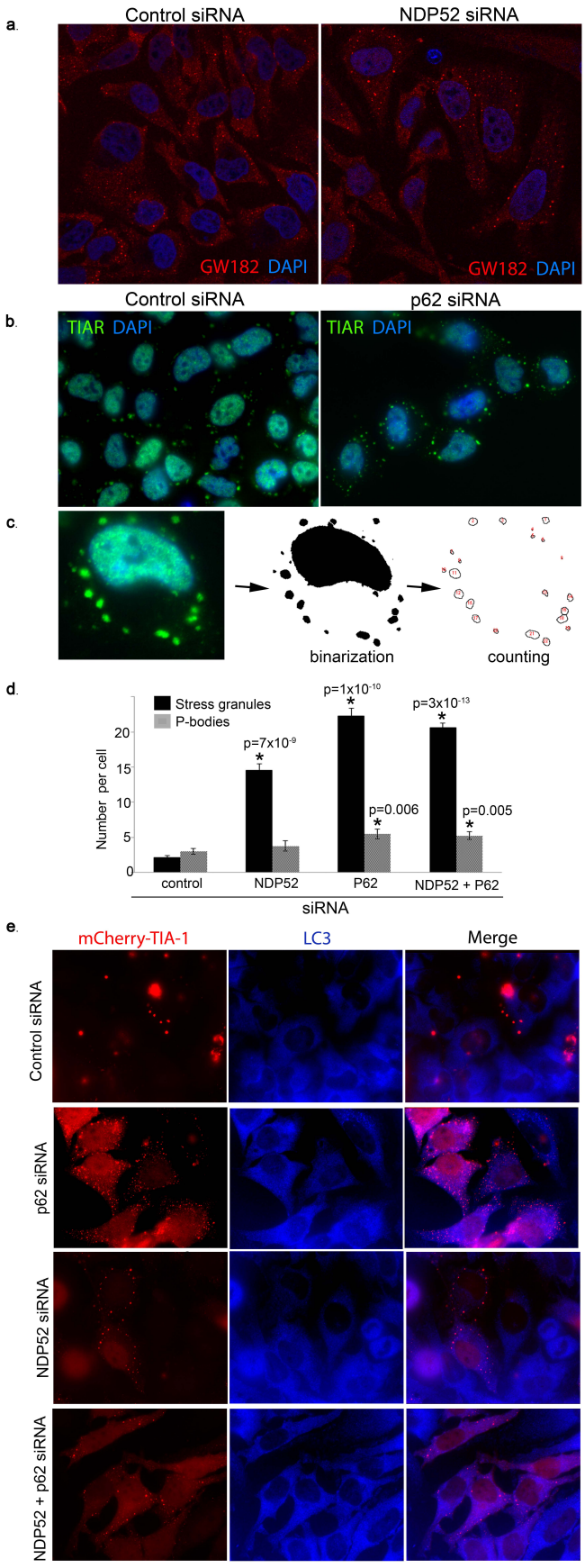
a.
Control siRNA
NDP52 siRNA
GW182 DAPI
GW182 DAPI
b.
Control siRNA
p62 siRNA
TIAR DAPI
TIAR DAPI
c.
binarization
counting
d.
Stress granules
P-bodies
Number per cell
p=7x10-9
p=1x10-10
p=0.006
p=3x10-13
p=0.005
control
NDP52
P62
NDP52 + P62
siRNA
e.
mCherry-TIA-1
LC3
Merge
Control siRNA
p62 siRNA
NDP52 siRNA
NDP52 + p62 siRNA

Figure 25: Depletion of P62 and NDP52 causes stress granules and P-bodies to accumulate

(**a**) Representative images of P-bodies (serum 18033 recognizing GW182) in cells treated with siRNA targeting NDP52 or control. (**b**) Representative images of stress granules (TIAR) in cells treated with siRNA targeting p62 or control. (**c**) Example of the process used to quantify stress granules and P-bodies. Thresholds were set according to methods and images were binarized to black and white. Punctae from 0.5 to 10 pixel area were automatically counted using the Particle Analyzer function of ImageJ. (**d**) Relative number of foci of GFP-DCP1A or mCherry-TIA-1 in cells treated with siRNA targeting NDP52, P62, both or control. N=98 cells, 1638 stress granules, 466 P-bodies. (n=3, NDP52 $p=7x10^{-9}$ stress granules; p62 $p=1x10^{-10}$ stress granules, p=0.006 P-bodies; NDP52+p62 $p=3 \times 10^{-13}$ stress granules, p=0.005 P-bodies). (**e**) Representative images of stress granules in cells treated with siRNA targeting p62, NDP52, both NDP52 and p62, or control. All scale bars are 10 μM.

NDP52 and p62 limit genomic insertions of retrotransposons

Knockdown of p62 or NDP52 (Figure 23a,b) increased levels of LINE-1 and *Alu* RNA (Figure 26a,b). Independent *Alu* elements of 250-350 nt also increased in cells depleted of NDP52 or p62 with siRNA (Figure 19a, Figure 26c,d). Knockdown of p62 or NDP52 also increased the rates of genomic insertion of LINE-1 and *Alu* (Figure 22k,l, Figure 26e,f). Together, this suggests that p62 and NDP52 selectively target stress granules and P-bodies containing retrotransposon RNA for degradation by autophagy, thereby preventing the insertion of LINE-1 and *Alu* into the genome.

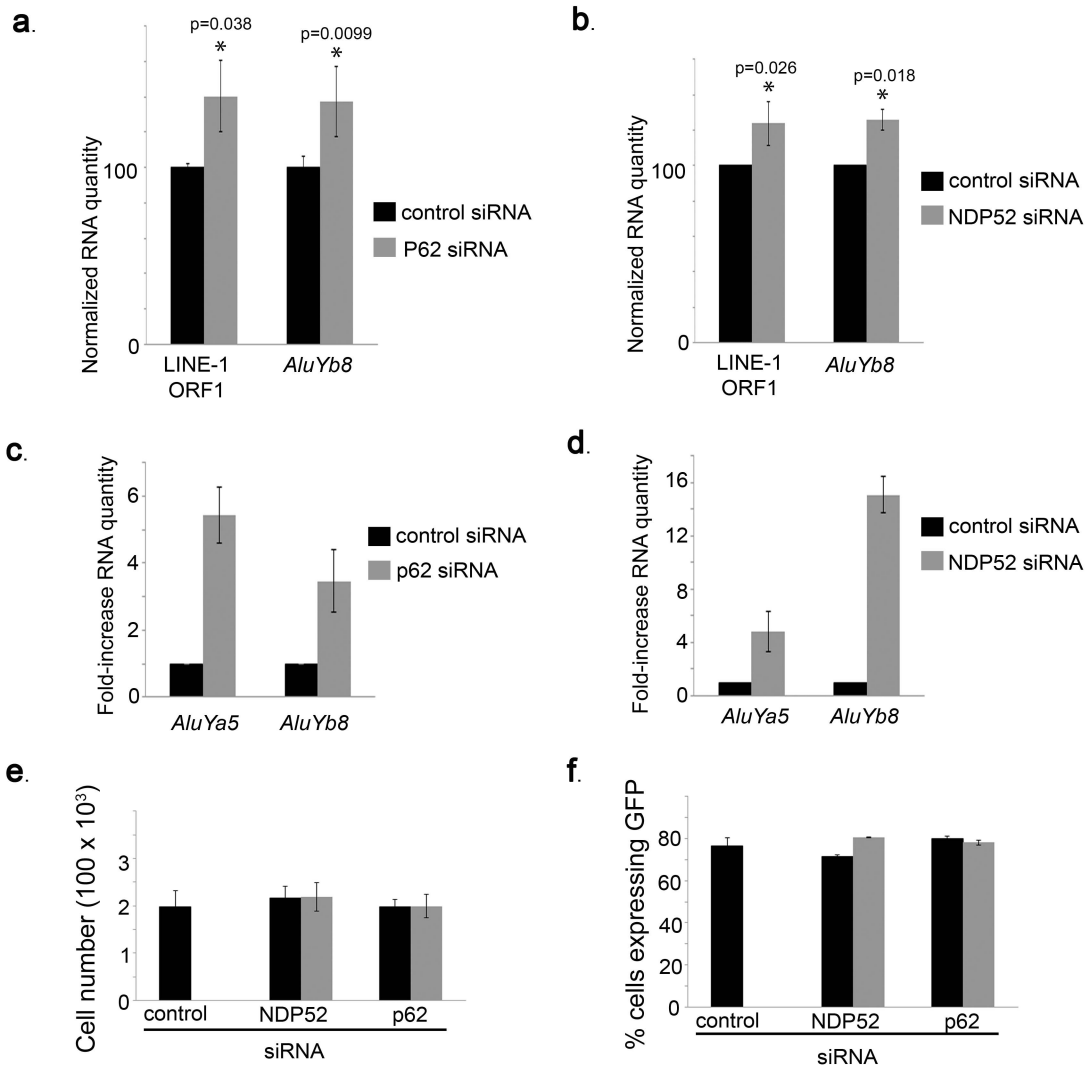

Figure 26: Depletion of P62 and NDP52 causes retrotransposon RNA to accumulate

(**a,b**) RT-qPCR analysis of levels of LINE-1 RNA (ORF1) and *AluYb8* in cells transfected with siRNA targeting (**a**) P62, (**b**) NDP52 or control. (**c,d**) RT-qPCR analysis of levels of *AluYa5* and *AluYb8* among RNA of 250-350 nt in cells transfected with siRNA targeting p62 (**c**) or NDP52 (**d**). (**e**) Percent of cells expressing GFP when co-transfected with plasmid expressing GFP and either of two independent siRNA (black and grey bars) targeting NDP52, P62 or control (n=3). (**f**) Relative number of cells at experiment's

termination if cells were transfected with either of two independent siRNA targeting NDP52, P62 or control (black and grey bars).

Beclin1/Atg6 mice accumulate retrotransposon insertions

BECLIN1/ATG6 (*BECN1/ATG6),* a gene required for autophagosome biogenesis (X. Qu et al., 2003), is lost in 40-70% of human breast and ovarian cancer patients (Levine & Kroemer, 2008). To examine whether *Becn1/Atg6* controls LINE-1 activity in a controlled system we used *Becn1/Atg6*$^{+/-}$ mice. Levels of LINE-1 RNA increased in ovaries of *Becn1/Atg6*$^{+/-}$ mice compared to wild-type (Figure 27a). We tested the relative number of LINE-1 genomic insertions using an established qPCR assay that is specific for the small number of active LINE-1 (approximately 1,290) and faithfully mirrors rates of insertion analyzed by genome sequencing (Baillie et al., 2011; Muotri et al., 2005). Importantly, this assay measures relative quantity of ORF2 (3' of LINE-1) normalized to the 5'UTR of LINE-1 which is truncated in virtually all new LINE-1 insertions (Beck et al., 2011). This ensures that *de novo* insertions of LINE-1 are measured rather than unrelated chromosomal amplification. In *Becn1/Atg6*$^{+/-}$ mice the relative number of LINE-1 insertions increased in ovary (13%, Figure 27b) compared to wild-type controls. This represents approximately 150 new insertions per cell in the ovary, in the range of LINE-1 insertions observed during neurogenesis (Muotri et al., 2010). Other studies had observed higher rates of LINE-1 insertions in brain and muscle than in liver and other tissues (Kano et al., 2009; Muotri et al., 2010). Screening other tissues for LINE-1 activity in *Becn1/Atg6*$^{+/-}$ mice we observed that levels of LINE-1 RNA increased in pre-frontal cortex (Figure 27c). Levels of genomic insertions of LINE-1 increased in pre-frontal cortex and muscle, but not liver (Figure 27c,d). This suggests that *Atg6/Becn1* and autophagy control retrotransposon RNA levels and retrotransposon-mediated genetic change in mice.

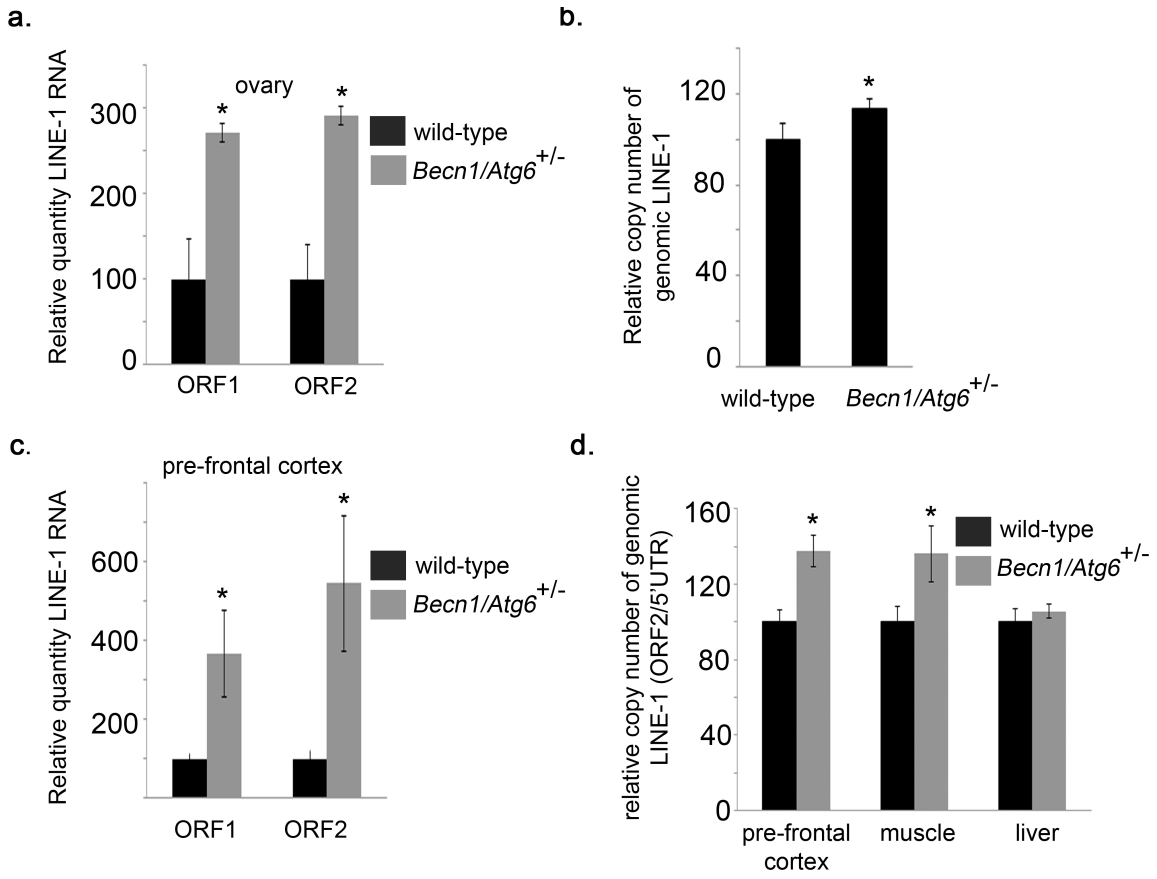

Figure 27: Levels of LINE-1 RNA and genomic insertions increase in mice with loss of *Becn1/Atg6*

(**a**) RT-qPCR analysis of the levels of LINE-1 ORF1 and ORF2 RNA in ovaries of *Becn1/Atg6*$^{+/-}$mice compared with wild-type controls (*n*=4 wild-type, *Becn1/Atg6*$^{+/-}$ mice). (**b**) qPCR analysis of relative number of genomic copies of LINE-1 ORF2 in ovaries of *Becn1/Atg6*$^{+/-}$mice and wild-type controls normalized to LINE-1 5′UTR and 5S rDNA (*n*=4 wild-type, 6 *Becn1/Atg6*$^{+/-}$ mice). **P*=0.02, *t*-test. (**c**) RT-qPCR analysis of the levels of LINE-1 ORF1 and ORF2 RNA in the prefrontal cortex of *Becn1/Atg6*$^{+/-}$ mice compared with wild-type controls (*n*=4 wild-type, *Becn1/Atg6*$^{+/-}$ mice). (**d**) qPCR analysis of relative number of genomic copies of LINE-1 ORF2 in muscle, liver and prefrontal cortex of *Becn1/Atg6*$^{+/-}$ mice and wild-type controls normalized to LINE-1 5′UTR and 5S rDNA (*n*=4 wild-type,

6 *Becn1/Atg6*$^{+/-}$ mice). *P=0.019 prefrontal cortex, P=0.048 muscle, analysis of variance. All error bars represent s.e. of the mean.

3.4 Discussion

Autophagy is a selective, stress-enhanced mechanism for degrading specific cytoplasmic contents. Despite critical roles for autophagy in cancer and several other diseases, surprisingly little is known about RNA degradation by autophagy. Data presented here strongly suggests that retrotransposon RNA is degraded by autophagy, and that impeding this process causes accumulation of retrotransposon RNA and genomic insertions. Evidence to date suggests that RNAs are targeted for autophagic degradation as part of RNA granules such as stress granules (Buchan et al., 2013; Dirac, Huthoff, Kjems, & Berkhout, 2002). Autophagy may be a more efficient mechanism for disposing of such large clusters of RNA than canonical RNA degradation complexes. Our evidence demonstrates that NDP52 preferentially localizes to P-bodies, while p62 preferentially localizes to stress granules, suggesting autophagy can selectively target distinct RNA granules (Figure 28). Intriguingly, emerging evidence suggests that pathology in amyotrophic lateral sclerosis (ALS) involves inhibited autophagic degradation of mutant proteins like TDP43 and FUS in stress granules (Buchan et al., 2013). Our identification of p62 as a selective autophagy receptor for degradation of stress granules, suggests a mechanism for the genetic implication of p62 in ALS (B. Mathew, Suresh, Anbazhagan, & Mathew, 2013).

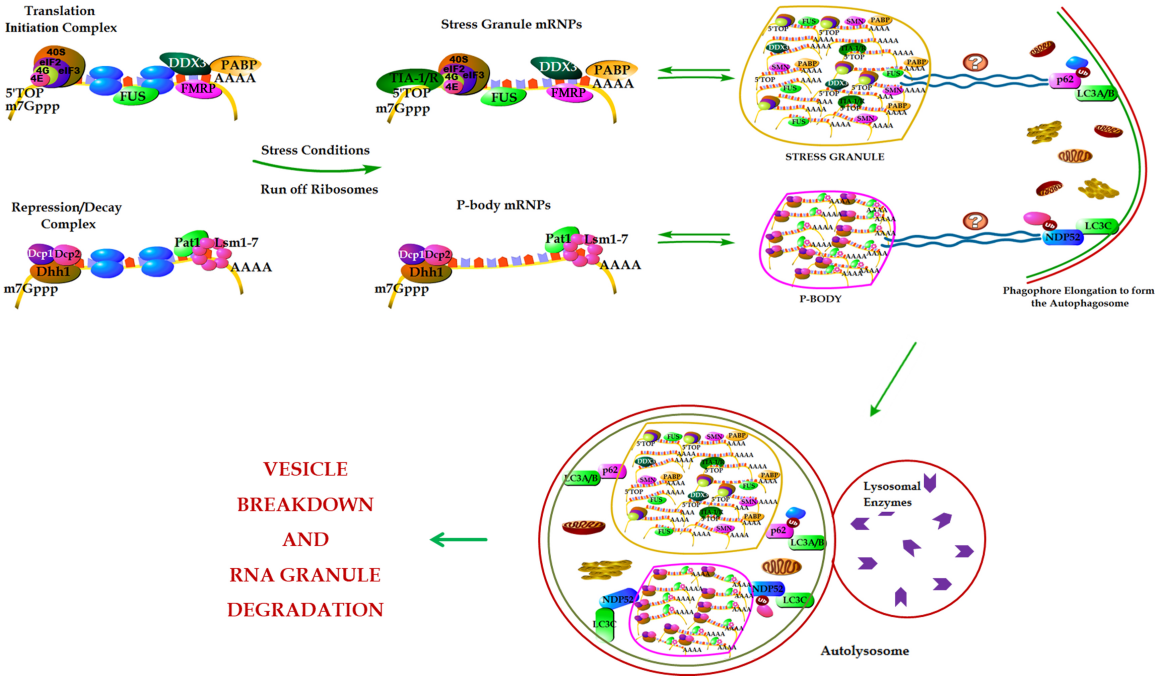

Figure 28: Schematic model of RNA granule clearance by autophagy

RNA granules - stress granules and processing bodies are degraded by preferential recruitment of selective autophagy receptors - p62 and NDP52 respectively.

Levels of LINE-1 RNA and genomic insertions also increase when a copy of the autophagy-critical gene *Becn1/Atg6* is lacking in mice, suggesting that loss of *BECN1/ATG6* which is common in ovarian, breast and prostate cancers may lead to LINE-1-induced genetic instability. A previous study demonstrated that *BECN/ATG61*$^{+/-}$ cells exhibit genetic instability and marks of DNA damage responses for unknown reasons (R. Mathew et al., 2007). LINE-1 and *Alu* retrotransposons instigate much more chromosomal instability than their insertions alone; LINE-1 ORF2p endonuclease activity generates double-stranded DNA breaks in great excess of those required for re-insertion of LINE-1 into the genome (Pepin et al., 2013). LINE-1 and *Alu* are also a frequent cause of interchromosomal translocations, intrachromosomal deletions, inversions, and amplifications (Dewannieux, Blaise, & Heidmann, 2005; Perez-Iratxeta et al., 1998;

Sandie et al., 2009). This suggests that unmoderated LINE-1 activity could contribute to the genomic instability caused by lack of autophagy in *BECN1/ATG6*$^{+/-}$ cells (R. Mathew et al., 2007). Interestingly, only 15% of *BECN1/ATG6*$^{+/-}$ mice develop tumours (X. Qu et al., 2003) suggesting the underlying process is stochastic, like the insertion of retrotransposons into the genome.

Mechanisms that promote genetic, or epigenetic diversity in response to stress may be favored by evolution (Netzel, Perez-Iratxeta, Bork, & Andrade, 2003). Proteins that suppress retrotransposons can act as capacitors or buffers of phenotypic diversity (Specchia et al., 2010). Many stresses induce transcription of retrotransposons and may promote somatic or inherited genetic change (Wissing et al., 2012). Our results suggest that autophagy, as a stress-induced response, tempers somatic variegation and evolutionary change by degrading retrotransposon RNA.

3.5 Methods

RT-qPCR

RT-qPCR was performed with the MiScript II Reverse Transcriptase system (Qiagen) and GoTaq® qPCR Master Mix (Promega A6002). The following primers were used, as described (Muotri et al., 2010) to quantify RNA in human cells: L1-ORF1: 5'-TCA AAG GAA AGC CCA TCA GAC TA-3', 5'-TGG CCC CCA CTC TCT TCT-3'; L1-5UTR: 5'-ACG GAA TCT CGC TGA TTG CTA-3', 5'-AAG CAA GCC TGG GCA ATG-3'; Alu-Sg: 5'-TTC GAG ACC AGC CTG GCC-3', 5'-CT CCC GGG TTC AAG CGA-3'; Alu-Ya5: 5'-TCC CGG CTA AAA CGG TGA AA-3', 5'-CTC CCA AGT AGC TGG GAC TAC AGG-3'; Alu-Yb8: 5'-ATC CTG GCT AAC AAG GTG AAA CCC-3', 5'-CGG ACT GCT GGA CTG CAG TG-3', β-actin: 5'-GGCATGGGTCAGAAGGATT- 3′ and 5′-GGGGTGTTGAAGGTCTCAAA- 3′; GAPDH: 5'-ATC TTC TTG TGC AGT GCC AG-3',

5’-TTT GCC ACT GCA AAT GGC AG-3’ For RT-qPCR of mouse tissues primers were designed as described (Muotri et al., 2010): 18S: 5’-ATG GTA GTC GCC GTG CCT AC-3’;5’- CCG GAA TCG AAC CCT GAT T-3’; mL1-ORF1a: 5’-ACT CAA AGC GAG GCA ACA CTA GA-3’;5’-GTT CCA GAT TTC TTT CCT AGG GTT TC-3’; mL1-ORF1b: 5’-AGG CTA CTA TAC CCA GCC AAA CTC T-3’;5’-TAC TTT GGT TTC TCC CTC TAT GAT AAT TG-3’; mL1-ORF2a: 5’-CCT CCA TTG TTG GTG GGA TT-3’;5’- GGA ACC GCC AGA CTG ATT TC-3’; mL1-Orf2b: 5’- CTG GCG AGG ATG TGG AGA A-3’; 5’-CCT GCA ATC CCA CCA ACA AT-3’. Relative quantities were calculated using the [delta][delta]CT method, normalizing to the geometric mean of β-actin and GAPDH.

Quantitative PCR (qPCR) of genomic LINE-1

Quantification of genomic insertions of LINE-1 was performed as described (Baillie et al., 2011; Muotri et al., 2010). Briefly, genomic DNA was isolated using GenElute Mammalian Genomic DNA Miniprep kits (Sigma, G1N70-1KT), which includes RNAse A treatment of genomic DNA. LINE-1 ORF2, 5’UTR or 5S rRNA were amplified in quadriplicate with the polymerase and primers previously described (Muotri et al., 2010) using GoTaq® qPCR Master Mix (Promega A6002). We calculated the percent increase in LINE-1 insertions as described (Baillie et al., 2011; Muotri et al., 2010). LINE-1 insertions are overwhelmingly (~99%) and severely truncated at the 5’ end, therefore the relative number of new insertions are estimated in this method normalizing LINE-1 ORF2 (3’) to LINE-1 5’UTR and 5S (Muotri et al., 2010) to avoid measuring genomic amplification due to other effects than LINE-1 insertion.

Cells and reagents

HeLa (CCL2, ATCC), 293T cells (CRL-3216, ATCC) OVCA 420 and OVCA 432 were cultured in DMEM containing 10% FBS and 2mM L-glutamine. The following plasmids

were gifts of J. Goodier (John Hopkins): GFP-MS2 (Mostowy & Cossart, 2012), LINE-1-MS2 (Goodier, Cheung, & Kazazian, 2012), Alu-MS2 (Goodier et al., 2012), GFP-ORF1p (Goodier, Zhang, Vetter, & Kazazian, 2007). GFP-Dcp1a (gift of W. Filipowicz, Freidrich Miescher Institute), GFP-Ge-1 (Bloch, Gulick, Bloch, & Yang, 2006), TIA-mCherry (gift of J. Cote, University of Ottawa) were also used. The following primary antibodies were used in this study: LC3 (Cell Signaling #2775), ORF1p (C. R. Harris et al., 2010) (a kind gift of C. Harris, University of Medicine and Dentistry of New Jersey), DICER (clone 13D6, Santa Cruz), NDP52 (ab688588), P62 (clone 3, BD Biosciences), DDX3 (A300-474A, Bethyl Labs), FMRP (clone 1C3, Millipore), TIAR (Cell Signaling Technology), Rck (#9407, Cell Signaling Technology), TOM20 (clone FL-145, Santa Cruz), Calnexin (polyclonal, Stressgen), and Alix (clone 2H12, Santa Cruz) and serum 18033 recognizing GW182 (Eystathioy et al., 2002) (a kind gift of M. Fritzler, University of Calgary). All antibodies were used at 1/500 dilutions. Silencer Select siRNAs (Life Technologies) were transfected with RNAiMax (Life Technologies). The siRNAs used were: ATG5 5′-AUAUCUCAUCCUGAUAUAGCgt-3′ (siRNA ID s18160) and 5′-AUGAGCUUCAAUUGCAUCCtt-3′ (siRNA ID s18158), P62 5′-siRNAUUUAAUGUAGAUUCGGAAGat-3′ (siRNA ID s16962) and 5′-UCUUUUCCCUCCGUGCUCCac-3′ (siRNA ID s16960) and NDP52 5′-siRNAAAAGUAACCCACAUGAAGGtg-3′ (siRNA ID s19996) and 5′-UUUGUUGUUUAGGUCAAUGgg-3′ (siRNA ID s19994).

Gel extraction of RNA for RT-qPCR of *Alu* RNA

RNA was separated on a 6% acrylamide gel and stained with ethidium bromide. The region between 250-350 nucleotides was excised with a scalpel and incubated with 400 µL of gel elution buffer (20 mM Tris-HCl, 0.25 M sodium acetate, 1 mM EDTA, 0.25% SDS, pH 7.5). The mixture was frozen on dry ice for 15 minutes and incubated at room

temperature overnight to allow RNA to diffuse from the gel. The mixture was subsequently centrifuged at 21 000 g for 10 min at room temperature. The supernatant was retrieved for RNA purification with Trizol reagent (Invitrogen).

Pulse-labeling of RNA with ethynyl-uridine

Pulse-labeling was performed with Click-iT technology using the Nascent RNA Click-iT kit (Life Technologies) according to manufacturer's instructions. Briefly, cells were plated at 2.5 x 10^5 per well in a 6 well plate and transfected with siRNA the following day. Forty-eight hours after transfection ethynyl-uridine (EU, 0.2 mM)) was added. Media was changed after one hour incubation and RNA was extracted immediately or after four more hours using Trizol reagent. EU incorporated in RNA (5 µg) was labeled with biotin (0.5 mM biotin azide per sample). Pulse-labeled, biotinylated RNA (500 ng) was captured using Dynabeads Streptavidin T1 magnetic beads and used as a template for cDNA synthesis using using SuperScript VILO cDNA Synthesis Kit (Life Technologies).

RNA decay with actinomycin D

Cells were plated in 6 well plates at a concentration of 2.5 x 10^5 per well. DMSO or Bafilomycin (400 nM, Millipore) were added to wells for 30 minutes, then Actinomycin D (Sigma-Aldrich) was added at a final concentration of 5 µg per ml. RNA was extracted from cells immediately, or 1, 4 or 8 h later using TRI reagent (Sigma, T9424-200ML), cDNAs were synthesized using SuperScript VILO cDNA Synthesis Kit (Invitrogen, 11754-250).

Alu retrotransposition assay

Retrotransposition assay was performed as described (Dewannieux et al., 2003; Goodier et al., 2012). In brief, 5x10^3 cells were plated in a 60mm dish. The following day

Alu-neo ^{Tet} (Dewannieux et al., 2003; Goodier et al., 2012) was co-tranfected with the retrotransposition driver plasmid pCEP 5'UTR ORF2-no neo (Alisch, Garcia-Perez, Muotri, Gage, & Moran, 2006) or pcDNA3.1 (control) and 10 nM of siRNA using Lipofectamine 2000 (Invitrogen). SiRNA alone was transfected as an additional control for selection. One week after transfection the cells were counted and $5x10^3$ cells were replated in 100 mm plates. The second day after replating, 600 µg per mL G418 (Life Technologies) was added and replaced every three days. After 10 days of selection, colonies were stained with crysal violet (Sigma-Aldrich), and counted.

LINE-1 retrotransposition assay

Retrotransposition assays were performed as described (Goodier et al., 2012). Briefly, 2.5×10^5 cells per well were seeded in 6-well dishes. The next day, 1.0 µg of 99 RPS-GFP PUR, containing LINE-1-RP coupled with an EGFP retrotransposition reporter cassette or 99 RPS-GFP JM111 PUR, containing LINE-1-RP with two point mutations in ORF1 that abolish retrotransposition (J. Lin et al., 2012)(gifts of J. Goodier) (Goodier et al., 2012; Takamura et al., 2011a), was co-transfected together with 10 nM of siRNA using Lipofectamine 2000 (Invitrogen). All transfections were in triplicate. Five days post-transfection, percent GFP-expressing cells was measured by flow cytometry (FC500, Beckman Coulter). To account for effects of siRNA-mediated knockdown on transfection efficiency, or cell proliferation/death, independent cells were transfected with EGFP-N1-expressing plasmid.

Fluorescence microscopy

Cells were prepared for microscopy as previously described (D. Gibbings, Leblanc, et al., 2012; D. Gibbings, Mostowy, S., Jay, F., Schwab, Y., Cossart, P., Voinnet, O., 2012). Cells were grown on 0.17 mm glass coverslips overnight before fixation in 2% PFA in

PBS (10 min). Cells were rinsed twice in PBS and incubated 10 min with 0.2% Triton-X-100 in PBS and 20 mM NH_4Cl. After washing with PBS, cells were blocked with 5% milk in PBS (1 h), washed three times in PBS and incubated with 5 µg per mL primary antibody overnight at 4°C, washed three times (10 min) in PBS and incubated with 1/300 dilution of highly cross-adsorbed secondary antibodies (goat anti-mouse Alexa488, or -633, anti-rabbit Alexa488 or -546 [Invitrogen], or anti-rabbit DyLight 405 [Jackson Immunoresearch]) for 1 h. After washing three times (10 min) cells were mounted with Vectashield Mounting Media and imaged on a Zeiss AxioObserver Z1 or a Zeiss 510 confocal Microscope.

Endogenous LINE-1 RNA was labeled using 48 Quasar570 labeled probes designed and produced by Biosearch Technologies (Petaluma, CA, USA). The sequence of L1 probes was: TTTGTTTACCTAAGCAAGCC, CTGTCTTTTTGTTTGTCTGT, CACTTAAGTCTGCAGAGGTT, CTCTCTTCAAAGCTGTCAGA, ATGGGTTTTCGGTGTAGATG, TCTTTGCCTTTGGTTTGAAT, AAGCACTTCTCTGTATTGGT, CATTCTTCACGTAGTTCTCG, ATATTTCTTGGAGGCTTTGC, GGGAAGTTCTCCTGGATAAT, TTGATGCAGTTTCTTCCTAG, CCCATTATTAATGTGTGGGA, TAATGTTGACAGTGGGGTGT, TTGACTTTCTGTCTCGTTGA, AGAGCTGAGTTCAATTCCTG, AGATGTCTATTAGGTCTGCT, TAGTTTGATTGCACTGTGGT, TATGTGGTGTCTTTGTTCTC, AATTTTGGATCTTTCCTGCT, AATGTGTTTGCTCTTGCTTT, TTTGTGTCTCTATTTCCTTC, TGCTAGCGGTCTATCAATTT, TTTGCGTAGAGGTGTTTGTA, CTTTTTTGGTTGTGTCTCTG, GTCAAAGGCTTTTTCTGCAT, GTGGGTTTGTCATAGATAGC, AAGGGAATGCTTCCAGTTTT, AATACCCTTTATTTCCTTCT,

AGGGACAATTTGACTTCCTC, TTCACATCCCTTGTAAGTTG,
TTTATTTCCTTGAGCAGTGG, TTCTTCCATTTGTTTGTGTC,
CTTTGTTCTTTTGGCTTAGG, GAAGTCAGGTAGTGTGATGC,
AAGGAAGGGATCCAGTTTCA, CTGAATGGTAATGCCTAGGT,
ATGGTAGTTTCTTTTGCTGT, GCGAAAATTTTCTCCCATGT,
CACTTTTTGATGGGGTTGTT, ATGTGTTTTTTGGCTGCATA,
CCATTCTAACTGGTGTGAGA, CCCACCAACAGTGTAAAAGT,
CACACTGACTTCCACAATGG, GGTATATACCCAGTAATGGG,
CGTGTGCATGTGTCTTTATA, CCAAGTCTTTGCTATTGTGA,
TCATTGTTGGACATTTGGGT, TATGCGGTGTTTGGTTTTTT.

For labeling with FISH probes, cells were fixed in 1% formaldehyde in PBS for 10 min, washed twice in PBS, permeabilized with 0.2% Triton X-100 (7 min), washed again and incubated (5 min) in 10% formamide in 2X SSC buffer. Subsequently 3 μM of LINE-1 FISH probes and 2.5 μg per mL of LC3 antibody were incubated with cells overnight at 37 C in hybridization buffer (0.1% Triton X-100, 0.1% Tween-20, 100 mg per mL dextran sulfate and 10% formamide in 2X SSC). Sections were incubated with secondary antibody (1 h), washed with PBS and mounted.

Quantification of microscopy

Image fields were randomly selected. The number of stress granules (labeled with anti-TIAR antibody) and P-bodies (labeled with 18033 serum recognizing GW182) were quantified using the automatic particle counting tool of ImageJ. To distinguish particles of interest from background with minimal user-bias, a threshold range was calculated using Li's Minimum Cross Entropy method (C. T. Li, PKS, 1998). Binary images were obtained upon applying the threshold settings (see Figure 24c). Pixel area size was set to 0.05-10

μm to exclude the nuclear staining of TIAR and foci were counted using the Analyze Particles function of ImageJ. The total number of stress granules or P-bodies was then divided by the number of cells.

To calculate the number of P-bodies (GFP-Dcp1a) or stress granules (mCherry-TIA-1) per cell, the total number of each was counted per cell, based on DAPI staining and differential interference contrast images. In Figure 22f, each P-body (GFP-Dcp1a) or stress granule (mCherry-TIA-1) in a cell was counted as being co-localized with p62, NDP52 or neither p62 or NDP52 / total number of P-bodies or stress granules in the cell. In Figure 22g, each P-body (GFP-Dcp1a) or stress granule (mCherry-TIA-1) in a cell was counted as being co-localized with p62 alone, NDP52 alone, or both p62 and NDP52 / total number of P-bodies or stress granules in the cell. P-bodies or stress granules co-localizing with neither are not included in Figure 22g. Co-efficients of co-localization were calculated using Just Another Co-localization Plugin (JACoP) (Bolte & Cordelieres, 2006).

Autophagosome purification

Autophagosomes were fractionated essentially as described (Sahu et al., 2011). Twenty 160 cm^2 plates of 293 cells were harvested into 0.25 M sucrose 10 mM HEPES pH 7.2, washed several times in the same solution, transferred into 0.25 M sucrose containing protease inhibitor cocktail (Roche, EDTA-free) and disrupted by nitrogen cavitation (Parr Instruments, 100 psi 30 sec, 50 psi 30 sec, 25 psi 8 min). Lysate was centrifuged twice at 2000g to eliminate intact cells and large debris. Supernatant was then centrifuged at 17 000 g (12 min) to pellet organelles. The pellet was resuspended in 0.25 M sucrose 10 mM HEPES pH 7.2 and treated with a mixture of RNAse A/T1 (Fermentas) for 10 min, 37 C. Organelles were then loaded at the bottom of a discontinuous Histodenz density

gradient (26%, 24%, 20%, and 15%) and centrifuged at 90 000 g for 3 h in an SW41 rotor (Beckman). Fractions at the interface of 15-20% and 20-24% densities are enriched in autophagosomes and autophagolysosomes respectively. Autophagosome-enriched fractions were used for all analyses.

Analysis of *Becn1/Atg6*$^{+/-}$ mice

All experiments were approved by the University of Ottawa Animal Care Committee according to Canadian Council on Animal Care guidelines. Four week-old *Becn1/Atg6*$^{+/-}$ female mice and wild-type littermates from two independent litters were euthanized and ovaries, pre-frontal cortex, muscle and liver were harvested, flash-frozen in liquid nitrogen and stored at -80 C prior to analysis as above. Analysis was not blinded.

Statistics

Two-tailed t-tests or ANOVA were employed to evaluate statistical significance of RT-qPCR, retrotransposition and microscopy quantifications on a minimum of three independent biological replicates.

3.6 Acknowledgements

The authors wish to thank Jocelyn Coté for helpful comments and kindly providing several antibodies and constructs. This work was supported in part by grants to DG (J.P. Bickell Foundation, Canadian Cancer Society Research Institute) and DL (NSERC Discovery Grant).

Chapter 4 - Manuscript #3

Atg5 disassociates the V1V0-ATPase to promote exosome production and tumor metastasis independent of canonical macroautophagy

Publication information:

Huishan Guo, Maneka Chitiprolu, Luc Roncevic, Charlotte Javalet, Fiona J. Hemming, My Tran Trung, Lingrui Meng, Elyse Latreille, Christiano Tanese de Souza, Danielle McCulloch, R. Mitchell Baldwin, Rebecca Auer, Jocelyn Côté, Ryan Charles Russell, Rémy Sadoul, Derrick Gibbings. “Atg5 Disassociates the V1V0-ATPase to Promote Exosome Production and Tumor Metastasis Independent of Canonical Macroautophagy”. Developmental Cell 2017 Dec 18;43(6):716-730.

Author’s contribution:

Designed the experiments: MC, HG, RCR, RMB, JC, RA, RS, DG. Performed the experiments and analyzed the data: MC, HG, LR, CJ, FJH, MTT, LM, EL, CTdS, DM. Helped write the paper: MC, HG, RS, DG. Conceived the study: DG.

MC contributions by figure: Figure 32b,i-l, Figure 33a,d-e,i-j, Figure 34c-e, Figure 35a-b, Figure 36a,e, Figure 37b-d

Atg5 disassociates the V1V0-ATPase to promote exosome production and tumor metastasis independent of canonical macroautophagy

Huishan Guo[1], Maneka Chitiprolu[1], Luc Roncevic[1], Charlotte Javalet[3,4], Fiona J. Hemming[3,4], My Tran Trung[1], Lingrui Meng[1], Elyse Latreille[1], Christiano Tanese de Souza[5], Danielle McCulloch[1], R. Mitchell Baldwin[1], Rebecca Auer[5], Jocelyn Côté[1], Ryan Charles Russell[1], Rémy Sadoul[3,4] and Derrick Gibbings[1,2]

1. Department of Cellular and Molecular Medicine, University of Ottawa, 3131 Roger Guindon Hall, 451 Smyth Road, Ottawa K1H 8M5, Canada

2. Ottawa Institute for System Biology, University of Ottawa, Ottawa K1H 8M5, Canada

3. Institut National de la Santé et de la Recherche Médicale (INSERM), U1216, 38042 Grenoble, France

4. Université Grenoble Alpes, Institut des Neurosciences, 38042 Grenoble, France

5. Ottawa Hospital Research Institute, Ottawa K1H 8L6, Canada

4.1 Abstract

Autophagy and autophagy-related genes (Atg) have been attributed prominent roles in tumorigenesis, tumor growth, and metastasis. Extracellular vesicles called exosomes are also implicated in cancer metastasis. Here, we demonstrate that exosome production is strongly reduced in cells lacking Atg5 and Atg16L1, but this is independent of Atg7 and canonical autophagy. Atg5 specifically decreases acidification of late endosomes where exosomes are produced, disrupting the acidifying V1V0-ATPase by removing a regulatory component, ATP6V1E1, into exosomes. The effect of Atg5 on exosome production promotes the migration and *in vivo* metastasis of orthotopic breast cancer cells. These findings uncover mechanisms controlling exosome release and identify means by which autophagy-related genes can contribute to metastasis in autophagy-independent pathways.

4.2 Introduction

Exosomes are 40-120 nm vesicles released by many cell types (Colombo, Raposo, & Thery, 2014). As endosomes mature their membranes bud inward to produce vesicles inside the endosomal lumen (Hanson & Cashikar, 2012). These Multivesicular Bodies (MVB) can subsequently fuse with the plasma membrane to release their intraluminal vesicles to the extracellular space where they are called exosomes (Colombo et al., 2014).

Mechanisms underlying exosome production are slowly being elucidated. ESCRT and ESCRT-associated proteins are required for budding of vesicles into endosomes (Colombo et al., 2013). Rab27a and b control fusion of MVB with the plasma membrane to release exosomes (Ostrowski et al., 2010). However, steps controlling MVB fate after generation of intraluminal vesicles and before release of exosomes have remained obscure.

A complex of Autophagy-related genes (Atg) including Atg5-Atg12 and Atg16L1 terminates an enzymatic cascade culminating in the covalent modification of LC3-I (Atg8) with the lipid phosphatidylethanolamine (PE) to form LC3-II (Bento et al., 2016). Generation of LC3-II is canonically involved in the expansion of the phagophore and its closure to form a double-membraned autophagosome. Autophagosomes then fuse with late endosomes and lysosomes to degrade their engulfed cytoplasmic contents (Bento et al., 2016). While examples of non-canonical autophagy have recently been described that are independent of Atg5 and Atg7, the majority of autophagy pathways described to date are dependent on these two canonical factors.

The Atg5-Atg12 and Atg16L1 complex, along with LC3 has also been observed to localize to endosomes and phagosomes to secure the acidification of these

compartments and lysosomal degradation of pathogens or apoptotic cells they enclose (Florey, Kim, Sandoval, Haynes, & Overholtzer, 2011; Martinez et al., 2015). Other studies have also shown that autophagy genes promotes lysosomal trafficking and degradation of endosomal contents (Peng et al., 2014; J. Zhou, S. H. Tan, et al., 2013). The mechanism underlying the effects of Atg5 on acidification of phagosomes and endosomes are unclear (Ktistakis & Tooze, 2016).

If Atg5, Atg16L1 and LC3 localize to multiple types of endosomes it is plausible that they localize to subpopulations of MVB producing exosomes as well, and could impact exosome biogenesis or release. Several studies have begun to investigate the effects of Atg genes on exosome production but the results of this research have frequently been contradictory. A unique covalent Atg3-12 complex, that like the Atg5-Atg12 complex requires Atg7 for its formation, promotes exosome release (Murrow et al., 2015). While this agrees with a subsequent report that Atg7 is required for release of hepatitis C in exosome-like vesicles (Shrivastava et al., 2016), it contradicts a previous report that Atg7 has no impact on exosome release (Sahu et al., 2011). Other studies have observed that Bafilomycin or other inhibitors of lysosomal acidification, that also can inhibit autophagy and autophagic degradation increase exosome release (Alvarez-Erviti et al., 2011). Effects of these inhibitors on exosome release have at times been attributed to a blockade in autophagy although the mechanism is unknown. These apparent contradictions may be due to the reliance of each of these studies on particular types of exosomes (e.g. hepatitis C virus containing) and Western blot to quantify exosome release. Western blot cannot differentiate whether effects are due to larger contaminating vesicles, effects on a subpopulation of exosomes or specific exosome contents (Colombo et al., 2013; Lotvall et al., 2014; Tauro et al., 2013). To avoid these possibilities, recent guidelines recommend at least two methods to quantify exosome

release including one that quantifies populations of exosomes using their characteristic size (Lotvall et al., 2014). In sum, the effect of genes required for autophagy like Atg5 and Atg16L1 on exosome production have not been studied, and published data on the effect of other Atg genes on exosome production are contradictory, suggesting that this subject requires more in-depth investigation.

Here, using multiple orthogonal approaches we demonstrate that Atg5 is required for exosome production but that this is independent of Atg7 and canonical autophagy. Atg5 detaches ATP6V1E1 from the V_1V_0-ATPase that acidifies MVB. This disassembles the V_1V_0-ATPase complex, decreases the acidification of MVB and promotes release of exosomes. Atg5-dependent control of exosome production increases migration of breast cancer cells *in vitro* and promotes metastasis *in vivo* in an orthotopic model of breast cancer.

4.3 Results

Exosome levels are decreased in cells lacking Atg5 and Atg16L1, but not Atg7

Exosome preparations obtained by differential ultracentrifugation from the human breast cancer cell line MDA-MB-231 and mouse embryonic fibroblast (MEF) cells were predominantly composed of 40-120 nm particles (Nanoparticle tracking, dynamic light scattering, Figure 29a, Figure 30a), enriched in exosome markers (Tsg101, Flotillin2) but not markers of cellular debris derived from distinct mitochondrial compartments (Tomm20, Figure 29b), and exhibited the appearance of exosomes by electron microscopy (Figure 30a) (Thery, Amigorena, Raposo, & Clayton, 2006). In comparison to their wild-type counterparts, exosome preparations from equivalent amounts of *Atg5*$^{-/-}$ MEF (Figure 30b) contained strikingly reduced levels of exosome markers (Flotillin2, Tsg101, Figure 29b) and exosome-sized particles by nanoparticle tracking and dynamic

light scattering (Figure 29a,c, Figure 30a-c). Exosome levels were similarly reduced in *ATG5*$^{-/-}$ human MDA-MB-231 cells (Figure 29a-c, Figure 30a-c). Decreased exosome production by *Atg5*$^{-/-}$ cells was not due to differential cell numbers attained at the end of exosome production (Figure 30d). Transiently repressing Atg5 in MEFs using a tetracycline-dependent system (Figure 29d), also reduced numbers of exosome-sized particles and levels of exosome markers in exosome preparations (Figure 29e,f). These effects were rescued by re-induction of Atg5 (Figure 29d-f). HCT-116 cells lacking Atg16L1 also produced less exosomes (Figure 29g). In contrast, exosome production measured by Western blot and particle concentration by nanoparticle tracking or dynamic light scattering was not decreased in *Atg7*$^{-/-}$ MEF, *Atg14*$^{-/-}$ MEF or when Atg7 was depleted with siRNA in MDA-MB-231 cells, despite LC3-II production being ablated (Figure 29h, Figure 30e-i).

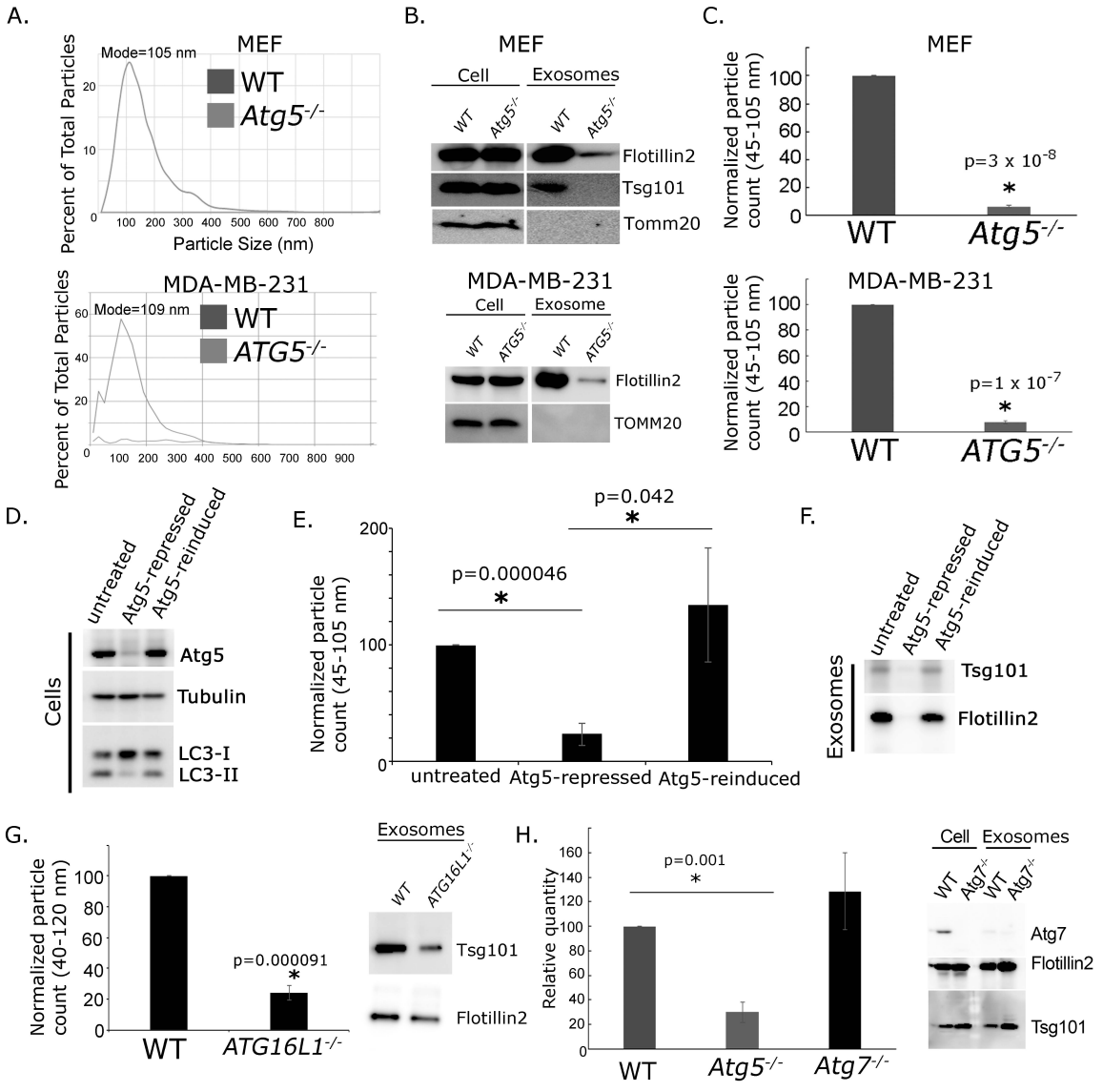

Figure 29: Exosome abundance is reduced in supernatants of *Atg5*$^{-/-}$ and *Atg16L1*$^{-/-}$ cells

(**a**) Representative histograms of a Nanosight Nanoparticle tracking analysis of exosomes produced by MEF and MDA-MB-231 wild-type and *Atg5*$^{-/-}$ cells showing percent of total particles (y-axis) vs. size (nm, x-axis). (**b**) Western blot of Flotillin2, Tsg101, and Tomm20 (negative control) in equal amounts of total cell lysates and exosome preparations from equal amounts of wild-type and *Atg5*$^{-/-}$ MEF and MDA-MB-231 cells. Irrelevant lanes between cell and exosome samples were removed. (**c**)

Normalized quantification of exosome-sized particles (45-105 nm) released by wild-type and *Atg5*$^{-/-}$ MEF and MDA-MB-231 cells using Nanoparticle tracking analysis (n=3). (**d**) Western blot of Atg5 and LC3 in MEF cells with doxycycline-repressed Atg5 cultured in parallel either in DMEM (untreated), DMEM containing doxycycline (Atg5-repressed), or DMEM containing doxycycline that was subsequently removed for 2 days (Atg5 re-induced). (**e**) Quantification of particles in exosome preparations from MEF with doxycycline-repressed Atg5 treated as in (d) using Nanoparticle tracking (n=3). (**f**) Western blot of Tsg101 and Flotillin2 in exosome preparations from equivalent amounts of MEF cells with doxycycline-repressible Atg5. (**g**) Quantification of particles in exosome preparations from wild-type and *ATG16L1*$^{-/-}$ HCT-116 using Nanoparticle tracking (n=3) and Western blot for exosome markers Tsg101 and Flotillin2 in exosome preparations from equal amounts of cells. (**h**) Quantification of particles in exosome preparations from wild-type, *Atg5*$^{-/-}$ and *Atg7*$^{-/-}$ MEF using dynamic light scattering intensity (n=3). Western blots quantify exosome markers in exosome preparations (Tsg101, Flotillin2) produced by equal amounts of cells and confirm Atg7 knockout in cells. At times, Western blots were run on the same samples on separate gels in parallel. Data are represented as mean +/- SEM.

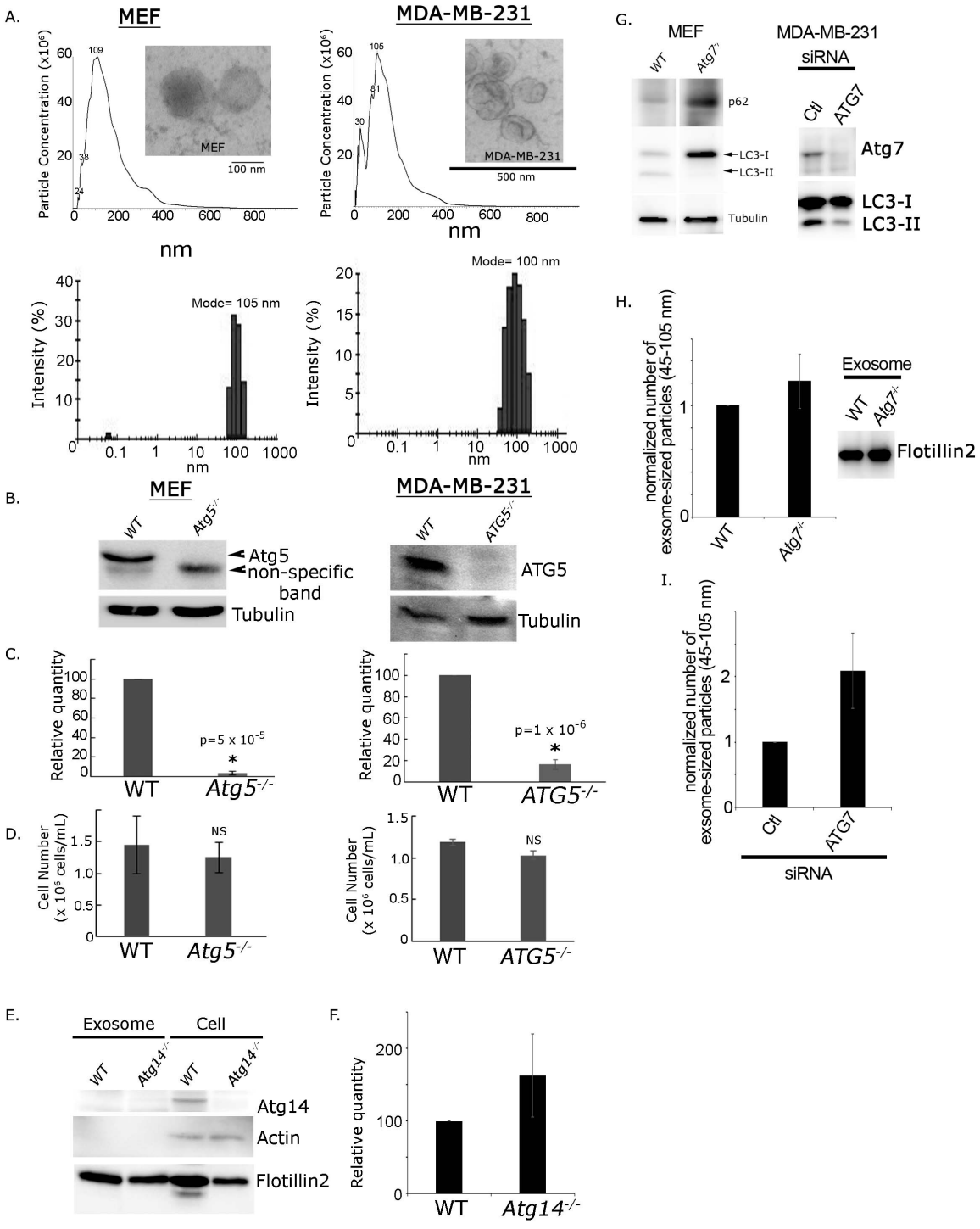

Figure 30: Atg5, but not Atg7 is required for exosome production

(**a**) Representative histograms of Nanoparticle tracking analysis measuring percent total particles (y-axis) vs. size (nm, x-axis) of exosome preparations from MEF and MDA-MB-231. Inset, electron microscopy images of exosome preparations from MEF and MDA-

MB-231 including scale bars (100 nm left, 500 nm right). Below, Dynamic light scattering histograms of exosome preparations representing intensity (relative number of particles) and size of particles. (**b**) Western blot of Atg5 and Tubulin (loading control) in equivalent amounts of wild-type and *Atg5*$^{-/-}$ MEF and MDA-MB-231 cells. (**c**) Quantification by dynamic light scattering of particles in exosome preparations from wild-type and *Atg5*$^{-/-}$ MEF and MDA-MB-231 cells. (**d**) Quantification of cell number by trypan blue exclusion (n=3) after culture of wild-type and *Atg5*$^{-/-}$ MEF and MDA-MB-231 cells for exosome production in (c). (**e**) Western blot of Atg14, Flotillin2 (exosome marker), and Actin (loading control for cell lysates) in lysates from equal amounts of cells and exosomes produced by equal amounts of cells (to assess changes in exosome production). (**f**) Quantification by dynamic light scattering of particles in exosome preparations from wild-type and *Atg14*$^{-/-}$ MEF cells (n=3). (**g**) Western blot of equivalent amounts of cell lysates from wild-type and *Atg7*$^{-/-}$ MEF for LC3, autophagy substrate p62 and Tubulin (loading control). As expected, *Atg7*$^{-/-}$ MEF do not convert LC3-I to LC3-II and accumulate p62. Right, Western blot of Atg7 and LC3 in equivalent amounts of MDA-MB-231 cells treated with control siRNA or siRNA targeting Atg7. Samples were run on the same gel and irrelevant lanes were excised in the Figure. (**h**) Nanoparticle tracking analysis quantification of exosome-sized particles (45-105 nm) released by wild-type and *Atg7*$^{-/-}$ MEF (n=3). Western blot of exosome marker Flotillin2 in exosome preparations produced by equal amounts of wild type and *Atg7*$^{-/-}$ MEF cells. (**i**) Nanoparticle tracking analysis quantification of exosome-sized particles (45-105 nm) released by MDA-MB-231 cells treated with control or Atg7 targeting siRNA (n=3). Data are represented as mean +/- SEM.

Atg5 does not affect exosome uptake from media

We sought to systematically identify the step of exosome biogenesis or re-uptake affected by *Atg5*. *Atg5*$^{-/-}$ MEFs exhibited no difference in uptake of DiO-labeled exosomes, or depletion of labeled exosomes from media, compared to wild-type cells (Figure 31a-c). This suggests that exosomes are not less abundant in cell culture supernatants of cells lacking functional *Atg5* because of increased cellular uptake of exosomes.

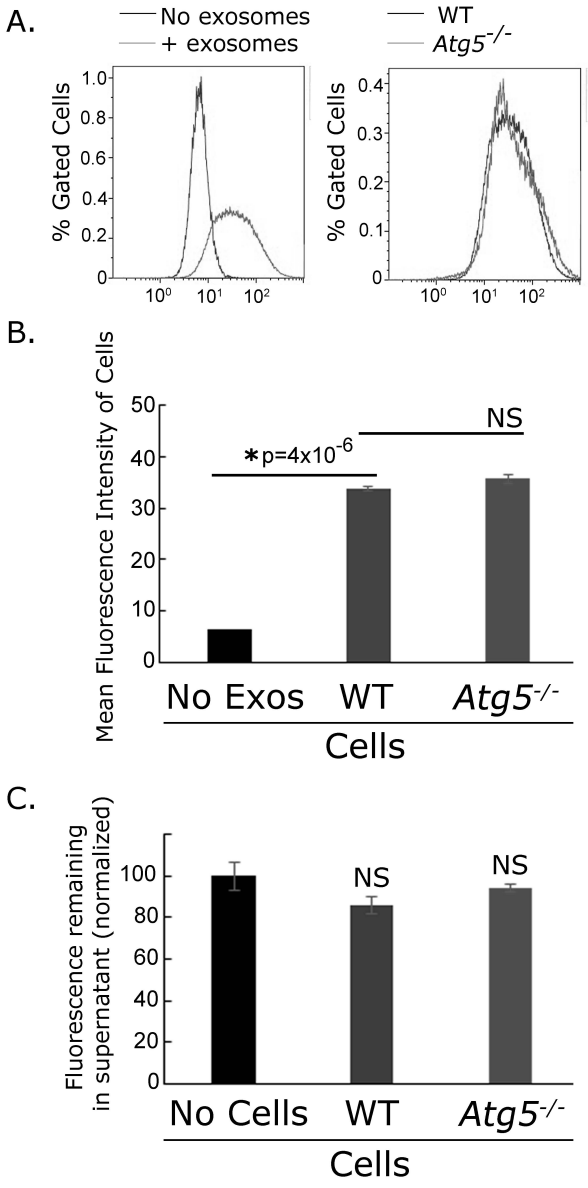

Figure 31: Uptake of exosomes from the extracellular space in *Atg5*$^{-/-}$ MEF is similar to wild-type MEF

(**a**) Representative flow cytometry histograms of cells incubated for 1 h with exosomes fluorescently labeled with DiO dye. (**b**) Fluorescence of wild-type and *Atg5*$^{-/-}$ MEF cells incubated with DiO-labeled exosome preparations from wild-type MEF cells for 1 h (n=3). Fluorescence was measured by flow cytometry (median). (**c**) Fluorescence remaining in supernatant after incubation of DiO-labeled exosome preparations with wild-type or *Atg5*$^{-/-}$ MEF cells (n=3). Data are represented as mean +/- SEM.

Atg5 does not affect budding of intraluminal vesicles into MVB

Production of a covalent Atg3-Atg12 complex that was recently demonstrated to be required for budding of intraluminal vesicles into MVB, was not decreased in *Atg5*$^{-/-}$ MEF (Figure 32a). *Atg5*$^{-/-}$ MDA-MB-231 and MEF also exhibited similar punctae of CD63, a hallmark exosome marker, inside endosomes labeled with Rab5, a marker frequently used to model budding into MVB involved in exosome production (Baietti et al., 2012; Gross, Chaudhary, Bartscherer, & Boutros, 2012; Trajkovic et al., 2008) (Figure 33a, Figure 32b). By electron microscopy, *Atg5*$^{-/-}$ MEF exhibited a significantly increased number of intraluminal vesicles per MVB and increased MVB diameter (Figure 33b-c, Figure 32d-g). Despite this, MVB intraluminal vesicles in *Atg5*$^{-/-}$ MEF were of similar size and morphology to MVB of wild-type cells (Figure 33b) and the percent of MVB exhibiting membrane invaginations, a measure of MVB budding and scission activity (Wemmer et al., 2011), was also unchanged (Figure 32c). Nor did MVB exhibit tubular or multicisternal protrusions in *Atg5*$^{-/-}$ MEF as observed with some ESCRT mutants with impaired budding (Figure 33b) (Razi & Futter, 2006). Together, this suggests that *Atg5* does not affect budding and scission of intraluminal vesicles into MVB (Futter, Collinson, Backer, & Hopkins, 2001; Hurley & Hanson, 2010).

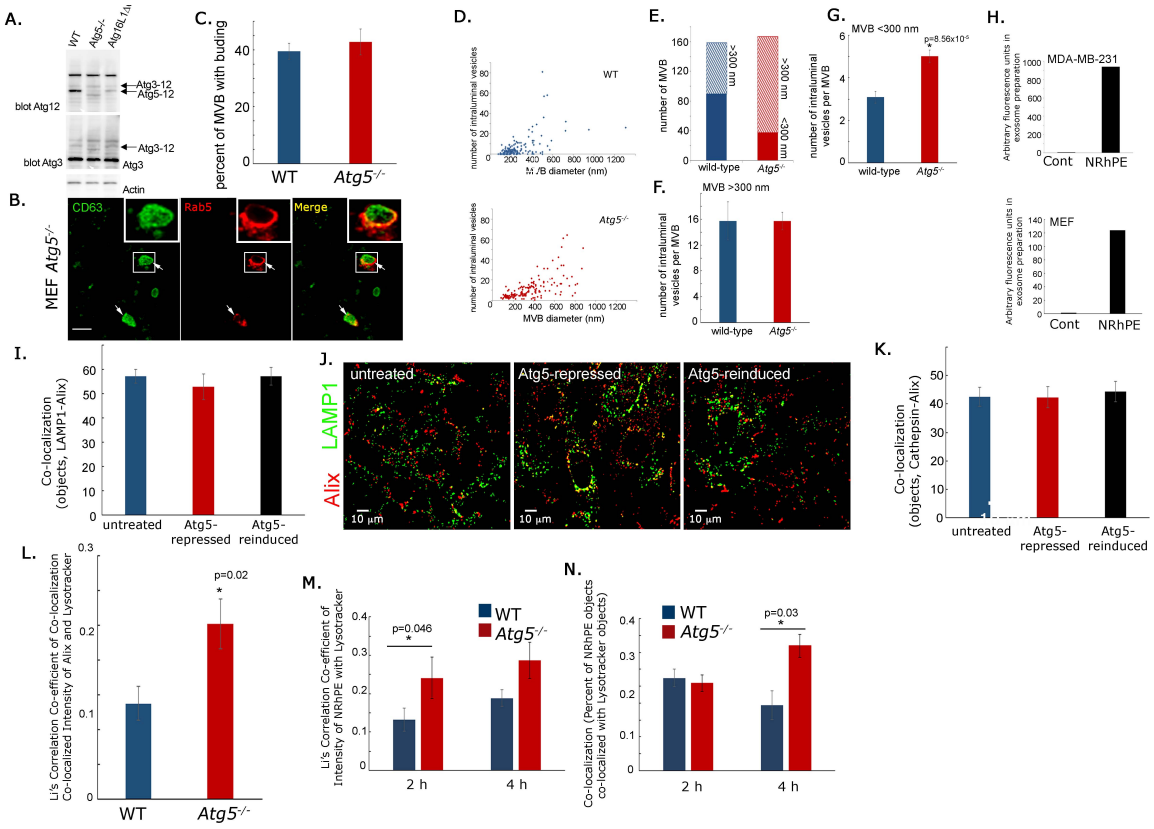

Figure 32: Multivesicular bodies exhibit increased acidification in the absence of Atg5

(**a**) Western blot for Atg12, Atg3 and Actin (control) in equivalent amounts of wild-type, *Atg5*$^{-/-}$, or *Atg16l1*$^{\Delta CCD}$ MEF. (**b**) Confocal microscopy of CD63 in Rab5+ organelles of *Atg5*$^{-/-}$ MEF. Scale bar = 1 µm. (**c**) Percent of MVB exhibiting budding of their membrane in wild-type and *Atg5*$^{-/-}$ MEF. Wild-type 167 MVB, *Atg5*$^{-/-}$ MEF 159 MVB. (**d**) Dot plot of number of intraluminal vesicles per MVB (y-axis) vs. MVB diameter (x-axis) in wild-type (WT) and *Atg5*$^{-/-}$ MEF. A shift toward larger MVB with more intraluminal vesicles can be seen in *Atg5*$^{-/-}$ MEF. Wild-type 996 intraluminal vesicles, *Atg5*$^{-/-}$ MEF 1726 intraluminal vesicles. WT 167 MVB, *Atg5*$^{-/-}$ MEF 159 MVB. (**e**) Number of MVB in wild-type and *Atg5*$^{-/-}$ MEF stratified by size (<300 nm solid bars and >300 nm lined bars). 167 MVB, *Atg5*$^{-/-}$ MEF 159 MVB. (**f**) Number of intraluminal vesicles per MVB of (>300 nm) in wild-type and *Atg5*$^{-/-}$ MEF. Wild-type 38 MVB, 598 intraluminal vesicles; *Atg5*$^{-/-}$ 90 MVB, 1382

intraluminal vesicles. (**g**) Number of intraluminal vesicles per MVB of (<300 nm) in wild-type and *Atg5*$^{-/-}$ MEF. Wild-type 129 MVB, 298 intraluminal vesicles; *Atg5*$^{-/-}$ 69 MVB, 347 intraluminal vesicles. All error bars represent SEM. (**h**) Quantification of NRhPE fluorescence in exosome preparations prepared by differential centrifugation from MDA-MB-231 and MEF treated with NRhPE or vehicle. (**i-k**) Co-localization of Alix with lysosomal markers (LAMP1, CathepsinB). Experiments were performed in MEF untreated, treated with 1 ng/mL doxycycline (2 d) to repress Atg5 (Atg-repressed) or treated with doxycycline and then left untreated for 2 d (Atg5-reinduced). (**i**) Quantification of co-localization of LAMP1 with Alix using automated segmentation and quantification of objects. (**j**) Representative images of mCherry-Alix co-localization with LAMP1 in MEF that were untreated, Atg5-repressed or Atg5-reinduced. LAMP1-tagBFP is pseudocolored green. Scale bar = 10 µm. (**k**) Quantification of co-localization of CathepsinB with Alix using object-based methods by SQASSH. (**l**) Quantification of the co-localization of mCherry-Alix with Lysotracker in wild-type or *Atg5*$^{-/-}$ MEF using Li's correlation co-efficient of fluorescent intensity. A total of 75 wild-type MEF and 51 *Atg5*$^{-/-}$ MEF cells were quantified. (**m**) Quantification of the co-localization of NRhPE with Lysotracker using Li's correlation co-efficient of fluorescent intensity in MEF wild-type and *Atg5*$^{-/-}$ cells. (**n**) Quantification of the co-localization of NRhPE with Lysotracker using automated segmentation and quantification of objects in MEF wild-type and *Atg5*$^{-/-}$ cells. Data are represented as mean +/- SEM.

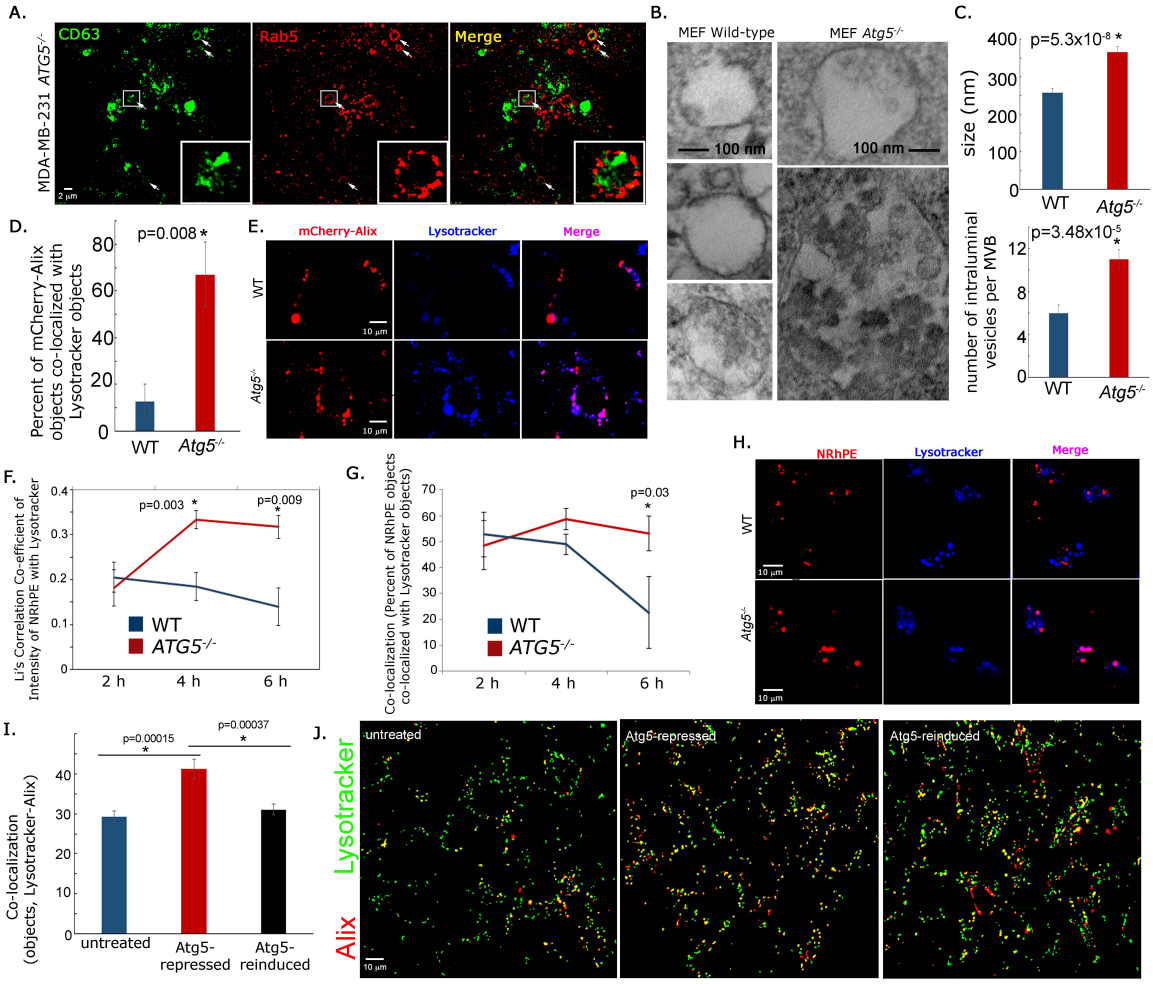

Figure 33: Loss of *Atg5* increases MVB size, intraluminal vesicle number and acidification

(**a**) STED microscopy of the exosome marker CD63 and the early endosome/MVB marker Rab5 in *ATG5*$^{-/-}$ MDA-MB-231 cells demonstrating punctate CD63 staining within Rab5+ endosomes. Scale bar = 2 µm. (**b**) Representative electron microscopy images of MVB in wild-type and *Atg5*$^{-/-}$ MEF cells. Scale of all images in wild-type or *Atg5*$^{-/-}$ group are identical, scale bar represents 100 nm. (**c**) Average size of MVB (upper) and number of intraluminal vesicles per MVB (lower) in wild-type and *Atg5*$^{-/-}$ MEF. Wild-type 167 MVB, *Atg5*$^{-/-}$ MEF 159, Wild-type 996 intraluminal vesicles, *Atg5*$^{-/-}$ MEF 1726 intraluminal vesicles. Electron microscopy data derived from two independent biological replicates. (**d**) Quantification of the co-localization of mCherry-Alix with Lysotracker in wild-type and

Atg5$^{-/-}$ MEF using automated segmentation and quantification of objects. A total of 75 wild-type MEF and 51 *Atg5*$^{-/-}$ MEF cells were quantified. (**e**) Representative images of co-localization of mCherry-Alix with Lysotracker in wild-type and *Atg5*$^{-/-}$ MEF. Scale bars represent 10 μm. (**f,g**) Quantification of the co-localization of the MVB marker NRhPE with Lysotracker using Li's correlation co-efficient (**f**) and automated segmentation and quantification of objects (**g**) in MDA-MB-231 wild-type and *ATG5*$^{-/-}$ cells. A total of 30-70 cells were quantified in each condition. (**h**) Representative images of NRhPE with Lysotracker in MDA-MB-231 cells at 4 h. Scale bars represent 10 μm. (**i**) Quantification of the co-localization of mCherry-Alix with Lysotracker using automated segmentation and quantification of objects in MEF cells either untreated, with Atg5 repressed, or Atg5 re-induced as in Figure 29d. A total of 30-70 cells were quantified in each condition. (**j**) Representative images of mCherry-Alix with Lysotracker in MEF cells in (i). Scale bars represent 10 μm. All data are represented as mean +/- SEM.

Loss of ATG5 increases MVB acidification independent of lysosomal fusion

By electron microscopy, we observed that *Atg5*$^{-/-}$ MEF exhibited a significantly increased number of intraluminal vesicles per MVB and increased MVB diameter (Figure 33b-c, Figure 32d-g), two signs of increased MVB acidification and maturation (Huotari & Helenius, 2011; Puchner, Walter, Kasper, Huang, & Lim, 2013). Markers of MVB that are also enriched in exosomes, namely NRhPE (N-lissamine rhodamine phosphatidylethanolamine) (Figure 32h) and mCherry-Alix (Vidal, Mangeat, & Hoekstra, 1997) exhibited unaltered co-localization with either of two lysosome markers (LAMP1, CathepsinB) in wild-type, Atg5-repressed, or Atg5-reinduced MEFs (Figure 32i-k). In contrast, co-localization of the exosome marker mCherry-Alix with Lysotracker that marks acidified compartments increased in *Atg5*$^{-/-}$ cells measured using two independent

measures of co-localization (Figure 33d,e, Figure 32l). Similarly, NRhPE co-localization with Lysotracker increased in *ATG5*$^{-/-}$ MDA-MB-231 cells not at early stages of endocytosis, but at time points when it accumulates in MVB (Vidal et al., 1997) (Figure 33f-h). Similar results were observed in *Atg5*$^{-/-}$ MEF (Figure 32m-n). Finally, Alix co-localization with Lysotracker increased upon repression of Atg5 by tetracycline and returned to normal upon rescue of Atg5 levels (Figure 33i,j).

In direct contrast with the effect of *Atg5* on MVB labeled with exosome markers *Atg5* promoted acidification of dextran-containing endosomal compartments as previously published (Florey et al., 2011; Ktistakis & Tooze, 2016; Martinez et al., 2015; Peng et al., 2014; J. Zhou, S. H. Tan, et al., 2013) (Figure 34a,b). Distinct from the effect of Atg5 on compartments containing Alix and NRhPE, repression of Atg5 reduced EGF trafficking to the lysosome (LAMP1, CathepsinB, Figure 34c-e) as previously reported. For reasons that are not clear this was not rescued when Atg5 was re-induced (Figure 34c-e). In sum, in *Atg5*$^{-/-}$ cells, MVB exhibit increased size and number of intraluminal vesicles and compartments containing MVB and exosome markers (mCherry-Alix, NRhPE) exhibit increased acidification (Lysotracker staining), but do not exhibit increased colocalization with lysosome markers (LAMP1, CathepsinB). Together, this suggests that MVB acidification is accentuated in *Atg5*$^{-/-}$ cells independent of lysosomal fusion and these effects contrast with other endosomal compartments (dextran, EGF).

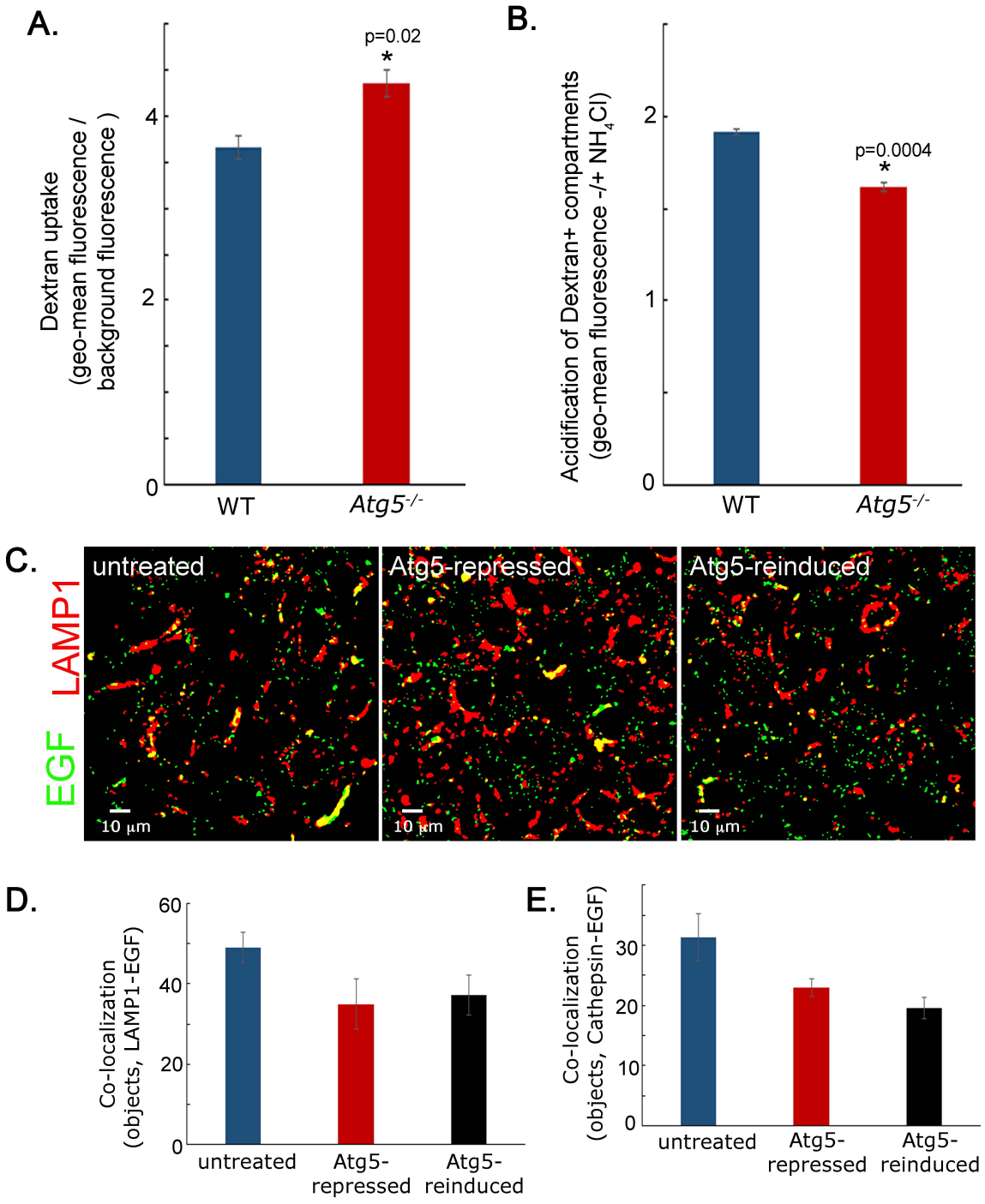

Figure 34: Atg5 does not increase acidification of dextran-containing compartments or localization of EGF to lysosomes

(**a**) Uptake of pHrodo labeled dextran by wild-type and *Atg5*$^{-/-}$ MEF. Geometric mean of fluorescent intensity was measured by flow cytometry. (**b**) Acidification of compartments

containing pHrodo labeled dextran in wild-type and *Atg5*$^{-/-}$ MEF after 20 minutes. Ratio of the geometric mean of fluorescent intensity measured by flow cytometry before vs. after addition of NH_4Cl to neutralize pH-dependent increase in fluorescence of pH-sensitive pHrodo dye. (**c**) Representative images of co-localization of Alexa488-EGF with LAMP1-tagBFP pseudocolored red. Scale bar = 10 µm. (**d**) Quantification of co-localization of LAMP1 with Alexa488-EGF using automated segmentation and quantification of objects. (**e**) Quantification of co-localization of Cathepsin with Alexa488-EGF automated segmentation and quantification of objects. Data are represented as mean +/- SEM.

Atg5 causes disassociation of ATP6V1E1 from the V_1V_0-ATPase at MVB

To further understand the relationship between ATG5 and MVB acidification, we investigated the V_1V_0-ATPase, a multi-molecular proton pump mediating acidification of endosomes and lysosomes (Cotter, Stransky, McGuire, & Forgac, 2015). We observed that ATP6V1E1, an exposed peripheral stalk component of the cytoplasmic V_1 complex co-localized with the MVB marker CD63 (Figure 35a). ATP6V1E1 was previously demonstrated in yeast and mammalian cells to detach from the V_1V_0-ATPase to decrease its activity (Sautin, Lu, Gaugler, Zhang, & Gluck, 2005; Toei, Saum, & Forgac, 2010). SiRNA targeting ATP6V1E1 diminished Lysotracker staining of cells to a similar extent as siRNA targeting other critical components of the V_1V_0-ATPase such as V0C (Figure 35b), demonstrating that ATP6V1E1 is capable of regulating the V_1V_0-ATPase in mammalian cells. To quantify detachment of ATP6V1E1 from the V_1V_0-ATPase in *Atg5*$^{-/-}$ cells we performed proximity ligation assays (PLA) for ATP6V1E1 and a core transmembrane component of the V_1V_0-ATPase, ATP6V0C. As expected, PLA dots indicating a close association of ATP6V1E1 with V_1V_0-ATPase were detected and dots were eliminated by siRNA targeting ATP6V1E1 validating the specificity of the assay (Figure 35c). Transient repression of Atg5 increased the amount of ATP6V1E1

associated with the V_1V_0-ATPase, and this returned to normal when Atg5 expression was restored (Figure 35d,e). Association of ATP6V1E1 with the V_1V_0-ATPase was also increased in cells genetically deleted of *Atg5* (Figure 35f), but was unaltered in *Atg7*$^{-/-}$ cells (Figure 35g). Loss of Atg5, but not Atg7 enhanced the association of ATP6V1E1 with the V_1V_0-ATPase at MVB marked by mCherry-Alix (Figure 35h). This mirrors the effect of Atg5, but not Atg7 on exosome production (Figure 29), suggesting that Atg5 detaches ATP6V1E1 from the V_1V_0-ATPase complex to regulate MVB acidification and exosome production independent of Atg7.

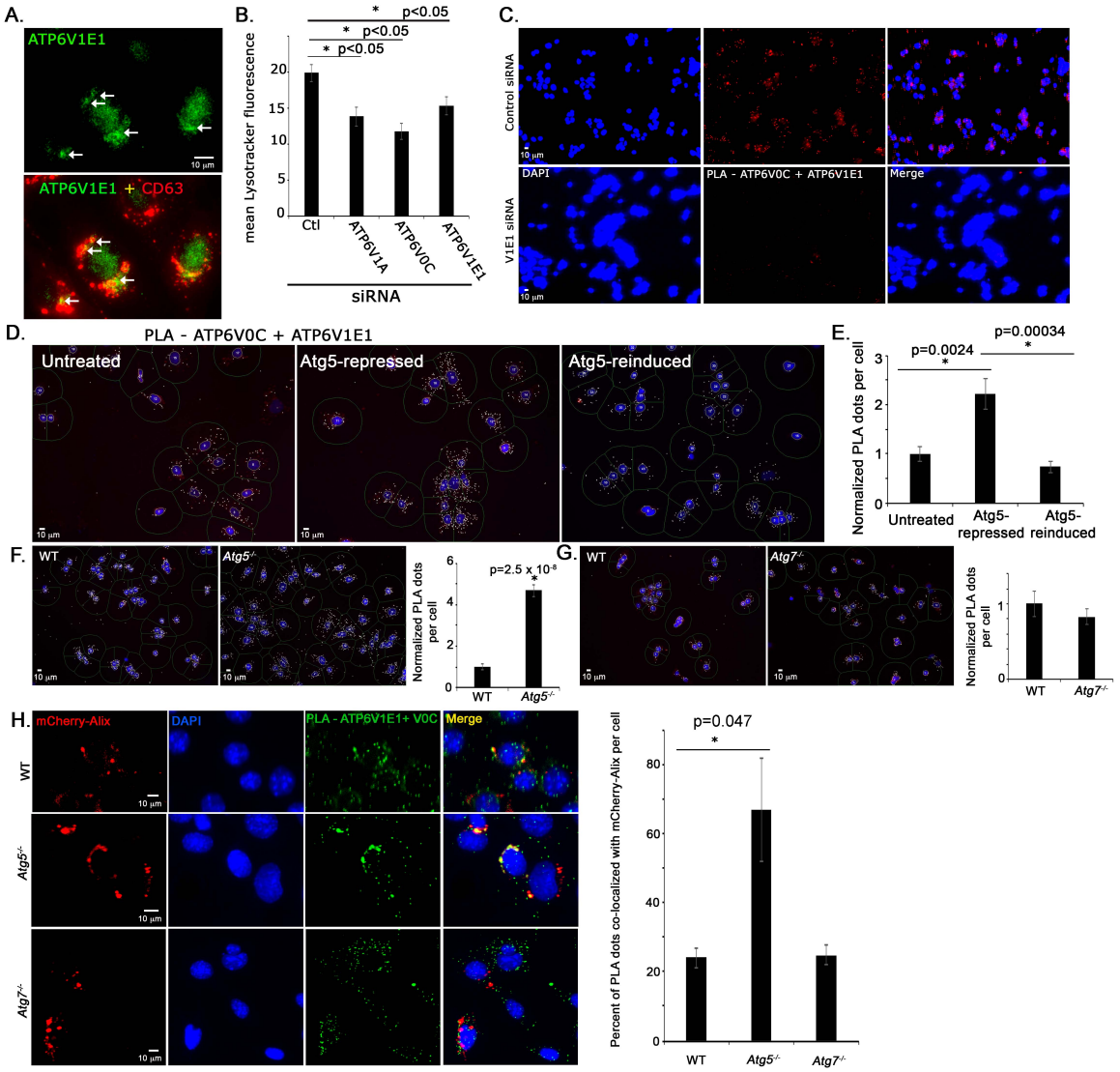

Figure 35: Atg5 disassociates ATP6V1E1 from the V_1V_0-ATPase

(**a**) Immunofluorescence microscopy of ATP6V1E1 showing its co-localization with the MVB and exosome marker Tsg101. Scale bars represent 10 μm. (**b**) Mean Lysotracker fluorescence measured in cells treated with siRNA targeting ATP6V1E1, ATP6V1A, ATP6V0C or control non-specific RNA. (**c**) Representative fluorescent microscopy image of proximity ligation assay signals demonstrating association of ATP6V1E1 with the core V_1V_0-ATPase component ATP6V0C that is lost in cells treated with siRNA targeting ATP6V1E1. Scale bars represent 10 μm. (**d**) Representative proximity ligation assay analyses of ATP6V1E1 with the core V_1V_0-ATPase component ATP6V0C in MEF cells that were untreated, Atg5-repressed (+Doxycycline), or Atg5-reinduced. Scale bars represent 10 μm. (**e**) Quantification of proximity ligations assays of ATP6V1E1 with ATP6V0C as in (d) in MEF cells that were untreated, Atg5-repressed (+Doxycycline), or Atg5-reinduced. (**f**) Representative proximity ligation assay analyses of ATP6V1E1 with ATP6V0C in MEF wild-type and *Atg5*$^{-/-}$ cells and their quantification. Scale bars represent 10 μm. (**g**) Representative proximity ligation assay analyses of ATP6V1E1 with ATP6V0C in MEF wild-type and *Atg7*$^{-/-}$ cells and their quantification. Scale bars represent 10 μm. (**h**) Representative proximity ligation assay analyses of ATP6V1E1 with ATP6V0C in MEF wild-type, *Atg5*$^{-/-}$ and *Atg7*$^{-/-}$ cells expressing mCherry-Alix. Graph of percent of mCherry-Alix punctae (MVB) that co-localize with proximity ligation assay signals of ATP6V1E1 with ATP6V0C. Scale bars represent 10 μm. All data are represented as mean +/- SEM.

The enrichment of LC3 in exosomes is diminished in cells lacking ATG5, not ATG7

We investigated how Atg5 might detach ATP6V1E1 from the V_1V_0-ATPase to affect MVB acidification. Atg5-mCherry localized to compartments co-labeled with both the exosome markers CD63 and Rab5 (Figure 36a). Interestingly, Atg5 and Atg16L1 were also

abundant in exosomes produced by multiple cell types compared to their levels in similar amounts of cell lysate (Figure 36b). The Atg5 complex binds LC3 and lipidates it to form LC3-II. LC3 was also abundant in these exosome preparations (Figure 36b). Remarkably, exosomes were strongly enriched in lipid-modified LC3-II (vs. unmodified LC3-I) compared to the ratio of LC3-II to LC3-I in the corresponding cell lysates (Figure 36b,c). This suggests that Atg5 and LC3 are sorted into exosomes. One mechanism by which Atg5 could detach ATP6V1E1 from the V_1V_0-ATPase complex at MVB would be for Atg5 to remove ATP6V1E1 into the intraluminal vesicles budding into MVB that become exosomes. In agreement with this possibility ATP6V1E1 detected with a specific antibody was also detected in exosomes (Figure 36d).

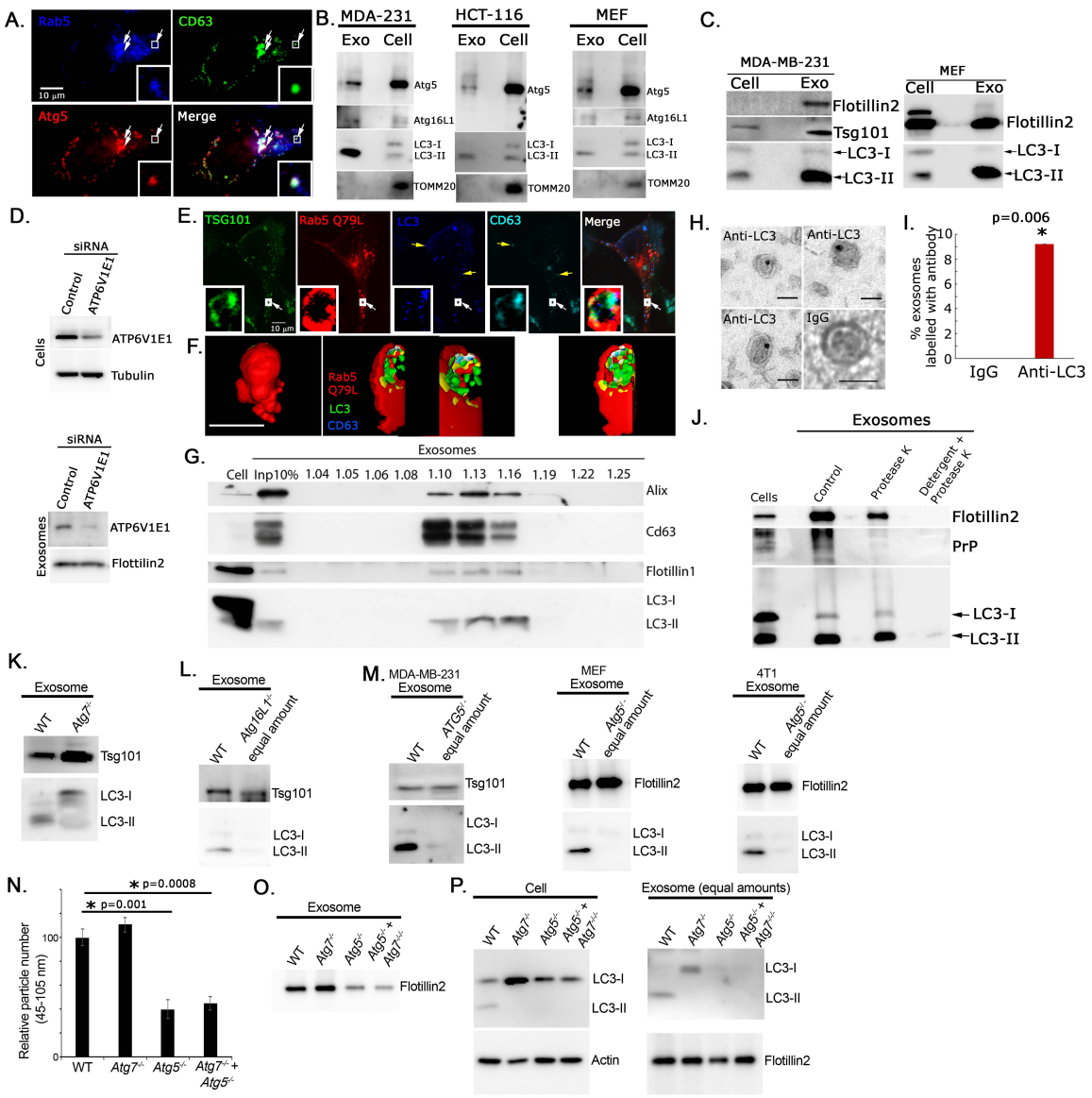

Figure 36: Atg5 recruits LC3 into exosomes

(**a**) Immunofluorescent microscopy highlighting Atg5 co-localization with punctae that are marked by both Rab5 and CD63 (white arrows). Scale bars represent 10 μm. (**b**) Western blot of Atg5, Atg16L1 and LC3 in equivalent amounts of exosomes or cells of several cell types. (**c**) Western blot of LC3 and exosome markers in (Tsg101, Flotillin2) in equivalent amounts of exosomes or cells (MDA-MB-231 and MEF). (**d**) Western blot of ATP6V1E1 in cells treated with siRNA targeting ATP6V1E1 and the exosomes they produce. Equal amounts of exosomes were used to show reduced levels of ATP6V1E1-

specific band in exosomes. (**e**) Confocal microscopy of Tsg101, CD63, LC3 and constitutively active dsRed-Rab5 Q79L in MDA-MB-231 cells. Scale bar = 10 μm (**f**) 3-D reconstruction of LC3 and CD63 inside endosomes labeled with constitutively active mutant dsRed-Rab5 Q79L in MDA-MB-231 cells. Scale bar = 1 μm (**g**) Western blot analysis of sucrose density gradient fractions of exosome preparations from Neuro2a cells for LC3 and exosome markers (Alix, CD63 and Flotillin1) showing partitioning of LC3 with exosomes at densities characteristic of exosomes. Inp=input. (**h**) Immunogold electron microscopy with anti-LC3 antibody in exosome preparations of Neuro2a cells. Scale bars = 100 nm. (**i**) Quantification of percent of exosomes labeled with LC3 antibody by electron microscopy (647 exosomes total in 3 replicates, no labeling was observed in samples labeled with control antibody). (**j**) Western blot of equivalent amounts of exosomes from Neuro2a cells mock treated, treated with protease K or treated with detergent and protease K. Blots for the proteins on the surface of exosomes (PrP) or inside exosomes (Flotillin2) are controls for the protease and detergent treatments. (**k**) Western blot of LC3 and exosome marker Tsg101 in equivalent amounts of exosomes produced by wild-type and *Atg7*$^{-/-}$ MEF to show alterations in specific cargoes in exosomes. (**l**) Western blot of LC3 and exosome marker Tsg101 in equivalent amounts of exosomes from wild-type and *Atg16L1*$^{-/-}$ HCT-116 to show alterations in specific cargoes in exosomes. (**m**) Western blot of LC3 and exosome marker Tsg101 in equal amounts of exosomes produced by wild-type and *Atg5*$^{-/-}$ MDA-MB-231, MEF or 4T1 cells to show alterations in specific cargoes in exosomes. (**n**) Quantification of particles in exosome preparations from equal numbers of wild-type and *Atg7*$^{-/-}$, *Atg5*$^{-/-}$ *and Atg5*$^{-/-}$*&Atg7*$^{-/-}$ MEF cells using Nanoparticle tracking (n=3) and (**o**) Western blot for exosome markers Flotillin2 in exosome preparations from equal amounts of cells. (**p**) Western blot of cells for LC3 and Beta-actin and of LC3 and exosome marker Flotillin2 in

equivalent amounts of exosomes from wild-type and *Atg7*$^{-/-}$, *Atg5*$^{-/-}$ *and Atg5*$^{-/-}$*&Atg7*$^{-/-}$ MEF to show alterations in specific cargoes in exosomes. Data are represented as mean +/- SEM.

We first sought to validate that LC3 was found in *bona fide* exosomes. LC3 was enriched in exosome preparations from multiple mouse and human cells (MEF, MDA-MB-231, HCT-116, Neuro2A, 3T3 Figure 36b, Figure 37a). If LC3 is found in exosomes it should co-localize with endosomes and the intraluminal vesicles of MVB. Constitutively-active Rab5 (Rab5-Q79L) enlarges endosomes and faithfully documents the budding of intraluminal vesicles into MVB during exosome biogenesis (Baietti et al., 2012; Gross et al., 2012; Trajkovic et al., 2008). Accordingly, punctae inside Rab5-Q79L endosomes were labeled by antibodies recognizing Alix, Tsg101 or CD63, established markers of intraluminal vesicles and exosomes (Figure 36e,f, Figure 37b-d). LC3 exhibited similar punctate staining within Rab5-Q79L+ endosomes (Figure 36e,f) that co-localized in part with exosome markers Alix, Tsg101 and CD63 in MEF and MDA-MB-231 cells (Figure 36e,f, Figure 37b-d). On sucrose density gradients of exosome preparations, LC3-II fractionated with the exosome markers Alix, CD63 and Flotillin-1 at densities characteristic of exosomes (Figure 36g) (Thery et al., 2006). Finally, LC3 antibody labeled vesicles of 30-100 nm in exosome preparations using electron microscopy (Figure 36h,i). Cumulatively this evidence demonstrates that LC3-II is enriched in *bona fide* exosomes from multiple cell types (Figure 36b-i).

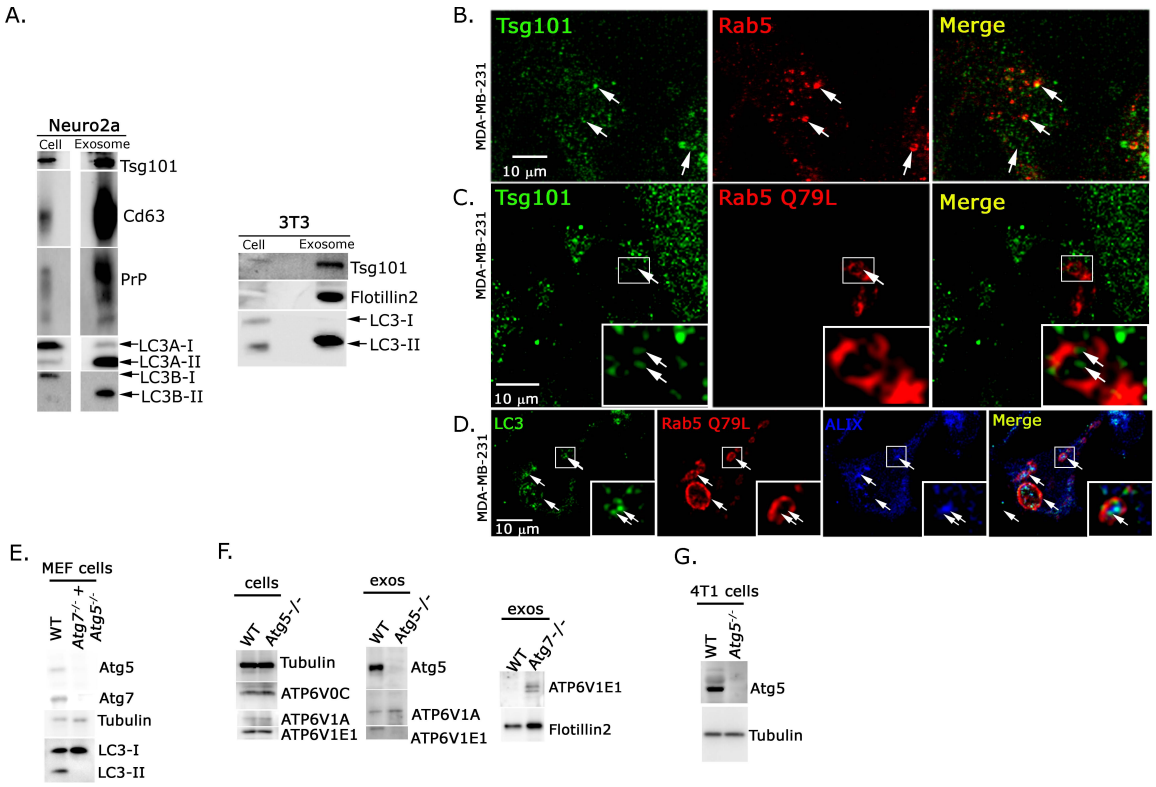

Figure 37: LC3 is found in exosomes and Atg5, but not Atg7, controls sorting of ATP6V1E1 into exosomes

(**a**) Western blot analysis of equivalent amounts (µg protein) of exosome preparations and total cell lysate from 3T3 and Neuro2a cells for exosome markers (Tsg101, CD63, PrP, Flotillin2) and LC3. Neuro2A cells and exosomes were blotted for both LC3A and LC3B. Neuro2a cell and exosome samples were run on the same gel and irrelevant lanes were excised in the Figure. (**b**) Confocal microscopy of Tsg101 with endogenous Rab5 in MDA-MB-231 cells. Scale bar = 10 µm. (**c**) Confocal microscopy of Tsg101 with constitutively active mutant dsRed-Rab5 Q79L in MDA-MB-231 cells. Scale bar = 10 µm. (**d**) Confocal microscopy of LC3 and the exosome marker Alix with constitutively active mutant dsRed-Rab5 Q79L in MDA-MB-231 cells. Scale bar = 10 µm. (**e**) Western blot of Atg5, Atg7, LC3 and Tubulin in MEF cells genetically deleted of both *Atg5* and *Atg7.* (**f**) Western blot of components of the the V_1V_0 ATPase in equivalent amounts of exosomes

produced by *Atg5*$^{-/-}$ or *Atg7*$^{-/-}$ MEF cells. (**g**) Western blot of Atg5 in equivalent amounts of wild-type and *Atg5*$^{-/-}$ 4T1 cells compared to loading control (Tubulin).

LC3-II could associate with the surface, not the lumen of exosomes following the fusion of autophagosomes with endosomes as the internal membrane of the autophagosome starts to degrade. LC3-II was sensitive to Protease K-digestion only after treatment of exosome preparations with detergent (Figure 36j), which suggests that LC3-II is enclosed inside exosomes. Reinforcing this, whereas exosomes from wild-type cells are enriched in lipid-modified LC3-II, *Atg7*$^{-/-}$ MEF that are incapable of canonical macroautophagy produce exosomes enriched in LC3-I (Figure 36k). This demonstrates that LC3 is recruited into exosomes by a process not requiring canonical macroautophagy or lipid modification of LC3.

Atg5 is abundant in exosomes (Figure 36b) and associates with LC3 suggesting Atg5 may recruit LC3 into exosomes. Accordingly, Western blot of equal amounts of exosomes from wild-type and *Atg5*$^{-/-}$ cells demonstrated that LC3 was nearly undetectable in exosomes from *Atg5*$^{-/-}$ cells (Figure 36m). Similar results were found in exosomes from cells lacking Atg16L1 (Figure 36l). In *Atg7*$^{-/-}$ cells LC3-I was recruited into exosomes at similar levels to LC3-II in wild-type cells (Figure 36k). This reinforces that exosome production and LC3 sorting into exosomes is independent of *Atg7* and the formation of LC3-II. Cells genetically deleted of both *Atg5* and *Atg7* exhibited reduced exosome production (Figure 36n,o, Figure 37e) and nearly eliminated the packaging of LC3-I into exosomes that was observed in *Atg7*$^{-/-}$ cells (Figure 36p). Together, this suggests that Atg5 and Atg16L1 are required for recruitment of either LC3-I or LC3-II into exosomes, while Atg7 and canonical macroautophagy are not required.

Atg5 recruits ATP6V1E1 into exosomes to control exosome production

Atg5 detaches ATP6V1E1 from the V_1V_0-ATPase. We tested whether LC3 could mediate this effect. Proximity ligation assays detected an association between ATP6V1E1 and LC3 that was lost when ATP6V1E1 was depleted with siRNA (Figure 38a). This suggests ATP6V1E1 is in the immediate vicinity of LC3 (Figure 38a). To test whether LC3 binds ATP6V1E1, ATP6V1E1 was immunoprecipitated (Figure 38b). LC3-I and LC3-II were pulled down in immunoprecipitates of ATP6V1E1 compared to immunoprecipitates of a non-specific isotype control antibody (Figure 38b). Specificity of the ATP6V1E1 band on Western blots was confirmed with siRNA targeting ATP6V1E1 (Figure 36d). Finally, recombinant LC3-I coated on beads pulled down ATP6V1E1 from cell lysates, as well as its known binding partner p62, compared to control beads alone (Figure 38c,d). Together, this strongly suggests that LC3 associates with ATP6V1E1.

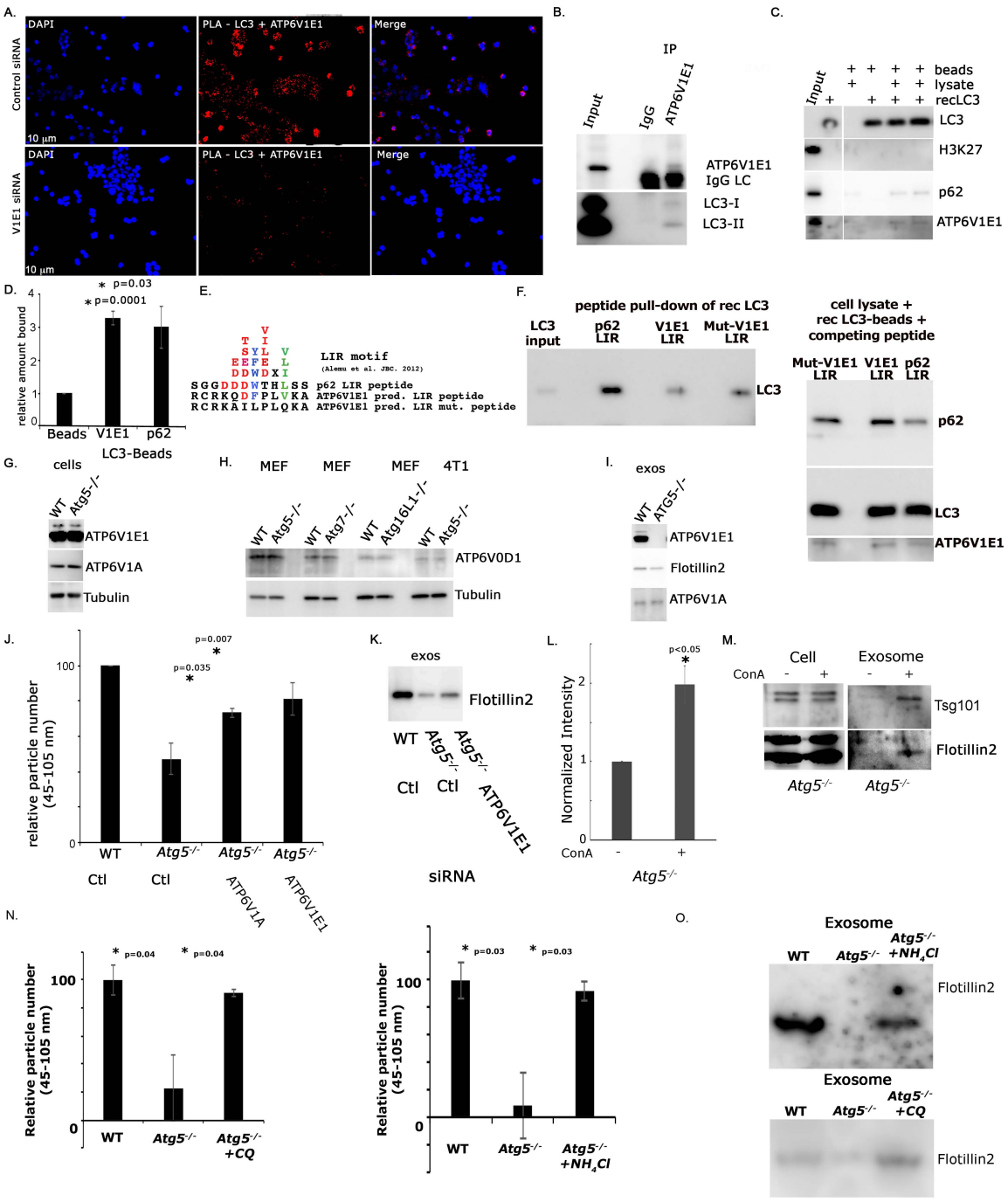

Figure 38: LC3 binds ATP6V1E1 and selectively removes it into exosomes to modulate exosome production

(**a**) Representative fluorescent microscopy of proximity ligation assay of ATP6V1E1 with LC3 in MEF. Signals are lost in cells treated with siRNA targeting ATP6V1E1 validating the specificity of the assay. Scale bars represent 10 µm. (**b**) Western blot of LC3 in

immunoprecipitates of ATP6V1E1 compared to negative control IgG. IgG LC indicates the IgG light chain band found in both ATP6V1E1 and control IgG immunoprecipitates. (**c**) Western blot of known LC3-interacting protein p62 (positive control), non-LC3 interacting protein H3K27 (negative control) and ATP6V1E1 in pull-downs of recombinant LC3. (**d**) Quantification of the LC3 pulldown experiments in (c) over 3 independent experiments. (**e**) Top, Canonical LIR motif is color-coded for acidic (red), aromatic (blue) or hydrophobic (green) residues with preferential LIR-motif amino acids stacked vertically at each position. Bottom, alignment of canonical LIR motif peptide with established p62 LIR peptide and predicted LIR peptide in ATP6V1E1 or a mutated version thereof. (**f**) Left, Western blot of LC3 after pulldown of recombinant LC3 with biotinylated peptides from p62 LIR motif, ATP6V1E1 predicted LIR motif, and a mutated version thereof (negative control). Right, Western blot of p62 and ATP6V1E1 in pulldowns from cell lysates with recombinant LC3 in the presence of a competitive excess of the indicated peptides. (**g**) Western blot of ATP6V1E1 and other components of the V_1V_0-ATPase in wild-type and *Atg5*$^{-/-}$ MEF cells. (**h**) Western blot of ATP6V1E1 and other components of the V_1V_0-ATPase in wild-type, *Atg5*$^{-/-}$, *Atg7*$^{-/}$, *Atg16L1*$^{-/-}$ MEF cells and *Atg5*$^{-/-}$ 4T1 cells. (**i**) Western blot of ATP6V1E1 and other components of the V_1V_0-ATPase in equivalent amounts of exosomes produced by wild-type and *ATG5*$^{-/-}$ MDA-MB-231 to show alterations in levels of specific cargoes in exosomes. (**j**) Quantification of exosome production by nanoparticle tracking analysis of particles (45-105 nm) in wild-type and *Atg5*$^{-/-}$ MEF treated with control non-specific siRNA or siRNA targeting ATP6V1E1 or ATP6V1A. (**k**) Western blot of exosome marker Flotillin2 in exosome preparations produced by equivalent amounts of wild-type and *Atg5*$^{-/-}$ MEF treated with control non-specific siRNA or siRNA targeting ATP6V1E1. (**l**) Quantification of exosome production using dynamic light scattering in *Atg5*$^{-/-}$ MEF treated with Concanamycin A or mock treated. (**m**) Western blot of exosome markers Tsg101 and

Flotillin2 in cells and exosome preparations from equivalent amounts of *Atg5*$^{-/-}$ MEF treated with Concanamycin or mock treated. (**n**) Quantification of exosome production by nanoparticle tracking analysis of particles (45-105 nm) in wild-type and *Atg5*$^{-/-}$ MEF either untreated or treated with Chloroquine (CQ) for 16 h (left) or with NH_4Cl for 30 min (right). (**o**) Quantification of exosome production by Western blot for Flotillin2 in exosome preparations produced by wild-type and *Atg5*$^{-/-}$ MEF either untreated or treated with 100 μM Chloroquine (CQ) for 16 h (bottom) or with 20 mM NH_4Cl for 30 min (top). Data are represented as mean +/- SEM.

LC3 binds many of its interactors using LIR (LC3-Interacting-Region) motifs. LIR motif prediction algorithms (Kalvari et al., 2014) did not detect a LIR motif in ATP6V1E1. Independently searching, we identified only one site that bore some resemblance to a canonical LIR motif (Figure 38e). Peptides of 4-18 amino acids including LIR motifs have been used in a wide variety of assays to bind LC3 and analyze LIR motifs (Johansen et al., 2017; Y. K. Lee et al., 2017). Peptides including the canonical p62 LIR motif, the putative ATP6V1E1 LIR motif, or a mutated version of the ATP6V1E1 peptide were synthesized (Figure 38e). Peptides from the established p62 LIR motif (a positive control) pulled down recombinant LC3, whereas LC3 bound at background levels to control mutated peptide and the putative ATP6V1E1 LIR motif peptide (Figure 38f). Recombinant LC3 pulled down p62 and ATP6V1E1 from cell lysates (Figure 38c,d). Peptide containing the p62 LIR motif competed with endogenous p62 binding demonstrating that the assay measures binding of LC3 to LIR-motifs (Figure 38f). Nonetheless, p62 LIR motif peptide had no effect on pulldown of ATP6V1E1 (Figure 38f) suggesting that LC3 does not use its LIR-binding region to associate with ATP6V1E1. Compared to mutated control peptide, the peptide containing the putative ATP6V1E1 LIR motif did not affect binding of LC3 to either p62 or ATP6V1E1 (Figure 38f). Together,

this suggests that ATP6V1E1 does not have a canonical LIR motif, and ATP6V1E1 associates with a site in LC3 that is independent of the LIR motif binding site.

In cells genetically deleted of Atg5$^{-/-}$ no evident change in levels of ATP6V1E1 or other components of the V_1V_0-ATPase including V1A, V0C or V0D were apparent (Figure 38g-h, Figure 37f). However, in parallel with the decrease in LC3 levels in exosomes produced by *Atg5*$^{-/-}$ cells, we observed a decrease in ATP6V1E1 levels in exosomes (Figure 38i, Figure 37f). Another component of the V_1 complex, ATP6V1A, could be detected at low levels in exosomes but its levels in exosomes were unchanged in exosomes produced by cells lacking Atg5 (Figure 38i, Figure 37f). This suggests that ATP6V1E1 is selectively recruited into exosomes in an Atg5 dependent manner.

Atg5 detaches ATP6V1E1 from the V_1V_0-ATPase complex (Figure 35d-h), removes ATP6V1E1 into exosomes (Figure 38g-i, Figure 37f), and causes decreased MVB acidification (Figure 33). If this is critical for the effect of Atg5 on exosome release then depleting ATP6V1E1 with siRNA should rescue exosome release in *Atg5*$^{-/-}$ cells. Accordingly, while exosome release was decreased in *Atg5*$^{-/-}$ cells, cells released more exosome size particles and exosome markers accumulated in exosome preparations when *Atg5*$^{-/-}$ cells were treated with siRNA targeting ATP6V1E1 (Figure 38j,k). If V_1V_0-ATPase complex inactivation is the critical effect of detaching ATP6V1E1 from the V_1V_0-ATPase complex then exosome release should also be restored in *Atg5*$^{-/-}$ cells by inhibiting the V_1V_0-ATPase by other means. In agreement, treating cells with siRNA targeting an independent component of the V_1V_0-ATPase complex, ATP6V1A rescued production of exosome-sized particles in *Atg5*$^{-/-}$ cells (Figure 38j). Similarly, chemically perturbing the V_1V_0-ATPase complex with Concanamycin rescued exosome production in *Atg5*$^{-/-}$ cells (Figure 38l,m). This strongly suggests that disrupting V_1V_0-ATPase complex is required to restore exosome release in *Atg5*$^{-/-}$ cells. V_1V_0-ATPase is

postulated to also be involved in fusion of organelles with lysosomes or for exocytosis, independent of its established role in endolysosomal acidification (D. Wang & Hiesinger, 2013). Chloroquine and NH_4Cl both increase endolysosomal pH independently of the V_1V_0-ATPase, and both rescued exosome production in *Atg5*$^{-/-}$ cells (Figure 38n,o). This suggests that the major effect of Atg5 on the V_1V_0-ATPase complex which controls exosome production is its increase of endolysosomal pH. Cumulatively, this suggests that Atg5 removes ATP6V1E1 into exosomes and away from the V_1V_0-ATPase complex thereby decreasing MVB acidification and allowing exosome release.

Atg5 affects migration and metastasis of cancer cells by controlling exosome release

Atg5 and autophagy have been attributed many roles in cancer. One emerging role for Atg5 is in controlling cancer metastasis. Western blotting confirmed the presence of several proteins linked to cancer cell invasion in exosomes including Vimentin, Ras, and β-catenin at relative enrichment (vs. cell lysate) comparable to exosome markers like Tsg101 (Figure 39a). Consequently, we hypothesized that *Atg5* may affect migration and invasion of cancer cells by controlling exosome release. To test this in a tractable model, exosomes purified from 10^5 cells of the highly invasive breast cancer cell line MDA-MB-231 were incubated with an equivalent number of MCF-7 cells, a minimally invasive breast cancer cell line. Exosomes from MDA-MB-231 cells promoted migration of MCF-7 cells in transwell and wound healing assays while exosomes from an equivalent number of *ATG5*$^{-/-}$ MDA-MB-231 cells had no effect (Figure 39b,c, Figure 40a,b). Exosomes from MDA-MB-231 cells also promoted invasion of MCF-7 cells through a matrigel-coated transwell chamber while exosomes from similar numbers of *ATG5*$^{-/-}$ MDA-MB-231 cells had no effect (Figure 39d, Figure 40c). These effects were due to decreased numbers of exosomes released by *ATG5*$^{-/-}$ MDA-MB-231 cells and not a change in their contents, as

supplementing with equivalent amounts of exosomes from wild-type or *ATG5*$^{-/-}$ MDA-MB-231 resulted in similar effects on migration and invasion of MCF-7 cells (Figure 39e).

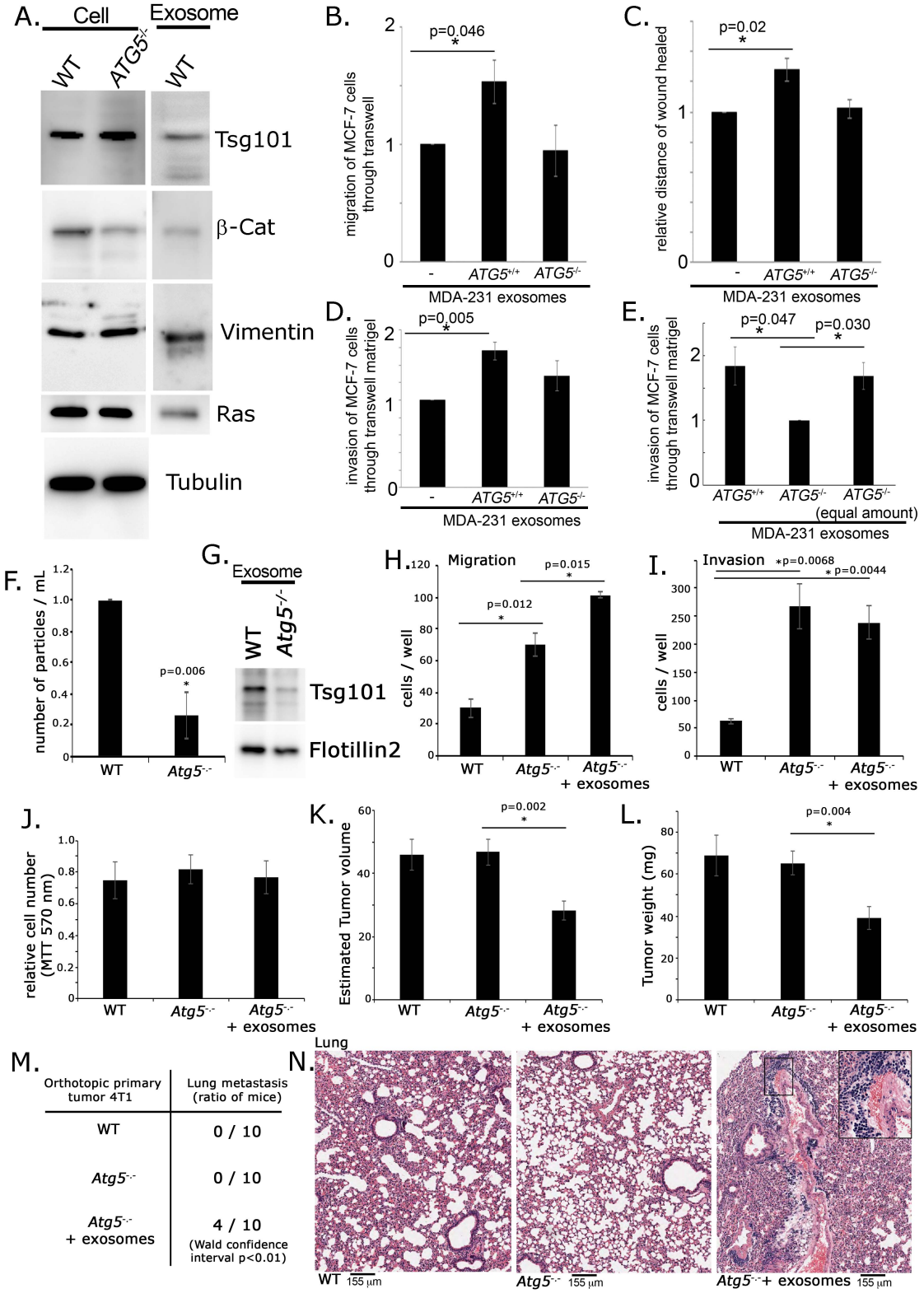

Orthotopic primary tumor 4T1	Lung metastasis (ratio of mice)
WT	0 / 10
Atg5$^{-/-}$	0 / 10
Atg5$^{-/-}$ + exosomes	4 / 10 (Wald confidence interval p<0.01)

Figure 39: Atg5 promotes migration and metastasis of breast cancer cells by increasing exosome production

(**a**) Western blot of wild-type and *ATG5*$^{-/-}$ MDA-MB-231 cells or wild-type exosomes for exosome markers (Tsg101) and proteins with roles in migration and metastasis (Vimentin, Ras, β-catenin). (**b**) Quantification of migration of MCF-7 cells through a transwell chamber upon incubation with no exosomes or exosomes from equivalent amounts of wild-type or *ATG5*$^{-/-}$ MDA-MB-231 cells. (**c**) Quantification of wound closure by MCF-7 cells incubated with no exosomes or exosomes from equivalent amounts of wild-type or *ATG5*$^{-/-}$ MDA-MB-231 cells. (**d**) Quantification of invasion of MCF-7 cells through a transwell chamber coated with matrigel upon incubation with no exosomes or exosomes from equivalent amounts of wild-type or *ATG5*$^{-/-}$ MDA-MB-231 cells. (**e**) Quantification of invasion of MCF-7 cells through a transwell chamber coated with matrigel upon incubation with exosomes from wild-type MDA-MB-231 cells, exosomes from an equivalent number of MDA-MB-231 ATG5$^{-/-}$ cells, or an equivalent amount of exosomes from ATG5$^{-/-}$ cells as produced by wild-type cells (equal amount exosome). (**f**) Quantification of exosome production by nanoparticle tracking analysis of particles (45-105 nm) in wild-type and *Atg5*$^{-/-}$ 4T1. (**g**) Western blot of exosome markers Tsg101 and Flotillin2 in exosome preparations produced by equivalent amounts of wild-type and *Atg5*$^{-/-}$ 4T1 cells. (**h**) Quantification of migration through a transwell chamber of wild-type, *Atg5*$^{-/-}$ or *Atg5*$^{-/-}$ 4T1 cells supplemented with exosomes from wild-type 4T1 cells. (**i**) Quantification of invasion through a matrigel coated transwell chamber of wild-type, *Atg5*$^{-/-}$ or *Atg5*$^{-/-}$ 4T1 cells pretreated with exosomes from wild-type 4T1 cells. (**j**) Quantification of cell quantity by MTT assay of wild-type, *Atg5*$^{-/-}$ or *Atg5*$^{-/-}$ 4T1 cells pretreated with exosomes from wild-type 4T1 cells after 48 h. (**k**) Estimated volume of primary tumor extracted from the mammary pad of mice implanted 2 weeks prior with wild-type, *Atg5*$^{-/-}$ or *Atg5*$^{-/-}$ 4T1 cells pre-treated with wild-type exosomes. Volume =

[width(2) x length]/2. (**l**) Tumor mass of primary tumor extracted from the mammary pad of mice implanted 2 weeks prior with wild-type, *Atg5*$^{-/-}$ or *Atg5*$^{-/-}$ 4T1 cells pre-treated with wild-type exosomes. (**m**) Table of number of mice with metastatic cancer nodes in at least one of 4 sections of the left lung lobe analyzed. (**n**) Images of haemotoxylin-eosin stained left lower lung lobe sections from mice implanted with wild-type, *Atg5*$^{-/-}$ or *Atg5*$^{-/-}$ 4T1 cells pre-treated with wild-type exosomes in the mammary pad three weeks after removal of the primary tumor. Scale bars represent 155 μm. Data are represented as mean +/- SEM. Western blots were run on separate gels in parallel using samples prepared in parallel.

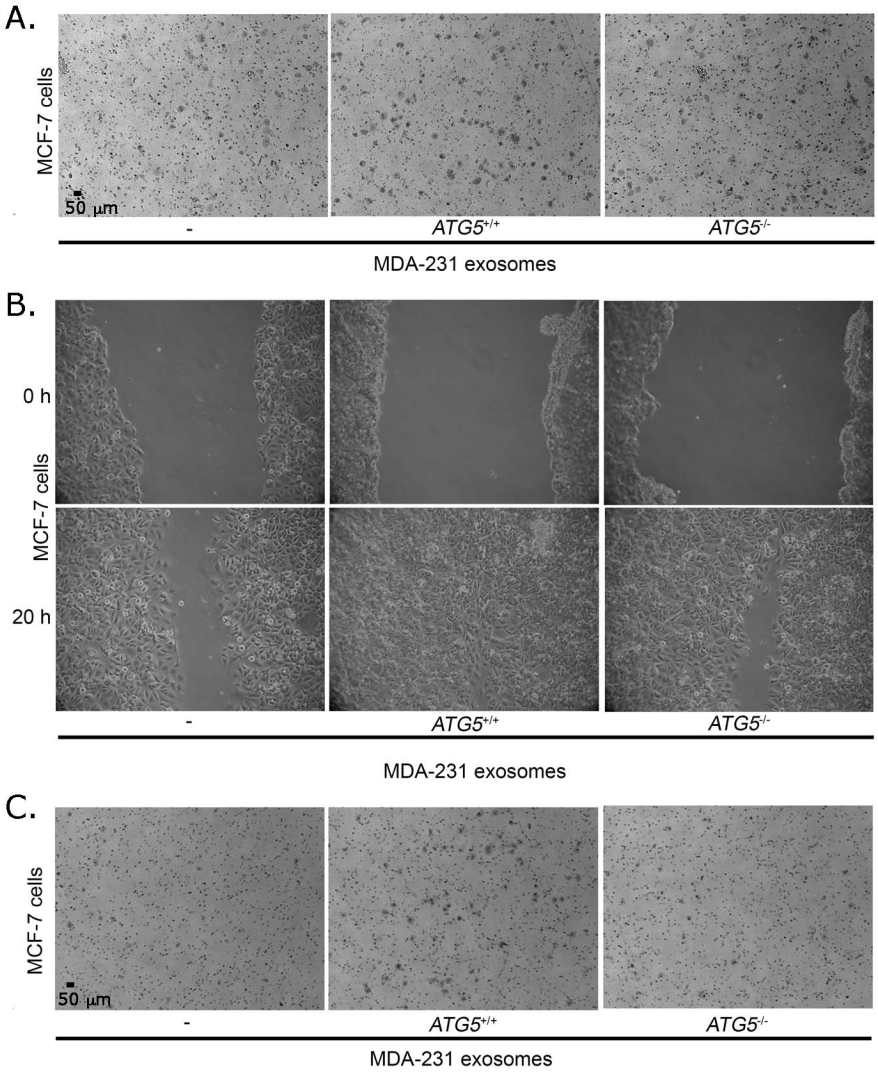

Figure 40: Atg5 is required for exosome production that promotes wound healing, migration and invasion of MDA-MB-231 breast cancer cells

(**a-c**) Representative images of MCF-7 cells incubated without exosomes, or with exosomes from equivalent amounts of wild-type or *ATG5*$^{-/-}$ MDA-MB-231 cells in (**a**) transwell migration assay (Scale bar = 50 μm), (**b**) wound healing assay (Images were acquired with a 4x objective lens) and (**c**) and transwell invasion assay. Cells in (a) and (c) were stained with crystal violet (Scale bar = 50 μm).

To investigate the effect of Atg5 on exosome-mediated spread of breast cancer in an orthotopic model we used 4T1 breast cancer cells. As with other cell lines tested, *Atg5*$^{-/-}$ 4T1 cells (Figure 37g) released fewer exosomes than wild-type cells (Figure 39f,g). Interestingly, migration and invasion of *Atg5*$^{-/-}$ 4T1 was increased, as measured by transwell assays, compared to its wild-type counterpart (Figure 39h,i). Replacing exosomes lacking in the media of *Atg5*$^{-/-}$ cells with wild-type exosomes further increased migration of 4T1 cells (Figure 39h). Cumulatively, results in MDA-MB-231 and 4T1 breast cancer cell lines suggest that loss of exosome production in *Atg5* knockout cells decreases migration of these cells.

To evaluate the *in vivo* consequences on metastasis of tumors we adopted the orthotopic 4T1 model of metastasis. People handling and injecting mice, measuring primary tumors and analyzing metastasis in tissues were blinded to treatment groups. 4T1 cells were washed in PBS and implanted in the mammary pad. Wild-type, and *Atg5*$^{-/-}$ 4T1 cells were compared to *Atg5*$^{-/-}$ cells whose lack of exosomes was supplemented by pre-treating with wild-type exosomes before implantation. Primary tumors formed after two weeks by wild-type and *Atg5*$^{-/-}$ 4T1 cells were equivalent in volume and mass, whereas the volume and mass of tumors from *Atg5*$^{-/-}$ cells supplemented with wild-type

exosomes was significantly reduced (Figure 39k,l), despite the unchanged proliferation of these cells *in vitro* (Figure 39j). Mice were sacrificed 3 weeks later. In this version of the 4T1 model previous evidence demonstrated that no metastatic nodules are observed in lung or other organs when primary tumors are removed at 2 weeks as performed here (Tao, Fang, Alroy, & Sahagian, 2008). Accordingly, no metastatic nodules were observed in sectioned lower left lung lobes of mice implanted with wild-type or *Atg5*$^{-/-}$ 4T1 cells. However, replacing the exosomes of *Atg5*$^{-/-}$ cells caused the appearance of metastatic nodules, which were confirmed by a clinical pathologist in 4 of 10 mice (Figure 39m,n, $p>0.01$ Wald's modified confidence interval). This suggests Atg5 is required for effective exosome production that enhances migration of breast cancer cells from the site of the primary tumor to establish metastasis.

4.4 Discussion

Existing literature has suggested contradicting effects of autophagy genes on exosome production. These papers frequently examined single genes, relied on Western blots to quantify exosomes, and examined extracellular vesicles with unique cargoes like hepatitis C virus in single cell types. Here we systematically evaluated the effects of multiple Atg genes often in more than one cell type and with more rigorous quantification of exosome quantity by nanoparticle tracking, dynamic light scattering and Western blot for canonical exosome markers. This evidence suggests that Atg5, independent of Atg7 and canonical macroautophagy, is critical for regulating exosome production. Effects of Atg6/Beclin1 on exosome production that were previously observed (Shrivastava et al., 2016) may be independent of autophagy. Beclin1 forms a complex with class III phosphinositide 3-kinase (PI3K) and dictates the allocation of class III PI3K between Atg14L1 complexes involved in phagophore formation for autophagy and complexes involved in budding of vesicles into MVB (McKnight et al., 2014). Therefore, Beclin1 is

likely to affect exosome production by altering the amount of class III PI3K participating in budding of vesicles into MVB (Futter et al., 2001) independent of autophagy and the mechanisms described here. As well, the increased release of exosomes previously observed when cells are treated with Bafilomycin and other inhibitors of the V_1V_0-ATPase complex (Alvarez-Erviti et al., 2011; Parolini et al., 2009) are likely independent of canonical autophagy as these inhibitors also increased exosome production in *Atg5*$^{-/-}$ cells (Figure 38). While our results demonstrate that exosome production is independent of canonical Atg7-dependent autophagy, autophagosome-like structures and degradation have been observed in cells lacking Atg7 (T. K. Chang et al., 2013; Ktistakis & Tooze, 2016; Nishida et al., 2016; Ra et al., 2016). Therefore, we cannot exclude that one of the complex emerging forms of Atg7-independent non-canonical autophagy participates in exosome production. However, in terms of membrane topology there is no straightforward model for how a large double-membraned autophagosome participates in generating ~100 nm intraluminal vesicles within endosomes. In contrast, Atg5, Atg16L1 and LC3 have been observed to localize to endosomes, phagosomes and lysosome-like granules that are related to MVB independent of double-membrane autophagosomes (Munz, 2017). Knowledge of exosome biogenesis and our data are consistent with a model in which Atg5, Atg16L1 and LC3 are found on the cytoplasmic surface of MVB and are packaged into intraluminal vesicles budding into MVB.

Atg5 is abundant in exosomes (Figure 36b) and is required for LC3 sorting into exosomes. LC3-I rather than LC3-II is sorted into exosomes in *Atg7*$^{-/-}$ cells, demonstrating that LC3 sorting into exosomes occurs without Atg7 and canonical autophagy (Figure 36k,n-p) and LC3-II is not required for exosome production. This suggests that Atg5 physically brings LC3 into exosomes. LC3 associates with the V_1V_o ATPase component ATP6V1E1 according to PLA assays (Figure 38a),

immunoprecipitations (Figure 38b) and pulldowns with recombinant LC3 (Figure 38c). Our data suggests that as LC3 is packaged into exosomes it takes ATP6V1E1 with it, thereby inactivating the V_1V_o-ATPase at MVB and causing MVB pH to increase in an Atg5-dependent manner. Several lines of evidence suggest that functions of the V_1V_o-ATPase in acidification and fusion of organelles can be dissected (D. Wang & Hiesinger, 2013). Exosome production in *Atg5*$^{-/-}$ cells was rescued by increasing endolysosomal pH for only 30 min with NH_4Cl to minimize secondary effects of neutralizing endolysosomal pH (Figure 38n-o). This suggests that the effect of the V_1V_o-ATPase on Atg5-dependent exosome production is due to effects on MVB acidification, but we cannot formally exclude a direct role of the V_1V_o-ATPase in membrane fusion in this process.

Atg5 decreased acidification of MVB (Figure 33). In contrast, Atg5 has been observed in other systems to increase acidification of LC3-associated compartments including autophagolysosomes, LC3-associated phagosomes and endosomes (Peng et al., 2014; Romao et al., 2013; Sanjuan et al., 2007; J. Zhou, S. H. Tan, et al., 2013). Consistent with this literature we found Atg5 promoted acidification or lysosomal fusion of compartments destined for degradation (EGF, dextran, Figure 34a-e), while limiting acidification of MVB containing exosome markers (Alix, NRhPE, Figure 33d-j, Figure 32i-l). This suggests Atg5 has contrasting effects on discrete populations of endosomes and MVB with distinct fates (lysosomal fusion, Golgi-trafficking, plasma membrane fusion). One model consistent with the evidence is that on MVB, LC3 may remove ATP6V1E1 into intraluminal vesicles/exosomes and decrease MVB acidification whereas when LC3 remains on the surface of the endosome, phagosome or autophagosome it may recruit ATP6V1E1 and anchor or stabilize the V_1V_o ATPase to promote acidification of these organelles.

Exosomes have been demonstrated to promote invasion of cancer cells (Kosaka, Yoshioka, Fujita, & Ochiya, 2016). Recent studies have highlighted a role for exosomes in trafficking to future sites of metastasis and establishing a metastatic niche for cancer cells to spread into (A. Hoshino et al., 2015). The present study demonstrates that exosomes also promote metastasis of cancer cells by acting directly on cancer cells to promote their migration from the site of the primary tumor. Our results demonstrate that one mechanism by which *Atg5* controls cancer cell migration and metastasis (Kenific, Wittmann, & Debnath, 2016; Sharifi et al., 2016) is to control release of exosomes (Figure 41). This effect of Atg5 on exosome release may contribute to the effects of autophagy on cancer cell invasion previously observed (Kenific et al., 2016; Sharifi et al., 2016). An increasing number of changes in growth factor and metabolic cues are being discovered to directly impact the Atg5-Atg16L1 complex by direct phosphorylation for example (Russell, Yuan, & Guan, 2014). Our results thus suggest that control of exosome release by Atg5-Atg16L1 may contribute to the complex effects of autophagy genes, autophagy activators or inhibitors, lysosome-targeting drugs, and tumor microenvironment on cancer metastasis.

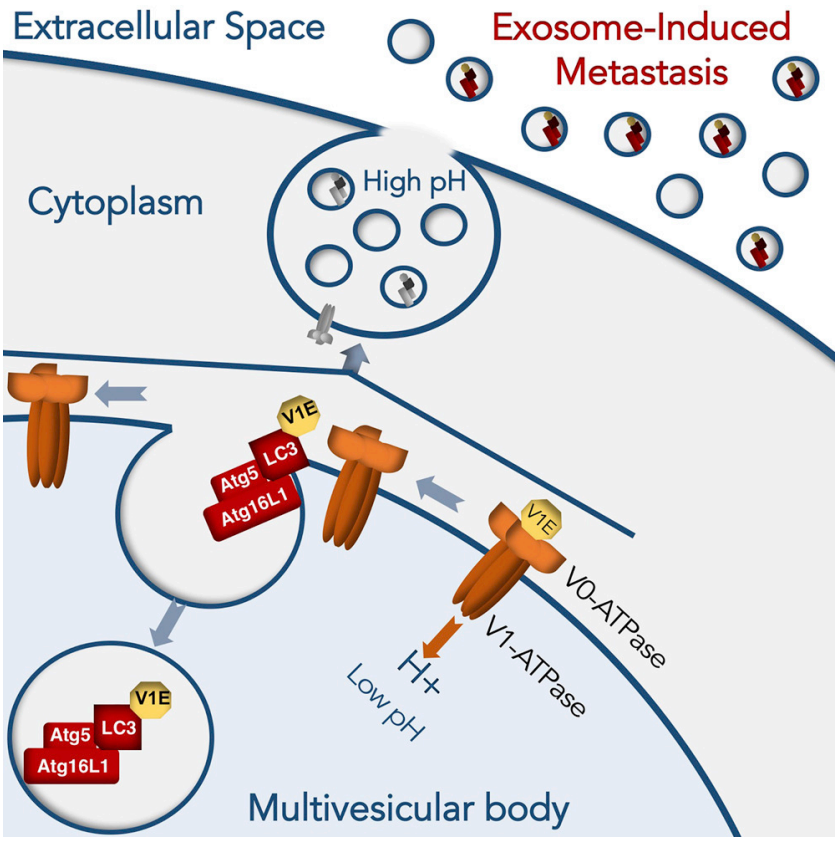

Figure 41: Schematic model of Atg5-mediated exosome production

Atg5 removes V1E from the V1V0-ATPase thereby inactivating the V1V0-ATPase, increasing MVB pH and enhancing exosome production.

4.5 Methods

Key Resources Table

*Due to the size of this table please refer to Appendix F

Contact for reagent and resource sharing

Further information and requests for resources and reagents should be directed to and will be fulfilled by the Lead Contact, Derrick Gibbings (gibbings@uottawa.ca).

Experimental models and subject details

Cell lines

Mouse embryonic fibroblasts (MEF) lacking a copy of *Atg5* (Kuma et al., 2004), and wild-type and *ATG16L1*$^{-/-}$ HCT-116 were a gift of D. Philpott (University of Toronto, Canada). *Atg7*$^{-/-}$ and *Atg14*$^{-/-}$ cells were a gift of Herbert Virgin (University of Washington). Doxycycline-regulated Atg5 MEF generated previously were also used (Hosokawa, Hara, & Mizushima, 2007).

MDA-MB-231 (HTB-26, ATCC) cells were genetically deleted of *ATG5* using Compozr Zinc Fingers technology (product number CKOZFND1217-1KT, Sigma-Aldrich). Mutation of *ATG5* was confirmed using Surveyor Mutation Detection Assay (706020, Transgenomic), PCR (ZFN primer F sequence was CAAAATGGGCCAAATAGCTAAA and ZFN primer R sequence was ACTTACCATTTTGCAATCCCA) and Western blot. All cells, including Neuro2A (CCL-131, ATCC) and 3T3 (CRL-1658, ATCC), were cultured in Dulbecco's Modified Eagle Medium (DMEM) containing 10% fetal bovine serum and penicillin-streptomycin. To generate 4T1 *Atg5*$^{-/-}$ cells Crispr Cas9 guide RNAs (gRNA) for murine ATG5 were generated using the online CRISPR design tool targeting exon 1 (http://crispr.mit.edu/). Atg5 knock-out 4T1 cell line for injection into mice was generated using the following gRNA: Top: caccGAAGATGTGCTTCGAGATGTGTGG, bottom: aaacCCACACATCTCGAAGCACATCTTC. To generate Atg7 & Atg5 double knockout MEF cells, Atg7 was knocked out using the following gRNA: Top: caccGAAGTTGAACGAGTACCGCC, Bottom: aaacGGCGGTACTCGTTCAACTTC on *Atg5*$^{-/-}$ MEFs. The knockout of each protein was confirmed using Western blot. Identity of cell lines was not authenticated by the authors.

Mice

Eight week old female Balb/C mice (Charles River) were randomized into 3 groups (10 mice per group) to receive $3X10^5$ 4T1 cells in 50 μl PBS injected in the lower mammary pad. Mice were housed at 4 per cage and fed with standard food and water *ad libitum*. All experiments involving mice were performed in accordance with relevant institutional and national guidelines and regulations and approved by the University of Ottawa Animal Care Committee.

Exosome enrichment

Exosomes were enriched by differential centrifugation as previously described (Thery et al., 2006). Briefly, cells were cultured in media containing 10% FBS previously depleted of exosomes by centrifugation at 100 000 g for 16 h (Thery et al., 2006). To purify exosomes, supernatant from cell cultures was centrifuged at 300 g (10 min), 2000 g (10 min) and 10 000 g (30 min, SW32 rotor). At each step the supernatant was recovered. After centrifugation at 100 000 g (1 h 10 min, SW32 rotor) the supernatant was removed and the pellet was resuspended. The pellet was washed in PBS by a final centrifugation at 100 000 g (20 min, TLA100.3 rotor). The exosome-enriched pellet was re-suspended in PBS for further analyses.

For density separation, exosomes were purified as described (Laulagnier, 2015). Briefly, Neuro2A cell culture media was collected, and a cocktail of protease inhibitors added (Roche). Media were cleared of debris by two successive centrifugation steps (2 000 g for 10 min, 20 000 g for 20 min) and filtration through a 0.22 μm filter (Millex GV PVDF, Millipore). The medium was centrifuged for 2 h at 100 000 g (2 h, SW32 rotor). The resulting pellet was resuspended in 0.211 M sucrose, 3 mM imidazole pH 7.4, and loaded onto a continuous sucrose gradient (0.3-1.4 M). Gradient was centrifuged at 200 000 g (18 h, SW41Ti rotor), and 10 fractions (1 ml) were collected. The sucrose density

of each fraction was determined by refractometry. Fractions were washed in 3 mM imidazole, pH 7.4, and centrifuged at 200,000 g (2 h, SW41Ti rotor). Exosome pellets were resuspended in Laemmli buffer and used for Western blot analysis.

Dynamic light scattering

Preparations of enriched exosomes were analyzed by dynamic light scattering on a Protein Solutions Dynapro Instrument using Dynamics V6 software. Data were acquired every 10 seconds at 4°C and 10% laser power for at least 200 seconds per sample. The intensity (Cnt/s) and size (nm) were generated automatically by the instrument.

Nanoparticle tracking analysis

Preparations of enriched exosomes were analyzed using either a Nanosight (Figure 29a,c) or a ParticleMetrix Zetaview Nanoparticle tracking instrument (all other graphs). Post-acquisition parameters on the Nanosight were: were Min Bright: 15, Min size: 10 nm, Max size: 200nm.

The ZetaView Nanoparticle Tracking instrument (ParticleMetrix) is calibrated for experiments following every instrument start-up. Focusing and alignment are performed automatically using 102nm polystyrene beads (Microtrac 900383). Exosome samples were diluted in PBS into the acceptable range for measurement (typically 1:1000 – 1:100,000). One mL of sample was injected into the machine and allowed to slow down according to the built in particle drift sensor. If the sample falls within the acceptable reading concentration range, video acquisition and analysis was performed using the following parameters. Acquisition Parameters: Sensitivity (85), Shutter speed (40), Frame rate per second (30), Resolution (Highest), Positions measured (11). Post-

acquisition parameters: Minimum brightness (15), Minimium size in pixels (10), Maximum size in pixels (500).

The analysis reports containing the particle size (nm) and concentration (particles/ml) were generated automatically. The particles between 45 nm and 105 nm were summed to quantify exosome-sized particles. In experiments in Figure 38n,o measuring exosome production after treating cells with NH_4Cl or Chloroquine for short time periods, background readings from exosome-depleted media alone were subtracted. Only in these experiments was the background reading high enough to impact the particle counts measured.

Exosome uptake assay

Exosomes purified using the procedure described above were re-suspended in 20 µl of PBS. Vybrant DIO Cell-Labeling Solution (V22886, Invitrogen) was used and the manufacturer's protocol was followed. Briefly, 5 µl of the cell-labeling solution was added to the exosome preparation and incubated for 20 min at 37°C. Excess label was removed by centrifugation (100,000g, 20 min, TLA 100.3 rotor) and the pellet was re-suspended in 500 µl of DMEM. Equal amounts of DIO-labeled exosomes were added to cells in triplicate and DMEM alone was added to control wells. Cells were incubated with DIO-labeled exosomes for 1 h. Supernatant was retained to measure uptake of DIO-labled exosomes by disappearance of fluorescence (Synergy H1 Hybrid Multi-Mode Microplate Reader, BioTek). To measure internalization of exosomes into cells, these were re-suspended in 500 µl of PBS for analysis on a flow cytometer (Beckman Coulter Cyan ADP 9).

Endosomal labeling and trafficking assays

To label MVB, cells were incubated with 3 μM NRhPE (Avanti Polar Lipids) at 4°C for 15 min then transferred to 37°C, 5% CO_2 for the indicated incubation times, as previously described (Vidal et al., 1997). pHrodo Green Dextran (10 kDa, ThermoFisher) was incubated with cells for 10 minutes and cells were transferred to ice for immediate analysis by flow cytometry. After initial readings 20 mM NH_4Cl was added to cells to neutralize the pH-dependent increase in pHrodo fluorescence to measure dextran internalization and acidification of dextran-containing compartments (geometric mean fluorescence intensity before/after NH_4Cl). To image EGFR trafficking cells were incubated with EGF-Alexa488 (100 ng/mL, ThermoFisher) in serum-free DMEM and imaged at 30 min where its localization in late endosomes and lysosomes is maximal (Vanlandingham & Ceresa, 2009).

Immunofluorescence microscopy

Cells were prepared for microscopy as previously described (D. Gibbings, Mostowy, S., Jay, F., Schwab, Y., Cossart, P., Voinnet, O., 2012). Cells cultured on coverslips (Deckgläser 18 mm Ø) were fixed in 2% paraformaldehyde in PBS (10 min) 48 h post transfection where cells were transfected. Cells were then rinsed twice in PBS and permeabilized with 0.2% Triton-X-100 in PBS containing 20 mM NH_4Cl (10 min). After washing with PBS, cells were blocked with 5% milk in PBS (1 hour), washed three times in PBS and incubated with 2-5 μg/ml primary antibody in PBS at 4°C overnight. Following primary incubation, cells were washed three times (5 min) in PBS and incubated for 1 hour at room temperature with 1/250 dilution of highly cross-adsorbed secondary antibodies (goat anti-mouse Alexa Fluor 488, 546 or 633, goat anti-rabbit Alexa Flour 488 or 546, goat anti-rat Alexa Fluor 546, donkey anti-goat Alexa Fluor 488 [ThermoFisher], or goat anti-rabbit DyLight 405 [Thermo Scientific]). After washing three

times (5 min), cells were mounted with Vectashield Mounting Media. For live cell imaging, cells were plated on Cellview culture dishes with 2.2 cm^2 glass bottom.

Epifluorescence microscopy was performed using a Zeiss AxioObserver.D1 or Zeiss AxioObserver.Z1 microscope. Images were acquired with a 63x Plan-Apochromat 1.4 Oil DIC objective and AxioCam MRm CCD (monochrome), using Zeiss AxioVision Rel. 4.8 software. Confocal microscopy was performed using a Zeiss LSM 510 Meta/AxioVert 200 microscope. Images were acquired with a 63x Plan-Apochromat 1.4 Oil DIC objective, 2 Photo Multiplier Tubes and 1 Meta detector, using Zeiss ZEN software. Confocal images for preparing 3D models were acquired in 0.5-1 µm Z-stacks.

Stimulated emission-depletion (STED) microscopy

Subconfluent cells were cultured on glass coverslips (Deckgläser 18 mm Ø). Forty-eight h after transfection, cells were fixed with 4% paraformaldehyde in 10 mM PBS (10 mM phosphate buffer - pH 7.2, 154 mM NaCl). After cells were washed with PBS at room temperature, then incubated overnight at 4°C with primary antibody prepared in Ab Buffer (10 mM PBS, 3% BSA, 0.3% Triton X-100). After washing, the cells were incubated for 1 hour at room temperature with STED CW-compatible secondary as well as tertiary antibodies prepared in Ab buffer. Cells were mounted with Prolong Gold ™ Antifade (P36930, Life Technology) mounting medium and cured for 24 h at room temperature before imaging. Secondary antibodies used include: ChromeoTM 505 anti-mouse IgG (15050, Active Motif, Concentration 1:500), Biotin-anti-rabbit IgG (B8895, Sigma, Concentration 1:800), Streptavidin V500 (561419, BD Horizon, Concentration 1:200).

Continuous wave stimulated emission depletion (STED CW) images were acquired using a Leica SP5/STED CW microscope, and a 100x oil immersion objective (HCX PL

APO CS 100x/1.40 OIL STED, Leica Germany) essentially as described (Y. Z. Zheng et al., 2011). Dual colour excitation of fluorophores was achieved using an argon-ion laser exciting at 458 nm and 514 nm respectively. STED depletion was achieved with a 592 nm CW laser line. Fluorescence outputs were captured in sequential scans using base parameters of 600 Hz frequency at a 2.54x zoom giving a resolution of 29.8 nm x 29.8 nm per pixel. The first scan at 514 nm excitation wavelength (ChromeoTM 505) was performed at 50% laser power, 750 gain, -0.3 offset, with frame averaging and accumulation of 3, and a detection window of 520 – 580 nm. The second scan at 458 nm excitation wavelength (streptavidin V500) was performed at 85% (LC3) or 55% (Rab5) laser power, 800 gain, -1.0 offset, with frame averaging and accumulation of 3, and a detection window of 465 – 485 nm. STED 592 depletion laser power was 100%. Images were processed using Leica STED deconvolution software (LAS AF v2.6.3.8173). First a point spread function (PSF) was generated using a Lorentz transformation of 70 nm. Then the image was deconvolved using the generated PSF and signal energy set to regularization parameter 0.05. Images were further processed using the baseline mean function, and background was reduced by 1500 (in the 16-bit image).

Image analysis

Images were analyzed using ImageJ software. Three-dimensional image renderings were made using ImageJ. Raw microscope image channels were thresholded and merged using the imbedded “Threshold > Triangle” and “Merge Channels” options, respectively. The composite image was rendered as a 3D image with the “Show Color Surfaces” plugin with the radius of smoothing set to 0.20 pixels.

To detect and quantify the colocalization of fluorescently labelled subcellular structures, we employed an object-based colocalization method named ‘SQUASSH’ (Segmentation

and QUantification of Subcellular SHapes) (Rizk et al., 2014). The ImageJ plugin - MosaicSuite was downloaded and run on each of the images. Background fluorescence was eliminated with a rolling ball window size of 10 pixels. For segmentation, PSF model for the wide-field microscope used was estimated to be 0.84 (xy) and 0.79 (z). Regularization parameter and minimum object intensity of channel 1 and channel 2 were set at 0.15, 0.075 and 0.15 respectively. A Gaussian noise model was used. Cell masks were set at 0.25 and 0.2 for channel 1 and channel 2 respectively. Another ImageJ plugin Just Another Co-localization Plugin (JACoP) was used to obtain Li's intensity correlation co-efficient of co-localization (Q. Li et al., 2004). In quantified experiments at least 3 slides were imaged per condition, with 5-7 images per slide and approximately 10 cells/image to provide data from about 250-350 cells.

Electron microscopy

Cultures of MEF cells were fixed *in situ* with 0.1 M cacodylate buffer containing 2% glutaraldehyde until processing for embedding. Cells were post-fixed in 1% osmium tetroxide (EMS, PA, USA) in cacodylate buffer at 4^{o}C. After washing in buffer, MEF cells were dehydrated in graded ethanol, infiltrated and embedded in Epon 812 (MECALAB, Québec, Canada), as described (Luft, 1961). Ultrathin sections were obtained using a Reichert Ultracut S ultramicrotome, and mounted on formvar-carbon coated nickel grids (MECALAB, Québec, Canada). Sections were stained with uranyl acetate and examination was performed with a Philips CM 100 electron microscope. To analyse MVB, we excluded organelles containing a signature double-membrane of autophagosomes or organelles that were electron dense like lysosomes or contained heterogenous luminal contents that are characteristic of lysosomes and autophagolysosomes (Huotari & Helenius, 2011). MVB frequently contained dense

surface patches associated with vesicle budding (Murk et al., 2003), and MVB exclusively containing vesicles of 30-120 nm were analysed (Huotari & Helenius, 2011).

LC3 was detected in exosome preparations by electron microscopy as previously described (Chivet et al., 2014). Briefly, Neuro2a cell culture media was collected, and a cocktail of protease inhibitors added (Roche). Media were cleared of debris by two successive centrifugation steps (2 000 g for 10 min, 20 000 g for 20 min) and filtration through a 0.22 µm filter (Millex GV PVDF, Millipore). The medium was centrifuged for 100 000 g (2 h, SW32 rotor). The resulting pellet was washed in PBS and resuspended in 40 µl 2 % paraformaldehyde in PBS. Four µL drops were spotted onto Formvar-carbon-coated grids for 20 min, treated with PBS-glycine (50 mM), blocked with PBS-BSA (10 mg/ml) then permeabilised with 0.05% saponin in PBS-BSA before consecutive incubation with rabbit anti-LC3A/B (Cell signalling, 1 h), followed by goat anti-rabbit 1.4 nm gold conjugated-F(ab') (Nanoprobes, 45 min). The grids were then fixed 1 min with 1 % glutaraldehyde in PBS and finally treated with the HQ silver intensification kit (Nanoprobes) for 6 min before negative staining. Grids were observed with a Jeol JEM 1200EX transmission electron microscope.

Recombinant LC3 pull-down

In brief, 0.5 µg of His-tagged recombinant LC3 (His-tag, Cat# ADI-APR-100-0200, Enzo Life Sciences) was rotated in 50 µl with 5 µl of His-tagged Dynabeads (Cat# 10103D, Thermofisher) in a binding/wash buffer (50 mM Sodium Phosphate, pH 8.0, 150 mM NaCl, 0.01% Tween®-20, 0.5% Triton X-100) at room temperature (RT) for 10 min. Then 150 µl of binding/wash buffer containing 5% BSA was added to the tubes and rotated for 5 minutes. Tubes were placed on a magnet and supernatant discarded. Cell lysate (100ul, 150ug) collected in Pull-down Buffer (3.25 mM Sodium phosphate pH 7.4,

70 mM NaCl, 0.01% Tween®-20, 0.5% Triton X-100) was incubated on a roller for 10 min. Supernatant was discarded and beads were washed 4 times with 300 μl Binding/Wash Buffer. His-LC3 was eluted with 150 mM Imidazole, 50 mM Sodium phosphate pH 8.0, 300 mM NaCl, 0.01% Tween®-20 with gentle shaking for 5 min. Supernatants were separated from beads on a magnet. The median intensities of bands for p62, ATP6V1E1 and background were quantified over 3 independent experiments using ImageQuantTL (GE Healthcare).

Experiments with competitive peptides were performed as above, except 50 μmoles of peptide was added during incubation with cell lysate. The following peptides were synthesized by Genscript with an N-terminal biotin: p62 LIR: SGGDDDWTHLSS, ATP6V1E1 putative LIR: RCRKQDFPLVKA, and ATP6V1E1 mutated putative LIR: RCRKAILPLQKA.

LC3-interacting region peptide pulldown assay

The following peptides were synthesized by Genscript with an N-terminal biotin: p62 LIR: SGGDDDWTHLSS, ATP6V1E1 putative LIR: RCRKQDFPLVKA, and ATP6V1E1 mutated putative LIR: RCRKAILPLQKA. Fifteen μl of Dynabeads® MyOne™ Streptavidin T1 (Cat#65601, ThermoFisher) were washed with PBS, then 10 nmoles of biotinylated peptides and 100 ng of recombinant LC3 were added. The mixture was rotated at 4 C overnight. The beads were then washed with PBS 3 times and collected for further Western analysis.

Scratch wound assay

MCF-7 cells were grown to confluence in 6 well plates containing DMEM with FBS. Wells were marked with a reference line through their center. Once cells reached

confluence they were scratch wounded using a 200 μl pipette tip (2 wounds/well perpendicular to the reference line), washed with PBS, and supplied with fresh media. Exosomes isolated from equivalent amounts of wild-type MDA-MB-231, *Atg5*$^{-/-}$ MDA-MB-231, or MCF-7 cells in 6 well plates were added to the media of scratch-wounded MCF-7 cells. An image on either side of the reference line at each scratch wound was taken at time 0 and 20 h. In each image, the distance of the wound was measured at 6 points including the largest and smallest distances.

Motility and invasion assay

Motility chambers (BD Bioscience, Cat#354578) and invasion chambers (BD Bioscience, Cat#354480) were rehydrated and equilibrated for 2 h with 500 µl of serum free DMEM media. After 2 h, the medium in the inserts was aspirated and inserts were placed into wells containing DMEM with 10% FBS. MCF-7 cells (50 x 10^3) were added to each chamber in serum-free media. Exosomes isolated from equivalent amounts of wild-type MDA-MB-231, *ATG5*$^{-/-}$ MDA-MB-231, or MCF-7 cells in 6 well plates were added to the media of MCF-7 cells. The chambers were incubated for 24 h with exosomes. The media was then removed and the upper surface of the membrane was scrubbed 20 times with a cotton swab. Cells on the lower surface of the scrubbed membranes were fixed and stained with Diff-Kwik kit (Thermo Fisher Cat# 9990700) according to the manufacturer's instruction.

Proximity ligation assays

Proximity ligation assays (PLA) were performed according to the manufacturer's protocol using the following reagents Duolink® In Situ Detection Reagents Green (Cat# DUO92014-100RXN, Sigma); Duolink® In Situ Detection Reagents Orange (Cat# DUO92007-100RXN, Sigma); Duolink® In Situ PLA® Probe Anti-Rabbit PLUS (Cat#

DUO92002, Sigma); Duolink® In Situ PLA® Probe Anti-Mouse MINUS (Cat# DUO92004, Sigma). In brief, cells were plated either on cover slips or glass slides at a concentration of 10^5/ml. Cells were fixed using 4% formaldehyde in PBS, then permeablized using 20 mM NH_4Cl, 0.2% Triton in PBS for 20 minutes at room temperature. Hydrophobic pen was used to enclose a 1 cm^2 area, then 40 μl of reaction volume was added. All subsequent incubations were performed at 37°C in a humid chamber. Non-specific binding was minimized with the manufacturer's blocking buffer for 30 min. Primary ATP6V1E1 (Host: mouse Cat# H00000529-M02, Abnova) and ATP6V0C Antibody (Cat# PA5-23972, Thermofisher), or ATP6V1E1 (Host: mouse Cat# H00000529-M02, Abnova) and Anti-LC3 antibody (Host: Rabbit, Cat# L7543-200UL, Sigma) were incubated with coverslips for 1 h (1:50, manufacturer's antibody diluent). Coverslips were washed with provided buffer A twice for 5 min, incubated with provided PLA probes for 1hr and washed with buffer A (twice, 5 min). Coverslips were incubated with ligation mix for 30 mins washed twice with buffer A and incubated with amplification mix. Coverslips were then washed with provided Buffer B twice (10 min), followed by 1 min washing with 0.01x Wash Buffer B. The samples were mounted with Duolink *In Situ* Mounting Medium with DAPI in dark for 15 min at room temperature. The images were taken using a Zeiss AxioObserver.Z1fluorescence microscope at 20X. In experiments including Alix-mCherry cells were fixed for PLA 30 hours post-transfection. Three biological replicates were performed for each condition. The Duolink® ImageTool (Cat# DUO90806-1EA, Sigma) was used to analyze images to obtain the number of PLA signals in the cytoplasm. Analyzed images in figures were generated automatically by the software. The number of signals per cell was calculated as Total number of Signals in Cytoplasm / Total number of Cells. The number of signals per cell was then normalized to the control.

Orthotopic model of 4T1 breast cancer

Equal amounts of 4T1 cells (wild-type and *Atg5*$^{-/-}$) were plated at a concentration of 10^6 per 10 cm dish, and pretreated either with vehicle or 10 μg of exosomes collected from 4T1 wild type cells for 6 days. Media and exosomes were changed every two days. Cells were collected, washed in PBS, counted and re-suspended in PBS. Eight week old female Balb/C mice (Charles River) were randomized into 3 groups (10 mice per group) to receive $3X10^5$ cells in 50 μl PBS injected in the lower mammary pad. Two weeks post-injection, the primary tumors were surgically excised. Primary tumors were weighed and measured using calipers and its volume was calculated using the formula (W x W x L)/2. Lower left lung lobes were collected 23 days after the removal of primary tumors and sectioned (5 μm, 20 sections). Every 5th section was stained using standard H&E staining. Stained sections were scanned using a Quorum Slide Scanner, and images were analyzed using Aperio imagescope (v12.3). All people handling or injecting cells into mice, removing and measuring tumors, staining and quantifying slides were blinded to the treatment groups. All experiments involving mice were performed in accordance with relevant institutional and national guidelines and regulations and approved by the University of Ottawa Animal Care Committee.

Quantification and statistical analysis

Two-tailed t-tests or ANOVA were employed to evaluate statistical significance, $p \leq 0.05$ was considered as significant. SPSS V21.0 was used for statistical analysis. Error bars represent SEM.

4.6 Acknowledgements

The authors would like to thank Manajeh Daneshmand for reviewing tissue sections from 4T1 metastasis models. The authors would like to thank Dana Philpott and Skip Virgin

for kindly providing MEF and HCT-116 knockout cells and Shoukat Dedhar for 4T1 cells. This research was funded by a grant from the National Sciences and Engineering Research Council of Canada (grant number 436104) and the Canadian Cancer Society Research Institute Grant number 702978 (D.G.). M.C. is supported by a Vanier Scholarship from the Canadian Institutes of Health Research. C.J. is supported by the Ministère de l'Enseignement Supérieur et de la Recherche. Work in the lab of R.S. was funded by the Institut National de la Santé et de la Recherche Médicale (Inserm), Université Joseph Fourier, Fondation France Alzheimer and ANR [grant number 08-Blanc-0271 (to R.S)]. R. M. B. was supported by a post-doctoral fellowship from the Canadian Institutes of Health Research. J.C. is a Canada Research Chair (Tier II) in RNA Metabolism funded through Canadian Institutes of Health Research.

Chapter 5 - General Discussion

Over the past two decades, our knowledge of autophagy in mechanistic and pathophysiological contexts has advanced tremendously. The three manuscripts presented in this thesis are a collection of research that investigated the emerging themes of misregulated autophagy in two human diseases - ALS and cancer. One general overarching link between these pathologies and several others is that defects in autophagy pathways have been observed throughout the progression of diseases (Giampieri et al., 2018). However, the many functions exerted by autophagy in vital biological processes leads to significant differences in its pathogenic mechanisms. For instance, autophagy functions as a stress-adaptive cytoprotective mechanism by eliminating misfolded proteins, damaged organelles or invading pathogens that cause several diseases. On the other hand, this stress-coping mechanism of autophagy is also exploited by treacherous cancer cells to establish tumours at distant-sites and become resistant to drugs or therapy. In addition, excessive autophagy causes undesirable cell death. Therefore, precise roles for autophagy in stress/disease contexts must be defined.

The three articles in this thesis represent the continuing efforts in the complex world of autophagy. They aim to fill the existing knowledge gaps and improve our current understanding of the various regulatory mechanisms, with the ultimate goal to selectively manipulate autophagy and autophagy-related processes for effective therapeutics. Specifically, while activating autophagy to degrade arginine methyl positive stress granules (Chapter 2) and retrotransposon RNA (Chapter 3) may be beneficial in ALS and cancer initiation contexts respectively, inactivating autophagy machinery proteins to impair exosome-mediated metastasis (Chapter 4) may be beneficial in the context of tumour progression.

5.1 Therapeutic targets for autophagy induction

5.1.1 Stress granules as ALS-linked pathological substrates of autophagy

Numerous links between autophagy and ALS have been established due to the growing number of disease-linked mutations in this degradation pathway (Ramesh & Pandey, 2017). However, how autophagy functionally protects from neurodegeneration in ALS remains obscure. In Chitiprolu *et al.*, 2018 (Chapter 2), we identified a critical and novel mechanism by which an ALS-linked autophagy receptor - p62 degrades ALS-linked cytoplasmic stress granules. Our work unified several ALS-linked proteins - p62, C9ORF72, SMN and FUS in one degradative pathway. Specifically, a complex of C9ORF72 and p62 bound a Tudor-domain containing protein - SMN to recognize proteins symmetrically methylated on arginines such as FUS. As a result, stress granule proteins significantly enriched in symmetrically methylated proteins were selectively targeted for autophagic clearance. FUS is conventionally known to harbour asymmetric dimethylarginines (Rappsilber, Friesen, Paushkin, Dreyfuss, & Mann, 2003). However, a previous study identified a FUS epitope that is likely recognized by a symmetric dimethylarginine-specific antibody (SYM10) (Boisvert et al., 2003). Additionally, predictions of a recent proteome-wide screen for PRMT5 targets also yielded FUS (Larsen et al., 2016). In agreement, our research demonstrated a previously undefined symmetric arginine methylation event on FUS (R218) controlled by an arginine methyltransferase not previously known to modify FUS (PRMT5); this methylation event triggered autophagic degradation of FUS.

Canonically, substrates degraded by autophagy are ubiquitinated. For instance, blocking the degradation of ubiquitinated SMN by the autophagy receptor - p62 has been tested as a therapeutic approach to promote motor neuron survival and longevity in

fly and mouse models of spinal muscular atrophy (Rodriguez-Muela et al., 2018). However more recently, autophagy receptors including Optineurin, Tecpr1 and Cbl have been suggested to target substrates for degradation by autophagy in ubiquitin-independent pathways (Khaminets et al., 2016). Recent reports highlight the ability of alternative post-translational modifications to target cargoes for autophagic degradation. For example when bacteria penetrate plasma membrane to enter the cytoplasm, glycosylation on the exterior face of the plasma membrane is introduced into the cytoplasm and recognized by Galectin-8 and NDP52 for degradation by autophagy. Intriguingly, during *C.elegans* embryogenesis an RNA-containing structure unique to germline cells called P granules is eliminated by autophagy after it is no longer required for development. Notably, this process requires arginine methylation of P granule proteins, but is independent of the *C.elegans* p62 homologue (S. Li et al., 2013). In combination with the observations herein, this hints that arginine methylation has more widespread roles than anticipated across species in priming substrates for degradation by autophagy. Most post-translational modifications (e.g. phosphorylation) have enzymes that remove the modification (e.g. phosphatases). If PRMTs are the writers and Tudor-domains are the readers of arginine methylation, our study demonstrates that autophagy may act as an eraser of arginine methylation in mammals.

Nine arginine methyltransferases (PRMTs) are known and nearly all generate either symmetric or asymmetric arginine dimethylation. We observed relatively higher enrichment of symmetric dimethylation in stress granules. PRMT5 and PRMT9 are the only enzymes that can generate symmetric dimethylarginine. Our C9ORF72 and p62 interactomes included several predicted PRMT5 substrates and 70% depletion of PRMT5 prevented elimination of most stress granules. It may be that other PRMTs such

as PRMT9 or alternate modifications or pathways also engage autophagy receptors to degrade stress granules by autophagy.

Arginine-methylated proteins are significantly enriched in RNA binding proteins (Q. Liu & Dreyfuss, 1995; M. C. Yu, 2011). Strikingly, a large proportion of proteins that are methylated on arginines (e.g., FUS, DDX3, G3BP1) or bind to methylated arginines (e.g., SMN, TDRD3, SND1) accumulate in stress granules. Interestingly, the C9ORF72 and p62 interactomes contained multiple RNA binding proteins with dimethylated arginines (FUS, HNRNPA1, HNRNPU, HNRNPUL1 and TAF15). This suggests that p62 may use SMN to dock on multiple arginine-methylated proteins in stress granules. Additionally, p62 may also use other Tudor-domain containing proteins such as TDRD3 or SND1 to recognize arginine-methylated stress granule proteins such as DDX3 or G3BP1.

Docking is a frequent phenomenon that unites biological processes involving distinct pathways or entities. For example DNA encoding ribosomes localizes adjacent to nucleolei and rRNA-binding proteins that then capture and assemble its transcriptional products (Wachtler et al., 1992). Similarly, we observed frequent docking of p62 to the surface of stress granules. Our electron microscopy evidence suggests that this docking may allow accessibility of p62 to LC3 and thereby promote autophagosome engulfment of stress granules.

We explored the accumulation of symmetrically dimethylated cytoplasmic aggregates in C9ORF72-ALS patients, as a loss of C9ORF72 may impact autophagy in these patients. Lack of mutations in *PRMT5* or *PRMT9* in ALS patients is indicative of a downstream defect in the clearance of symmetrically dimethylated cytoplasmic aggregates by C9ORF72-autophagy machinery. While C9ORF72 knockout mice do not have prominent

motor or motor neuron deficits (O'Rourke et al., 2016), it remains possible that C9ORF72 loss of function in patients with C9ORF72 repeat expansions contributes to ALS pathology alongside dipeptide and RNA repeats, other ALS-linked mutations and environmental stress factors. Indeed, patients harbouring mutations in additional ALS-associated genes in combination with C9ORF72 mutations have been described (Gross et al., 2012). In addition, mouse models recapitulating human disease may frequently fail to recapitulate disease pathology in a distinct animal with a shorter lifespan as observed with most Parkinson's disease mutations (Beal, 2010).

p62 is associated with oxidative stress response. Besides selective autophagy, p62 functions in multiple pathways such as the Keap1–Nrf2 pathway and mTORC1 activation (Katsuragi, Ichimura, & Komatsu, 2015). Our mass-spectrometric analysis of p62 interactors under oxidative stress yielded a novel function for p62 in RNA binding and splicing function. Our evidence confirmed the role of p62 in regulating alternative splicing of various mRNA targets that are also alternatively spliced by ALS-linked protein - FUS. Additionally, p62's ability to detect stress granules that are significantly enriched in RNA and RNA binding proteins also indicates its potential function in RNA metabolism such as RNA splicing. With dysfunctional RNA-processing and RNA-mediated toxicity gaining increasing recognition as contributors to ALS pathogenesis, future studies discovering novel (i) RNA processing functions for existing ALS proteins such as p62 or (ii) mutations in RNA binding proteins may lead to better patient stratification for efficacious personalized medicine (Donnelly, Grima, & Sattler, 2014).

Overall, Chitiprolu *et al.*, 2018 suggests a two-step model for ALS pathology. According to literature, the first step involves expression of dipeptide repeats which drive the formation of inclusions in C9ORF72-linked ALS (Chew et al., 2015). Our evidence suggests a second step that controls the ability of cells to eliminate these inclusions.

Reduced levels of normal C9ORF72 caused by repeat expansions in its first intron may prevent these inclusions from being eliminated by autophagy and thereby contribute to their accumulation and attendant pathology in these patients. Our work has unified mechanisms critical to autophagy, RNA biology, arginine-methylation and ALS. Therapeutically, small molecules binding p62 to mimic p62-C9ORF72 interaction hold promise to selectively degrade disease-specific substrates such as stress granules by autophagy. This research encourages future studies to develop activators of PRMTs in addition to the small molecule inhibitors currently being studied as anti-cancer therapeutics. In addition, it remains to be seen if activating symmetric arginine dimethylation of arginine-glycine (RG) dipeptide repeat expansions of C9ORF72 may prevent neurodegeneration due to the degradation of repeats by p62-mediated autophagy. Thus, aiming to uncover fundamental mechanisms involved in ALS pathology, our work identified specific targets to treat ALS.

5.1.2 Retrotransposon RNAs as pathological substrates of autophagy in cancer

Defective autophagy has critical roles in tumorigenesis and has been targeted in over 100 clinical trials (Chude & Amaravadi, 2017; Galluzzi et al., 2015). Autophagy as a protector against genomic instability is believed to mediate tumour suppression during early stages of tumour development (White, Karp, Strohecker, Guo, & Mathew, 2010). For example, impaired autophagy due to deletion of one copy of *Becn1* promotes (i) unexplained DNA damage and chromosome instability and (ii) various malignancies such as lymphomas, lung and liver carcinomas (R. Mathew et al., 2007; X. Qu et al., 2003; Yue et al., 2003). However, how autophagy protects from genetic instability and cancer remains elusive. In Guo *et al.*, 2014 (Chapter 3), we employed several innovative approaches in cell culture and mice to discover that impairing degradation of retrotransposon RNA by autophagy increases LINE-1 insertions in the genome. This is

the first robust demonstration in the literature that a specific RNA is degraded by autophagy in mammalian systems with functional impact. Further, the study significantly impacts our current models for the role of autophagy in cancer.

Emerging evidence has revealed connections between the RNA world and autophagy. Only recently, the focus for autophagy substrates has shifted from proteins and organelles to RNA and associated binding proteins. A significant proportion of cellular RNAs, including rRNA and tRNA, are highly structured and bound by proteins thereby rendering them less accessible to the conventional RNA decay mechanisms such as deadenylases, decapping enzymes, exoribonucleolytic decay, nonsense-mediated decay, no-go decay or non-stop decay (Frankel, Lubas, & Lund, 2017). Thus, autophagy may represent an efficient mechanism for RNA turnover. Indeed, pioneering studies demonstrated RNA degradation in a lysosome-dependent pathway (Balavoine et al., 1990; Heydrick et al., 1991; Lardeux & Mortimore, 1987; Mortimore, Lardeux, & Heydrick, 1989; Sameshima, Liebhaber, & Schlessinger, 1981). However, the mechanistic details for the sequestration of RNA within autophagosomes and subsequent degradation within lysosomes have not been extensively studied. Through our research, we demonstrated selective autophagic degradation of retrotransposon RNA accumulated within cytoplasmic RNA granules. A recent study also provided evidence for RNA selectivity via lysosomal receptor-mediated uptake and degradation (Aizawa et al., 2016; Hase et al., 2015). To fully understand the impact of RNA degradation by autophagy, future studies should delineate the genome-wide definition of RNAs enclosed within autophagosomes under various stresses/disease contexts.

Autophagy receptors confer selectivity to cargos by physically linking specific substrates to growing phagophores. Both the autophagy receptors - p62 and NDP52 bind cargos modified with multiple ubiquitin chains. While p62 has been previously shown to target

aggregated proteins and cytosolic bacteria, NDP52 has targeted intracellular bacteria and damaged mitochondria (Gatica, Lahiri, & Klionsky, 2018). Our research for the first time expanded the repertoire of substrates to include RNA substrates, for each of the two selective autophagy receptors. We demonstrated that two autophagy receptors were recruited at times to RNA granules, but one dominantly co-localized with and eliminated the RNA granule. A likely explanation of this is that the complex composition of stress granules generates multiple signals which recruit distinct autophagy receptors. Stress granule composition is variable and stress dependent (Protter & Parker, 2016). For instance, we anticipate that stress granules or aggregates induced by FUS or TDP-43 mutations or chemotherapy drugs may have overlapping but differing content and therefore vary with respect to which autophagy receptor is dominant in recognizing and eliminating them.

RNA stress granules are detected in various tumours often induced in response to radio- and chemotherapies (Fournier et al., 2010; Moeller et al., 2004; Szaflarski et al., 2016). They further contribute to cancer metastasis and cancer cell survival. Therefore, targeted elimination of stress granules can boost killing of cancer cells (Somasekharan et al., 2015). Guo *et al.*, 2014 contributes to our previous study implicating stress granules as crucibles for ALS pathogenesis (Chapter 2). Advancing from the work of Roy Parker that ALS-linked mutations in VCP block autophagic degradation of stress granules (Buchan et al., 2013), we identified that the selective autophagy receptors p62 and NDP52 target stress granules and processing bodies containing retrotransposon RNA for degradation by autophagy. While localization of LINE-1 to stress granules has been reported as a host cell defense mechanism to prevent LINE-1 retrotransposition, our mechanism of targeted degradation of stress granules containing retrotransposon RNA suggests an irreversible defense strategy under persistent stress conditions (X. Li

et al., 2013; Moldovan & Moran, 2015). Taken together, therapeutic strategies targeting pathological stress granules may lead to a dysfunctional stress response that prevents cancer cells from adapting to and surviving further stress (tumour microenvironment), ultimately killing cancer cells.

Several recent papers suggest that retrotransposons are major sources of somatic variegation exhibiting increased activity in cancers (Helman et al., 2014). Our work demonstrated that lack of *Atg6/Beclin1* leads to accumulation of LINE-1 insertions in mice that may contribute to genetic instability and tumorigenesis in 40-75% cases of breast, ovarian, and prostate cancers with inhibited autophagy (Liang et al., 1999). Recent evidence identifying cancer-causing *BRCA1* mutations adjacent to *BECN1* questions the role of *BECN1* in tumour suppression. While deletions of both *BRCA1* and *BECN1* or *BRCA1* alone were identified in cancers, mutations of *BECN1* alone were not found indicating *BRCA1* loss as a primary driver of tumour development in these cancers (Laddha, Ganesan, Chan, & White, 2014a). There may, however, be tumour or cancer types such as hepatomas that require characterization at the genomic level, where autophagy-promoting genes may indeed be mutated to cause cancer. In agreement, reduced expression of *BECN1* (but not low *BRCA1*) has been linked to advanced tumour grade and poor prognosis in estrogen receptor-negative subtypes of human breast cancer (Tang et al., 2015). Additionally, an autophagy-independent mechanism for *BECN1* loss promoting tumour development in pre-malignant cells cannot be ruled out (Elgendy et al., 2014). Thus, the impact of *BECN1* loss on cancer initiation may involve undefined complex pathways.

In evolutionary terms, retrotransposons account for 25% of interindividual variation and are hypothesized to frequently drive speciation (Kidd et al., 2010). Evolutionary selection occurs in stressful environments and autophagy is a pre-eminent response to most

stresses. It is possible that defects in autophagy in combination with elevated genetic instability in the early stages of tumour development may drive diversification beyond Darwinian natural selection. This may then result in generation of distinct populations of cancer cells at a rapid pace unmatched by their rate of elimination. Therefore, the mechanism of autophagy buffering genetic and potentially evolutionary change by degrading retrotransposons may be relevant for future anti-cancer therapeutic interventions. With the emergence of resistance to cancer drugs being the major barrier to cure many cancers (Holohan, Van Schaeybroeck, Longley, & Johnston, 2013), employing autophagy activators, like mTOR inhibitors, as part of therapeutic cocktails may prove powerful in limiting tumour evolution and minimizing drug resistance in a broad swathe of cancers.

5.2 Therapeutic targets for autophagy inhibition

5.2.1 Autophagy-related protein as a mediator of exosome release and cancer progression

Active autophagy, hijacked by malignant cancer cells, has been attributed roles in tumour progression by maintaining redox and metabolic homeostasis, and preserving the functionality of cancer stem cells (K. Liu et al., 2017; Perera et al., 2015). During the late stages of cancer progression i.e., following malignancy, autophagic responses may be essential to survival and growth of cancer cells in the tumour microenvironment. For example, tissue-specific deletion of *Atg5* or *Atg7* in models of *KRAS* ^{G12D}-driven lung and pancreatic carcinogenesis favours the accumulation of dysfunctional mitochondria, impairs the cellular respiratory capacity and delays the progression of adenocarcinomas (Rao et al., 2014; Strohecker et al., 2013; A. Yang et al., 2014). Moreover, genetic and pharmacological inhibition of autophagy-related factors diminishes the tumorigenic

potential of malignant cells (Galluzzi, Bravo-San Pedro, Demaria, Formenti, & Kroemer, 2017; J. Y. Guo, Xia, & White, 2013). However, how specific autophagy-related proteins and processes mediate proliferative, invasive, and/or metastatic phenotypes and poor disease outcome have not yet been established. In Guo *et al.*, 2017 (Chapter 4), we discovered that Atg5 and Atg16L1 are required for exosome production (quantity) and this promotes metastasis independent of canonical autophagy. This suggests that some effects attributed to autophagy in cancer may be mediated by exosomes and part of efforts to therapeutically inhibit autophagy in cancer should be redirected to exosomes.

Prior work demonstrates that the ESCRT complex, which participates in exosome biogenesis at MVB, is required for autophagy in ways that are undefined and potentially indirect (Hurley, 2015; Rusten & Stenmark, 2009). Interestingly, ESCRT-dependent budding in MVB to form exosomes and phagophore maturation into autophagosomes share morphological and molecular traits. Both involve recruitment of ubiquitinated substrates to phosphatidyl-inositol-3-phosphate-enriched membranes whose expansion and fusion is driven by Vps34 (Hanson & Cashikar, 2012; Henne, Stenmark, & Emr, 2013; Mizushima, Yoshimori, & Ohsumi, 2011). Both Atg and ESCRT proteins are required for unconventional secretion of some proteins lacking signal peptide sequences, including IL-1β and *Dictyostelium* Acb1 (Bruns et al., 2011; Dupont et al., 2011; Duran et al., 2010; Y. Qu, Franchi, Nunez, & Dubyak, 2007). If these proteins are released with exosomes, as has been suggested (Duran et al., 2010; Piccioli & Rubartelli, 2013), our current findings may help explain how Atg proteins contribute to unconventional secretion. In agreement, another group has reported that Atg proteins control exosome biogenesis (Murrow et al., 2015). However, our study details a comprehensive quantification of exosome production incorporating techniques such as

nanoparticle tracking, dynamic light scattering and Western blotting for multiple exosome markers.

We demonstrated that similar to autophagosomes, exosomes are strongly enriched in LC3-II compared to LC3-I and Atg5 is required for exosome production. However, cells depleted of another *Atg* gene - *Atg7* produced equivalent quantities of exosomes despite their inability to produce LC3-II or generate autophagosomes. Thus, Atg7 may be expendable for other functions of Atg proteins at alternate sites such as exosome production and release.

Non-degradative roles for Atg proteins, independent of their roles in autophagy, have been described (Bestebroer et al., 2013; Deretic et al., 2012). Subsets of Atg proteins required for autophagy are frequently engaged in processes such as extracellular release including exosome release (here) and release of specialized lysosome-related organelles including melanosomes, mast cell granules and Paneth cell granules (Cadwell et al., 2008; DeSelm et al., 2011; Ebato et al., 2008; Ganesan et al., 2008; Marino et al., 2010; K. K. Patel et al., 2013; Ushio et al., 2011). One commonality among these diverse types of structures is the involvement of ESCRT, Rab27a/b and tetraspanin proteins in their biogenesis (Baietti et al., 2012; Bobrie et al., 2012; de Saint Basile, Menasche, & Fischer, 2010; Marks, Heijnen, & Raposo, 2013; Ostrowski et al., 2010; Truschel et al., 2009). The possibility that multiple Atg proteins impact endosomal trafficking and extracellular release needs to be systematically investigated.

Our results demonstrated increased exosome production upon inhibition of mTOR or disruption of MVB maturation and lysosomal fusion. This suggests that stress stimuli from tumor microenvornments causing mTOR inhibition, may contribute to the increased exosome production associated with many cancers (Peinado et al., 2012). In addition to

the ability of exosomes to transfer phenotypes of invasiveness and metastasis to new cells (Peinado et al., 2012), a recent study demonstrated that exosomes can make naïve cells tumorigenic (Melo et al., 2014). This suggests that our novel Atg5-dependent mechanism promotes cancer by the regional and systemic spread of cancer cell exosomes, which mediate invasion and metastasis of existing cancer cells and the genesis of new cancer cells. Taken together, selective targeting of *Atg5* or exosomes may prevent exosome-mediated spread of phenotypes such as cancer therapy resistance and ultimately promote tumor cell death.

5.3 Conclusion and Future Directions

Overall, the collection of manuscripts presented here unveils several novel mechanisms of autophagy implicated in ALS and cancer. Both autophagy inducers and autophagy inhibitors are available for clinical use and can have beneficial effects against neurodegeneration and cancer (mTOR inhibitors, hydroxychloroquine). While most neurodegenerative diseases may benefit from autophagy activation, a major challenge to using these drugs clinically in individual cancer patients is deciding whether an inhibitor or an activator of autophagy may be beneficial (H. Harris & Rubinsztein, 2011; Onorati, Dyczynski, Ojha, & Amaravadi, 2018). This decision may be aided by knowledge of the status of autophagy in a tumour. For instance, the presence of LC3 in exosomes and the regulation of exosome abundance by *Atg5*, mTOR inhibitors and inhibitors of lysosomal fusion suggests that exosomes sampled from blood, urine or other fluids may provide a real-time diagnostic (Sehgal, Chen, Gibbings, Sah, & Bumcrot, 2014) of autophagy status or mTOR activity in tumours or distant tissues. Additionally, aggregation-prone proteins involved in many neurodegenerative diseases, such as the prion protein (PrP) (Fevrier et al., 2004), amyloid-β (Rajendran et al., 2006), and α-synuclein (Danzer et al., 2012) traffic between cells in exosomes and contribute to

the spread of at least some of these diseases throughout the body (Aguzzi & Rajendran, 2009). Similar, HIV-1 uses exosomes to traffic out of macrophages in an Atg7-dependent manner (Fang et al., 2007; Kyei et al., 2009). Since many of these pathological proteins and pathogens are also degraded by autophagy (H. Harris & Rubinsztein, 2012), it is possible that LC3 may recruit these pathogenic proteins into exosomes enabling their intercellular spread. While mTOR inhibitors may help control these neurodegenerative diseaeses or HIV-1 by activating their autophagic degradation (H. Harris & Rubinsztein, 2012), they may simultaneously contribute to spread of these diseases by enhancing their release in exosomes.

Future investigations are required to delineate the therapeutic potential of (i) activating autophagic degradation of retrotransposon RNA and RNA granules, and (ii) inhibiting autophagy factors and exosome mediated spread of phenotypes. Firstly, the effect of retrotransposon RNA degradation on spontaneous transformation and emergence of resistance to chemotherapeutics in cell culture and xenograft models of cancer has to be analyzed. Secondly to identify RNAs degraded within RNA granules, genome-wide associations and candidate gene studies need to be performed. In addition, autophagy activating drugs eliminating stress granules selectively while ameliorating disease phenotypes have to be screened and characterized. Thirdly, the effect of various autophagy proteins and/or disease models on exosome contents, communication, and spread of phenotype (misfolded proteins, metastasis or drug resistance) has to be systematically undertaken. Altogether, this fount of knowledge would allow us to therapeutically modulate unexploited functions of autophagy that are emerging as critical in the pathogenesis of human diseases.

6.0 Appendix A

This table can be found on page 17 at:

https://static-content.springer.com/esm/art%3A10.1038%2Fs41467-018-05273-7/MediaObjects/41467_2018_5273_MOESM1_ESM.pdf

7.0 Appendix B

This table can be downloaded at:

https://static-content.springer.com/esm/art%3A10.1038%2Fs41467-018-05273-7/MediaObjects/41467_2018_5273_MOESM3_ESM.xlsx

8.0 Appendix C

This table can be found on page 24 at:

https://static-content.springer.com/esm/art%3A10.1038%2Fs41467-018-05273-7/MediaObjects/41467_2018_5273_MOESM1_ESM.pdf

9.0 Appendix D

This table can be downloaded at:

https://static-content.springer.com/esm/art%3A10.1038%2Fs41467-018-05273-7/MediaObjects/41467_2018_5273_MOESM4_ESM.xlsx

10.0 Appendix E

This table can be downloaded at:

https://static-content.springer.com/esm/art%3A10.1038%2Fs41467-018-05273-7/MediaObjects/41467_2018_5273_MOESM5_ESM.xlsx

11.0 Appendix F

Reagent or Resource	Source	Identifier
Antibodies		
Alix (immunofluorescence, Host: mouse)	BD Transduction Laboratories	Clone: 49/AIP1
Alix (Host: mouse)	Cell Signaling Technology	Cat#: 2171; RRID: AB_2299455
Atg5 (Host: rabbit)	Cell Signaling Technology	Cat#: 8540; RRID: AB_10828728
Atg7 (Host: rabbit)	Cell Signaling Technology	Cat#: 8558; RRID: AB_10831194
Atg12 (Host: rabbit)	Cell Signaling Technology	Cat#: 4180; RRID: AB_1903898
Atg3 (Host: rabbit)	Cell Signaling Technology	Cat#: 3415; RRID: AB_2059244
Human CD63 (Host: mouse)	Santa Cruz	Cat#: Sc-5275; RRID: AB_627877
Mouse CD63 (Host: mouse)	MBL International	Clone: R5G2; RRID: AB_1278815
LC3A/B (Host: rabbit)	Cell Signaling Technology	Cat#: 4108; RRID: AB_2137703
Flotillin2 (Host: rabbit)	Cell Signaling Technology	Cat#: 3436; RRID: AB_2106572
Tsg101 (Host: mouse)	Genetex	Clone: 4A10; RRID: AB_373239

Reagent or Resource	Source	Identifier
Tomm20 (Host: rabbit)	Santa Cruz	Clone FL-145; RRID: AB_2207533
Rab5 (Host: rabbit)	Cell Signaling Technology	Cat#: 3547; RRID: AB_2300649
ChromeoTM 505 anti-mouse IgG	Active Motif	Cat#: 15050
Biotin-anti-rabbit IgG	Sigma-Aldrich	Cat#: B8895; RRID: AB_258649
Streptavidin V500	BD Horizon	Cat#: 56149
1.4 nm NanoGold conjugated-F(ab')	Nanoprobes	Cat#: 2003; RRID: AB_2687591
ATP6V1E1 (Host: rabbit)	ThermoFisher	Cat#: PA5-29899; RRID: AB_2547373
ATP6V1E1 (PLA assay, Host: mouse)	Abnova	Clone 4E11; RRID: AB_10628559
ATP6V1A (Host: rabbit)	Abcam	RRID: Ab137574
ATP6V0C (Host: rabbit)	ThermoFisher	Cat#: PA5-23972; RRID: AB_2541472
ATP6V0D1 (Host: mouse)	Abcam	Cat#: Ab56441; RRID: AB_940402
LC3B (Host: rabbit)	Sigma-Aldrich	Cat#: L7543; RRID: AB_796155
Alix (density gradient, Host: rabbit)	Covolab	Cat#: Pab0204
Flotillin1 (density gradient, Host: mouse)	BD Transduction Laboratories	Cat#: 610820; RRID: AB_398139

Reagent or Resource	Source	Identifier
GFP (Host: mouse)	Abcam	Cat#: Ab3277; RRID: AB_308705
Goat anti-mouse Alexa Fluor 488	ThermoFisher	Cat#: A11029; RRID: AB_138404
Goat anti-mouse Alexa Fluor 546	ThermoFisher	Cat#: A11030; RRID: AB_144695
Goat anti-mouse Alexa Fluor 633	ThermoFisher	Cat#: A21052; RRID: AB_141459
Goat anti-rabbit Alexa Fluor 488	ThermoFisher	Cat#: A11034; RRID: AB_2576217
Goat anti-rabbit Alexa Fluor 546	ThermoFisher	Cat#: A11035; RRID: AB_143051
Anti-goat Alexa Fluor 488	ThermoFisher	Cat#: A11015; RRID: AB_141362
Anti-rat Alexa Fluor 546	ThermoFisher	Cat#: A11081; RRID: AB_141738
Goat anti-rabbit DyLight 405	ThermoFisher	Cat#: 35550; RRID: AB_1965945
Chemicals, Peptides, and Recombinant Proteins		
p62 LIR: biotin-SGGDDDWTHLSS	Genscript	>75% purity
ATP6V1E1 putative LIR: biotin-RCRKQDFPLVKA	Genscript	>75% purity
ATP6V1E1 mutated putative LIR: biotin-RCRKAILPLQKA	Genscript	>75% purity

Reagent or Resource	Source	Identifier
p62 LIR: SGGDDDWTHLSS	Genscript	>75% purity
ATP6V1E1 putative LIR: RCRKQDFPLVKA	Genscript	>75% purity
ATP6V1E1 mutated putative LIR: RCRKAILPLQKA	Genscript	>75% purity
His-tagged recombinant LC3	Enzo Life Sciences	ADI-APR-100-0200
1% Osmium Tetroxide	Electron Microscopy Sciences	19110
Epon 812	Mecalab	3137N
Prolong Gold Antifade	ThermoFisher	P36930
Critical Commercial Assays		
ATG5 Compozr Zinc Fingers	Sigma-Aldrich	CKOZFND1217-1KT
Lysotracker Blue	ThermoFisher	L7526
Lipofectamine 2000	ThermoFisher	11668-019
Vybrant DIO Cell-Labeling Solution	ThermoFisher	V22886
phRodo Green Dextran (10 kDa)	ThermoFisher	P35368
EGF-biotin-Alexa488	ThermoFisher	E13345
Lissamine Rhodamine B phosphatidylethanolamine 16:0	Avanti Polar Lipids	810158
HQ Silver Intensification Kit	Nanoprobes	2012

Reagent or Resource	Source	Identifier
Duolink® In Situ Detection Reagents Green	Sigma-Aldrich	DUO92014-100RXN
Duolink® In Situ Detection Reagents Orange	Sigma-Aldrich	DUO92007-100RXN
Duolink® In Situ PLA® Probe Anti-Rabbit PLUS	Sigma-Aldrich	DUO92002
Duolink® In Situ PLA® Probe Anti-Mouse MINUS	Sigma-Aldrich	DUO92004
Experimental Models: Cell Lines		
MDA-MB-231 (female, breast cancer cell line)	ATCC	HTB-26
4T1 (female, breast cancer cell line)	ATCC	CRL-2539
Neuro2a (male, neuroblastoma)	ATCC	CCL-131
3T3 (male)	ATCC	CRL-1658
Mouse embryonic fibroblasts (sex unavailable)	Dana Philpott (University of Toronto)	
Mouse embryonic fibroblasts (*Atg5*$^{-/-}$, sex unavailable)	Dana Philpott (University of Toronto)	
Wild-type and *ATG16L1*$^{-/-}$ HCT-116 (male)	Dana Philpott (University of Toronto)	
Mouse embryonic fibroblasts (*Atg7*$^{-/-}$, sex unavailable)	Herbert Virgin (Washington University)	

Reagent or Resource	Source	Identifier
Mouse embryonic fibroblasts (*Atg16L1*$^{-/-}$, sex unavailable)	Herbert Virgin (Washington University)	(Cadwell et al., 2008)
Mouse embryonic fibroblasts (*Atg14*$^{-/-}$, sex unavailable)	Herbert Virgin (Washington University)	
Mouse embryonic fibroblasts (*Atg5*$^{-/-}$ with inducible *Atg5*, sex unavailable)	Noboru Mizushima (University of Tokyo), via XiaoHui Zha (University of Ottawa)	(Hosokawa et al., 2007)
Experimental Models: Organisms/Strains		
Balb/c mice (female, 8 weeks)	Charles River	Strain 028
Oligonucleotides		
ATP6V1E1 Silencer Select SiRNA Sense: CCCAAAGACUAAAGAUUAUtt Anti-Sense: AUAAUCUUUAGUCUUUGGGtt	ThermoFisher	ID: s1803
ATP6V1A Silencer Select SiRNA Sense: CAUGGUCCAUUAUUCGUGAtt Anti-Sense: UCACGAAUAAUGGACCAUGtg;	ThermoFisher	ID: s1793
ATP6V1E1 Silencer Select SiRNA Sense: GCAAUCCCUAUGUAUAAAtt Anti-Sense: UUUUAUACAUAGGGAUUGCtt	ThermoFisher	ID: s62774
ATG7 Silencer Select SiRNA Sense:GGAACACUGUAUAACACCAtt	ThermoFisher	ID: s20650

Reagent or Resource	Source	Identifier
Anti-Sense:UGGUGUUAUACAGUGUUCCaa		
Silencer Select Negative Control siRNA 1	ThermoFisher	4390843
Atg5 Crispr Guide RNA Top: caccGAAGATGTGCTTCGA GATGTGTGG, Bottom: aaacCCACACATCTCGAAGCACATCTTC.	IDT	custom
Atg7 Crispr Guide RNA Top: caccGAAGTTGAACGAGTACCGCC, Bottom: aaacGGCGGTACTCGTTCAACTTC	IDT	custom
Recombinant DNA		
DsRed-Rab5-QL	Addgene	29688 (Taelman et al., 2010)
DsRed-Rab5-WT	Addgene	13050 (Sharma et al., 2003)
pmCherry-ATG5	Addgene	13095 (Hamacher-Brady et al., 2007)
mCherry-Alix	Addgene	21504 (H. H. Lee, Elia, Ghirlando, Lippincott-Schwartz, & Hurley, 2008) 611
HcRed-hLC3	Addgene	24991 (Tanida et al., 2008)
HcRed-LC3deltaGly221	Addgene	24992 (Tanida et al., 2008)

Reagent or Resource	Source	Identifier
TagBFP-LAMP1	Addgene	55263 (Rizzo, Davidson, & Piston, 2009)
EBFP2-CathepsinB	Addgene	55236 (Rizzo et al., 2009)
GFP-p62	Peter Kim	(Pankiv et al., 2007)
GFP-p62deltaLIR	Peter Kim	(Pankiv et al., 2007)
Other		
Motility Chamber	BD Bioscience	354578
Invasion Chamber	BD Bioscience	354480
Diff-Kwik	ThermoFisher	9990700
Dynabeads MyOne Streptavidin T1	ThermoFisher	65601
His-tagged DynaBeads	ThermoFisher	1013D

12.0 Appendix G

CHITIPROLU, MANEKA

LinkedIn: www.linkedin.com/in/**maneka-chitiprolu**

SUMMARY

- Drug delivery researcher, bioengineer and Vanier scholar, with 6+ years of experience in combining fascinating discoveries of basic research with practical solutions for human health, with proven ability to (i) critically review literature, design structured strategies and deliver impactful, innovative results, (ii) manage and complete projects while meeting stringent deadlines.
  https://med.uottawa.ca/en/news/uottawa-researchers-dr-derrick-gibbings-lab-connect-dots-cause-als
  https://med.uottawa.ca/en/news/researchers-uncover-significant-trigger-cancer-metastasis
- Confident public speaker with strong writing and presentation skills that led to dissemination of complex scientific ideas to multidisciplinary audience as evidenced through 4 publications, 10+ posters and talks at international conferences, 10+ awards, scholarships and research grants.
- Inspiring team player and leader with the ability to work autonomously as well as in collaborative environments that led to initiatives focused on graduate student career development facilitated by 10+ networking events, 5 workshops, 20+ speakers with procurement of funding.

EDUCATION AND PROFESSIONAL EXPERIENCE

1. Doctoral Candidate, Derrick Gibbings Lab, University of Ottawa, Canada **2013 - 2018, Expected**

- CGPA 9.67/10 with an uncommon **distinction** on comprehensive exam testing the knowledge and skill to be successful
- Discovered and **published** novel mechanisms to eliminate toxic RNA/protein aggregates associated with neurodegenerative diseases such as **ALS**; achieved **40% improvement** in clearance of toxic proteins observed in the disease
- Performed confocal and super-resolution **microscopy**, and employed image analyses tools to demonstrate therapeutic effects of exosomes leading to a **45% reduction** in cancer metastasis upon targeting a gene of interest
- Engineered RNA-containing exosomes as diagnostic and **drug delivery** vehicles to treat diseases by developing reporter assays based on **multiparameter flow cytometry**
- Designed, initiated and managed a parallel project independently, for **mentoring** and training a summer student

2. Bachelor's Thesis, Indian Institute of Technology Madras, India **September 2011 - May 2013**
Bachelor of Technology in Biotechnology with a Minor in Operations Research **2009 - 2013**

- CGPA of 8.99/10 (ranked 3rd in 45) with an outstanding **10/10** on thesis; Thesis supervisor - Dr. Madhulika Dixit
- Identified and **published** key proteins in the blood whose levels are suppressed by 40-50% in **pre-diabetic**, Indian men
- Mastered the isolation of human Peripheral Blood Mono-nuclear Cells for in-vitro culture and stimulation, and experimental **techniques** such as immunofluorescence, cell adhesion, cell death and cell viability assays
- Discovered the functional relevance of specific female sex **hormones** regulating vascular homeostasis

3. Summer Trainee, Goethe-University, Germany **May 2012 - July 2012**

- Identified Vitamin D to boost endothelial **regeneration** of carotid arteries post injury in diabetes; Supervisor - Dr. Ralf Brandes
- Employed **in-vivo mouse models** of diabetes, vessel dissections, culture and stimulation of primary endothelial cells, endothelial migration and wound healing assays, colony forming assays, FACS analyses

4. Summer Trainee, Centre for Cellular and Molecular Biology, India **May 2011 - July 2011**

- Pursued **mathematical and computational biology** to accurately simulate cancer events of ErbB signaling cascade including 828 biochemical reactions and 4 transmembrane kinases; Supervisor - Dr. Somdatta Sinha
- Studied the **simulated** dynamics of phosphorylated molecules in a dose-response manner of drug stimulation to quantify effective dosage, using *CellDesigner* and *SimBiology* - **MATLAB** tool

PUBLICATIONS

- **Maneka Chitiprolu** et al. (2018). *A C9ORF72 and P62 Complex Detects Arginine Methylation to Clear Stress Granules by Autophagy.* Nature Communications
- Huishan Guo, **Maneka Chitiprolu** et al. (2017). *Atg5 Disassociates the V1V0-ATPase to Promote Exosome Production and Tumor Metastasis Independent of Canonical Macroautophagy.* Developmental Cell
- Huishan Guo, **Maneka Chitiprolu** et al. (2014). *Autophagy supports genomic stability by degrading retrotransposon RNA.* Nature Communications
- Abel Arul Nathan, Mallu Abhiram Charan Tej, **Maneka Chitiprolu** et al. (2014). *Impaired glucose tolerance alters functional ability of peripheral blood-derived mononuclear cells in Asian Indian men.* Diabetes and Vascular Disease Research

❖ Reviewed 3 manuscripts submitted to international journals of Oncogene, Scientific Reports and Biochemistry and Cell Biology

SKILLS

- **Laboratory Skills:** CRISPR, In vitro cell culture, Primary culture, Stable lenti-viral transduction, siRNA and DNA transfection, Protein purification, Western blotting, RNA extraction and qRT-PCR, Immunofluorescence (human brain and spinal cord), Immunohistochemistry, Immunoprecipitation, Peptide pulldown assay, Flow cytometry, Cloning, Cell death and cell viability assays, Exosome and Autophagosome isolations, Subcellular fractionation, Luciferase reporter assays, In vitro methylation assay
- **Computer Skills:** Photoshop, NGS and Mass Spectrometry Analysis, ImageJ, Excel, PowerPoint, Outlook, Prism, MATLAB, R
- **Certifications:** Employability Skills, Writing in the Sciences, Statistics in Medicine, Community Outreach and Media Relations in the Sciences, Project Management, Strategy Management

NATIONAL AND INTERNATIONAL EXPOSURE

- Invited for **oral presentations** to academic as well as non-academic audience:
  - **1 of 50** chosen speakers, Selective Autophagy, Keystone Symposia, Kyoto, **Japan**, 2018
  - **1 of 7 out of 93** applicants, Ottawa International Conference on Neuromuscular Disease & Biology, 2017
  - **1 of 23** chosen speakers, ALS Canada Research Forum, Toronto, 2017
  - **1 of 6 out of 50** applicants, Annual Departmental Research Day, University of Ottawa, 2015
- Submitted novel scientific abstracts and succinctly presented **posters**:
  - 60th Annual Canadian Society for Molecular Biosciences Conference, Ottawa, 2017
  - National Cancer Institute RNA Biology Symposium, Bethesda, **United States**, 2017
  - 27th International Symposium on ALS/MND, Dublin, **Ireland**, 2016
  - Autophagy: Molecular and Physiological Mechanisms, Keystone Symposia, Whistler, **Canada**, 2016
  - EMBO | EMBL Symposia: The Complex Life of mRNA, Heidelberg, **Germany**, 2014
- **Best poster prize** of 48 presenters, Dept. of Cellular and Molecular Medicine/Neuroscience - **250 Canadian dollars**, 2014
- **2nd for best poster** of 34 presenters, Dept. of Cellular and Molecular Medicine - **100 Canadian dollars**, 2014

Selected AWARDS

- Top **0.5%** to receive to receive **Vanier Graduate Scholarship - 150,000 Canadian dollars**, 2016
- Received **ALS Canada** Cycle of Hope **Doctoral** Research **Award - 75,000 Canadian dollars**, 2015
- Received Larry Haffner **Fellowship**, **Parkinson** Research Consortium - **30,000 Canadian dollars**, 2014
- Honored with Faculty of Medicine **Award of Excellence** in Graduate Studies - **500 Canadian dollars**, 2014
- Received an undergraduate summer **grant** from **German Research Foundation - 2,238 Euros**, 2012
- Received an undergraduate summer **fellowship**, **Indian Academy of Sciences - 12,000 Rupees**, 2011
- Top **1.28%** to be admitted to the **Indian Statistical Institute**, 2009
- Top **1.5%**, to be admitted to the **Indian Institute of Technology**, 2009

LEADERSHIP EXPERIENCE

- **Committee Member, Trainee Workshops, Canadian Society of Molecular Biosciences Meeting** **2017**
  - Brought-in 50% of speakers and secured 30% of funding to organize professional development & career networking events
- **Committee Member, Advances in Biomedical Sciences Seminar Series, University of Ottawa** **2015-2016**
  - Led professional development initiatives for 200 students, overseeing guest lectures from a record 9 international speakers
- **Committee Member, Department Graduate Student Council, University of Ottawa** **2015-2016**
  - Facilitated social and academic events (Grant and Scholarship Writing), atleast 1event/month, for a student population of 60
- **Career Coordinator, Department of Biotechnology, IIT Madras** **2011-2012**
  - Designed the department brochure to market student interests to potential employers
  - Managed 600 students, 100 recruiting companies and 50 fellow coordinators to schedule a one month job fair
  - Contacted 47 companies including one new pharmaceutical company to participate in the job fair
- **Co-founder and Event Coordinator – *BioDocks!*, Technical Festival (ISO 9001-2000), IIT Madras** **2011**
  - Identified a valuable Industry Defined Problem and created the 1st biotechnology competition on Bio-Modeling to solve it
  - Organized lecture series | Addressed the broad problem of pose prediction using docking scoring functions of *AutDock4.2*
- **Photography Coordinator, Technical (Shaastra) and Cultural (Saarang) Festivals, IIT Madras** **2010-2012**
  - Led 10 volunteers to photograph over 120 events | Worked with a team of 10 coordinators
  - Pictured Stop Motion Videos; Designated photographer for a live concert with footfall of over 8000

INTERESTS AND ACTIVITIES

- Trained classical **dancer**, performed at over 35 events for **1000s of spectators**; media shared by Justin Trudeau *2015-Present*
- Volunteered with ***Let's Talk Science*** conducting 7 public events, 3 classroom visits, teaching **30 - 6000 children/event***2015-2017*
- Volunteered and raised **$15,000** for **ALS, Muscular Dystrophy and Parkinson's** with a 100 uOttawa team members *2014-2016*
- Reviewed 3 manuscripts for the **peer-reviewed Journal of Medicine** at University of Ottawa *2016-2017*
- Other Interests: Traveling, Fiction, Squash, Sketching

13.0 References

Abe, K., Itoyama, Y., Sobue, G., Tsuji, S., Aoki, M., Doyu, M., . . . Edaravone, A. L. S. Study Group. (2014). Confirmatory double-blind, parallel-group, placebo-controlled study of efficacy and safety of edaravone (MCI-186) in amyotrophic lateral sclerosis patients. *Amyotroph Lateral Scler Frontotemporal Degener, 15*(7-8), 610-617. doi: 10.3109/21678421.2014.959024

Abel, O., Powell, J. F., Andersen, P. M., & Al-Chalabi, A. (2012). ALSoD: A user-friendly online bioinformatics tool for amyotrophic lateral sclerosis genetics. *Hum Mutat, 33*(9), 1345-1351. doi: 10.1002/humu.22157

Acosta, J. R., Goldsbury, C., Winnick, C., Badrock, A. P., Fraser, S. T., Laird, A. S., . . . Cole, N. J. (2014). Mutant human FUS Is ubiquitously mislocalized and generates persistent stress granules in primary cultured transgenic zebrafish cells. *PLoS One, 9*(6), e90572. doi: 10.1371/journal.pone.0090572

Adjibade, P., St-Sauveur, V. G., Quevillon Huberdeau, M., Fournier, M. J., Savard, A., Coudert, L., . . . Mazroui, R. (2015). Sorafenib, a multikinase inhibitor, induces formation of stress granules in hepatocarcinoma cells. *Oncotarget, 6*(41), 43927-43943. doi: 10.18632/oncotarget.5980

Aguzzi, A., & Rajendran, L. (2009). The transcellular spread of cytosolic amyloids, prions, and prionoids. *Neuron, 64*(6), 783-790. doi: 10.1016/j.neuron.2009.12.016

Aita, V. M., Liang, X. H., Murty, V. V., Pincus, D. L., Yu, W., Cayanis, E., . . . Levine, B. (1999). Cloning and genomic organization of beclin 1, a candidate tumor suppressor gene on chromosome 17q21. *Genomics, 59*(1), 59-65. doi: 10.1006/geno.1999.5851

Aizawa, S., Fujiwara, Y., Contu, V. R., Hase, K., Takahashi, M., Kikuchi, H., . . . Kabuta, T. (2016). Lysosomal putative RNA transporter SIDT2 mediates direct uptake of RNA by lysosomes. *Autophagy, 12*(3), 565-578. doi: 10.1080/15548627.2016.1145325

Al-Nedawi, K., Meehan, B., Micallef, J., Lhotak, V., May, L., Guha, A., & Rak, J. (2008). Intercellular transfer of the oncogenic receptor EGFRvIII by microvesicles derived from tumour cells. *Nat Cell Biol, 10*(5), 619-624. doi: 10.1038/ncb1725

Alisch, R. S., Garcia-Perez, J. L., Muotri, A. R., Gage, F. H., & Moran, J. V. (2006). Unconventional translation of mammalian LINE-1 retrotransposons. *Genes Dev, 20*(2), 210-224. doi: 20/2/210 [pii]

10.1101/gad.1380406

Almeida, S., Gascon, E., Tran, H., Chou, H. J., Gendron, T. F., Degroot, S., . . . Gao, F. B. (2013). Modeling key pathological features of frontotemporal dementia with C9ORF72 repeat expansion in iPSC-derived human neurons. *Acta Neuropathol, 126*(3), 385-399. doi: 10.1007/s00401-013-1149-y

Almendro, V., Marusyk, A., & Polyak, K. (2013). Cellular heterogeneity and molecular evolution in cancer. *Annu Rev Pathol, 8*, 277-302. doi: 10.1146/annurev-pathol-020712-163923

Alvarez-Erviti, L., Seow, Y., Schapira, A. H., Gardiner, C., Sargent, I. L., Wood, M. J., & Cooper, J. M. (2011). Lysosomal dysfunction increases exosome-mediated alpha-synuclein release and transmission. *Neurobiol Dis, 42*(3), 360-367. doi: 10.1016/j.nbd.2011.01.029

Amaya, C., Fader, C. M., & Colombo, M. I. (2015). Autophagy and proteins involved in vesicular trafficking. *FEBS Lett, 589*(22), 3343-3353. doi: 10.1016/j.febslet.2015.09.021

Anderson, P., & Kedersha, N. (2008). Stress granules: the Tao of RNA triage. *Trends Biochem Sci, 33*(3), 141-150. doi: 10.1016/j.tibs.2007.12.003

Anderson, P., Kedersha, N., & Ivanov, P. (2015). Stress granules, P-bodies and cancer. *Biochim Biophys Acta, 1849*(7), 861-870. doi: 10.1016/j.bbagrm.2014.11.009

Anthony, K., & Gallo, J. M. (2010). Aberrant RNA processing events in neurological disorders. *Brain Res, 1338*, 67-77. doi: 10.1016/j.brainres.2010.03.008

Antonioli, M., Di Rienzo, M., Piacentini, M., & Fimia, G. M. (2017). Emerging Mechanisms in Initiating and Terminating Autophagy. *Trends Biochem Sci, 42*(1), 28-41. doi: 10.1016/j.tibs.2016.09.008

Arai, T., Hasegawa, M., Akiyama, H., Ikeda, K., Nonaka, T., Mori, H., . . . Oda, T. (2006). TDP-43 is a component of ubiquitin-positive tau-negative inclusions in frontotemporal lobar degeneration and amyotrophic lateral sclerosis. *Biochem Biophys Res Commun, 351*(3), 602-611. doi: 10.1016/j.bbrc.2006.10.093

Azmi, A. S., Bao, B., & Sarkar, F. H. (2013). Exosomes in cancer development, metastasis, and drug resistance: a comprehensive review. *Cancer Metastasis Rev, 32*(3-4), 623-642. doi: 10.1007/s10555-013-9441-9

Bachand, F., Boisvert, F. M., Cote, J., Richard, S., & Autexier, C. (2002). The product of the survival of motor neuron (SMN) gene is a human telomerase-associated protein. *Mol Biol Cell, 13*(9), 3192-3202. doi: 10.1091/mbc.E02-04-0216

Bader, C. A., Shandala, T., Ng, Y. S., Johnson, I. R., & Brooks, D. A. (2015). Atg9 is required for intraluminal vesicles in amphisomes and autolysosomes. *Biol Open, 4*(11), 1345-1355. doi: 10.1242/bio.013979

Baechtold, H., Kuroda, M., Sok, J., Ron, D., Lopez, B. S., & Akhmedov, A. T. (1999). Human 75-kDa DNA-pairing protein is identical to the pro-oncoprotein TLS/FUS and is able to promote D-loop formation. *J Biol Chem, 274*(48), 34337-34342.

Baietti, M. F., Zhang, Z., Mortier, E., Melchior, A., Degeest, G., Geeraerts, A., . . . David, G. (2012). Syndecan-syntenin-ALIX regulates the biogenesis of exosomes. *Nat Cell Biol, 14*(7), 677-685. doi: 10.1038/ncb2502

Baillie, J. K., Barnett, M. W., Upton, K. R., Gerhardt, D. J., Richmond, T. A., De Sapio, F., . . . Faulkner, G. J. (2011). Somatic retrotransposition alters the genetic landscape of the human brain. *Nature, 479*(7374), 534-537. doi: 10.1038/nature10531

Balavoine, S., Feldmann, G., & Lardeux, B. (1990). Rates of RNA degradation in isolated rat hepatocytes. Effects of amino acids and inhibitors of lysosomal function. *Eur J Biochem, 189*(3), 617-623.

Balavoine, S., Feldmann, G., & Lardeux, B. (1993). Regulation of RNA degradation in cultured rat hepatocytes: effects of specific amino acids and insulin. *J Cell Physiol, 156*(1), 56-62. doi: 10.1002/jcp.1041560109

Balavoine, S., Rogier, E., Feldmann, G., & Lardeux, B. (1992). Responsiveness of RNA degradation to amino acids in cultured rat hepatocytes: comparison with isolated rat hepatocytes. *J Cell Physiol, 150*(1), 149-157. doi: 10.1002/jcp.1041500120

Ballou, L. M., & Lin, R. Z. (2008). Rapamycin and mTOR kinase inhibitors. *J Chem Biol, 1*(1-4), 27-36. doi: 10.1007/s12154-008-0003-5

Bandyopadhyay, U., Kaushik, S., Varticovski, L., & Cuervo, A. M. (2008). The chaperone-mediated autophagy receptor organizes in dynamic protein complexes at the lysosomal membrane. *Mol Cell Biol, 28*(18), 5747-5763. doi: 10.1128/MCB.02070-07

Barmada, S. J., Serio, A., Arjun, A., Bilican, B., Daub, A., Ando, D. M., . . . Finkbeiner, S. (2014). Autophagy induction enhances TDP43 turnover and survival in neuronal ALS models. *Nat Chem Biol, 10*(8), 677-685. doi: 10.1038/nchembio.1563

Baron, D. M., Kaushansky, L. J., Ward, C. L., Sama, R. R., Chian, R. J., Boggio, K. J., . . . Bosco, D. A. (2013). Amyotrophic lateral sclerosis-linked FUS/TLS alters stress granule assembly and dynamics. *Mol Neurodegener, 8*, 30. doi: 10.1186/1750-1326-8-30

Baselga, J., Campone, M., Piccart, M., Burris, H. A., 3rd, Rugo, H. S., Sahmoud, T., . . . Hortobagyi, G. N. (2012). Everolimus in postmenopausal hormone-receptor-positive advanced breast cancer. *N Engl J Med, 366*(6), 520-529. doi: 10.1056/NEJMoa1109653

Batzer, M. A., & Deininger, P. L. (2002). Alu repeats and human genomic diversity. *Nat Rev Genet, 3*(5), 370-379. doi: 10.1038/nrg798

Beal, M. F. (2010). Parkinson's disease: a model dilemma. *Nature, 466*(7310), S8-10. doi: 10.1038/466S8a

Beck, C. R., Collier, P., Macfarlane, C., Malig, M., Kidd, J. M., Eichler, E. E., . . . Moran, J. V. (2010). LINE-1 retrotransposition activity in human genomes. *Cell, 141*(7), 1159-1170. doi: 10.1016/j.cell.2010.05.021

Beck, C. R., Garcia-Perez, J. L., Badge, R. M., & Moran, J. V. (2011). LINE-1 elements in structural variation and disease. *Annu Rev Genomics Hum Genet, 12*, 187-215. doi: 10.1146/annurev-genom-082509-141802

Becker, L. A., Huang, B., Bieri, G., Ma, R., Knowles, D. A., Jafar-Nejad, P., . . . Gitler, A. D. (2017). Therapeutic reduction of ataxin-2 extends lifespan and reduces pathology in TDP-43 mice. *Nature, 544*(7650), 367-371. doi: 10.1038/nature22038

Bedford, M. T., & Clarke, S. G. (2009). Protein arginine methylation in mammals: who, what, and why. *Mol Cell, 33*(1), 1-13. doi: 10.1016/j.molcel.2008.12.013

Belzil, V. V., Bauer, P. O., Prudencio, M., Gendron, T. F., Stetler, C. T., Yan, I. K., . . . Petrucelli, L. (2013). Reduced C9orf72 gene expression in c9FTD/ALS is caused by histone trimethylation, an epigenetic event detectable in blood. *Acta Neuropathol, 126*(6), 895-905. doi: 10.1007/s00401-013-1199-1

Belzil, V. V., Daoud, H., Desjarlais, A., Bouchard, J. P., Dupre, N., Camu, W., . . . Rouleau, G. A. (2011). Analysis of OPTN as a causative gene for amyotrophic lateral sclerosis. *Neurobiol Aging, 32*(3), 555 e513-554. doi: 10.1016/j.neurobiolaging.2010.10.001

Belzil, V. V., Valdmanis, P. N., Dion, P. A., Daoud, H., Kabashi, E., Noreau, A., . . . Rouleau, G. A. (2009). Mutations in FUS cause FALS and SALS in French and French Canadian populations. *Neurology, 73*(15), 1176-1179. doi: 10.1212/WNL.0b013e3181bbfeef

Bennett, E. A., Keller, H., Mills, R. E., Schmidt, S., Moran, J. V., Weichenrieder, O., & Devine, S. E. (2008). Active Alu retrotransposons in the human genome. *Genome Res, 18*(12), 1875-1883. doi: 10.1101/gr.081737.108

Bentmann, E., Neumann, M., Tahirovic, S., Rodde, R., Dormann, D., & Haass, C. (2012). Requirements for stress granule recruitment of fused in sarcoma (FUS) and TAR DNA-binding protein of 43 kDa (TDP-43). *J Biol Chem, 287*(27), 23079-23094. doi: 10.1074/jbc.M111.328757

Bento, C. F., Renna, M., Ghislat, G., Puri, C., Ashkenazi, A., Vicinanza, M., . . . Rubinsztein, D. C. (2016). Mammalian Autophagy: How Does It Work? *Annu Rev Biochem, 85*, 685-713. doi: 10.1146/annurev-biochem-060815-014556

Berg, T. O., Fengsrud, M., Stromhaug, P. E., Berg, T., & Seglen, P. O. (1998). Isolation and characterization of rat liver amphisomes. Evidence for fusion of autophagosomes with both early and late endosomes. *J Biol Chem, 273*(34), 21883-21892.

Bestebroer, J., V'Kovski, P., Mauthe, M., & Reggiori, F. (2013). Hidden behind autophagy: the unconventional roles of ATG proteins. *Traffic, 14*(10), 1029-1041. doi: 10.1111/tra.12091

Bhattacharya, S., Pal, K., Sharma, A. K., Dutta, S. K., Lau, J. S., Yan, I. K., . . . Mukhopadhyay, D. (2014). GAIP interacting protein C-terminus regulates autophagy and exosome biogenesis of pancreatic cancer through metabolic pathways. *PLoS One, 9*(12), e114409. doi: 10.1371/journal.pone.0114409

Birgisdottir, A. B., Lamark, T., & Johansen, T. (2013). The LIR motif - crucial for selective autophagy. *J Cell Sci, 126*(Pt 15), 3237-3247. doi: 10.1242/jcs.126128

Bloch, D. B., Gulick, T., Bloch, K. D., & Yang, W. H. (2006). Processing body autoantibodies reconsidered. *Rna, 12*(5), 707-709.

Blokhuis, A. M., Groen, E. J., Koppers, M., van den Berg, L. H., & Pasterkamp, R. J. (2013). Protein aggregation in amyotrophic lateral sclerosis. *Acta Neuropathol, 125*(6), 777-794. doi: 10.1007/s00401-013-1125-6

Bobrie, A., Krumeich, S., Reyal, F., Recchi, C., Moita, L. F., Seabra, M. C., . . . Thery, C. (2012). Rab27a supports exosome-dependent and -independent mechanisms that modify the tumor microenvironment and can promote tumor progression. *Cancer Res, 72*(19), 4920-4930. doi: 10.1158/0008-5472.CAN-12-0925

Boeynaems, S., Bogaert, E., Kovacs, D., Konijnenberg, A., Timmerman, E., Volkov, A., . . . Van Den Bosch, L. (2017). Phase Separation of C9orf72 Dipeptide Repeats Perturbs Stress Granule Dynamics. *Mol Cell, 65*(6), 1044-1055 e1045. doi: 10.1016/j.molcel.2017.02.013

Boisvert, F. M., Cote, J., Boulanger, M. C., Cleroux, P., Bachand, F., Autexier, C., & Richard, S. (2002). Symmetrical dimethylarginine methylation is required for the localization of SMN in Cajal bodies and pre-mRNA splicing. *J Cell Biol, 159*(6), 957-969. doi: 10.1083/jcb.200207028

Boisvert, F. M., Cote, J., Boulanger, M. C., & Richard, S. (2003). A proteomic analysis of arginine-methylated protein complexes. *Mol Cell Proteomics, 2*(12), 1319-1330. doi: 10.1074/mcp.M300088-MCP200

Bolte, S., & Cordelieres, F. P. (2006). A guided tour into subcellular colocalization analysis in light microscopy. *J Microsc, 224*(Pt 3), 213-232. doi: 10.1111/j.1365-2818.2006.01706.x

Bosco, D. A., Lemay, N., Ko, H. K., Zhou, H., Burke, C., Kwiatkowski, T. J., Jr., . . . Hayward, L. J. (2010). Mutant FUS proteins that cause amyotrophic lateral sclerosis incorporate into stress granules. *Hum Mol Genet, 19*(21), 4160-4175. doi: 10.1093/hmg/ddq335

Brady, O. A., Meng, P., Zheng, Y., Mao, Y., & Hu, F. (2011). Regulation of TDP-43 aggregation by phosphorylation and p62/SQSTM1. *J Neurochem, 116*(2), 248-259. doi: 10.1111/j.1471-4159.2010.07098.x

Brandman, O., & Hegde, R. S. (2016). Ribosome-associated protein quality control. *Nat Struct Mol Biol, 23*(1), 7-15. doi: 10.1038/nsmb.3147

Bremang, M., Cuomo, A., Agresta, A. M., Stugiewicz, M., Spadotto, V., & Bonaldi, T. (2013). Mass spectrometry-based identification and characterisation of lysine and arginine methylation in the human proteome. *Mol Biosyst, 9*(9), 2231-2247. doi: 10.1039/c3mb00009e

Brouha, B., Schustak, J., Badge, R. M., Lutz-Prigge, S., Farley, A. H., Moran, J. V., & Kazazian, H. H., Jr. (2003). Hot L1s account for the bulk of retrotransposition in the human population. *Proc Natl Acad Sci U S A, 100*(9), 5280-5285. doi: 10.1073/pnas.0831042100

0831042100 [pii]

Bruijn, L. I., Houseweart, M. K., Kato, S., Anderson, K. L., Anderson, S. D., Ohama, E., . . . Cleveland, D. W. (1998). Aggregation and motor neuron toxicity of an ALS-linked SOD1 mutant independent from wild-type SOD1. *Science, 281*(5384), 1851-1854.

Bruns, C., McCaffery, J. M., Curwin, A. J., Duran, J. M., & Malhotra, V. (2011). Biogenesis of a novel compartment for autophagosome-mediated unconventional protein secretion. *J Cell Biol, 195*(6), 979-992. doi: 10.1083/jcb.201106098

Buchan, J. R., Kolaitis, R. M., Taylor, J. P., & Parker, R. (2013). Eukaryotic stress granules are cleared by autophagy and Cdc48/VCP function. *Cell, 153*(7), 1461-1474. doi: 10.1016/j.cell.2013.05.037

Buchan, J. R., & Parker, R. (2009). Eukaryotic stress granules: the ins and outs of translation. *Mol Cell, 36*(6), 932-941. doi: 10.1016/j.molcel.2009.11.020

Buschow, S. I., Nolte-'t Hoen, E. N., van Niel, G., Pols, M. S., ten Broeke, T., Lauwen, M., . . . Stoorvogel, W. (2009). MHC II in dendritic cells is targeted to lysosomes

or T cell-induced exosomes via distinct multivesicular body pathways. *Traffic, 10*(10), 1528-1542. doi: TRA963 [pii]

10.1111/j.1600-0854.2009.00963.x

Bussing, I., Slack, F. J., & Grosshans, H. (2008). let-7 microRNAs in development, stem cells and cancer. *Trends Mol Med, 14*(9), 400-409. doi: 10.1016/j.molmed.2008.07.001

Caccamo, A., Majumder, S., Deng, J. J., Bai, Y., Thornton, F. B., & Oddo, S. (2009). Rapamycin rescues TDP-43 mislocalization and the associated low molecular mass neurofilament instability. *J Biol Chem, 284*(40), 27416-27424. doi: 10.1074/jbc.M109.031278

Cadwell, K., Liu, J. Y., Brown, S. L., Miyoshi, H., Loh, J., Lennerz, J. K., . . . Virgin, H. W. th. (2008). A key role for autophagy and the autophagy gene Atg16l1 in mouse and human intestinal Paneth cells. *Nature, 456*(7219), 259-263. doi: 10.1038/nature07416

Cancer Genome Atlas, Network. (2012). Comprehensive molecular portraits of human breast tumours. *Nature, 490*(7418), 61-70. doi: 10.1038/nature11412

Cancer Genome Atlas Research, Network. (2011). Integrated genomic analyses of ovarian carcinoma. *Nature, 474*(7353), 609-615. doi: 10.1038/nature10166

Castillo, K., Nassif, M., Valenzuela, V., Rojas, F., Matus, S., Mercado, G., . . . Hetz, C. (2013). Trehalose delays the progression of amyotrophic lateral sclerosis by enhancing autophagy in motoneurons. *Autophagy, 9*(9), 1308-1320. doi: 10.4161/auto.25188

Cemma, M., Kim, P. K., & Brumell, J. H. (2011). The ubiquitin-binding adaptor proteins p62/SQSTM1 and NDP52 are recruited independently to bacteria-associated microdomains to target Salmonella to the autophagy pathway. *Autophagy, 7*(3), 341-345.

Chang, C. F., Lee, Y. C., Lee, K. H., Lin, H. C., Chen, C. L., Shen, C. J., & Huang, C. C. (2016). Therapeutic effect of berberine on TDP-43-related pathogenesis in FTLD and ALS. *J Biomed Sci, 23*(1), 72. doi: 10.1186/s12929-016-0290-z

Chang, T. K., Shravage, B. V., Hayes, S. D., Powers, C. M., Simin, R. T., Wade Harper, J., & Baehrecke, E. H. (2013). Uba1 functions in Atg7- and Atg3-independent autophagy. *Nat Cell Biol, 15*(9), 1067-1078. doi: 10.1038/ncb2804

Chen, C., Nott, T. J., Jin, J., & Pawson, T. (2011). Deciphering arginine methylation: Tudor tells the tale. *Nat Rev Mol Cell Biol, 12*(10), 629-642. doi: 10.1038/nrm3185

Chen, L., Dahlstrom, J. E., Chandra, A., Board, P., & Rangasamy, D. (2012). Prognostic value of LINE-1 retrotransposon expression and its subcellular localization in breast cancer. *Breast Cancer Res Treat, 136*(1), 129-142. doi: 10.1007/s10549-012-2246-7

Chen, Y. D., Fang, Y. T., Cheng, Y. L., Lin, C. F., Hsu, L. J., Wang, S. Y., . . . Lin, Y. S. (2017). Exophagy of annexin A2 via RAB11, RAB8A and RAB27A in IFN-gamma-stimulated lung epithelial cells. *Sci Rep, 7*(1), 5676. doi: 10.1038/s41598-017-06076-4

Chew, J., Gendron, T. F., Prudencio, M., Sasaguri, H., Zhang, Y. J., Castanedes-Casey, M., . . . Petrucelli, L. (2015). Neurodegeneration. C9ORF72 repeat expansions in mice cause TDP-43 pathology, neuronal loss, and behavioral deficits. *Science, 348*(6239), 1151-1154. doi: 10.1126/science.aaa9344

Chivet, M., Javalet, C., Laulagnier, K., Blot, B., Hemming, F. J., & Sadoul, R. (2014). Exosomes secreted by cortical neurons upon glutamatergic synapse activation specifically interact with neurons. *J Extracell Vesicles, 3*, 24722. doi: 10.3402/jev.v3.24722

Choi, J., Jung, W., & Koo, J. S. (2013). Expression of autophagy-related markers beclin-1, light chain 3A, light chain 3B and p62 according to the molecular subtype of breast cancer. *Histopathology, 62*(2), 275-286. doi: 10.1111/his.12002

Chude, C. I., & Amaravadi, R. K. (2017). Targeting Autophagy in Cancer: Update on Clinical Trials and Novel Inhibitors. *Int J Mol Sci, 18*(6). doi: 10.3390/ijms18061279

Cleaver, J. E., Lam, E. T., & Revet, I. (2009). Disorders of nucleotide excision repair: the genetic and molecular basis of heterogeneity. *Nat Rev Genet, 10*(11), 756-768. doi: 10.1038/nrg2663

Cleveland, D. W., & Rothstein, J. D. (2001). From Charcot to Lou Gehrig: deciphering selective motor neuron death in ALS. *Nat Rev Neurosci, 2*(11), 806-819. doi: 10.1038/35097565

Codogno, P., Mehrpour, M., & Proikas-Cezanne, T. (2011). Canonical and non-canonical autophagy: variations on a common theme of self-eating? *Nat Rev Mol Cell Biol, 13*(1), 7-12. doi: 10.1038/nrm3249

Colombo, M., Moita, C., van Niel, G., Kowal, J., Vigneron, J., Benaroch, P., . . . Raposo, G. (2013). Analysis of ESCRT functions in exosome biogenesis, composition and secretion highlights the heterogeneity of extracellular vesicles. *J Cell Sci, 126*(Pt 24), 5553-5565. doi: 10.1242/jcs.128868

Colombo, M., Raposo, G., & Thery, C. (2014). Biogenesis, secretion, and intercellular interactions of exosomes and other extracellular vesicles. *Annu Rev Cell Dev Biol, 30*, 255-289. doi: 10.1146/annurev-cellbio-101512-122326

Colombrita, C., Zennaro, E., Fallini, C., Weber, M., Sommacal, A., Buratti, E., . . . Ratti, A. (2009). TDP-43 is recruited to stress granules in conditions of oxidative insult. *J Neurochem, 111*(4), 1051-1061. doi: 10.1111/j.1471-4159.2009.06383.x

Conicella, A. E., Zerze, G. H., Mittal, J., & Fawzi, N. L. (2016). ALS Mutations Disrupt Phase Separation Mediated by alpha-Helical Structure in the TDP-43 Low-Complexity C-Terminal Domain. *Structure, 24*(9), 1537-1549. doi: 10.1016/j.str.2016.07.007

Cook, K. L., Shajahan, A. N., & Clarke, R. (2011). Autophagy and endocrine resistance in breast cancer. *Expert Rev Anticancer Ther, 11*(8), 1283-1294. doi: 10.1586/era.11.111

Cooper-Knock, J., Walsh, M. J., Higginbottom, A., Robin Highley, J., Dickman, M. J., Edbauer, D., . . . Shaw, P. J. (2014). Sequestration of multiple RNA recognition motif-containing proteins by C9orf72 repeat expansions. *Brain, 137*(Pt 7), 2040-2051. doi: 10.1093/brain/awu120

Cornelis, G., Heidmann, O., Degrelle, S. A., Vernochet, C., Lavialle, C., Letzelter, C., . . . Dupressoir, A. (2013). Captured retroviral envelope syncytin gene associated with the unique placental structure of higher ruminants. *Proc Natl Acad Sci U S A, 110*(9), E828-837. doi: 10.1073/pnas.1215787110

Corrado, L., Del Bo, R., Castellotti, B., Ratti, A., Cereda, C., Penco, S., . . . Silani, V. (2010). Mutations of FUS gene in sporadic amyotrophic lateral sclerosis. *J Med Genet, 47*(3), 190-194. doi: 10.1136/jmg.2009.071027

Cote, J., Boisvert, F. M., Boulanger, M. C., Bedford, M. T., & Richard, S. (2003). Sam68 RNA binding protein is an in vivo substrate for protein arginine N-methyltransferase 1. *Mol Biol Cell, 14*(1), 274-287. doi: 10.1091/mbc.E02-08-0484

Cote, J., & Richard, S. (2005). Tudor domains bind symmetrical dimethylated arginines. *J Biol Chem, 280*(31), 28476-28483. doi: 10.1074/jbc.M414328200

Cotter, K., Stransky, L., McGuire, C., & Forgac, M. (2015). Recent Insights into the Structure, Regulation, and Function of the V-ATPases. *Trends Biochem Sci, 40*(10), 611-622. doi: 10.1016/j.tibs.2015.08.005

Cox, J., & Mann, M. (2008). MaxQuant enables high peptide identification rates, individualized p.p.b.-range mass accuracies and proteome-wide protein quantification. *Nat Biotechnol, 26*(12), 1367-1372. doi: 10.1038/nbt.1511

Crazzolara, R., Cisterne, A., Thien, M., Hewson, J., Baraz, R., Bradstock, K. F., & Bendall, L. J. (2009). Potentiating effects of RAD001 (Everolimus) on vincristine therapy in childhood acute lymphoblastic leukemia. *Blood, 113*(14), 3297-3306. doi: 10.1182/blood-2008-02-137752

Da Cruz, S., & Cleveland, D. W. (2011). Understanding the role of TDP-43 and FUS/TLS in ALS and beyond. *Curr Opin Neurobiol, 21*(6), 904-919. doi: 10.1016/j.conb.2011.05.029

Daigle, J. G., Lanson, N. A., Jr., Smith, R. B., Casci, I., Maltare, A., Monaghan, J., . . . Pandey, U. B. (2013). RNA-binding ability of FUS regulates neurodegeneration, cytoplasmic mislocalization and incorporation into stress granules associated with FUS carrying ALS-linked mutations. *Hum Mol Genet, 22*(6), 1193-1205. doi: 10.1093/hmg/dds526

Danzer, K. M., Kranich, L. R., Ruf, W. P., Cagsal-Getkin, O., Winslow, A. R., Zhu, L., . . . McLean, P. J. (2012). Exosomal cell-to-cell transmission of alpha synuclein oligomers. *Mol Neurodegener, 7*, 42. doi: 10.1186/1750-1326-7-42

Davidson, Y. S., Barker, H., Robinson, A. C., Thompson, J. C., Harris, J., Troakes, C., . . . Mann, D. M. (2014). Brain distribution of dipeptide repeat proteins in frontotemporal lobar degeneration and motor neurone disease associated with expansions in C9ORF72. *Acta Neuropathol Commun, 2*, 70. doi: 10.1186/2051-5960-2-70

De Leeuw, F., Zhang, T., Wauquier, C., Huez, G., Kruys, V., & Gueydan, C. (2007). The cold-inducible RNA-binding protein migrates from the nucleus to cytoplasmic stress granules by a methylation-dependent mechanism and acts as a translational repressor. *Exp Cell Res, 313*(20), 4130-4144. doi: 10.1016/j.yexcr.2007.09.017

de Saint Basile, G., Menasche, G., & Fischer, A. (2010). Molecular mechanisms of biogenesis and exocytosis of cytotoxic granules. *Nat Rev Immunol, 10*(8), 568-579. doi: 10.1038/nri2803

Decker, C. J., & Parker, R. (2012). P-bodies and stress granules: possible roles in the control of translation and mRNA degradation. *Cold Spring Harb Perspect Biol, 4*(9), a012286. doi: 10.1101/cshperspect.a012286

DeJesus-Hernandez, M., Mackenzie, I. R., Boeve, B. F., Boxer, A. L., Baker, M., Rutherford, N. J., . . . Rademakers, R. (2011). Expanded GGGGCC hexanucleotide repeat in noncoding region of C9ORF72 causes chromosome 9p-linked FTD and ALS. *Neuron, 72*(2), 245-256. doi: 10.1016/j.neuron.2011.09.011

Deng, H. X., Chen, W., Hong, S. T., Boycott, K. M., Gorrie, G. H., Siddique, N., . . . Siddique, T. (2011). Mutations in UBQLN2 cause dominant X-linked juvenile and adult-onset ALS and ALS/dementia. *Nature, 477*(7363), 211-215. doi: 10.1038/nature10353

Deng, H. X., Zhai, H., Bigio, E. H., Yan, J., Fecto, F., Ajroud, K., . . . Siddique, T. (2010). FUS-immunoreactive inclusions are a common feature in sporadic and non-SOD1 familial amyotrophic lateral sclerosis. *Ann Neurol, 67*(6), 739-748. doi: 10.1002/ana.22051

Deosaran, E., Larsen, K. B., Hua, R., Sargent, G., Wang, Y., Kim, S., . . . Kim, P. K. (2013). NBR1 acts as an autophagy receptor for peroxisomes. *J Cell Sci, 126*(Pt 4), 939-952. doi: 10.1242/jcs.114819

Deretic, V., Jiang, S., & Dupont, N. (2012). Autophagy intersections with conventional and unconventional secretion in tissue development, remodeling and inflammation. *Trends Cell Biol, 22*(8), 397-406. doi: 10.1016/j.tcb.2012.04.008

DeSelm, C. J., Miller, B. C., Zou, W., Beatty, W. L., van Meel, E., Takahata, Y., . . . Virgin, H. W. (2011). Autophagy proteins regulate the secretory component of osteoclastic bone resorption. *Dev Cell, 21*(5), 966-974. doi: 10.1016/j.devcel.2011.08.016

Deter, R. L., & De Duve, C. (1967). Influence of glucagon, an inducer of cellular autophagy, on some physical properties of rat liver lysosomes. *J Cell Biol, 33*(2), 437-449.

Dewannieux, M., Blaise, S., & Heidmann, T. (2005). Identification of a functional envelope protein from the HERV-K family of human endogenous retroviruses. *J Virol, 79*(24), 15573-15577. doi: 10.1128/JVI.79.24.15573-15577.2005

Dewannieux, M., Esnault, C., & Heidmann, T. (2003). LINE-mediated retrotransposition of marked Alu sequences. *Nat Genet, 35*(1), 41-48. doi: 10.1038/ng1223

ng1223 [pii]

Dewey, C. M., Cenik, B., Sephton, C. F., Dries, D. R., Mayer, P., 3rd, Good, S. K., . . . Yu, G. (2011). TDP-43 is directed to stress granules by sorbitol, a novel physiological osmotic and oxidative stressor. *Mol Cell Biol, 31*(5), 1098-1108. doi: 10.1128/MCB.01279-10

Dewey, C. M., Cenik, B., Sephton, C. F., Johnson, B. A., Herz, J., & Yu, G. (2012). TDP-43 aggregation in neurodegeneration: are stress granules the key? *Brain Res, 1462*, 16-25. doi: 10.1016/j.brainres.2012.02.032

Dirac, A. M., Huthoff, H., Kjems, J., & Berkhout, B. (2002). Requirements for RNA heterodimerization of the human immunodeficiency virus type 1 (HIV-1) and HIV-2 genomes. *J Gen Virol, 83*(Pt 10), 2533-2542.

Dirks, R. W., Van Dorp, A. G., Van Minnen, J., Fransen, J. A., Van der Ploeg, M., & Raap, A. K. (1992). Electron microscopic detection of RNA sequences by non-radioactive in situ hybridization in the mollusk Lymnaea stagnalis. *J Histochem Cytochem, 40*(11), 1647-1657.

Dolzhanskaya, N., Merz, G., Aletta, J. M., & Denman, R. B. (2006). Methylation regulates the intracellular protein-protein and protein-RNA interactions of FMRP. *J Cell Sci, 119*(Pt 9), 1933-1946. doi: 10.1242/jcs.02882

Donnelly, C. J., Grima, J. C., & Sattler, R. (2014). Aberrant RNA homeostasis in amyotrophic lateral sclerosis: potential for new therapeutic targets? *Neurodegener Dis Manag, 4*(6), 417-437. doi: 10.2217/nmt.14.36

Donnelly, C. J., Zhang, P. W., Pham, J. T., Haeusler, A. R., Mistry, N. A., Vidensky, S., . . . Rothstein, J. D. (2013). RNA toxicity from the ALS/FTD C9ORF72 expansion is mitigated by antisense intervention. *Neuron, 80*(2), 415-428. doi: 10.1016/j.neuron.2013.10.015

Dormann, D., Madl, T., Valori, C. F., Bentmann, E., Tahirovic, S., Abou-Ajram, C., . . . Haass, C. (2012). Arginine methylation next to the PY-NLS modulates Transportin binding and nuclear import of FUS. *EMBO J, 31*(22), 4258-4275. doi: 10.1038/emboj.2012.261

Dormann, D., Rodde, R., Edbauer, D., Bentmann, E., Fischer, I., Hruscha, A., . . . Haass, C. (2010). ALS-associated fused in sarcoma (FUS) mutations disrupt Transportin-mediated nuclear import. *EMBO J, 29*(16), 2841-2857. doi: 10.1038/emboj.2010.143

Duesberg, P., Stindl, R., & Hehlmann, R. (2000). Explaining the high mutation rates of cancer cells to drug and multidrug resistance by chromosome reassortments that are catalyzed by aneuploidy. *Proc Natl Acad Sci U S A, 97*(26), 14295-14300. doi: 10.1073/pnas.97.26.14295

Dupont, N., Jiang, S., Pilli, M., Ornatowski, W., Bhattacharya, D., & Deretic, V. (2011). Autophagy-based unconventional secretory pathway for extracellular delivery of IL-1beta. *EMBO J, 30*(23), 4701-4711. doi: 10.1038/emboj.2011.398

Duran, J. M., Anjard, C., Stefan, C., Loomis, W. F., & Malhotra, V. (2010). Unconventional secretion of Acb1 is mediated by autophagosomes. *J Cell Biol, 188*(4), 527-536. doi: 10.1083/jcb.200911154

Ebato, C., Uchida, T., Arakawa, M., Komatsu, M., Ueno, T., Komiya, K., . . . Watada, H. (2008). Autophagy is important in islet homeostasis and compensatory increase of beta cell mass in response to high-fat diet. *Cell Metab, 8*(4), 325-332. doi: 10.1016/j.cmet.2008.08.009

El-Naggar, A. M., Veinotte, C. J., Cheng, H., Grunewald, T. G., Negri, G. L., Somasekharan, S. P., . . . Sorensen, P. H. (2015). Translational Activation of

HIF1alpha by YB-1 Promotes Sarcoma Metastasis. *Cancer Cell, 27*(5), 682-697. doi: 10.1016/j.ccell.2015.04.003

Elgendy, M., Ciro, M., Abdel-Aziz, A. K., Belmonte, G., Dal Zuffo, R., Mercurio, C., . . . Minucci, S. (2014). Beclin 1 restrains tumorigenesis through Mcl-1 destabilization in an autophagy-independent reciprocal manner. *Nat Commun, 5*, 5637. doi: 10.1038/ncomms6637

Emde, A., Eitan, C., Liou, L. L., Libby, R. T., Rivkin, N., Magen, I., . . . Hornstein, E. (2015). Dysregulated miRNA biogenesis downstream of cellular stress and ALS-causing mutations: a new mechanism for ALS. *EMBO J, 34*(21), 2633-2651. doi: 10.15252/embj.201490493

Errafiy, R., Aguado, C., Ghislat, G., Esteve, J. M., Gil, A., Loutfi, M., & Knecht, E. (2013). PTEN increases autophagy and inhibits the ubiquitin-proteasome pathway in glioma cells independently of its lipid phosphatase activity. *PLoS One, 8*(12), e83318. doi: 10.1371/journal.pone.0083318

Evans, J. D., Peddigari, S., Chaurasiya, K. R., Williams, M. C., & Martin, S. L. (2011). Paired mutations abolish and restore the balanced annealing and melting activities of ORF1p that are required for LINE-1 retrotransposition. *Nucleic Acids Res, 39*(13), 5611-5621. doi: 10.1093/nar/gkr171

Evrony, G. D., Cai, X., Lee, E., Hills, L. B., Elhosary, P. C., Lehmann, H. S., . . . Walsh, C. A. (2012). Single-neuron sequencing analysis of L1 retrotransposition and somatic mutation in the human brain. *Cell, 151*(3), 483-496. doi: 10.1016/j.cell.2012.09.035

Eystathioy, T., Chan, E. K., Tenenbaum, S. A., Keene, J. D., Griffith, K., & Fritzler, M. J. (2002). A phosphorylated cytoplasmic autoantigen, GW182, associates with a unique population of human mRNAs within novel cytoplasmic speckles. *Mol Biol Cell, 13*(4), 1338-1351.

Fan, A. C., & Leung, A. K. (2016). RNA Granules and Diseases: A Case Study of Stress Granules in ALS and FTLD. *Adv Exp Med Biol, 907*, 263-296. doi: 10.1007/978-3-319-29073-7_11

Fang, Y., Wu, N., Gan, X., Yan, W., Morrell, J. C., & Gould, S. J. (2007). Higher-order oligomerization targets plasma membrane proteins and HIV gag to exosomes. *PLoS Biol, 5*(6), e158. doi: 06-PLBI-RA-2411R2 [pii]

10.1371/journal.pbio.0050158

Farg, M. A., Sundaramoorthy, V., Sultana, J. M., Yang, S., Atkinson, R. A., Levina, V., . . . Atkin, J. D. (2014). C9ORF72, implicated in amytrophic lateral sclerosis and frontotemporal dementia, regulates endosomal trafficking. *Hum Mol Genet, 23*(13), 3579-3595. doi: 10.1093/hmg/ddu068

Farre, J. C., Manjithaya, R., Mathewson, R. D., & Subramani, S. (2008). PpAtg30 tags peroxisomes for turnover by selective autophagy. *Dev Cell, 14*(3), 365-376. doi: 10.1016/j.devcel.2007.12.011

Farre, J. C., & Subramani, S. (2004). Peroxisome turnover by micropexophagy: an autophagy-related process. *Trends Cell Biol, 14*(9), 515-523. doi: 10.1016/j.tcb.2004.07.014

Faulkner, G. J., Kimura, Y., Daub, C. O., Wani, S., Plessy, C., Irvine, K. M., . . . Carninci, P. (2009). The regulated retrotransposon transcriptome of mammalian cells. *Nat Genet, 41*(5), 563-571. doi: ng.368 [pii]

10.1038/ng.368

Fecto, F., Yan, J., Vemula, S. P., Liu, E., Yang, Y., Chen, W., . . . Siddique, T. (2011). SQSTM1 mutations in familial and sporadic amyotrophic lateral sclerosis. *Arch Neurol, 68*(11), 1440-1446. doi: 10.1001/archneurol.2011.250

Fernandes, N., Eshleman, N., & Buchan, J. R. (2018). Stress Granules and ALS: A Case of Causation or Correlation? *Adv Neurobiol, 20*, 173-212. doi: 10.1007/978-3-319-89689-2_7

Fevrier, B., Vilette, D., Archer, F., Loew, D., Faigle, W., Vidal, M., . . . Raposo, G. (2004). Cells release prions in association with exosomes. *Proc Natl Acad Sci U S A, 101*(26), 9683-9688. doi: 10.1073/pnas.0308413101

0308413101 [pii]

Fimia, G. M., Kroemer, G., & Piacentini, M. (2013). Molecular mechanisms of selective autophagy. *Cell Death Differ, 20*(1), 1-2. doi: 10.1038/cdd.2012.97

Florey, O., Kim, S. E., Sandoval, C. P., Haynes, C. M., & Overholtzer, M. (2011). Autophagy machinery mediates macroendocytic processing and entotic cell death by targeting single membranes. *Nat Cell Biol, 13*(11), 1335-1343. doi: 10.1038/ncb2363

Forman, M. S., Trojanowski, J. Q., & Lee, V. M. (2004). Neurodegenerative diseases: a decade of discoveries paves the way for therapeutic breakthroughs. *Nat Med, 10*(10), 1055-1063. doi: 10.1038/nm1113

Fornai, F., Longone, P., Cafaro, L., Kastsiuchenka, O., Ferrucci, M., Manca, M. L., . . . Paparelli, A. (2008). Lithium delays progression of amyotrophic lateral sclerosis. *Proc Natl Acad Sci U S A, 105*(6), 2052-2057. doi: 10.1073/pnas.0708022105

Forostyak, S., & Sykova, E. (2017). Neuroprotective Potential of Cell-Based Therapies in ALS: From Bench to Bedside. *Front Neurosci, 11*, 591. doi: 10.3389/fnins.2017.00591

Fouad, Y. A., & Aanei, C. (2017). Revisiting the hallmarks of cancer. *Am J Cancer Res, 7*(5), 1016-1036.

Fournier, M. J., Gareau, C., & Mazroui, R. (2010). The chemotherapeutic agent bortezomib induces the formation of stress granules. *Cancer Cell Int, 10*, 12. doi: 10.1186/1475-2867-10-12

Fracchiolla, D., Sawa-Makarska, J., Zens, B., Ruiter, A., Zaffagnini, G., Brezovich, A., . . . Martens, S. (2016). Mechanism of cargo-directed Atg8 conjugation during selective autophagy. *Elife, 5*. doi: 10.7554/eLife.18544

Frankel, L. B., Lubas, M., & Lund, A. H. (2017). Emerging connections between RNA and autophagy. *Autophagy, 13*(1), 3-23. doi: 10.1080/15548627.2016.1222992

Freischmidt, A., Wieland, T., Richter, B., Ruf, W., Schaeffer, V., Muller, K., . . . Weishaupt, J. H. (2015). Haploinsufficiency of TBK1 causes familial ALS and fronto-temporal dementia. *Nat Neurosci, 18*(5), 631-636. doi: 10.1038/nn.4000

Fussner, E., Djuric, U., Strauss, M., Hotta, A., Perez-Iratxeta, C., Lanner, F., . . . Bazett-Jones, D. P. (2011). Constitutive heterochromatin reorganization during somatic cell reprogramming. *EMBO J, 30*(9), 1778-1789. doi: 10.1038/emboj.2011.96

Futter, C. E., Collinson, L. M., Backer, J. M., & Hopkins, C. R. (2001). Human VPS34 is required for internal vesicle formation within multivesicular endosomes. *J Cell Biol, 155*(7), 1251-1264. doi: 10.1083/jcb.200108152

Gal, J., Strom, A. L., Kwinter, D. M., Kilty, R., Zhang, J., Shi, P., . . . Zhu, H. (2009). Sequestosome 1/p62 links familial ALS mutant SOD1 to LC3 via an ubiquitin-independent mechanism. *J Neurochem, 111*(4), 1062-1073. doi: 10.1111/j.1471-4159.2009.06388.x

Gal, J., Zhang, J., Kwinter, D. M., Zhai, J., Jia, H., Jia, J., & Zhu, H. (2011). Nuclear localization sequence of FUS and induction of stress granules by ALS mutants. *Neurobiol Aging, 32*(12), 2323 e2327-2340. doi: 10.1016/j.neurobiolaging.2010.06.010

Galluzzi, L., Baehrecke, E. H., Ballabio, A., Boya, P., Bravo-San Pedro, J. M., Cecconi, F., . . . Kroemer, G. (2017). Molecular definitions of autophagy and related processes. *EMBO J, 36*(13), 1811-1836. doi: 10.15252/embj.201796697

Galluzzi, L., Bravo-San Pedro, J. M., Demaria, S., Formenti, S. C., & Kroemer, G. (2017). Activating autophagy to potentiate immunogenic chemotherapy and radiation therapy. *Nat Rev Clin Oncol, 14*(4), 247-258. doi: 10.1038/nrclinonc.2016.183

Galluzzi, L., Pietrocola, F., Bravo-San Pedro, J. M., Amaravadi, R. K., Baehrecke, E. H., Cecconi, F., . . . Kroemer, G. (2015). Autophagy in malignant transformation and cancer progression. *EMBO J, 34*(7), 856-880. doi: 10.15252/embj.201490784

Ganesan, A. K., Ho, H., Bodemann, B., Petersen, S., Aruri, J., Koshy, S., . . . White, M. A. (2008). Genome-wide siRNA-based functional genomics of pigmentation identifies novel genes and pathways that impact melanogenesis in human cells. *PLoS Genet, 4*(12), e1000298. doi: 10.1371/journal.pgen.1000298

Gao, X., Zacharek, A., Salkowski, A., Grignon, D. J., Sakr, W., Porter, A. T., & Honn, K. V. (1995). Loss of heterozygosity of the BRCA1 and other loci on chromosome 17q in human prostate cancer. *Cancer Res, 55*(5), 1002-1005.

Gareau, C., Fournier, M. J., Filion, C., Coudert, L., Martel, D., Labelle, Y., & Mazroui, R. (2011). p21(WAF1/CIP1) upregulation through the stress granule-associated protein CUGBP1 confers resistance to bortezomib-mediated apoptosis. *PLoS One, 6*(5), e20254. doi: 10.1371/journal.pone.0020254

Gasior, S. L., Preston, G., Hedges, D. J., Gilbert, N., Moran, J. V., & Deininger, P. L. (2007). Characterization of pre-insertion loci of de novo L1 insertions. *Gene, 390*(1-2), 190-198. doi: 10.1016/j.gene.2006.08.024

Gatica, D., Lahiri, V., & Klionsky, D. J. (2018). Cargo recognition and degradation by selective autophagy. *Nat Cell Biol, 20*(3), 233-242. doi: 10.1038/s41556-018-0037-z

Geisler, S., Holmstrom, K. M., Skujat, D., Fiesel, F. C., Rothfuss, O. C., Kahle, P. J., & Springer, W. (2010). PINK1/Parkin-mediated mitophagy is dependent on VDAC1 and p62/SQSTM1. *Nat Cell Biol, 12*(2), 119-131. doi: 10.1038/ncb2012

Gerlinger, M., Rowan, A. J., Horswell, S., Larkin, J., Endesfelder, D., Gronroos, E., . . . Swanton, C. (2012). Intratumor heterogeneity and branched evolution revealed by multiregion sequencing. *N Engl J Med, 366*(10), 883-892. doi: 10.1056/NEJMoa1113205

Giampieri, F., Afrin, S., Forbes-Hernandez, T. Y., Gasparrini, M., Cianciosi, D., Reboredo-Rodriguez, P., . . . Battino, M. (2018). Autophagy in Human Health and Disease: Novel Therapeutic Opportunities. *Antioxid Redox Signal*. doi: 10.1089/ars.2017.7234

Gibbings, D., Leblanc, P., Jay, F., Pontier, D., Michel, F., Schwab, Y., . . . Voinnet, O. (2012). Human prion protein binds Argonaute and promotes accumulation of microRNA effector complexes. *Nat Struct Mol Biol, 19*(5), 517-524, S511. doi: 10.1038/nsmb.2273

Gibbings, D., Mostowy, S., Jay, F., Schwab, Y., Cossart, P., & Voinnet, O. (2012). Selective autophagy degrades DICER and AGO2 and regulates miRNA activity. *Nat Cell Biol, 14*(12), 1314-1321. doi: 10.1038/ncb2611

Gibbings, D., Mostowy, S., Jay, F., Schwab, Y., Cossart, P., Voinnet, O. (2012). Selective autophagy degrades DICER and AGO2 and regulates miRNA activity. *Nature Cell Biology, in press*.

Gijselinck, I., Van Langenhove, T., van der Zee, J., Sleegers, K., Philtjens, S., Kleinberger, G., . . . Van Broeckhoven, C. (2012). A C9orf72 promoter repeat expansion in a Flanders-Belgian cohort with disorders of the frontotemporal lobar degeneration-amyotrophic lateral sclerosis spectrum: a gene identification study. *Lancet Neurol, 11*(1), 54-65. doi: 10.1016/S1474-4422(11)70261-7

Gill, A., Kidd, J., Vieira, F., Thompson, K., & Perrin, S. (2009). No benefit from chronic lithium dosing in a sibling-matched, gender balanced, investigator-blinded trial using a standard mouse model of familial ALS. *PLoS One, 4*(8), e6489. doi: 10.1371/journal.pone.0006489

Goodier, J. L., Cheung, L. E., & Kazazian, H. H., Jr. (2012). MOV10 RNA helicase is a potent inhibitor of retrotransposition in cells. *PLoS Genet, 8*(10), e1002941. doi: 10.1371/journal.pgen.1002941

Goodier, J. L., Cheung, L. E., & Kazazian, H. H., Jr. (2013). Mapping the LINE1 ORF1 protein interactome reveals associated inhibitors of human retrotransposition. *Nucleic Acids Res*. doi: 10.1093/nar/gkt512

Goodier, J. L., Mandal, P. K., Zhang, L., & Kazazian, H. H., Jr. (2010). Discrete subcellular partitioning of human retrotransposon RNAs despite a common mechanism of genome insertion. *Hum Mol Genet, 19*(9), 1712-1725. doi: ddq048 [pii]

10.1093/hmg/ddq048

Goodier, J. L., Zhang, L., Vetter, M. R., & Kazazian, H. H., Jr. (2007). LINE-1 ORF1 protein localizes in stress granules with other RNA-binding proteins, including components of RNA interference RNA-induced silencing complex. *Mol Cell Biol, 27*(18), 6469-6483. doi: 10.1128/MCB.00332-07

Gordon, P. B., & Seglen, P. O. (1988). Prelysosomal convergence of autophagic and endocytic pathways. *Biochem Biophys Res Commun, 151*(1), 40-47.

Goulet, I., Boisvenue, S., Mokas, S., Mazroui, R., & Cote, J. (2008). TDRD3, a novel Tudor domain-containing protein, localizes to cytoplasmic stress granules. *Hum Mol Genet, 17*(19), 3055-3074. doi: 10.1093/hmg/ddn203

Grabocka, E., & Bar-Sagi, D. (2016). Mutant KRAS Enhances Tumor Cell Fitness by Upregulating Stress Granules. *Cell, 167*(7), 1803-1813 e1812. doi: 10.1016/j.cell.2016.11.035

Gross, J. C., Chaudhary, V., Bartscherer, K., & Boutros, M. (2012). Active Wnt proteins are secreted on exosomes. *Nat Cell Biol, 14*(10), 1036-1045. doi: 10.1038/ncb2574

Grunt, T. W., & Mariani, G. L. (2012). Targeting the PI3K/AKT/mTOR Pathway in Breast Cancer. *Curr Cancer Drug Targets*.

Guevel, L., Lavoie, J. R., Perez-Iratxeta, C., Rouger, K., Dubreil, L., Feron, M., . . . Megeney, L. A. (2011). Quantitative proteomic analysis of dystrophic dog muscle. *J Proteome Res, 10*(5), 2465-2478. doi: 10.1021/pr2001385

Guo, A., Gu, H., Zhou, J., Mulhern, D., Wang, Y., Lee, K. A., . . . Comb, M. J. (2014). Immunoaffinity enrichment and mass spectrometry analysis of protein methylation. *Mol Cell Proteomics, 13*(1), 372-387. doi: 10.1074/mcp.O113.027870

Guo, H., Chitiprolu, M., Gagnon, D., Meng, L., Perez-Iratxeta, C., Lagace, D., & Gibbings, D. (2014). Autophagy supports genomic stability by degrading retrotransposon RNA. *Nat Commun, 5*, 5276. doi: 10.1038/ncomms6276

Guo, J. Y., Karsli-Uzunbas, G., Mathew, R., Aisner, S. C., Kamphorst, J. J., Strohecker, A. M., . . . White, E. (2013). Autophagy suppresses progression of K-ras-induced lung tumors to oncocytomas and maintains lipid homeostasis. *Genes Dev, 27*(13), 1447-1461. doi: 10.1101/gad.219642.113

Guo, J. Y., Xia, B., & White, E. (2013). Autophagy-mediated tumor promotion. *Cell, 155*(6), 1216-1219. doi: 10.1016/j.cell.2013.11.019

Guo, W., Gao, Y., Li, N., Shao, F., Wang, C., Wang, P., . . . He, J. (2017). Exosomes: New players in cancer (Review). *Oncol Rep, 38*(2), 665-675. doi: 10.3892/or.2017.5714

Haeusler, A. R., Donnelly, C. J., & Rothstein, J. D. (2016). The expanding biology of the C9orf72 nucleotide repeat expansion in neurodegenerative disease. *Nat Rev Neurosci, 17*(6), 383-395. doi: 10.1038/nrn.2016.38

Hamacher-Brady, A., Brady, N. R., Logue, S. E., Sayen, M. R., Jinno, M., Kirshenbaum, L. A., . . . Gustafsson, A. B. (2007). Response to myocardial ischemia/reperfusion injury involves Bnip3 and autophagy. *Cell Death Differ, 14*(1), 146-157. doi: 10.1038/sj.cdd.4401936

Han, T. W., Kato, M., Xie, S., Wu, L. C., Mirzaei, H., Pei, J., . . . McKnight, S. L. (2012). Cell-free formation of RNA granules: bound RNAs identify features and components of cellular assemblies. *Cell, 149*(4), 768-779. doi: 10.1016/j.cell.2012.04.016

Hanahan, D., & Weinberg, R. A. (2011). Hallmarks of cancer: the next generation. *Cell, 144*(5), 646-674. doi: 10.1016/j.cell.2011.02.013

Hancks, D. C., & Kazazian, H. H., Jr. (2012). Active human retrotransposons: variation and disease. *Curr Opin Genet Dev, 22*(3), 191-203. doi: 10.1016/j.gde.2012.02.006

Hanna, R. A., Quinsay, M. N., Orogo, A. M., Giang, K., Rikka, S., & Gustafsson, A. B. (2012). Microtubule-associated protein 1 light chain 3 (LC3) interacts with Bnip3 protein to selectively remove endoplasmic reticulum and mitochondria via autophagy. *J Biol Chem, 287*(23), 19094-19104. doi: 10.1074/jbc.M111.322933

Hanson, P. I., & Cashikar, A. (2012). Multivesicular body morphogenesis. *Annu Rev Cell Dev Biol, 28*, 337-362. doi: 10.1146/annurev-cellbio-092910-154152

Hara, T., Nakamura, K., Matsui, M., Yamamoto, A., Nakahara, Y., Suzuki-Migishima, R., . . . Mizushima, N. (2006). Suppression of basal autophagy in neural cells causes neurodegenerative disease in mice. *Nature, 441*(7095), 885-889. doi: 10.1038/nature04724

Harms, M. B., Cady, J., Zaidman, C., Cooper, P., Bali, T., Allred, P., . . . Baloh, R. H. (2013). Lack of C9ORF72 coding mutations supports a gain of function for repeat expansions in amyotrophic lateral sclerosis. *Neurobiol Aging, 34*(9), 2234 e2213-2239. doi: 10.1016/j.neurobiolaging.2013.03.006

Harris, C. R., Normart, R., Yang, Q., Stevenson, E., Haffty, B. G., Ganesan, S., . . . Tang, L. H. (2010). Association of nuclear localization of a long interspersed nuclear element-1 protein in breast tumors with poor prognostic outcomes. *Genes Cancer, 1*(2), 115-124. doi: 10.1177/1947601909360812

Harris, H., & Rubinsztein, D. C. (2011). Control of autophagy as a therapy for neurodegenerative disease. *Nat Rev Neurol, 8*(2), 108-117. doi: 10.1038/nrneurol.2011.200

Harris, H., & Rubinsztein, D. C. (2012). Control of autophagy as a therapy for neurodegenerative disease. *Nat Rev Neurol, 8*(2), 108-117. doi: 10.1038/nrneurol.2011.200

Hart, P. J. (2006). Pathogenic superoxide dismutase structure, folding, aggregation and turnover. *Curr Opin Chem Biol, 10*(2), 131-138. doi: 10.1016/j.cbpa.2006.02.034

Hase, K., Fujiwara, Y., Kikuchi, H., Aizawa, S., Hakuno, F., Takahashi, S., . . . Kabuta, T. (2015). RNautophagy/DNautophagy possesses selectivity for RNA/DNA substrates. *Nucleic Acids Res, 43*(13), 6439-6449. doi: 10.1093/nar/gkv579

He, C., & Klionsky, D. J. (2009). Regulation mechanisms and signaling pathways of autophagy. *Annu Rev Genet, 43*, 67-93. doi: 10.1146/annurev-genet-102808-114910

He, W. S., Dai, X. F., Jin, M., Liu, C. W., & Rent, J. H. (2012). Hypoxia-induced autophagy confers resistance of breast cancer cells to ionizing radiation. *Oncol Res, 20*(5-6), 251-258.

Helman, E., Lawrence, M. S., Stewart, C., Sougnez, C., Getz, G., & Meyerson, M. (2014). Somatic retrotransposition in human cancer revealed by whole-genome and exome sequencing. *Genome Res, 24*(7), 1053-1063. doi: 10.1101/gr.163659.113

Henne, W. M., Stenmark, H., & Emr, S. D. (2013). Molecular mechanisms of the membrane sculpting ESCRT pathway. *Cold Spring Harb Perspect Biol, 5*(9). doi: 10.1101/cshperspect.a016766

Hershko, A., & Ciechanover, A. (1998). The ubiquitin system. *Annu Rev Biochem, 67*, 425-479. doi: 10.1146/annurev.biochem.67.1.425

Heydrick, S. J., Lardeux, B. R., & Mortimore, G. E. (1991). Uptake and degradation of cytoplasmic RNA by hepatic lysosomes. Quantitative relationship to RNA turnover. *J Biol Chem, 266*(14), 8790-8796.

Higginbotham, J. N., Demory Beckler, M., Gephart, J. D., Franklin, J. L., Bogatcheva, G., Kremers, G. J., . . . Coffey, R. J. (2011). Amphiregulin exosomes increase cancer cell invasion. *Curr Biol, 21*(9), 779-786. doi: 10.1016/j.cub.2011.03.043

Hillwig, M. S., Contento, A. L., Meyer, A., Ebany, D., Bassham, D. C., & Macintosh, G. C. (2011). RNS2, a conserved member of the RNase T2 family, is necessary for ribosomal RNA decay in plants. *Proc Natl Acad Sci U S A, 108*(3), 1093-1098. doi: 10.1073/pnas.1009809108

Hirano, M., Nakamura, Y., Saigoh, K., Sakamoto, H., Ueno, S., Isono, C., . . . Kusunoki, S. (2013). Mutations in the gene encoding p62 in Japanese patients with amyotrophic lateral sclerosis. *Neurology, 80*(5), 458-463. doi: 10.1212/WNL.0b013e31827f0fe5

Hoell, J. I., Larsson, E., Runge, S., Nusbaum, J. D., Duggimpudi, S., Farazi, T. A., . . . Tuschl, T. (2011). RNA targets of wild-type and mutant FET family proteins. *Nat Struct Mol Biol, 18*(12), 1428-1431. doi: 10.1038/nsmb.2163

Holohan, C., Van Schaeybroeck, S., Longley, D. B., & Johnston, P. G. (2013). Cancer drug resistance: an evolving paradigm. *Nat Rev Cancer, 13*(10), 714-726. doi: 10.1038/nrc3599

Hoogstraat, M., de Pagter, M. S., Cirkel, G. A., van Roosmalen, M. J., Harkins, T. T., Duran, K., . . . Kloosterman, W. P. (2014). Genomic and transcriptomic plasticity in treatment-naive ovarian cancer. *Genome Res, 24*(2), 200-211. doi: 10.1101/gr.161026.113

Hormozdiari, F., Alkan, C., Ventura, M., Hajirasouliha, I., Malig, M., Hach, F., . . . Eichler, E. E. (2011). Alu repeat discovery and characterization within human genomes. *Genome Res, 21*(6), 840-849. doi: 10.1101/gr.115956.110

Hoshino, A., Costa-Silva, B., Shen, T. L., Rodrigues, G., Hashimoto, A., Tesic Mark, M., . . . Lyden, D. (2015). Tumour exosome integrins determine organotropic metastasis. *Nature, 527*(7578), 329-335. doi: 10.1038/nature15756

Hoshino, D., Kirkbride, K. C., Costello, K., Clark, E. S., Sinha, S., Grega-Larson, N., . . . Weaver, A. M. (2013). Exosome secretion is enhanced by invadopodia and drives invasive behavior. *Cell Rep, 5*(5), 1159-1168. doi: 10.1016/j.celrep.2013.10.050

Hosokawa, N., Hara, Y., & Mizushima, N. (2007). Generation of cell lines with tetracycline-regulated autophagy and a role for autophagy in controlling cell size. *FEBS Lett, 581*(15), 2623-2629. doi: 10.1016/j.febslet.2007.05.061

Hu, Y. L., DeLay, M., Jahangiri, A., Molinaro, A. M., Rose, S. D., Carbonell, W. S., & Aghi, M. K. (2012). Hypoxia-induced autophagy promotes tumor cell survival and adaptation to antiangiogenic treatment in glioblastoma. *Cancer Res, 72*(7), 1773-1783. doi: 10.1158/0008-5472.CAN-11-3831

Hua, Y., & Zhou, J. (2004). Survival motor neuron protein facilitates assembly of stress granules. *FEBS Lett, 572*(1-3), 69-74. doi: 10.1016/j.febslet.2004.07.010

Huang, E. J., Zhang, J., Geser, F., Trojanowski, J. Q., Strober, J. B., Dickson, D. W., . . . Lomen-Hoerth, C. (2010). Extensive FUS-immunoreactive pathology in juvenile amyotrophic lateral sclerosis with basophilic inclusions. *Brain Pathol, 20*(6), 1069-1076. doi: 10.1111/j.1750-3639.2010.00413.x

Huotari, J., & Helenius, A. (2011). Endosome maturation. *EMBO J, 30*(17), 3481-3500. doi: 10.1038/emboj.2011.286

Hurley, J. H. (2015). ESCRTs are everywhere. *EMBO J, 34*(19), 2398-2407. doi: 10.15252/embj.201592484

Hurley, J. H., & Hanson, P. I. (2010). Membrane budding and scission by the ESCRT machinery: it's all in the neck. *Nat Rev Mol Cell Biol, 11*(8), 556-566. doi: 10.1038/nrm2937

Hwang, S., Maloney, N. S., Bruinsma, M. W., Goel, G., Duan, E., Zhang, L., . . . Virgin, H. W. (2012). Nondegradative role of Atg5-Atg12/ Atg16L1 autophagy protein complex in antiviral activity of interferon gamma. *Cell Host Microbe, 11*(4), 397-409. doi: 10.1016/j.chom.2012.03.002

Ichimura, Y., Kirisako, T., Takao, T., Satomi, Y., Shimonishi, Y., Ishihara, N., . . . Ohsumi, Y. (2000). A ubiquitin-like system mediates protein lipidation. *Nature, 408*(6811), 488-492. doi: 10.1038/35044114

Inami, Y., Waguri, S., Sakamoto, A., Kouno, T., Nakada, K., Hino, O., . . . Komatsu, M. (2011). Persistent activation of Nrf2 through p62 in hepatocellular carcinoma cells. *J Cell Biol, 193*(2), 275-284. doi: 10.1083/jcb.201102031

Ito, D., Seki, M., Tsunoda, Y., Uchiyama, H., & Suzuki, N. (2011). Nuclear transport impairment of amyotrophic lateral sclerosis-linked mutations in FUS/TLS. *Ann Neurol, 69*(1), 152-162. doi: 10.1002/ana.22246

Ito, H., Fujita, K., Nakamura, M., Wate, R., Kaneko, S., Sasaki, S., . . . Kusaka, H. (2011). Optineurin is co-localized with FUS in basophilic inclusions of ALS with FUS mutation and in basophilic inclusion body disease. *Acta Neuropathol, 121*(4), 555-557. doi: 10.1007/s00401-011-0809-z

Ittner, L. M., Halliday, G. M., Kril, J. J., Gotz, J., Hodges, J. R., & Kiernan, M. C. (2015). FTD and ALS--translating mouse studies into clinical trials. *Nat Rev Neurol, 11*(6), 360-366. doi: 10.1038/nrneurol.2015.65

Iwata, A., Riley, B. E., Johnston, J. A., & Kopito, R. R. (2005). HDAC6 and microtubules are required for autophagic degradation of aggregated huntingtin. *J Biol Chem, 280*(48), 40282-40292. doi: 10.1074/jbc.M508786200

Izquierdo-Useros, N., Puertas, M. C., Borras, F. E., Blanco, J., & Martinez-Picado, J. (2011). Exosomes and retroviruses: the chicken or the egg? *Cell Microbiol, 13*(1), 10-17. doi: 10.1111/j.1462-5822.2010.01542.x

Jain, K., Paranandi, K. S., Sridharan, S., & Basu, A. (2013). Autophagy in breast cancer and its implications for therapy. *Am J Cancer Res, 3*(3), 251-265.

Jain, S., Wheeler, J. R., Walters, R. W., Agrawal, A., Barsic, A., & Parker, R. (2016). ATPase-Modulated Stress Granules Contain a Diverse Proteome and Substructure. *Cell, 164*(3), 487-498. doi: 10.1016/j.cell.2015.12.038

Jiang, J., Zhu, Q., Gendron, T. F., Saberi, S., McAlonis-Downes, M., Seelman, A., . . . Lagier-Tourenne, C. (2016). Gain of Toxicity from ALS/FTD-Linked Repeat Expansions in C9ORF72 Is Alleviated by Antisense Oligonucleotides Targeting GGGGCC-Containing RNAs. *Neuron, 90*(3), 535-550. doi: 10.1016/j.neuron.2016.04.006

Jiang, S., Wells, C. D., & Roach, P. J. (2011). Starch-binding domain-containing protein 1 (Stbd1) and glycogen metabolism: Identification of the Atg8 family interacting motif (AIM) in Stbd1 required for interaction with GABARAPL1. *Biochem Biophys Res Commun, 413*(3), 420-425. doi: 10.1016/j.bbrc.2011.08.106

Johansen, T., Birgisdottir, A. B., Huber, J., Kniss, A., Dotsch, V., Kirkin, V., & Rogov, V. V. (2017). Methods for Studying Interactions Between Atg8/LC3/GABARAP and LIR-Containing Proteins. *Methods Enzymol, 587*, 143-169. doi: 10.1016/bs.mie.2016.10.023

Johansen, T., & Lamark, T. (2011). Selective autophagy mediated by autophagic adapter proteins. *Autophagy, 7*(3), 279-296.

Jovicic, A., Mertens, J., Boeynaems, S., Bogaert, E., Chai, N., Yamada, S. B., . . . Gitler, A. D. (2015). Modifiers of C9orf72 dipeptide repeat toxicity connect nucleocytoplasmic transport defects to FTD/ALS. *Nat Neurosci, 18*(9), 1226-1229. doi: 10.1038/nn.4085

Ju, J. S., Fuentealba, R. A., Miller, S. E., Jackson, E., Piwnica-Worms, D., Baloh, R. H., & Weihl, C. C. (2009). Valosin-containing protein (VCP) is required for autophagy and is disrupted in VCP disease. *J Cell Biol, 187*(6), 875-888. doi: 10.1083/jcb.200908115

Kabashi, E., Valdmanis, P. N., Dion, P., Spiegelman, D., McConkey, B. J., Vande Velde, C., . . . Rouleau, G. A. (2008). TARDBP mutations in individuals with sporadic and familial amyotrophic lateral sclerosis. *Nat Genet, 40*(5), 572-574. doi: 10.1038/ng.132

Kabeya, Y., Mizushima, N., Ueno, T., Yamamoto, A., Kirisako, T., Noda, T., . . . Yoshimori, T. (2000). LC3, a mammalian homologue of yeast Apg8p, is localized in autophagosome membranes after processing. *EMBO J, 19*(21), 5720-5728. doi: 10.1093/emboj/19.21.5720

Kalvari, I., Tsompanis, S., Mulakkal, N. C., Osgood, R., Johansen, T., Nezis, I. P., & Promponas, V. J. (2014). iLIR: A web resource for prediction of Atg8-family interacting proteins. *Autophagy, 10*(5), 913-925. doi: 10.4161/auto.28260

Kanki, T., Wang, K., Cao, Y., Baba, M., & Klionsky, D. J. (2009). Atg32 is a mitochondrial protein that confers selectivity during mitophagy. *Dev Cell, 17*(1), 98-109. doi: 10.1016/j.devcel.2009.06.014

Kano, H., Godoy, I., Courtney, C., Vetter, M. R., Gerton, G. L., Ostertag, E. M., & Kazazian, H. H., Jr. (2009). L1 retrotransposition occurs mainly in embryogenesis

and creates somatic mosaicism. *Genes Dev, 23*(11), 1303-1312. doi: 10.1101/gad.1803909

Karanasios, E., Walker, S. A., Okkenhaug, H., Manifava, M., Hummel, E., Zimmermann, H., . . . Ktistakis, N. T. (2016). Autophagy initiation by ULK complex assembly on ER tubulovesicular regions marked by ATG9 vesicles. *Nat Commun, 7*, 12420. doi: 10.1038/ncomms12420

Kato, M., Han, T. W., Xie, S., Shi, K., Du, X., Wu, L. C., . . . McKnight, S. L. (2012). Cell-free formation of RNA granules: low complexity sequence domains form dynamic fibers within hydrogels. *Cell, 149*(4), 753-767. doi: 10.1016/j.cell.2012.04.017

Katsuragi, Y., Ichimura, Y., & Komatsu, M. (2015). p62/SQSTM1 functions as a signaling hub and an autophagy adaptor. *FEBS J, 282*(24), 4672-4678. doi: 10.1111/febs.13540

Kaushik, S., & Cuervo, A. M. (2012). Chaperone-mediated autophagy: a unique way to enter the lysosome world. *Trends Cell Biol, 22*(8), 407-417. doi: 10.1016/j.tcb.2012.05.006

Kedersha, N., Stoecklin, G., Ayodele, M., Yacono, P., Lykke-Andersen, J., Fritzler, M. J., . . . Anderson, P. (2005). Stress granules and processing bodies are dynamically linked sites of mRNP remodeling. *J Cell Biol, 169*(6), 871-884. doi: 10.1083/jcb.200502088

Kemp, J. R., & Longworth, M. S. (2015). Crossing the LINE Toward Genomic Instability: LINE-1 Retrotransposition in Cancer. *Front Chem, 3*, 68. doi: 10.3389/fchem.2015.00068

Kenific, C. M., & Debnath, J. (2015). Cellular and metabolic functions for autophagy in cancer cells. *Trends Cell Biol, 25*(1), 37-45. doi: 10.1016/j.tcb.2014.09.001

Kenific, C. M., Wittmann, T., & Debnath, J. (2016). Autophagy in adhesion and migration. *J Cell Sci, 129*(20), 3685-3693. doi: 10.1242/jcs.188490

Khaminets, A., Behl, C., & Dikic, I. (2016). Ubiquitin-Dependent And Independent Signals In Selective Autophagy. *Trends Cell Biol, 26*(1), 6-16. doi: 10.1016/j.tcb.2015.08.010

Kidd, J. M., Graves, T., Newman, T. L., Fulton, R., Hayden, H. S., Malig, M., . . . Eichler, E. E. (2010). A human genome structural variation sequencing resource reveals insights into mutational mechanisms. *Cell, 143*(5), 837-847. doi: 10.1016/j.cell.2010.10.027

Kihara, A., Noda, T., Ishihara, N., & Ohsumi, Y. (2001). Two distinct Vps34 phosphatidylinositol 3-kinase complexes function in autophagy and carboxypeptidase Y sorting in Saccharomyces cerevisiae. *J Cell Biol, 152*(3), 519-530.

Kim, B., Ha, M., Loeff, L., Chang, H., Simanshu, D. K., Li, S., . . . Kim, V. N. (2015). TUT7 controls the fate of precursor microRNAs by using three different uridylation mechanisms. *EMBO J, 34*(13), 1801-1815. doi: 10.15252/embj.201590931

Kim, H. J., Kim, N. C., Wang, Y. D., Scarborough, E. A., Moore, J., Diaz, Z., . . . Taylor, J. P. (2013). Mutations in prion-like domains in hnRNPA2B1 and hnRNPA1

cause multisystem proteinopathy and ALS. *Nature, 495*(7442), 467-473. doi: 10.1038/nature11922

Kim, M. J., Woo, S. J., Yoon, C. H., Lee, J. S., An, S., Choi, Y. H., . . . Lee, S. J. (2011). Involvement of autophagy in oncogenic K-Ras-induced malignant cell transformation. *J Biol Chem, 286*(15), 12924-12932. doi: 10.1074/jbc.M110.138958

Kim, S., Kim do, H., Jung, W. H., & Koo, J. S. (2013). Metabolic phenotypes in triple-negative breast cancer. *Tumour Biol, 34*(3), 1699-1712. doi: 10.1007/s13277-013-0707-1

Kimmelman, A. C. (2011). The dynamic nature of autophagy in cancer. *Genes Dev, 25*(19), 1999-2010. doi: 10.1101/gad.17558811

King, H. W., Michael, M. Z., & Gleadle, J. M. (2012). Hypoxic enhancement of exosome release by breast cancer cells. *BMC Cancer, 12*, 421. doi: 10.1186/1471-2407-12-421

Kino, Y., Washizu, C., Aquilanti, E., Okuno, M., Kurosawa, M., Yamada, M., . . . Nukina, N. (2011). Intracellular localization and splicing regulation of FUS/TLS are variably affected by amyotrophic lateral sclerosis-linked mutations. *Nucleic Acids Res, 39*(7), 2781-2798. doi: 10.1093/nar/gkq1162

Kirkin, V., Lamark, T., Sou, Y. S., Bjorkoy, G., Nunn, J. L., Bruun, J. A., . . . Johansen, T. (2009). A role for NBR1 in autophagosomal degradation of ubiquitinated substrates. *Mol Cell, 33*(4), 505-516. doi: 10.1016/j.molcel.2009.01.020

Klionsky, D. J., Abdalla, F. C., Abeliovich, H., Abraham, R. T., Acevedo-Arozena, A., Adeli, K., . . . Zuckerbraun, B. (2012). Guidelines for the use and interpretation of assays for monitoring autophagy. *Autophagy, 8*(4), 445-544.

Komatsu, M., Waguri, S., Chiba, T., Murata, S., Iwata, J., Tanida, I., . . . Tanaka, K. (2006). Loss of autophagy in the central nervous system causes neurodegeneration in mice. *Nature, 441*(7095), 880-884. doi: 10.1038/nature04723

Komatsu, M., Waguri, S., Koike, M., Sou, Y. S., Ueno, T., Hara, T., . . . Tanaka, K. (2007). Homeostatic levels of p62 control cytoplasmic inclusion body formation in autophagy-deficient mice. *Cell, 131*(6), 1149-1163. doi: 10.1016/j.cell.2007.10.035

Komatsu, M., Waguri, S., Ueno, T., Iwata, J., Murata, S., Tanida, I., . . . Chiba, T. (2005). Impairment of starvation-induced and constitutive autophagy in Atg7-deficient mice. *J Cell Biol, 169*(3), 425-434. doi: 10.1083/jcb.200412022

Korac, J., Schaeffer, V., Kovacevic, I., Clement, A. M., Jungblut, B., Behl, C., . . . Dikic, I. (2013). Ubiquitin-independent function of optineurin in autophagic clearance of protein aggregates. *J Cell Sci, 126*(Pt 2), 580-592. doi: 10.1242/jcs.114926

Kornblihtt, A. R., de la Mata, M., Fededa, J. P., Munoz, M. J., & Nogues, G. (2004). Multiple links between transcription and splicing. *RNA, 10*(10), 1489-1498. doi: 10.1261/rna.7100104

Kosaka, N., Yoshioka, Y., Fujita, Y., & Ochiya, T. (2016). Versatile roles of extracellular vesicles in cancer. *J Clin Invest, 126*(4), 1163-1172. doi: 10.1172/JCI81130

Kraft, C., Deplazes, A., Sohrmann, M., & Peter, M. (2008). Mature ribosomes are selectively degraded upon starvation by an autophagy pathway requiring the Ubp3p/Bre5p ubiquitin protease. *Nat Cell Biol, 10*(5), 602-610. doi: 10.1038/ncb1723

Krick, R., Muehe, Y., Prick, T., Bremer, S., Schlotterhose, P., Eskelinen, E. L., . . . Thumm, M. (2008). Piecemeal microautophagy of the nucleus requires the core macroautophagy genes. *Mol Biol Cell, 19*(10), 4492-4505. doi: 10.1091/mbc.E08-04-0363

Ktistakis, N. T., & Tooze, S. A. (2016). Digesting the Expanding Mechanisms of Autophagy. *Trends Cell Biol, 26*(8), 624-635. doi: 10.1016/j.tcb.2016.03.006

Kuma, A., Hatano, M., Matsui, M., Yamamoto, A., Nakaya, H., Yoshimori, T., . . . Mizushima, N. (2004). The role of autophagy during the early neonatal starvation period. *Nature, 432*(7020), 1032-1036. doi: 10.1038/nature03029

Kumar, V., Kashav, T., Islam, A., Ahmad, F., & Hassan, M. I. (2016). Structural insight into C9orf72 hexanucleotide repeat expansions: Towards new therapeutic targets in FTD-ALS. *Neurochem Int, 100*, 11-20. doi: 10.1016/j.neuint.2016.08.008

Kundu, M., & Thompson, C. B. (2008). Autophagy: basic principles and relevance to disease. *Annu Rev Pathol, 3*, 427-455. doi: 10.1146/annurev.pathmechdis.2.010506.091842

Kung, C. P., Budina, A., Balaburski, G., Bergenstock, M. K., & Murphy, M. (2011). Autophagy in tumor suppression and cancer therapy. *Crit Rev Eukaryot Gene Expr, 21*(1), 71-100.

Kuo, S. Y., Castoreno, A. B., Aldrich, L. N., Lassen, K. G., Goel, G., Dancik, V., . . . Xavier, R. J. (2015). Small-molecule enhancers of autophagy modulate cellular disease phenotypes suggested by human genetics. *Proc Natl Acad Sci U S A, 112*(31), E4281-4287. doi: 10.1073/pnas.1512289112

Kurosawa, M., Matsumoto, G., Kino, Y., Okuno, M., Kurosawa-Yamada, M., Washizu, C., . . . Nukina, N. (2015). Depletion of p62 reduces nuclear inclusions and paradoxically ameliorates disease phenotypes in Huntington's model mice. *Hum Mol Genet, 24*(4), 1092-1105. doi: 10.1093/hmg/ddu522

Kwiatkowski, T. J., Jr., Bosco, D. A., Leclerc, A. L., Tamrazian, E., Vanderburg, C. R., Russ, C., . . . Brown, R. H., Jr. (2009). Mutations in the FUS/TLS gene on chromosome 16 cause familial amyotrophic lateral sclerosis. *Science, 323*(5918), 1205-1208. doi: 10.1126/science.1166066

Kwon, M. J., Baek, W., Ki, C. S., Kim, H. Y., Koh, S. H., Kim, J. W., & Kim, S. H. (2012). Screening of the SOD1, FUS, TARDBP, ANG, and OPTN mutations in Korean patients with familial and sporadic ALS. *Neurobiol Aging, 33*(5), 1017 e1017-1023. doi: 10.1016/j.neurobiolaging.2011.12.003

Kyei, G. B., Dinkins, C., Davis, A. S., Roberts, E., Singh, S. B., Dong, C., . . . Deretic, V. (2009). Autophagy pathway intersects with HIV-1 biosynthesis and regulates viral yields in macrophages. *J Cell Biol, 186*(2), 255-268. doi: 10.1083/jcb.200903070

Laddha, S. V., Ganesan, S., Chan, C. S., & White, E. (2014a). Mutational landscape of the essential autophagy gene BECN1 in human cancers. *Mol Cancer Res, 12*(4), 485-490. doi: 10.1158/1541-7786.MCR-13-0614

Laddha, S. V., Ganesan, S., Chan, C. S., & White, E. (2014b). Mutational Landscape of the Essential Autophagy Gene BECN1 in Human Cancers. *Mol Cancer Res*. doi: 10.1158/1541-7786.MCR-13-0614

Lagier-Tourenne, C., Baughn, M., Rigo, F., Sun, S., Liu, P., Li, H. R., . . . Ravits, J. (2013). Targeted degradation of sense and antisense C9orf72 RNA foci as therapy for ALS and frontotemporal degeneration. *Proc Natl Acad Sci U S A, 110*(47), E4530-4539. doi: 10.1073/pnas.1318835110

Lagier-Tourenne, C., & Cleveland, D. W. (2009). Rethinking ALS: the FUS about TDP-43. *Cell, 136*(6), 1001-1004. doi: 10.1016/j.cell.2009.03.006

Lagier-Tourenne, C., Polymenidou, M., & Cleveland, D. W. (2010). TDP-43 and FUS/TLS: emerging roles in RNA processing and neurodegeneration. *Hum Mol Genet, 19*(R1), R46-64. doi: 10.1093/hmg/ddq137

Lagier-Tourenne, C., Polymenidou, M., Hutt, K. R., Vu, A. Q., Baughn, M., Huelga, S. C., . . . Yeo, G. W. (2012). Divergent roles of ALS-linked proteins FUS/TLS and TDP-43 intersect in processing long pre-mRNAs. *Nat Neurosci, 15*(11), 1488-1497. doi: 10.1038/nn.3230

Lamb, C. A., Yoshimori, T., & Tooze, S. A. (2013). The autophagosome: origins unknown, biogenesis complex. *Nat Rev Mol Cell Biol, 14*(12), 759-774. doi: 10.1038/nrm3696

Lardeux, B. R., Heydrick, S. J., & Mortimore, G. E. (1987). RNA degradation in perfused rat liver as determined from the release of [14C]cytidine. *J Biol Chem, 262*(30), 14507-14513.

Lardeux, B. R., Heydrick, S. J., & Mortimore, G. E. (1988). Rates of rat liver RNA degradation in vivo as determined from cytidine release during brief cyclic perfusion in situ. *Biochem J, 252*(2), 363-367.

Lardeux, B. R., & Mortimore, G. E. (1987). Amino acid and hormonal control of macromolecular turnover in perfused rat liver. Evidence for selective autophagy. *J Biol Chem, 262*(30), 14514-14519.

Larsen, S. C., Sylvestersen, K. B., Mund, A., Lyon, D., Mullari, M., Madsen, M. V., . . . Nielsen, M. L. (2016). Proteome-wide analysis of arginine monomethylation reveals widespread occurrence in human cells. *Sci Signal, 9*(443), rs9. doi: 10.1126/scisignal.aaf7329

Lattante, S., de Calbiac, H., Le Ber, I., Brice, A., Ciura, S., & Kabashi, E. (2015). Sqstm1 knock-down causes a locomotor phenotype ameliorated by rapamycin in a zebrafish model of ALS/FTLD. *Hum Mol Genet, 24*(6), 1682-1690. doi: 10.1093/hmg/ddu580

Laulagnier, K., Javalet C., Hemming, F.J., Sadoul, R. (2015). Purification and analysis of exosomes released by mature cortical neurons following synaptic activation. *Methods in Molecular Biology*.

Lazarou, M., Sliter, D. A., Kane, L. A., Sarraf, S. A., Wang, C., Burman, J. L., . . . Youle, R. J. (2015). The ubiquitin kinase PINK1 recruits autophagy receptors to induce mitophagy. *Nature, 524*(7565), 309-314. doi: 10.1038/nature14893

Le Ber, I., Camuzat, A., Guerreiro, R., Bouya-Ahmed, K., Bras, J., Nicolas, G., . . . Genetic Research Network on, Ftd Ftd-Als. (2013). SQSTM1 mutations in French patients with frontotemporal dementia or frontotemporal dementia with amyotrophic lateral sclerosis. *JAMA Neurol, 70*(11), 1403-1410. doi: 10.1001/jamaneurol.2013.3849

Lee, E., Iskow, R., Yang, L., Gokcumen, O., Haseley, P., Luquette, L. J., 3rd, . . . Cancer Genome Atlas Research, Network. (2012). Landscape of somatic retrotransposition in human cancers. *Science, 337*(6097), 967-971. doi: 10.1126/science.1222077

Lee, H. H., Elia, N., Ghirlando, R., Lippincott-Schwartz, J., & Hurley, J. H. (2008). Midbody targeting of the ESCRT machinery by a noncanonical coiled coil in CEP55. *Science, 322*(5901), 576-580. doi: 10.1126/science.1162042

Lee, J., & Bedford, M. T. (2002). PABP1 identified as an arginine methyltransferase substrate using high-density protein arrays. *EMBO Rep, 3*(3), 268-273. doi: 10.1093/embo-reports/kvf052

Lee, J. Y., Koga, H., Kawaguchi, Y., Tang, W., Wong, E., Gao, Y. S., . . . Yao, T. P. (2010). HDAC6 controls autophagosome maturation essential for ubiquitin-selective quality-control autophagy. *EMBO J, 29*(5), 969-980. doi: 10.1038/emboj.2009.405

Lee, K. H., Zhang, P., Kim, H. J., Mitrea, D. M., Sarkar, M., Freibaum, B. D., . . . Taylor, J. P. (2016). C9orf72 Dipeptide Repeats Impair the Assembly, Dynamics, and Function of Membrane-Less Organelles. *Cell, 167*(3), 774-788 e717. doi: 10.1016/j.cell.2016.10.002

Lee, Y. B., Chen, H. J., Peres, J. N., Gomez-Deza, J., Attig, J., Stalekar, M., . . . Shaw, C. E. (2013). Hexanucleotide repeats in ALS/FTD form length-dependent RNA foci, sequester RNA binding proteins, and are neurotoxic. *Cell Rep, 5*(5), 1178-1186. doi: 10.1016/j.celrep.2013.10.049

Lee, Y. J., Wei, H. M., Chen, L. Y., & Li, C. (2014). Localization of SERBP1 in stress granules and nucleoli. *FEBS J, 281*(1), 352-364. doi: 10.1111/febs.12606

Lee, Y. K., Jun, Y. W., Choi, H. E., Huh, Y. H., Kaang, B. K., Jang, D. J., & Lee, J. A. (2017). Development of LC3/GABARAP sensors containing a LIR and a hydrophobic domain to monitor autophagy. *EMBO J, 36*(8), 1100-1116. doi: 10.15252/embj.201696315

Lemmens, R., Moore, M. J., Al-Chalabi, A., Brown, R. H., Jr., & Robberecht, W. (2010). RNA metabolism and the pathogenesis of motor neuron diseases. *Trends Neurosci, 33*(5), 249-258. doi: 10.1016/j.tins.2010.02.003

Lenzi, J., De Santis, R., de Turris, V., Morlando, M., Laneve, P., Calvo, A., . . . Bozzoni, I. (2015). ALS mutant FUS proteins are recruited into stress granules in induced pluripotent stem cell-derived motoneurons. *Dis Model Mech, 8*(7), 755-766. doi: 10.1242/dmm.020099

Levine, B., & Klionsky, D. J. (2004). Development by self-digestion: molecular mechanisms and biological functions of autophagy. *Dev Cell, 6*(4), 463-477.

Levine, B., & Kroemer, G. (2008). Autophagy in the pathogenesis of disease. *Cell, 132*(1), 27-42. doi: 10.1016/j.cell.2007.12.018

Li, CH; Tam, PKS. (1998). An Iterative Algorithm for Minimum Cross Entropy Thresholding. *Pattern Recognition Letters, 19*(8), 771-776.

Li, Q., Lau, A., Morris, T. J., Guo, L., Fordyce, C. B., & Stanley, E. F. (2004). A syntaxin 1, Galpha(o), and N-type calcium channel complex at a presynaptic nerve terminal: analysis by quantitative immunocolocalization. *J Neurosci, 24*(16), 4070-4081. doi: 10.1523/JNEUROSCI.0346-04.2004

Li, Q., Lee, J. A., & Black, D. L. (2007). Neuronal regulation of alternative pre-mRNA splicing. *Nat Rev Neurosci, 8*(11), 819-831. doi: 10.1038/nrn2237

Li, S., Yang, P., Tian, E., & Zhang, H. (2013). Arginine methylation modulates autophagic degradation of PGL granules in C. elegans. *Mol Cell, 52*(3), 421-433. doi: 10.1016/j.molcel.2013.09.014

Li, X., Zhang, J., Jia, R., Cheng, V., Xu, X., Qiao, W., . . . Cen, S. (2013). The MOV10 helicase inhibits LINE-1 mobility. *J Biol Chem, 288*(29), 21148-21160. doi: 10.1074/jbc.M113.465856

Li, Y., Guo, Y., Wang, X., Yu, X., Duan, W., Hong, K., . . . Li, C. (2015). Trehalose decreases mutant SOD1 expression and alleviates motor deficiency in early but not end-stage amyotrophic lateral sclerosis in a SOD1-G93A mouse model. *Neuroscience, 298*, 12-25. doi: 10.1016/j.neuroscience.2015.03.061

Li, Y. R., King, O. D., Shorter, J., & Gitler, A. D. (2013). Stress granules as crucibles of ALS pathogenesis. *J Cell Biol, 201*(3), 361-372. doi: 10.1083/jcb.201302044

Liang, X. H., Jackson, S., Seaman, M., Brown, K., Kempkes, B., Hibshoosh, H., & Levine, B. (1999). Induction of autophagy and inhibition of tumorigenesis by beclin 1. *Nature, 402*(6762), 672-676. doi: 10.1038/45257

Lin, J., Jin, X., Bu, Y., Cao, D., Zhang, N., Li, S., . . . Jiang, Y. (2012). Efficient synthesis of RITA and its analogues: derivation of analogues with improved antiproliferative activity via modulation of p53/miR-34a pathway. *Org Biomol Chem, 10*(48), 9734-9746. doi: 10.1039/c2ob26627j

Lin, Y., Protter, D. S., Rosen, M. K., & Parker, R. (2015). Formation and Maturation of Phase-Separated Liquid Droplets by RNA-Binding Proteins. *Mol Cell, 60*(2), 208-219. doi: 10.1016/j.molcel.2015.08.018

Ling, J. P., Pletnikova, O., Troncoso, J. C., & Wong, P. C. (2015). TDP-43 repression of nonconserved cryptic exons is compromised in ALS-FTD. *Science, 349*(6248), 650-655. doi: 10.1126/science.aab0983

Ling, S. C., Polymenidou, M., & Cleveland, D. W. (2013). Converging mechanisms in ALS and FTD: disrupted RNA and protein homeostasis. *Neuron, 79*(3), 416-438. doi: 10.1016/j.neuron.2013.07.033

Liu-Yesucevitz, L., Bilgutay, A., Zhang, Y. J., Vanderweyde, T., Citro, A., Mehta, T., . . . Wolozin, B. (2010). Tar DNA binding protein-43 (TDP-43) associates with stress granules: analysis of cultured cells and pathological brain tissue. *PLoS One, 5*(10), e13250. doi: 10.1371/journal.pone.0013250

Liu, J., Zhang, Y., Liu, A., Wang, J., Li, L., Chen, X., . . . Liu, Y. (2016). Distinct Dasatinib-Induced Mechanisms of Apoptotic Response and Exosome Release in

Imatinib-Resistant Human Chronic Myeloid Leukemia Cells. *Int J Mol Sci, 17*(4), 531. doi: 10.3390/ijms17040531

Liu, K., Lee, J., Kim, J. Y., Wang, L., Tian, Y., Chan, S. T., . . . Ou, J. J. (2017). Mitophagy Controls the Activities of Tumor Suppressor p53 to Regulate Hepatic Cancer Stem Cells. *Mol Cell, 68*(2), 281-292 e285. doi: 10.1016/j.molcel.2017.09.022

Liu, L., Feng, D., Chen, G., Chen, M., Zheng, Q., Song, P., . . . Chen, Q. (2012). Mitochondrial outer-membrane protein FUNDC1 mediates hypoxia-induced mitophagy in mammalian cells. *Nat Cell Biol, 14*(2), 177-185. doi: 10.1038/ncb2422

Liu, Q., & Dreyfuss, G. (1995). In vivo and in vitro arginine methylation of RNA-binding proteins. *Mol Cell Biol, 15*(5), 2800-2808.

Liu, X. M., Sun, L. L., Hu, W., Ding, Y. H., Dong, M. Q., & Du, L. L. (2015). ESCRTs Cooperate with a Selective Autophagy Receptor to Mediate Vacuolar Targeting of Soluble Cargos. *Mol Cell, 59*(6), 1035-1042. doi: 10.1016/j.molcel.2015.07.034

Liu, Y. L., Yang, P. M., Shun, C. T., Wu, M. S., Weng, J. R., & Chen, C. C. (2010). Autophagy potentiates the anti-cancer effects of the histone deacetylase inhibitors in hepatocellular carcinoma. *Autophagy, 6*(8), 1057-1065.

Lock, R., Kenific, C. M., Leidal, A. M., Salas, E., & Debnath, J. (2014). Autophagy-dependent production of secreted factors facilitates oncogenic RAS-driven invasion. *Cancer Discov, 4*(4), 466-479. doi: 10.1158/2159-8290.CD-13-0841

Lockstone, H. E. (2011). Exon array data analysis using Affymetrix power tools and R statistical software. *Brief Bioinform, 12*(6), 634-644. doi: 10.1093/bib/bbq086

Lotvall, J., Hill, A. F., Hochberg, F., Buzas, E. I., Di Vizio, D., Gardiner, C., . . . Thery, C. (2014). Minimal experimental requirements for definition of extracellular vesicles and their functions: a position statement from the International Society for Extracellular Vesicles. *J Extracell Vesicles, 3*, 26913. doi: 10.3402/jev.v3.26913

Luft, J. H. (1961). Improvements in epoxy resin embedding methods. *J Biophys Biochem Cytol, 9*, 409-414.

Lv, M. M., Zhu, X. Y., Chen, W. X., Zhong, S. L., Hu, Q., Ma, T. F., . . . Zhao, J. H. (2014). Exosomes mediate drug resistance transfer in MCF-7 breast cancer cells and a probable mechanism is delivery of P-glycoprotein. *Tumour Biol, 35*(11), 10773-10779. doi: 10.1007/s13277-014-2377-z

Lykke-Andersen, S., & Jensen, T. H. (2015). Nonsense-mediated mRNA decay: an intricate machinery that shapes transcriptomes. *Nat Rev Mol Cell Biol, 16*(11), 665-677. doi: 10.1038/nrm4063

Mackenzie, I. R., Frick, P., Grasser, F. A., Gendron, T. F., Petrucelli, L., Cashman, N. R., . . . Neumann, M. (2015). Quantitative analysis and clinico-pathological correlations of different dipeptide repeat protein pathologies in C9ORF72 mutation carriers. *Acta Neuropathol, 130*(6), 845-861. doi: 10.1007/s00401-015-1476-2

Mackenzie, I. R., Frick, P., & Neumann, M. (2014). The neuropathology associated with repeat expansions in the C9ORF72 gene. *Acta Neuropathol, 127*(3), 347-357. doi: 10.1007/s00401-013-1232-4

Mackenzie, I. R., Munoz, D. G., Kusaka, H., Yokota, O., Ishihara, K., Roeber, S., . . . Neumann, M. (2011). Distinct pathological subtypes of FTLD-FUS. *Acta Neuropathol, 121*(2), 207-218. doi: 10.1007/s00401-010-0764-0

Maharjan, N., Kunzli, C., Buthey, K., & Saxena, S. (2016). C9ORF72 Regulates Stress Granule Formation and Its Deficiency Impairs Stress Granule Assembly, Hypersensitizing Cells to Stress. *Mol Neurobiol*. doi: 10.1007/s12035-016-9850-1

Majcher, V., Goode, A., James, V., & Layfield, R. (2015). Autophagy receptor defects and ALS-FTLD. *Mol Cell Neurosci, 66*(Pt A), 43-52. doi: 10.1016/j.mcn.2015.01.002

Majounie, E., Renton, A. E., Mok, K., Dopper, E. G., Waite, A., Rollinson, S., . . . Traynor, B. J. (2012). Frequency of the C9orf72 hexanucleotide repeat expansion in patients with amyotrophic lateral sclerosis and frontotemporal dementia: a cross-sectional study. *Lancet Neurol, 11*(4), 323-330. doi: 10.1016/S1474-4422(12)70043-1

Mandell, M. A., Jain, A., Arko-Mensah, J., Chauhan, S., Kimura, T., Dinkins, C., . . . Deretic, V. (2014). TRIM proteins regulate autophagy and can target autophagic substrates by direct recognition. *Dev Cell, 30*(4), 394-409. doi: 10.1016/j.devcel.2014.06.013

Marino, G., Fernandez, A. F., Cabrera, S., Lundberg, Y. W., Cabanillas, R., Rodriguez, F., . . . Lopez-Otin, C. (2010). Autophagy is essential for mouse sense of balance. *J Clin Invest, 120*(7), 2331-2344. doi: 10.1172/JCI42601

Marks, M. S., Heijnen, H. F., & Raposo, G. (2013). Lysosome-related organelles: unusual compartments become mainstream. *Curr Opin Cell Biol, 25*(4), 495-505. doi: 10.1016/j.ceb.2013.04.008

Martin, K. C., & Ephrussi, A. (2009). mRNA localization: gene expression in the spatial dimension. *Cell, 136*(4), 719-730. doi: 10.1016/j.cell.2009.01.044

Martin S. Taylor, John LaCava, Paolo Mita, Kelly R. Molloy, Cheng Ran Lisa Huang, Donghui Li, Emily M. Adney, Hua Jiang, Kathleen H. Burns, Brian T. Chait, Michael P. Rout, Jef D. Boeke, Lixin Dai. (2013). Affinity Proteomics Reveals Human Host Factors Implicated in Discrete Stages of LINE-1 Retrotransposition. *Cell, 155*(5), 1034-1048.

Martinez-Vicente, M., Talloczy, Z., Wong, E., Tang, G., Koga, H., Kaushik, S., . . . Cuervo, A. M. (2010). Cargo recognition failure is responsible for inefficient autophagy in Huntington's disease. *Nat Neurosci, 13*(5), 567-576. doi: 10.1038/nn.2528

Martinez, J., Malireddi, R. K., Lu, Q., Cunha, L. D., Pelletier, S., Gingras, S., . . . Green, D. R. (2015). Molecular characterization of LC3-associated phagocytosis reveals distinct roles for Rubicon, NOX2 and autophagy proteins. *Nat Cell Biol, 17*(7), 893-906. doi: 10.1038/ncb3192

Marusyk, A., Almendro, V., & Polyak, K. (2012). Intra-tumour heterogeneity: a looking glass for cancer? *Nat Rev Cancer, 12*(5), 323-334. doi: 10.1038/nrc3261

Maruyama, H., Morino, H., Ito, H., Izumi, Y., Kato, H., Watanabe, Y., . . . Kawakami, H. (2010). Mutations of optineurin in amyotrophic lateral sclerosis. *Nature, 465*(7295), 223-226. doi: 10.1038/nature08971

Mathew, B., Suresh, J., Anbazhagan, S., & Mathew, G. E. (2013). Pyrazoline: a promising scaffold for the inhibition of monoamine oxidase. *Cent Nerv Syst Agents Med Chem, 13*(3), 195-206.

Mathew, R., Karp, C. M., Beaudoin, B., Vuong, N., Chen, G., Chen, H. Y., . . . White, E. (2009). Autophagy suppresses tumorigenesis through elimination of p62. *Cell, 137*(6), 1062-1075. doi: 10.1016/j.cell.2009.03.048

Mathew, R., Kongara, S., Beaudoin, B., Karp, C. M., Bray, K., Degenhardt, K., . . . White, E. (2007). Autophagy suppresses tumor progression by limiting chromosomal instability. *Genes Dev, 21*(11), 1367-1381. doi: 10.1101/gad.1545107

Matsumoto, G., Stojanovic, A., Holmberg, C. I., Kim, S., & Morimoto, R. I. (2005). Structural properties and neuronal toxicity of amyotrophic lateral sclerosis-associated Cu/Zn superoxide dismutase 1 aggregates. *J Cell Biol, 171*(1), 75-85. doi: 10.1083/jcb.200504050

Matsumoto, G., Wada, K., Okuno, M., Kurosawa, M., & Nukina, N. (2011). Serine 403 phosphorylation of p62/SQSTM1 regulates selective autophagic clearance of ubiquitinated proteins. *Mol Cell, 44*(2), 279-289. doi: 10.1016/j.molcel.2011.07.039

Matus, S., Bosco, D. A., & Hetz, C. (2014). Autophagy meets fused in sarcoma-positive stress granules. *Neurobiol Aging, 35*(12), 2832-2835. doi: 10.1016/j.neurobiolaging.2014.08.019

Mazroui, R., Huot, M. E., Tremblay, S., Filion, C., Labelle, Y., & Khandjian, E. W. (2002). Trapping of messenger RNA by Fragile X Mental Retardation protein into cytoplasmic granules induces translation repression. *Hum Mol Genet, 11*(24), 3007-3017.

McClelland, S. E., Burrell, R. A., & Swanton, C. (2009). Chromosomal instability: a composite phenotype that influences sensitivity to chemotherapy. *Cell Cycle, 8*(20), 3262-3266.

McDonald, K. K., Aulas, A., Destroismaisons, L., Pickles, S., Beleac, E., Camu, W., . . . Vande Velde, C. (2011). TAR DNA-binding protein 43 (TDP-43) regulates stress granule dynamics via differential regulation of G3BP and TIA-1. *Hum Mol Genet, 20*(7), 1400-1410. doi: 10.1093/hmg/ddr021

McKnight, N. C., Zhong, Y., Wold, M. S., Gong, S., Phillips, G. R., Dou, Z., . . . Yue, Z. (2014). Beclin 1 is required for neuron viability and regulates endosome pathways via the UVRAG-VPS34 complex. *PLoS Genet, 10*(10), e1004626. doi: 10.1371/journal.pgen.1004626

Meister, G., Eggert, C., Buhler, D., Brahms, H., Kambach, C., & Fischer, U. (2001). Methylation of Sm proteins by a complex containing PRMT5 and the putative U snRNP assembly factor pICln. *Curr Biol, 11*(24), 1990-1994.

Melo, S. A., Sugimoto, H., O'Connell, J. T., Kato, N., Villanueva, A., Vidal, A., . . . Kalluri, R. (2014). Cancer Exosomes Perform Cell-Independent MicroRNA Biogenesis

and Promote Tumorigenesis. *Cancer Cell, 26*(5), 707-721. doi: 10.1016/j.ccell.2014.09.005

Menzies, F. M., Fleming, A., Caricasole, A., Bento, C. F., Andrews, S. P., Ashkenazi, A., . . . Rubinsztein, D. C. (2017). Autophagy and Neurodegeneration: Pathogenic Mechanisms and Therapeutic Opportunities. *Neuron, 93*(5), 1015-1034. doi: 10.1016/j.neuron.2017.01.022

Milano, V., Piao, Y., LaFortune, T., & de Groot, J. (2009). Dasatinib-induced autophagy is enhanced in combination with temozolomide in glioma. *Mol Cancer Ther, 8*(2), 394-406. doi: 10.1158/1535-7163.MCT-08-0669

Millecamps, S., Boillee, S., Chabrol, E., Camu, W., Cazeneuve, C., Salachas, F., . . . LeGuern, E. (2011). Screening of OPTN in French familial amyotrophic lateral sclerosis. *Neurobiol Aging, 32*(3), 557 e511-553. doi: 10.1016/j.neurobiolaging.2010.11.005

Miller, T. M., Pestronk, A., David, W., Rothstein, J., Simpson, E., Appel, S. H., . . . Cudkowicz, M. E. (2013). An antisense oligonucleotide against SOD1 delivered intrathecally for patients with SOD1 familial amyotrophic lateral sclerosis: a phase 1, randomised, first-in-man study. *Lancet Neurol, 12*(5), 435-442. doi: 10.1016/S1474-4422(13)70061-9

Mindell, J. A. (2012). Lysosomal acidification mechanisms. *Annu Rev Physiol, 74*, 69-86. doi: 10.1146/annurev-physiol-012110-142317

Mizielinska, S., Gronke, S., Niccoli, T., Ridler, C. E., Clayton, E. L., Devoy, A., . . . Isaacs, A. M. (2014). C9orf72 repeat expansions cause neurodegeneration in Drosophila through arginine-rich proteins. *Science, 345*(6201), 1192-1194. doi: 10.1126/science.1256800

Mizushima, N., & Komatsu, M. (2011). Autophagy: renovation of cells and tissues. *Cell, 147*(4), 728-741. doi: 10.1016/j.cell.2011.10.026

Mizushima, N., Levine, B., Cuervo, A. M., & Klionsky, D. J. (2008). Autophagy fights disease through cellular self-digestion. *Nature, 451*(7182), 1069-1075. doi: 10.1038/nature06639

Mizushima, N., Noda, T., Yoshimori, T., Tanaka, Y., Ishii, T., George, M. D., . . . Ohsumi, Y. (1998). A protein conjugation system essential for autophagy. *Nature, 395*(6700), 395-398. doi: 10.1038/26506

Mizushima, N., Yoshimori, T., & Ohsumi, Y. (2011). The role of Atg proteins in autophagosome formation. *Annu Rev Cell Dev Biol, 27*, 107-132. doi: 10.1146/annurev-cellbio-092910-154005

Moeller, B. J., Cao, Y., Li, C. Y., & Dewhirst, M. W. (2004). Radiation activates HIF-1 to regulate vascular radiosensitivity in tumors: role of reoxygenation, free radicals, and stress granules. *Cancer Cell, 5*(5), 429-441.

Moldovan, J. B., & Moran, J. V. (2015). The Zinc-Finger Antiviral Protein ZAP Inhibits LINE and Alu Retrotransposition. *PLoS Genet, 11*(5), e1005121. doi: 10.1371/journal.pgen.1005121

Molliex, A., Temirov, J., Lee, J., Coughlin, M., Kanagaraj, A. P., Kim, H. J., . . . Taylor, J. P. (2015). Phase separation by low complexity domains promotes stress granule

assembly and drives pathological fibrillization. *Cell, 163*(1), 123-133. doi: 10.1016/j.cell.2015.09.015

Morales, C. R., & Hecht, N. B. (1994). Poly(A)+ ribonucleic acids are enriched in spermatocyte nuclei but not in chromatoid bodies in the rat testis. *Biol Reprod, 50*(2), 309-319.

Morimoto, N., Nagai, M., Ohta, Y., Miyazaki, K., Kurata, T., Morimoto, M., . . . Abe, K. (2007). Increased autophagy in transgenic mice with a G93A mutant SOD1 gene. *Brain Res, 1167*, 112-117. doi: 10.1016/j.brainres.2007.06.045

Mortimore, G. E., Lardeux, B. R., & Heydrick, S. J. (1989). Mechanism and control of protein and RNA degradation in the rat hepatocyte: two modes of autophagic sequestration. *Revis Biol Celular, 20*, 79-96.

Mostowy, S., & Cossart, P. (2012). Septins: the fourth component of the cytoskeleton. *Nat Rev Mol Cell Biol, 13*(3), 183-194. doi: 10.1038/nrm3284

Motley, A. M., Nuttall, J. M., & Hettema, E. H. (2012). Pex3-anchored Atg36 tags peroxisomes for degradation in Saccharomyces cerevisiae. *EMBO J, 31*(13), 2852-2868. doi: 10.1038/emboj.2012.151

Motzer, R. J., Escudier, B., Oudard, S., Hutson, T. E., Porta, C., Bracarda, S., . . . Group, Record- Study. (2008). Efficacy of everolimus in advanced renal cell carcinoma: a double-blind, randomised, placebo-controlled phase III trial. *Lancet, 372*(9637), 449-456. doi: 10.1016/S0140-6736(08)61039-9

Mukherjee, A., Patel, B., Koga, H., Cuervo, A. M., & Jenny, A. (2016). Selective endosomal microautophagy is starvation-inducible in Drosophila. *Autophagy, 12*(11), 1984-1999. doi: 10.1080/15548627.2016.1208887

Munoz, M. J., Perez Santangelo, M. S., Paronetto, M. P., de la Mata, M., Pelisch, F., Boireau, S., . . . Kornblihtt, A. R. (2009). DNA damage regulates alternative splicing through inhibition of RNA polymerase II elongation. *Cell, 137*(4), 708-720. doi: 10.1016/j.cell.2009.03.010

Munz, C. (2017). The Macroautophagy Machinery in Endo- and Exocytosis. *J Mol Biol, 429*(4), 473-485. doi: 10.1016/j.jmb.2016.11.028

Muotri, A. R., Chu, V. T., Marchetto, M. C., Deng, W., Moran, J. V., & Gage, F. H. (2005). Somatic mosaicism in neuronal precursor cells mediated by L1 retrotransposition. *Nature, 435*(7044), 903-910. doi: nature03663 [pii]

10.1038/nature03663

Muotri, A. R., Marchetto, M. C., Coufal, N. G., Oefner, R., Yeo, G., Nakashima, K., & Gage, F. H. (2010). L1 retrotransposition in neurons is modulated by MeCP2. *Nature, 468*(7322), 443-446. doi: nature09544 [pii]

10.1038/nature09544

Muotri, A. R., Zhao, C., Marchetto, M. C., & Gage, F. H. (2009). Environmental influence on L1 retrotransposons in the adult hippocampus. *Hippocampus, 19*(10), 1002-1007. doi: 10.1002/hipo.20564

Murakami, T., Qamar, S., Lin, J. Q., Schierle, G. S., Rees, E., Miyashita, A., . . . St George-Hyslop, P. (2015). ALS/FTD Mutation-Induced Phase Transition of FUS

Liquid Droplets and Reversible Hydrogels into Irreversible Hydrogels Impairs RNP Granule Function. *Neuron, 88*(4), 678-690. doi: 10.1016/j.neuron.2015.10.030

Murk, J. L., Humbel, B. M., Ziese, U., Griffith, J. M., Posthuma, G., Slot, J. W., . . . Kleijmeer, M. J. (2003). Endosomal compartmentalization in three dimensions: implications for membrane fusion. *Proc Natl Acad Sci U S A, 100*(23), 13332-13337. doi: 10.1073/pnas.2232379100

Murrow, L., Malhotra, R., & Debnath, J. (2015). ATG12-ATG3 interacts with Alix to promote basal autophagic flux and late endosome function. *Nat Cell Biol, 17*(3), 300-310. doi: 10.1038/ncb3112

Myers, J. S., Vincent, B. J., Udall, H., Watkins, W. S., Morrish, T. A., Kilroy, G. E., . . . Batzer, M. A. (2002). A comprehensive analysis of recently integrated human Ta L1 elements. *Am J Hum Genet, 71*(2), 312-326. doi: 10.1086/341718

Netzel, R., Perez-Iratxeta, C., Bork, P., & Andrade, M. A. (2003). The way we write. *EMBO Rep, 4*(5), 446-451. doi: 10.1038/sj.embor.embor833

Neumann, M., Sampathu, D. M., Kwong, L. K., Truax, A. C., Micsenyi, M. C., Chou, T. T., . . . Lee, V. M. (2006). Ubiquitinated TDP-43 in frontotemporal lobar degeneration and amyotrophic lateral sclerosis. *Science, 314*(5796), 130-133. doi: 10.1126/science.1134108

Nishida, Y., Arakawa, S., Fujitani, K., Yamaguchi, H., Mizuta, T., Kanaseki, T., . . . Shimizu, S. (2016). Corrigendum: Discovery of Atg5/Atg7-independent alternative macroautophagy. *Nature, 533*(7601), 130. doi: 10.1038/nature16538

Nixon, R. A. (2013). The role of autophagy in neurodegenerative disease. *Nat Med, 19*(8), 983-997. doi: 10.1038/nm.3232

Noda, N. N., & Inagaki, F. (2015). Mechanisms of Autophagy. *Annu Rev Biophys, 44*, 101-122. doi: 10.1146/annurev-biophys-060414-034248

Novak, I., Kirkin, V., McEwan, D. G., Zhang, J., Wild, P., Rozenknop, A., . . . Dikic, I. (2010). Nix is a selective autophagy receptor for mitochondrial clearance. *EMBO Rep, 11*(1), 45-51. doi: 10.1038/embor.2009.256

O'Rourke, J. G., Bogdanik, L., Yanez, A., Lall, D., Wolf, A. J., Muhammad, A. K., . . . Baloh, R. H. (2016). C9orf72 is required for proper macrophage and microglial function in mice. *Science, 351*(6279), 1324-1329. doi: 10.1126/science.aaf1064

Ogawa, M., Yoshikawa, Y., Kobayashi, T., Mimuro, H., Fukumatsu, M., Kiga, K., . . . Sasakawa, C. (2011). A Tecpr1-dependent selective autophagy pathway targets bacterial pathogens. *Cell Host Microbe, 9*(5), 376-389. doi: 10.1016/j.chom.2011.04.010

Okamoto, K., Kondo-Okamoto, N., & Ohsumi, Y. (2009). Mitochondria-anchored receptor Atg32 mediates degradation of mitochondria via selective autophagy. *Dev Cell, 17*(1), 87-97. doi: 10.1016/j.devcel.2009.06.013

Onorati, A. V., Dyczynski, M., Ojha, R., & Amaravadi, R. K. (2018). Targeting autophagy in cancer. *Cancer, 124*(16), 3307-3318. doi: 10.1002/cncr.31335

Orvedahl, A., Sumpter, R., Jr., Xiao, G., Ng, A., Zou, Z., Tang, Y., . . . Levine, B. (2011). Image-based genome-wide siRNA screen identifies selective autophagy factors. *Nature, 480*(7375), 113-117. doi: 10.1038/nature10546

Ostertag, E. M., Prak, E. T., DeBerardinis, R. J., Moran, J. V., & Kazazian, H. H., Jr. (2000). Determination of L1 retrotransposition kinetics in cultured cells. *Nucleic Acids Res, 28*(6), 1418-1423.

Ostrowski, M., Carmo, N. B., Krumeich, S., Fanget, I., Raposo, G., Savina, A., . . . Thery, C. (2010). Rab27a and Rab27b control different steps of the exosome secretion pathway. *Nat Cell Biol, 12*(1), 19-30; sup pp 11-13. doi: 10.1038/ncb2000

Panas, M. D., Ivanov, P., & Anderson, P. (2016). Mechanistic insights into mammalian stress granule dynamics. *J Cell Biol, 215*(3), 313-323. doi: 10.1083/jcb.201609081

Pankiv, S., Clausen, T. H., Lamark, T., Brech, A., Bruun, J. A., Outzen, H., . . . Johansen, T. (2007). p62/SQSTM1 binds directly to Atg8/LC3 to facilitate degradation of ubiquitinated protein aggregates by autophagy. *J Biol Chem, 282*(33), 24131-24145. doi: 10.1074/jbc.M702824200

Papinski, D., Schuschnig, M., Reiter, W., Wilhelm, L., Barnes, C. A., Maiolica, A., . . . Kraft, C. (2014). Early steps in autophagy depend on direct phosphorylation of Atg9 by the Atg1 kinase. *Mol Cell, 53*(3), 471-483. doi: 10.1016/j.molcel.2013.12.011

Parker, S. J., Meyerowitz, J., James, J. L., Liddell, J. R., Crouch, P. J., Kanninen, K. M., & White, A. R. (2012). Endogenous TDP-43 localized to stress granules can subsequently form protein aggregates. *Neurochem Int, 60*(4), 415-424. doi: 10.1016/j.neuint.2012.01.019

Parolini, I., Federici, C., Raggi, C., Lugini, L., Palleschi, S., De Milito, A., . . . Fais, S. (2009). Microenvironmental pH is a key factor for exosome traffic in tumor cells. *J Biol Chem, 284*(49), 34211-34222. doi: 10.1074/jbc.M109.041152

Pasto, A., Pagotto, A., Pilotto, G., De Paoli, A., De Salvo, G. L., Baldoni, A., . . . Amadori, A. (2017). Resistance to glucose starvation as metabolic trait of platinum-resistant human epithelial ovarian cancer cells. *Oncotarget, 8*(4), 6433-6445. doi: 10.18632/oncotarget.14118

Patel, A., Lee, H. O., Jawerth, L., Maharana, S., Jahnel, M., Hein, M. Y., . . . Alberti, S. (2015). A Liquid-to-Solid Phase Transition of the ALS Protein FUS Accelerated by Disease Mutation. *Cell, 162*(5), 1066-1077. doi: 10.1016/j.cell.2015.07.047

Patel, K. K., Miyoshi, H., Beatty, W. L., Head, R. D., Malvin, N. P., Cadwell, K., . . . Stappenbeck, T. S. (2013). Autophagy proteins control goblet cell function by potentiating reactive oxygen species production. *EMBO J, 32*(24), 3130-3144. doi: 10.1038/emboj.2013.233

Peinado, H., Aleckovic, M., Lavotshkin, S., Matei, I., Costa-Silva, B., Moreno-Bueno, G., . . . Lyden, D. (2012). Melanoma exosomes educate bone marrow progenitor cells toward a pro-metastatic phenotype through MET. *Nat Med, 18*(6), 883-891. doi: 10.1038/nm.2753

Peng, J., Zhang, R., Cui, Y., Liu, H., Zhao, X., Huang, L., . . . Yu, L. (2014). Atg5 regulates late endosome and lysosome biogenesis. *Sci China Life Sci, 57*(1), 59-68. doi: 10.1007/s11427-013-4588-8

Pepin, D., Paradis, F., Perez-Iratxeta, C., Picketts, D. J., & Vanderhyden, B. C. (2013). The imitation switch ATPase Snf2l is required for superovulation and regulates Fgl2 in differentiating mouse granulosa cells. *Biol Reprod, 88*(6), 142. doi: 10.1095/biolreprod.112.105742

Perera, R. M., Stoykova, S., Nicolay, B. N., Ross, K. N., Fitamant, J., Boukhali, M., . . . Bardeesy, N. (2015). Transcriptional control of autophagy-lysosome function drives pancreatic cancer metabolism. *Nature, 524*(7565), 361-365. doi: 10.1038/nature14587

Perez-Iratxeta, C., Halloy, J., Moran, F., Martiel, J. L., & Goldbeter, A. (1998). Coexistence of multiple propagating wave-fronts in a regulated enzyme reaction model: link with birhythmicity and multi-threshold excitability. *Biophys Chem, 74*(3), 197-207.

Peters, O. M., Cabrera, G. T., Tran, H., Gendron, T. F., McKeon, J. E., Metterville, J., . . . Brown, R. H., Jr. (2015). Human C9ORF72 Hexanucleotide Expansion Reproduces RNA Foci and Dipeptide Repeat Proteins but Not Neurodegeneration in BAC Transgenic Mice. *Neuron, 88*(5), 902-909. doi: 10.1016/j.neuron.2015.11.018

Piao, Y. S., Wakabayashi, K., Kakita, A., Yamada, M., Hayashi, S., Morita, T., . . . Takahashi, H. (2003). Neuropathology with clinical correlations of sporadic amyotrophic lateral sclerosis: 102 autopsy cases examined between 1962 and 2000. *Brain Pathol, 13*(1), 10-22.

Piccioli, P., & Rubartelli, A. (2013). The secretion of IL-1beta and options for release. *Semin Immunol, 25*(6), 425-429. doi: 10.1016/j.smim.2013.10.007

Pilli, M., Arko-Mensah, J., Ponpuak, M., Roberts, E., Master, S., Mandell, M. A., . . . Deretic, V. (2012). TBK-1 promotes autophagy-mediated antimicrobial defense by controlling autophagosome maturation. *Immunity, 37*(2), 223-234. doi: 10.1016/j.immuni.2012.04.015

Pizzasegola, C., Caron, I., Daleno, C., Ronchi, A., Minoia, C., Carri, M. T., & Bendotti, C. (2009). Treatment with lithium carbonate does not improve disease progression in two different strains of SOD1 mutant mice. *Amyotroph Lateral Scler, 10*(4), 221-228. doi: 10.1080/17482960902803440

Poillet-Perez, L., Despouy, G., Delage-Mourroux, R., & Boyer-Guittaut, M. (2015). Interplay between ROS and autophagy in cancer cells, from tumor initiation to cancer therapy. *Redox Biol, 4*, 184-192. doi: 10.1016/j.redox.2014.12.003

Pratt, M. A., Tibbo, E., Robertson, S. J., Jansson, D., Hurst, K., Perez-Iratxeta, C., . . . Niu, M. Y. (2009). The canonical NF-kappaB pathway is required for formation of luminal mammary neoplasias and is activated in the mammary progenitor population. *Oncogene, 28*(30), 2710-2722. doi: 10.1038/onc.2009.131

Protter, D. S., & Parker, R. (2016). Principles and Properties of Stress Granules. *Trends Cell Biol, 26*(9), 668-679. doi: 10.1016/j.tcb.2016.05.004

Puchner, E. M., Walter, J. M., Kasper, R., Huang, B., & Lim, W. A. (2013). Counting molecules in single organelles with superresolution microscopy allows tracking of the endosome maturation trajectory. *Proc Natl Acad Sci U S A, 110*(40), 16015-16020. doi: 10.1073/pnas.1309676110

Puri, C., Renna, M., Bento, C. F., Moreau, K., & Rubinsztein, D. C. (2013). Diverse autophagosome membrane sources coalesce in recycling endosomes. *Cell, 154*(6), 1285-1299. doi: 10.1016/j.cell.2013.08.044

Qiu, H., Lee, S., Shang, Y., Wang, W. Y., Au, K. F., Kamiya, S., . . . Huang, E. J. (2014). ALS-associated mutation FUS-R521C causes DNA damage and RNA splicing defects. *J Clin Invest, 124*(3), 981-999. doi: 10.1172/JCI72723

Qu, X., Yu, J., Bhagat, G., Furuya, N., Hibshoosh, H., Troxel, A., . . . Levine, B. (2003). Promotion of tumorigenesis by heterozygous disruption of the beclin 1 autophagy gene. *J Clin Invest, 112*(12), 1809-1820. doi: 10.1172/JCI20039

Qu, Y., Franchi, L., Nunez, G., & Dubyak, G. R. (2007). Nonclassical IL-1 beta secretion stimulated by P2X7 receptors is dependent on inflammasome activation and correlated with exosome release in murine macrophages. *J Immunol, 179*(3), 1913-1925.

Quinsay, M. N., Thomas, R. L., Lee, Y., & Gustafsson, A. B. (2010). Bnip3-mediated mitochondrial autophagy is independent of the mitochondrial permeability transition pore. *Autophagy, 6*(7), 855-862.

Ra, E. A., Lee, T. A., Won Kim, S., Park, A., Choi, H. J., Jang, I., . . . Park, B. (2016). TRIM31 promotes Atg5/Atg7-independent autophagy in intestinal cells. *Nat Commun, 7*, 11726. doi: 10.1038/ncomms11726

Rabin, S. J., Kim, J. M., Baughn, M., Libby, R. T., Kim, Y. J., Fan, Y., . . . Ravits, J. (2010). Sporadic ALS has compartment-specific aberrant exon splicing and altered cell-matrix adhesion biology. *Hum Mol Genet, 19*(2), 313-328. doi: 10.1093/hmg/ddp498

Rajendran, L., Honsho, M., Zahn, T. R., Keller, P., Geiger, K. D., Verkade, P., & Simons, K. (2006). Alzheimer's disease beta-amyloid peptides are released in association with exosomes. *Proc Natl Acad Sci U S A, 103*(30), 11172-11177.

Ramesh Babu, J., Lamar Seibenhener, M., Peng, J., Strom, A. L., Kemppainen, R., Cox, N., . . . Wooten, M. W. (2008). Genetic inactivation of p62 leads to accumulation of hyperphosphorylated tau and neurodegeneration. *J Neurochem, 106*(1), 107-120. doi: 10.1111/j.1471-4159.2008.05340.x

Ramesh, N., & Pandey, U. B. (2017). Autophagy Dysregulation in ALS: When Protein Aggregates Get Out of Hand. *Front Mol Neurosci, 10*, 263. doi: 10.3389/fnmol.2017.00263

Rao, S., Tortola, L., Perlot, T., Wirnsberger, G., Novatchkova, M., Nitsch, R., . . . Penninger, J. M. (2014). A dual role for autophagy in a murine model of lung cancer. *Nat Commun, 5*, 3056. doi: 10.1038/ncomms4056

Raposo, G., & Stoorvogel, W. (2013). Extracellular vesicles: exosomes, microvesicles, and friends. *J Cell Biol, 200*(4), 373-383. doi: 10.1083/jcb.201211138

Rappsilber, J., Friesen, W. J., Paushkin, S., Dreyfuss, G., & Mann, M. (2003). Detection of arginine dimethylated peptides by parallel precursor ion scanning mass spectrometry in positive ion mode. *Anal Chem, 75*(13), 3107-3114.

Razi, M., & Futter, C. E. (2006). Distinct roles for Tsg101 and Hrs in multivesicular body formation and inward vesiculation. *Mol Biol Cell, 17*(8), 3469-3483. doi: 10.1091/mbc.e05-11-1054

Record, M., Carayon, K., Poirot, M., & Silvente-Poirot, S. (2014). Exosomes as new vesicular lipid transporters involved in cell-cell communication and various pathophysiologies. *Biochim Biophys Acta, 1841*(1), 108-120. doi: 10.1016/j.bbalip.2013.10.004

Renton, A. E., Majounie, E., Waite, A., Simon-Sanchez, J., Rollinson, S., Gibbs, J. R., . . . Traynor, B. J. (2011). A hexanucleotide repeat expansion in C9ORF72 is the cause of chromosome 9p21-linked ALS-FTD. *Neuron, 72*(2), 257-268. doi: 10.1016/j.neuron.2011.09.010

Richter, B., Sliter, D. A., Herhaus, L., Stolz, A., Wang, C., Beli, P., . . . Dikic, I. (2016). Phosphorylation of OPTN by TBK1 enhances its binding to Ub chains and promotes selective autophagy of damaged mitochondria. *Proc Natl Acad Sci U S A, 113*(15), 4039-4044. doi: 10.1073/pnas.1523926113

Rizk, A., Paul, G., Incardona, P., Bugarski, M., Mansouri, M., Niemann, A., . . . Sbalzarini, I. F. (2014). Segmentation and quantification of subcellular structures in fluorescence microscopy images using Squassh. *Nat Protoc, 9*(3), 586-596. doi: 10.1038/nprot.2014.037

Rizzo, M. A., Davidson, M. W., & Piston, D. W. (2009). Fluorescent protein tracking and detection: fluorescent protein structure and color variants. *Cold Spring Harb Protoc, 2009*(12), pdb top63. doi: 10.1101/pdb.top63

Rodriguez-Muela, N., Parkhitko, A., Grass, T., Gibbs, R. M., Norabuena, E. M., Perrimon, N., . . . Rubin, L. L. (2018). Blocking p62-dependent SMN degradation ameliorates spinal muscular atrophy disease phenotypes. *J Clin Invest, 128*(7), 3008-3023. doi: 10.1172/JCI95231

Rogov, V., Dotsch, V., Johansen, T., & Kirkin, V. (2014). Interactions between autophagy receptors and ubiquitin-like proteins form the molecular basis for selective autophagy. *Mol Cell, 53*(2), 167-178. doi: 10.1016/j.molcel.2013.12.014

Romao, S., Gasser, N., Becker, A. C., Guhl, B., Bajagic, M., Vanoaica, D., . . . Munz, C. (2013). Autophagy proteins stabilize pathogen-containing phagosomes for prolonged MHC II antigen processing. *J Cell Biol, 203*(5), 757-766. doi: 10.1083/jcb.201308173

Rubino, E., Rainero, I., Chio, A., Rogaeva, E., Galimberti, D., Fenoglio, P., . . . Group, Todem Study. (2012). SQSTM1 mutations in frontotemporal lobar degeneration and amyotrophic lateral sclerosis. *Neurology, 79*(15), 1556-1562. doi: 10.1212/WNL.0b013e31826e25df

Rubinsztein, D. C., Codogno, P., & Levine, B. (2012). Autophagy modulation as a potential therapeutic target for diverse diseases. *Nat Rev Drug Discov, 11*(9), 709-730. doi: 10.1038/nrd3802

Russell, R. C., Yuan, H. X., & Guan, K. L. (2014). Autophagy regulation by nutrient signaling. *Cell Res, 24*(1), 42-57. doi: 10.1038/cr.2013.166

Rusten, T. E., & Stenmark, H. (2009). How do ESCRT proteins control autophagy? *J Cell Sci, 122*(Pt 13), 2179-2183.

Ryu, H. H., Jun, M. H., Min, K. J., Jang, D. J., Lee, Y. S., Kim, H. K., & Lee, J. A. (2014). Autophagy regulates amyotrophic lateral sclerosis-linked fused in sarcoma-positive stress granules in neurons. *Neurobiol Aging, 35*(12), 2822-2831. doi: 10.1016/j.neurobiolaging.2014.07.026

Safaei, R., Larson, B. J., Cheng, T. C., Gibson, M. A., Otani, S., Naerdemann, W., & Howell, S. B. (2005). Abnormal lysosomal trafficking and enhanced exosomal export of cisplatin in drug-resistant human ovarian carcinoma cells. *Mol Cancer Ther, 4*(10), 1595-1604. doi: 10.1158/1535-7163.MCT-05-0102

Sahu, R., Kaushik, S., Clement, C. C., Cannizzo, E. S., Scharf, B., Follenzi, A., . . . Santambrogio, L. (2011). Microautophagy of cytosolic proteins by late endosomes. *Dev Cell, 20*(1), 131-139. doi: 10.1016/j.devcel.2010.12.003

Saito, H., Inazawa, J., Saito, S., Kasumi, F., Koi, S., Sagae, S., . . . Nakamura, Y. (1993). Detailed deletion mapping of chromosome 17q in ovarian and breast cancers: 2-cM region on 17q21.3 often and commonly deleted in tumors. *Cancer Res, 53*(14), 3382-3385.

Sama, R. R., Ward, C. L., Kaushansky, L. J., Lemay, N., Ishigaki, S., Urano, F., & Bosco, D. A. (2013). FUS/TLS assembles into stress granules and is a prosurvival factor during hyperosmolar stress. *J Cell Physiol, 228*(11), 2222-2231. doi: 10.1002/jcp.24395

Sameshima, M., Liebhaber, S. A., & Schlessinger, D. (1981). Dual pathways for ribonucleic acid turnover in WI-38 but not in I-cell human diploid fibroblasts. *Mol Cell Biol, 1*(1), 75-81.

Sandie, R., Palidwor, G. A., Huska, M. R., Porter, C. J., Krzyzanowski, P. M., Muro, E. M., . . . Andrade-Navarro, M. A. (2009). Recent developments in StemBase: a tool to study gene expression in human and murine stem cells. *BMC Res Notes, 2*, 39. doi: 10.1186/1756-0500-2-39

Sanjuan, M. A., Dillon, C. P., Tait, S. W., Moshiach, S., Dorsey, F., Connell, S., . . . Green, D. R. (2007). Toll-like receptor signalling in macrophages links the autophagy pathway to phagocytosis. *Nature, 450*(7173), 1253-1257. doi: 10.1038/nature06421

Sarkar, S., & Rubinsztein, D. C. (2008). Small molecule enhancers of autophagy for neurodegenerative diseases. *Mol Biosyst, 4*(9), 895-901. doi: 10.1039/b804606a

Sarraf, S. A., Raman, M., Guarani-Pereira, V., Sowa, M. E., Huttlin, E. L., Gygi, S. P., & Harper, J. W. (2013). Landscape of the PARKIN-dependent ubiquitylome in response to mitochondrial depolarization. *Nature, 496*(7445), 372-376. doi: 10.1038/nature12043

Sautin, Y. Y., Lu, M., Gaugler, A., Zhang, L., & Gluck, S. L. (2005). Phosphatidylinositol 3-kinase-mediated effects of glucose on vacuolar H+-ATPase assembly, translocation, and acidification of intracellular compartments in renal epithelial cells. *Mol Cell Biol, 25*(2), 575-589. doi: 10.1128/MCB.25.2.575-589.2005

Scaramuzzino, C., Monaghan, J., Milioto, C., Lanson, N. A., Jr., Maltare, A., Aggarwal, T., . . . Pandey, U. B. (2013). Protein arginine methyltransferase 1 and 8 interact with FUS to modify its sub-cellular distribution and toxicity in vitro and in vivo. *PLoS One, 8*(4), e61576. doi: 10.1371/journal.pone.0061576

Scekic-Zahirovic, J., Sendscheid, O., El Oussini, H., Jambeau, M., Sun, Y., Mersmann, S., . . . Dupuis, L. (2016). Toxic gain of function from mutant FUS protein is crucial to trigger cell autonomous motor neuron loss. *EMBO J, 35*(10), 1077-1097. doi: 10.15252/embj.201592559

Schludi, M. H., & Edbauer, D. (2018). Targeting RNA G-quadruplexes as new treatment strategy for C9orf72 ALS/FTD. *EMBO Mol Med, 10*(1), 4-6. doi: 10.15252/emmm.201708572

Schludi, M. H., May, S., Grasser, F. A., Rentzsch, K., Kremmer, E., Kupper, C., . . . Edbauer, D. (2015). Erratum to: Distribution of dipeptide repeat proteins in cellular models and C9orf72 mutation cases suggests link to transcriptional silencing. *Acta Neuropathol, 130*(4), 557-558. doi: 10.1007/s00401-015-1464-6

Schrider, D. R., Navarro, F. C., Galante, P. A., Parmigiani, R. B., Camargo, A. A., Hahn, M. W., & de Souza, S. J. (2013). Gene copy-number polymorphism caused by retrotransposition in humans. *PLoS Genet, 9*(1), e1003242. doi: 10.1371/journal.pgen.1003242

Sehgal, A., Chen, Q., Gibbings, D., Sah, D. W., & Bumcrot, D. (2014). Tissue-specific gene silencing monitored in circulating RNA. *RNA, 20*(2), 143-149. doi: 10.1261/rna.042507.113

Selvakumaran, M., Amaravadi, R. K., Vasilevskaya, I. A., & O'Dwyer, P. J. (2013). Autophagy inhibition sensitizes colon cancer cells to antiangiogenic and cytotoxic therapy. *Clin Cancer Res, 19*(11), 2995-3007. doi: 10.1158/1078-0432.CCR-12-1542

Shaid, S., Brandts, C. H., Serve, H., & Dikic, I. (2012). Ubiquitination and selective autophagy. *Cell death and differentiation*. doi: 10.1038/cdd.2012.72

Shaid, S., Brandts, C. H., Serve, H., & Dikic, I. (2013). Ubiquitination and selective autophagy. *Cell Death Differ, 20*(1), 21-30. doi: 10.1038/cdd.2012.72

Shannon, P., Markiel, A., Ozier, O., Baliga, N. S., Wang, J. T., Ramage, D., . . . Ideker, T. (2003). Cytoscape: a software environment for integrated models of biomolecular interaction networks. *Genome Res, 13*(11), 2498-2504. doi: 10.1101/gr.1239303

Sharifi, M. N., Mowers, E. E., Drake, L. E., Collier, C., Chen, H., Zamora, M., . . . Macleod, K. F. (2016). Autophagy Promotes Focal Adhesion Disassembly and Cell Motility of Metastatic Tumor Cells through the Direct Interaction of Paxillin with LC3. *Cell Rep, 15*(8), 1660-1672. doi: 10.1016/j.celrep.2016.04.065

Sharma, D. K., Choudhury, A., Singh, R. D., Wheatley, C. L., Marks, D. L., & Pagano, R. E. (2003). Glycosphingolipids internalized via caveolar-related endocytosis rapidly merge with the clathrin pathway in early endosomes and form microdomains for recycling. *J Biol Chem, 278*(9), 7564-7572. doi: 10.1074/jbc.M210457200

Sheffield, P., Garrard, S., & Derewenda, Z. (1999). Overcoming expression and purification problems of RhoGDI using a family of "parallel" expression vectors. *Protein Expr Purif, 15*(1), 34-39. doi: 10.1006/prep.1998.1003

Shen, Y., Liang, L. Z., Hong, M. H., Xiong, Y., Wei, M., & Zhu, X. F. (2008). [Expression and clinical significance of microtubule-associated protein 1 light chain 3 (LC3) and Beclin1 in epithelial ovarian cancer]. *Ai Zheng, 27*(6), 595-599.

Shevchenko, A., Tomas, H., Havlis, J., Olsen, J. V., & Mann, M. (2006). In-gel digestion for mass spectrometric characterization of proteins and proteomes. *Nat Protoc, 1*(6), 2856-2860. doi: 10.1038/nprot.2006.468

Shi, Y., Lin, S., Staats, K. A., Li, Y., Chang, W. H., Hung, S. T., . . . Ichida, J. K. (2018). Haploinsufficiency leads to neurodegeneration in C9ORF72 ALS/FTD human induced motor neurons. *Nat Med, 24*(3), 313-325. doi: 10.1038/nm.4490

Shih, J. W., Wang, W. T., Tsai, T. Y., Kuo, C. Y., Li, H. K., & Wu Lee, Y. H. (2012). Critical roles of RNA helicase DDX3 and its interactions with eIF4E/PABP1 in stress granule assembly and stress response. *Biochem J, 441*(1), 119-129. doi: 10.1042/BJ20110739

Shrivastava, S., Devhare, P., Sujijantarat, N., Steele, R., Kwon, Y. C., Ray, R., & Ray, R. B. (2016). Knockdown of Autophagy Inhibits Infectious Hepatitis C Virus Release by the Exosomal Pathway. *J Virol, 90*(3), 1387-1396. doi: 10.1128/JVI.02383-15

Shukla, R., Upton, K. R., Munoz-Lopez, M., Gerhardt, D. J., Fisher, M. E., Nguyen, T., . . . Faulkner, G. J. (2013). Endogenous retrotransposition activates oncogenic pathways in hepatocellular carcinoma. *Cell, 153*(1), 101-111. doi: 10.1016/j.cell.2013.02.032

Singh, S. S., Vats, S., Chia, A. Y., Tan, T. Z., Deng, S., Ong, M. S., . . . Kumar, A. P. (2018). Dual role of autophagy in hallmarks of cancer. *Oncogene, 37*(9), 1142-1158. doi: 10.1038/s41388-017-0046-6

Solyom, S., Ewing, A. D., Rahrmann, E. P., Doucet, T., Nelson, H. H., Burns, M. B., . . . Kazazian, H. H., Jr. (2012). Extensive somatic L1 retrotransposition in colorectal tumors. *Genome Res, 22*(12), 2328-2338. doi: 10.1101/gr.145235.112

Somasekharan, S. P., El-Naggar, A., Leprivier, G., Cheng, H., Hajee, S., Grunewald, T. G., . . . Sorensen, P. H. (2015). YB-1 regulates stress granule formation and tumor progression by translationally activating G3BP1. *J Cell Biol, 208*(7), 913-929. doi: 10.1083/jcb.201411047

Soo, K. Y., Halloran, M., Sundaramoorthy, V., Parakh, S., Toth, R. P., Southam, K. A., . . . Atkin, J. D. (2015). Rab1-dependent ER-Golgi transport dysfunction is a common pathogenic mechanism in SOD1, TDP-43 and FUS-associated ALS. *Acta Neuropathol, 130*(5), 679-697. doi: 10.1007/s00401-015-1468-2

Sorbara, M. T., Ellison, L. K., Ramjeet, M., Travassos, L. H., Jones, N. L., Girardin, S. E., & Philpott, D. J. (2013). The protein ATG16L1 suppresses inflammatory cytokines induced by the intracellular sensors Nod1 and Nod2 in an autophagy-independent manner. *Immunity, 39*(5), 858-873. doi: 10.1016/j.immuni.2013.10.013

Souquere, S., Mollet, S., Kress, M., Dautry, F., Pierron, G., & Weil, D. (2009). Unravelling the ultrastructure of stress granules and associated P-bodies in human cells. *J Cell Sci, 122*(Pt 20), 3619-3626. doi: 10.1242/jcs.054437

Specchia, V., Piacentini, L., Tritto, P., Fanti, L., D'Alessandro, R., Palumbo, G., . . . Bozzetti, M. P. (2010). Hsp90 prevents phenotypic variation by suppressing the mutagenic activity of transposons. *Nature, 463*(7281), 662-665. doi: nature08739 [pii]

10.1038/nature08739

Sreedharan, J., Blair, I. P., Tripathi, V. B., Hu, X., Vance, C., Rogelj, B., . . . Shaw, C. E. (2008). TDP-43 mutations in familial and sporadic amyotrophic lateral sclerosis. *Science, 319*(5870), 1668-1672. doi: 10.1126/science.1154584

Stieber, A., Gonatas, J. O., & Gonatas, N. K. (2000a). Aggregates of mutant protein appear progressively in dendrites, in periaxonal processes of oligodendrocytes, and in neuronal and astrocytic perikarya of mice expressing the SOD1(G93A) mutation of familial amyotrophic lateral sclerosis. *J Neurol Sci, 177*(2), 114-123.

Stieber, A., Gonatas, J. O., & Gonatas, N. K. (2000b). Aggregation of ubiquitin and a mutant ALS-linked SOD1 protein correlate with disease progression and fragmentation of the Golgi apparatus. *J Neurol Sci, 173*(1), 53-62.

Stolz, A., Ernst, A., & Dikic, I. (2014). Cargo recognition and trafficking in selective autophagy. *Nat Cell Biol, 16*(6), 495-501. doi: 10.1038/ncb2979

Strohecker, A. M., Guo, J. Y., Karsli-Uzunbas, G., Price, S. M., Chen, G. J., Mathew, R., . . . White, E. (2013). Autophagy sustains mitochondrial glutamine metabolism and growth of BrafV600E-driven lung tumors. *Cancer Discov, 3*(11), 1272-1285. doi: 10.1158/2159-8290.CD-13-0397

Stuffers, S., Sem Wegner, C., Stenmark, H., & Brech, A. (2009). Multivesicular endosome biogenesis in the absence of ESCRTs. *Traffic, 10*(7), 925-937. doi: 10.1111/j.1600-0854.2009.00920.x

Sugihara, K., Maruyama, H., Kamada, M., Morino, H., & Kawakami, H. (2011). Screening for OPTN mutations in amyotrophic lateral sclerosis in a mainly Caucasian population. *Neurobiol Aging, 32*(10), 1923 e1929-1910. doi: 10.1016/j.neurobiolaging.2011.03.024

Sui, X., Chen, R., Wang, Z., Huang, Z., Kong, N., Zhang, M., . . . Pan, H. (2013). Autophagy and chemotherapy resistance: a promising therapeutic target for cancer treatment. *Cell Death Dis, 4*, e838. doi: 10.1038/cddis.2013.350

Sullivan, P. M., Zhou, X., Robins, A. M., Paushter, D. H., Kim, D., Smolka, M. B., & Hu, F. (2016). The ALS/FTLD associated protein C9orf72 associates with SMCR8 and WDR41 to regulate the autophagy-lysosome pathway. *Acta Neuropathol Commun, 4*(1), 51. doi: 10.1186/s40478-016-0324-5

Sun, S., Ling, S. C., Qiu, J., Albuquerque, C. P., Zhou, Y., Tokunaga, S., . . . Cleveland, D. W. (2015). ALS-causative mutations in FUS/TLS confer gain and loss of function by altered association with SMN and U1-snRNP. *Nat Commun, 6*, 6171. doi: 10.1038/ncomms7171

Swanton, C., Nicke, B., Schuett, M., Eklund, A. C., Ng, C., Li, Q., . . . Downward, J. (2009). Chromosomal instability determines taxane response. *Proc Natl Acad Sci U S A, 106*(21), 8671-8676. doi: 10.1073/pnas.0811835106

Sylvestersen, K. B., Horn, H., Jungmichel, S., Jensen, L. J., & Nielsen, M. L. (2014). Proteomic analysis of arginine methylation sites in human cells reveals dynamic regulation during transcriptional arrest. *Mol Cell Proteomics, 13*(8), 2072-2088. doi: 10.1074/mcp.O113.032748

Szaflarski, W., Fay, M. M., Kedersha, N., Zabel, M., Anderson, P., & Ivanov, P. (2016). Vinca alkaloid drugs promote stress-induced translational repression and stress granule formation. *Oncotarget, 7*(21), 30307-30322. doi: 10.18632/oncotarget.8728

Taelman, V. F., Dobrowolski, R., Plouhinec, J. L., Fuentealba, L. C., Vorwald, P. P., Gumper, I., . . . De Robertis, E. M. (2010). Wnt signaling requires sequestration of glycogen synthase kinase 3 inside multivesicular endosomes. *Cell, 143*(7), 1136-1148. doi: 10.1016/j.cell.2010.11.034

Takamura, A., Komatsu, M., Hara, T., Sakamoto, A., Kishi, C., Waguri, S., . . . Mizushima, N. (2011a). Autophagy-deficient mice develop multiple liver tumors. *Genes Dev, 25*(8), 795-800. doi: 10.1101/gad.2016211

Takamura, A., Komatsu, M., Hara, T., Sakamoto, A., Kishi, C., Waguri, S., . . . Mizushima, N. (2011b). Autophagy-deficient mice develop multiple liver tumors. *Genes & development, 25*(8), 795-800. doi: 10.1101/gad.2016211

Tamai, K., Tanaka, N., Nakano, T., Kakazu, E., Kondo, Y., Inoue, J., . . . Sugamura, K. (2010). Exosome secretion of dendritic cells is regulated by Hrs, an ESCRT-0 protein. *Biochem Biophys Res Commun, 399*(3), 384-390. doi: 10.1016/j.bbrc.2010.07.083

Tang, H., Sebti, S., Titone, R., Zhou, Y., Isidoro, C., Ross, T. S., . . . Levine, B. (2015). Decreased BECN1 mRNA Expression in Human Breast Cancer is Associated with Estrogen Receptor-Negative Subtypes and Poor Prognosis. *EBioMedicine, 2*(3), 255-263. doi: 10.1016/j.ebiom.2015.01.008

Tanida, I., Yamaji, T., Ueno, T., Ishiura, S., Kominami, E., & Hanada, K. (2008). Consideration about negative controls for LC3 and expression vectors for four colored fluorescent protein-LC3 negative controls. *Autophagy, 4*(1), 131-134.

Tao, K., Fang, M., Alroy, J., & Sahagian, G. G. (2008). Imagable 4T1 model for the study of late stage breast cancer. *BMC Cancer, 8*, 228. doi: 10.1186/1471-2407-8-228

Tauro, B. J., Greening, D. W., Mathias, R. A., Mathivanan, S., Ji, H., & Simpson, R. J. (2013). Two distinct populations of exosomes are released from LIM1863 colon carcinoma cell-derived organoids. *Mol Cell Proteomics, 12*(3), 587-598. doi: 10.1074/mcp.M112.021303

Taylor, J. P., Brown, R. H., Jr., & Cleveland, D. W. (2016). Decoding ALS: from genes to mechanism. *Nature, 539*(7628), 197-206. doi: 10.1038/nature20413

Teo, G., Koh, H., Fermin, D., Lambert, J. P., Knight, J. D., Gingras, A. C., & Choi, H. (2016). SAINTq: Scoring protein-protein interactions in affinity purification - mass spectrometry experiments with fragment or peptide intensity data. *Proteomics, 16*(15-16), 2238-2245. doi: 10.1002/pmic.201500499

Teyssou, E., Takeda, T., Lebon, V., Boillee, S., Doukoure, B., Bataillon, G., . . . Millecamps, S. (2013). Mutations in SQSTM1 encoding p62 in amyotrophic lateral sclerosis: genetics and neuropathology. *Acta Neuropathol, 125*(4), 511-522. doi: 10.1007/s00401-013-1090-0

Thery, C., Amigorena, S., Raposo, G., & Clayton, A. (2006). Isolation and characterization of exosomes from cell culture supernatants and biological fluids. *Curr Protoc Cell Biol, Chapter 3*, Unit 3 22. doi: 10.1002/0471143030.cb0322s30

Thompson, P. A., Brewster, A. M., Kim-Anh, D., Baladandayuthapani, V., Broom, B. M., Edgerton, M. E., . . . Bondy, M. L. (2011). Selective genomic copy number imbalances and probability of recurrence in early-stage breast cancer. *PLoS One, 6*(8), e23543. doi: 10.1371/journal.pone.0023543

Thurston, T. L., Ryzhakov, G., Bloor, S., von Muhlinen, N., & Randow, F. (2009). The TBK1 adaptor and autophagy receptor NDP52 restricts the proliferation of ubiquitin-coated bacteria. *Nat Immunol, 10*(11), 1215-1221. doi: 10.1038/ni.1800

Tian, T., Zhu, Y. L., Hu, F. H., Wang, Y. Y., Huang, N. P., & Xiao, Z. D. (2013). Dynamics of exosome internalization and trafficking. *J Cell Physiol, 228*(7), 1487-1495. doi: 10.1002/jcp.24304

Tiloca, C., Ratti, A., Pensato, V., Castucci, A., Soraru, G., Del Bo, R., . . . Consortium, Slagen. (2012). Mutational analysis of VCP gene in familial amyotrophic lateral sclerosis. *Neurobiol Aging, 33*(3), 630 e631-632. doi: 10.1016/j.neurobiolaging.2011.10.025

Toei, M., Saum, R., & Forgac, M. (2010). Regulation and isoform function of the V-ATPases. *Biochemistry, 49*(23), 4715-4723. doi: 10.1021/bi100397s

Tradewell, M. L., Yu, Z., Tibshirani, M., Boulanger, M. C., Durham, H. D., & Richard, S. (2012). Arginine methylation by PRMT1 regulates nuclear-cytoplasmic localization and toxicity of FUS/TLS harbouring ALS-linked mutations. *Hum Mol Genet, 21*(1), 136-149. doi: 10.1093/hmg/ddr448

Trajkovic, K., Hsu, C., Chiantia, S., Rajendran, L., Wenzel, D., Wieland, F., . . . Simons, M. (2008). Ceramide triggers budding of exosome vesicles into multivesicular endosomes. *Science, 319*(5867), 1244-1247.

Traynor, B. J., Alexander, M., Corr, B., Frost, E., & Hardiman, O. (2003). An outcome study of riluzole in amyotrophic lateral sclerosis--a population-based study in Ireland, 1996-2000. *J Neurol, 250*(4), 473-479. doi: 10.1007/s00415-003-1026-z

Truschel, S. T., Simoes, S., Setty, S. R., Harper, D. C., Tenza, D., Thomas, P. C., . . . Marks, M. S. (2009). ESCRT-I function is required for Tyrp1 transport from early endosomes to the melanosome limiting membrane. *Traffic, 10*(9), 1318-1336. doi: 10.1111/j.1600-0854.2009.00955.x

Tu, P. H., Raju, P., Robinson, K. A., Gurney, M. E., Trojanowski, J. Q., & Lee, V. M. (1996). Transgenic mice carrying a human mutant superoxide dismutase transgene develop neuronal cytoskeletal pathology resembling human amyotrophic lateral sclerosis lesions. *Proc Natl Acad Sci U S A, 93*(7), 3155-3160.

Turinsky, A. L., Razick, S., Turner, B., Donaldson, I. M., & Wodak, S. J. (2014). Navigating the global protein-protein interaction landscape using iRefWeb. *Methods Mol Biol, 1091*, 315-331. doi: 10.1007/978-1-62703-691-7_22

Ugras, S. E., & Shorter, J. (2012). RNA-Binding Proteins in Amyotrophic Lateral Sclerosis and Neurodegeneration. *Neurol Res Int, 2012*, 432780. doi: 10.1155/2012/432780

Uhlmann, T., Geoghegan, V. L., Thomas, B., Ridlova, G., Trudgian, D. C., & Acuto, O. (2012). A method for large-scale identification of protein arginine methylation. *Mol Cell Proteomics, 11*(11), 1489-1499. doi: 10.1074/mcp.M112.020743

Ushio, H., Ueno, T., Kojima, Y., Komatsu, M., Tanaka, S., Yamamoto, A., . . . Nakano, H. (2011). Crucial role for autophagy in degranulation of mast cells. *J Allergy Clin Immunol, 127*(5), 1267-1276 e1266. doi: 10.1016/j.jaci.2010.12.1078

Uttenweiler, A., & Mayer, A. (2008). Microautophagy in the yeast Saccharomyces cerevisiae. *Methods Mol Biol, 445*, 245-259. doi: 10.1007/978-1-59745-157-4_16

Vader, P., Breakefield, X. O., & Wood, M. J. (2014). Extracellular vesicles: emerging targets for cancer therapy. *Trends Mol Med, 20*(7), 385-393. doi: 10.1016/j.molmed.2014.03.002

van Blitterswijk, M., & Landers, J. E. (2010). RNA processing pathways in amyotrophic lateral sclerosis. *Neurogenetics, 11*(3), 275-290. doi: 10.1007/s10048-010-0239-4

Van Deerlin, V. M., Leverenz, J. B., Bekris, L. M., Bird, T. D., Yuan, W., Elman, L. B., . . . Yu, C. E. (2008). TARDBP mutations in amyotrophic lateral sclerosis with TDP-43 neuropathology: a genetic and histopathological analysis. *Lancet Neurol, 7*(5), 409-416. doi: 10.1016/S1474-4422(08)70071-1

van Zundert, B., & Brown, R. H., Jr. (2017). Silencing strategies for therapy of SOD1-mediated ALS. *Neurosci Lett, 636*, 32-39. doi: 10.1016/j.neulet.2016.07.059

Vance, C., Rogelj, B., Hortobagyi, T., De Vos, K. J., Nishimura, A. L., Sreedharan, J., . . . Shaw, C. E. (2009). Mutations in FUS, an RNA processing protein, cause familial amyotrophic lateral sclerosis type 6. *Science, 323*(5918), 1208-1211. doi: 10.1126/science.1165942

Vanlandingham, P. A., & Ceresa, B. P. (2009). Rab7 regulates late endocytic trafficking downstream of multivesicular body biogenesis and cargo sequestration. *J Biol Chem, 284*(18), 12110-12124. doi: 10.1074/jbc.M809277200

Varshavsky, A. (2017). The Ubiquitin System, Autophagy, and Regulated Protein Degradation. *Annu Rev Biochem, 86*, 123-128. doi: 10.1146/annurev-biochem-061516-044859

Vaught, D. B., Stanford, J. C., Young, C., Hicks, D. J., Wheeler, F., Rinehart, C., . . . Cook, R. S. (2012). HER3 is required for HER2-induced preneoplastic changes to the breast epithelium and tumor formation. *Cancer Res, 72*(10), 2672-2682. doi: 10.1158/0008-5472.CAN-11-3594

Venkatraman, P., Wetzel, R., Tanaka, M., Nukina, N., & Goldberg, A. L. (2004). Eukaryotic proteasomes cannot digest polyglutamine sequences and release

them during degradation of polyglutamine-containing proteins. *Mol Cell, 14*(1), 95-104.

Vidal, M., Mangeat, P., & Hoekstra, D. (1997). Aggregation reroutes molecules from a recycling to a vesicle-mediated secretion pathway during reticulocyte maturation. *J Cell Sci, 110 (Pt 16)*, 1867-1877.

Vilas-Boas Fde, A., da Silva, A. M., de Sousa, L. P., Lima, K. M., Vago, J. P., Bittencourt, L. F., . . . Barcelos, L. S. (2016). Impairment of stress granule assembly via inhibition of the eIF2alpha phosphorylation sensitizes glioma cells to chemotherapeutic agents. *J Neurooncol, 127*(2), 253-260. doi: 10.1007/s11060-015-2043-3

Wachtler, F., Schofer, C., Mosgoller, W., Weipoltshammer, K., Schwarzacher, H. G., Guichaoua, M., . . . et al. (1992). Human ribosomal RNA gene repeats are localized in the dense fibrillar component of nucleoli: light and electron microscopic in situ hybridization in human Sertoli cells. *Exp Cell Res, 198*(1), 135-143.

Wahl, M. C., Will, C. L., & Luhrmann, R. (2009). The spliceosome: design principles of a dynamic RNP machine. *Cell, 136*(4), 701-718. doi: 10.1016/j.cell.2009.02.009

Waite, A. J., Baumer, D., East, S., Neal, J., Morris, H. R., Ansorge, O., & Blake, D. J. (2014). Reduced C9orf72 protein levels in frontal cortex of amyotrophic lateral sclerosis and frontotemporal degeneration brain with the C9ORF72 hexanucleotide repeat expansion. *Neurobiol Aging, 35*(7), 1779 e1775-1779 e1713. doi: 10.1016/j.neurobiolaging.2014.01.016

Walport, L. J., Hopkinson, R. J., Chowdhury, R., Schiller, R., Ge, W., Kawamura, A., & Schofield, C. J. (2016). Arginine demethylation is catalysed by a subset of JmjC histone lysine demethylases. *Nat Commun, 7*, 11974. doi: 10.1038/ncomms11974

Wang-Johanning, F., Frost, A. R., Jian, B., Epp, L., Lu, D. W., & Johanning, G. L. (2003). Quantitation of HERV-K env gene expression and splicing in human breast cancer. *Oncogene, 22*(10), 1528-1535. doi: 10.1038/sj.onc.1206241

Wang-Johanning, F., Radvanyi, L., Rycaj, K., Plummer, J. B., Yan, P., Sastry, K. J., . . . Johanning, G. L. (2008). Human endogenous retrovirus K triggers an antigen-specific immune response in breast cancer patients. *Cancer Res, 68*(14), 5869-5877. doi: 10.1158/0008-5472.CAN-07-6838

Wang, D., & Hiesinger, P. R. (2013). The vesicular ATPase: a missing link between acidification and exocytosis. *J Cell Biol, 203*(2), 171-173. doi: 10.1083/jcb.201309130

Wang, I. F., Guo, B. S., Liu, Y. C., Wu, C. C., Yang, C. H., Tsai, K. J., & Shen, C. K. (2012). Autophagy activators rescue and alleviate pathogenesis of a mouse model with proteinopathies of the TAR DNA-binding protein 43. *Proc Natl Acad Sci U S A, 109*(37), 15024-15029. doi: 10.1073/pnas.1206362109

Wang, I. F., Tsai, K. J., & Shen, C. K. (2013). Autophagy activation ameliorates neuronal pathogenesis of FTLD-U mice: a new light for treatment of TARDBP/TDP-43 proteinopathies. *Autophagy, 9*(2), 239-240. doi: 10.4161/auto.22526

Wang, J., & Wu, G. S. (2014). Role of autophagy in cisplatin resistance in ovarian cancer cells. *J Biol Chem, 289*(24), 17163-17173. doi: 10.1074/jbc.M114.558288

Wang, R. C., Wei, Y., An, Z., Zou, Z., Xiao, G., Bhagat, G., . . . Levine, B. (2012). Akt-mediated regulation of autophagy and tumorigenesis through Beclin 1 phosphorylation. *Science, 338*(6109), 956-959. doi: 10.1126/science.1225967

Wang, X., Fan, H., Ying, Z., Li, B., Wang, H., & Wang, G. (2010). Degradation of TDP-43 and its pathogenic form by autophagy and the ubiquitin-proteasome system. *Neurosci Lett, 469*(1), 112-116. doi: 10.1016/j.neulet.2009.11.055

Wang, X., Lu, G., Li, L., Yi, J., Yan, K., Wang, Y., . . . Shao, G. (2014). HUWE1 interacts with BRCA1 and promotes its degradation in the ubiquitin-proteasome pathway. *Biochem Biophys Res Commun, 444*(3), 290-295. doi: 10.1016/j.bbrc.2013.12.053

Watanabe, M., Dykes-Hoberg, M., Culotta, V. C., Price, D. L., Wong, P. C., & Rothstein, J. D. (2001). Histological evidence of protein aggregation in mutant SOD1 transgenic mice and in amyotrophic lateral sclerosis neural tissues. *Neurobiol Dis, 8*(6), 933-941. doi: 10.1006/nbdi.2001.0443

Webster, C. P., Smith, E. F., Bauer, C. S., Moller, A., Hautbergue, G. M., Ferraiuolo, L., . . . De Vos, K. J. (2016). The C9orf72 protein interacts with Rab1a and the ULK1 complex to regulate initiation of autophagy. *EMBO J, 35*(15), 1656-1676. doi: 10.15252/embj.201694401

Wei, H., Wei, S., Gan, B., Peng, X., Zou, W., & Guan, J. L. (2011). Suppression of autophagy by FIP200 deletion inhibits mammary tumorigenesis. *Genes Dev, 25*(14), 1510-1527. doi: 10.1101/gad.2051011

Wemmer, M., Azmi, I., West, M., Davies, B., Katzmann, D., & Odorizzi, G. (2011). Bro1 binding to Snf7 regulates ESCRT-III membrane scission activity in yeast. *J Cell Biol, 192*(2), 295-306. doi: 10.1083/jcb.201007018

White, E. (2012). Deconvoluting the context-dependent role for autophagy in cancer. *Nat Rev Cancer, 12*(6), 401-410. doi: 10.1038/nrc3262

White, E., Karp, C., Strohecker, A. M., Guo, Y., & Mathew, R. (2010). Role of autophagy in suppression of inflammation and cancer. *Curr Opin Cell Biol, 22*(2), 212-217. doi: 10.1016/j.ceb.2009.12.008

Wild, P., Farhan, H., McEwan, D. G., Wagner, S., Rogov, V. V., Brady, N. R., . . . Dikic, I. (2011). Phosphorylation of the autophagy receptor optineurin restricts Salmonella growth. *Science, 333*(6039), 228-233. doi: 10.1126/science.1205405

Williams, K. L., Warraich, S. T., Yang, S., Solski, J. A., Fernando, R., Rouleau, G. A., . . . Blair, I. P. (2012). UBQLN2/ubiquilin 2 mutation and pathology in familial amyotrophic lateral sclerosis. *Neurobiol Aging, 33*(10), 2527 e2523-2510. doi: 10.1016/j.neurobiolaging.2012.05.008

Wissing, S., Munoz-Lopez, M., Macia, A., Yang, Z., Montano, M., Collins, W., . . . Greene, W. C. (2012). Reprogramming somatic cells into iPS cells activates LINE-1 retroelement mobility. *Hum Mol Genet, 21*(1), 208-218. doi: 10.1093/hmg/ddr455

Wolozin, B. (2012). Regulated protein aggregation: stress granules and neurodegeneration. *Mol Neurodegener, 7*, 56. doi: 10.1186/1750-1326-7-56

Wong, Y. C., & Holzbaur, E. L. (2014). Optineurin is an autophagy receptor for damaged mitochondria in parkin-mediated mitophagy that is disrupted by an ALS-linked mutation. *Proc Natl Acad Sci U S A, 111*(42), E4439-4448. doi: 10.1073/pnas.1405752111

Wooten, M. W., Geetha, T., Babu, J. R., Seibenhener, M. L., Peng, J., Cox, N., . . . Moscat, J. (2008). Essential role of sequestosome 1/p62 in regulating accumulation of Lys63-ubiquitinated proteins. *J Biol Chem, 283*(11), 6783-6789. doi: 10.1074/jbc.M709496200

Wroe, R., Wai-Ling Butler, A., Andersen, P. M., Powell, J. F., & Al-Chalabi, A. (2008). ALSOD: the Amyotrophic Lateral Sclerosis Online Database. *Amyotroph Lateral Scler, 9*(4), 249-250. doi: 10.1080/17482960802146106

Xi, Z., Zinman, L., Moreno, D., Schymick, J., Liang, Y., Sato, C., . . . Rogaeva, E. (2013). Hypermethylation of the CpG island near the G4C2 repeat in ALS with a C9orf72 expansion. *Am J Hum Genet, 92*(6), 981-989. doi: 10.1016/j.ajhg.2013.04.017

Xiao, S., MacNair, L., McGoldrick, P., McKeever, P. M., McLean, J. R., Zhang, M., . . . Robertson, J. (2015). Isoform-specific antibodies reveal distinct subcellular localizations of C9orf72 in amyotrophic lateral sclerosis. *Ann Neurol, 78*(4), 568-583. doi: 10.1002/ana.24469

Yamano, K., Fogel, A. I., Wang, C., van der Bliek, A. M., & Youle, R. J. (2014). Mitochondrial Rab GAPs govern autophagosome biogenesis during mitophagy. *Elife, 3*, e01612. doi: 10.7554/eLife.01612

Yang, A., Rajeshkumar, N. V., Wang, X., Yabuuchi, S., Alexander, B. M., Chu, G. C., . . . Kimmelman, A. C. (2014). Autophagy is critical for pancreatic tumor growth and progression in tumors with p53 alterations. *Cancer Discov, 4*(8), 905-913. doi: 10.1158/2159-8290.CD-14-0362

Yang, S., Wang, X., Contino, G., Liesa, M., Sahin, E., Ying, H., . . . Kimmelman, A. C. (2011). Pancreatic cancers require autophagy for tumor growth. *Genes Dev, 25*(7), 717-729. doi: 10.1101/gad.2016111

Yang, Y., Hadjikyriacou, A., Xia, Z., Gayatri, S., Kim, D., Zurita-Lopez, C., . . . Bedford, M. T. (2015). PRMT9 is a type II methyltransferase that methylates the splicing factor SAP145. *Nat Commun, 6*, 6428. doi: 10.1038/ncomms7428

Yang, Z., & Klionsky, D. J. (2010). Eaten alive: a history of macroautophagy. *Nat Cell Biol, 12*(9), 814-822. doi: 10.1038/ncb0910-814

Yazbeck, V. Y., Buglio, D., Georgakis, G. V., Li, Y., Iwado, E., Romaguera, J. E., . . . Younes, A. (2008). Temsirolimus downregulates p21 without altering cyclin D1 expression and induces autophagy and synergizes with vorinostat in mantle cell lymphoma. *Exp Hematol, 36*(4), 443-450. doi: 10.1016/j.exphem.2007.12.008

Yin, J., Yan, X., Yao, X., Zhang, Y., Shan, Y., Mao, N., . . . Pan, L. (2012). Secretion of annexin A3 from ovarian cancer cells and its association with platinum resistance in ovarian cancer patients. *J Cell Mol Med, 16*(2), 337-348. doi: 10.1111/j.1582-4934.2011.01316.x

Yoshino, H., & Kimura, A. (2006). Investigation of the therapeutic effects of edaravone, a free radical scavenger, on amyotrophic lateral sclerosis (Phase II study). *Amyotroph Lateral Scler, 7*(4), 241-245. doi: 10.1080/17482960600881870

Yu, M. C. (2011). The Role of Protein Arginine Methylation in mRNP Dynamics. *Mol Biol Int, 2011*, 163827. doi: 10.4061/2011/163827

Yu, P., Lubben, W., Slomka, H., Gebler, J., Konert, M., Cai, C., . . . Bauer, S. (2012). Nucleic acid-sensing Toll-like receptors are essential for the control of endogenous retrovirus viremia and ERV-induced tumors. *Immunity, 37*(5), 867-879. doi: 10.1016/j.immuni.2012.07.018

Yue, Z., Jin, S., Yang, C., Levine, A. J., & Heintz, N. (2003). Beclin 1, an autophagy gene essential for early embryonic development, is a haploinsufficient tumor suppressor. *Proc Natl Acad Sci U S A, 100*(25), 15077-15082. doi: 10.1073/pnas.2436255100

Zaffagnini, G., & Martens, S. (2016). Mechanisms of Selective Autophagy. *J Mol Biol, 428*(9 Pt A), 1714-1724. doi: 10.1016/j.jmb.2016.02.004

Zagouri, F., Sergentanis, T. N., Chrysikos, D., Filipits, M., & Bartsch, R. (2012). mTOR inhibitors in breast cancer: a systematic review. *Gynecol Oncol, 127*(3), 662-672. doi: 10.1016/j.ygyno.2012.08.040

Zhang, H. G., & Grizzle, W. E. (2014). Exosomes: a novel pathway of local and distant intercellular communication that facilitates the growth and metastasis of neoplastic lesions. *Am J Pathol, 184*(1), 28-41. doi: 10.1016/j.ajpath.2013.09.027

Zhang, K., Shi, P., An, T., Wang, Q., Wang, J., Li, Z., . . . Guo, Y. (2013). Food restriction-induced autophagy modulates degradation of mutant SOD1 in an amyotrophic lateral sclerosis mouse model. *Brain Res, 1519*, 112-119. doi: 10.1016/j.brainres.2013.04.050

Zhang, L., Yu, J., Pan, H., Hu, P., Hao, Y., Cai, W., . . . Yuan, J. (2007). Small molecule regulators of autophagy identified by an image-based high-throughput screen. *Proc Natl Acad Sci U S A, 104*(48), 19023-19028. doi: 10.1073/pnas.0709695104

Zhang, X., Chen, S., Song, L., Tang, Y., Shen, Y., Jia, L., & Le, W. (2014). MTOR-independent, autophagic enhancer trehalose prolongs motor neuron survival and ameliorates the autophagic flux defect in a mouse model of amyotrophic lateral sclerosis. *Autophagy, 10*(4), 588-602. doi: 10.4161/auto.27710

Zhang, X., Li, L., Chen, S., Yang, D., Wang, Y., Zhang, X., . . . Le, W. (2011). Rapamycin treatment augments motor neuron degeneration in SOD1(G93A) mouse model of amyotrophic lateral sclerosis. *Autophagy, 7*(4), 412-425.

Zhang, Y., Yan, L., Zhou, Z., Yang, P., Tian, E., Zhang, K., . . . Zhang, H. (2009). SEPA-1 mediates the specific recognition and degradation of P granule components by autophagy in C. elegans. *Cell, 136*(2), 308-321. doi: 10.1016/j.cell.2008.12.022

Zhao, J., Rycaj, K., Geng, S., Li, M., Plummer, J. B., Yin, B., . . . Wang-Johanning, F. (2011). Expression of Human Endogenous Retrovirus Type K Envelope Protein is a Novel Candidate Prognostic Marker for Human Breast Cancer. *Genes Cancer, 2*(9), 914-922. doi: 10.1177/1947601911431841

Zhao, K., Du, J., Han, X., Goodier, J. L., Li, P., Zhou, X., . . . Yu, X. F. (2013). Modulation of LINE-1 and Alu/SVA retrotransposition by Aicardi-Goutieres syndrome-related SAMHD1. *Cell Rep, 4*(6), 1108-1115. doi: 10.1016/j.celrep.2013.08.019

Zhao, Z., Fux, B., Goodwin, M., Dunay, I. R., Strong, D., Miller, B. C., . . . Virgin, H. W. (2008). Autophagosome-independent essential function for the autophagy protein Atg5 in cellular immunity to intracellular pathogens. *Cell Host Microbe, 4*(5), 458-469. doi: 10.1016/j.chom.2008.10.003

Zheng, Y. T., Shahnazari, S., Brech, A., Lamark, T., Johansen, T., & Brumell, J. H. (2009). The adaptor protein p62/SQSTM1 targets invading bacteria to the autophagy pathway. *J Immunol, 183*(9), 5909-5916. doi: 10.4049/jimmunol.0900441

Zheng, Y. Z., Boscher, C., Inder, K. L., Fairbank, M., Loo, D., Hill, M. M., . . . Foster, L. J. (2011). Differential impact of caveolae and caveolin-1 scaffolds on the membrane raft proteome. *Mol Cell Proteomics, 10*(10), M110 007146. doi: 10.1074/mcp.M110.007146

Zhou, J., Tan, S. H., Nicolas, V., Bauvy, C., Yang, N. D., Zhang, J., . . . Shen, H. M. (2013). Activation of lysosomal function in the course of autophagy via mTORC1 suppression and autophagosome-lysosome fusion. *Cell Res, 23*(4), 508-523. doi: 10.1038/cr.2013.11

Zhou, J., Wang, J., Cheng, Y., Chi, Y. J., Fan, B., Yu, J. Q., & Chen, Z. (2013). NBR1-mediated selective autophagy targets insoluble ubiquitinated protein aggregates in plant stress responses. *PLoS Genet, 9*(1), e1003196. doi: 10.1371/journal.pgen.1003196

Zhou, Y., Liu, S., Liu, G., Ozturk, A., & Hicks, G. G. (2013). ALS-associated FUS mutations result in compromised FUS alternative splicing and autoregulation. *PLoS Genet, 9*(10), e1003895. doi: 10.1371/journal.pgen.1003895

Zinszner, H., Sok, J., Immanuel, D., Yin, Y., & Ron, D. (1997). TLS (FUS) binds RNA in vivo and engages in nucleo-cytoplasmic shuttling. *J Cell Sci, 110 (Pt 15)*, 1741-1750.

Zu, T., Gibbens, B., Doty, N. S., Gomes-Pereira, M., Huguet, A., Stone, M. D., . . . Ranum, L. P. (2011). Non-ATG-initiated translation directed by microsatellite expansions. *Proc Natl Acad Sci U S A, 108*(1), 260-265. doi: 10.1073/pnas.1013343108